School of Chemical and Petroleum Engineering

Department of Chemical Engineering

Catalytic Oxidation of Toxic Organics in Aqueous Solution for Wastewater Treatment

Edy Saputra

This thesis is presented for the degree of

Doctor of Philosophy

of

Curtin University

September 2013

Declaration

To the best of my knowledge and belief this thesis contains no material previously published by any other person except where due acknowledgment has been made.

This thesis contains no material which has been accepted for the award of any other degree or diploma in any university.

Signature : ……

Date : ……

Acknowledgement

I would like to thank profusely to my main supervisor Prof. Shaobin Wang and co-supervisor Prof. Ha Ming Ang for their guidance, encouragement and patience during my Doctoral Program in the Department of Chemical Engineering, Curtin University. The enthusiasm and inspiration from them, makes me excited to do my research project. I also thank Prof. Moses O. Tade as a chairman of the thesis committee who has held regular meetings to support and assist in resolving any problems that occur in my research. With excellent support from all of them my research and thesis can be completed. Furthermore, I extend sincere thanks also to all the lab technicians at Chemical Engineering Department, Karen Haynes and the team members who have given so much assistance in my research. Without them, my experiment would not be successful. I extend special thanks also to my research colleague, Muhammad Syaifullah, who has helped me in my critical periods of my study.

I am thankful to DIKTI sponsor of National Education of Indonesia Government who has provided scholarships for my Doctoral Program. Thanks also go to Prof. Ashaluddin Jalil, the rector of Riau University, my home university, and Prof. Amir Awaluddin as a director of International office and also his staff members, who provided so much assistance in solving problems of my scholarship and other issues.

Lastly, and most importantly, a special thank is made to my beloved wife Erni Liana and my children, Izzah, Ibad, Rido, and Anisa, all my family: Mamak, Kak Yamin, Yeni, Epi, Iwan, Ican, and Yade for their immense support, and also my deceased beloved father.

Summary

This research is focused on catalytic oxidation of toxic organics in aqueous solution for wastewater treatment. Active metals, manganese (Mn), cobalt (Co) and Iron (Fe) have been used to synthesize several catalysts such as α-, β-, γ-MnO_2, MnO, α-Mn_2O_3, γ-Mn_3O_4, α-Mn_2O_3@α-MnO_2 core/shell, Mn/AC, Mn/GO, Co_3O_4, Fe_3O_4, using hydrothermal, solvothermal, sol-gel, and impregnation methods. Those synthesized catalysts have been characterized and tested in heterogeneous activation of peroxymonosulfate for phenol degradation in aqueous solutions. They showed varying activities in activation of peroxymonosulfate to generate sulfate radicals for phenol degradation, depending on surface area, crystalline structure, and oxidation states. Further, it was observed that adsorption may increase the probability of reaction between peroxymonosulfate and phenol, and phenol degradation on all heterogeneous catalysts followed the first-order kinetics. Moreover, it was also found that several parameters such as the concentration of phenol, catalyst loading, peroxymonosulfate loading, and temperature are key factors affecting the phenol oxidation process.

Publication by the author

1. Saputra, E., Muhammad, S., Sun, H., Ang, H. M., Tadé, M. O., Wang, S., *Different Crystallographic One-dimensional MnO_2 Nanomaterials and Their Superior Performance in Catalytic Phenol Degradation.* Environ. Sci. Technol., 2013, **47** (11), 5882–5887.

2. Saputra, E., Muhammad, S., Sun, H., Ang, H. M., Tadé, M. O., Wang, S., *Manganese Oxides at Different Oxidation States for Heterogeneous Activation of Peroxymonosulfate for Phenol Degradation in Aqueous Solution.* Applied Catalysis B: Environmental, **142-143** (2013), 729-735.

3. Saputra, E., Muhammad, S., Sun, H., Ang, H. M., Tadé, M. O., Wang, S., *A comparative study of spinel structured Mn_3O_4, Co_3O_4 and Fe_3O_4 nanoparticles in catalytic oxidation of phenolic contaminants in aqueous solutions.* Journal of Colloid and Interface Science, **407** (2013) 467–473.

4. Saputra, E., Muhammad, S., Sun, H., Ang, H. M., Tadé, M. O., Wang, S., *Activated carbons as green and effective catalysts for generation of reactive radicals in degradation of aqueous phenol.* DOI: 10.1039/C3RA42455C, RSC Adv., 2013.

5. Saputra, E., Muhammad, S., Sun, H., Ang, H. M., Tadé, M. O., Wang, S., *α-MnO_2 activation of peroxymonosulfate for catalytic phenol degradation in aqueous solutions.* Catalysis Communications, **26** (2012) 144-148.

6. Saputra, E., Muhammad, S., Sun, H., Ang, H. M., Tadé, M. O., Wang, S., *Red mud and fly ash supported Co catalysts for phenol oxidation.* Catalysis Today 2012, **190** (1), 68-72.

7. Muhammad, S., Saputra, E., Sun, H., Izidoro, J. d. C., Fungaro, D. A., Ang, H. M., Tade, M. O., Wang, S. *Coal fly ash supported Co_3O_4 catalysts for phenol degradation using peroxymonosulfate*. *RSC Advances 2012, **2** (13) 5645-5650.*

8. Muhammad, S., Saputra, E., Sun, H., Ang, H.M., Tade, M., Wang, S. *Heterogeneous Catalytic Oxidation of Aqueous Phenol on Red Mud Supported Cobalt Catalysts*. *Industrial & Engineering Chemistry Research, **51** (2012) 15351−15359.*

9. Saputra, E., Utama, P. S., Muhammad, S., Sun, H., Ang, H. M., Tadé, M. O., Wang, S., *Removal of Phenolic Contaminants Using Sulfate Radicals Activated by Mn_3O_4, Co_3O_4 and Fe_3O_4 Catalysts*, Proceeding for "Moving towards the New Chapter in Chemical Engineering amongst ASEAN Region", the 5th Regional Conference on Chemical Engineering, 7 – 8 February 2013, Pattaya, Thailand.

10. Sun, H., Saputra, E., Ang, H. M., Tadé, M. O., Wang, S., *Cobalt-exchanged natural zeolites (Australian and Indonesian) for catalytic oxidation of phenol solutions*, 17th International Zeolite Conference, July 7-12, 2013, Moscow, Russia.

11. Saputra, E., Muhammad, S., Sun, H., Ang, H. M., Tadé, M. O., Wang, S. *Green Catalytic Degradation of Aqueous Contaminants by Activated Carbon*, 5th International Symposium on Carbon for Catalysis, CARBOCAT-V, June 28-30, 2012, Brixten-Italy.

12. Muhammad, S., Saputra, E., Tade, M. O., Wang, S., *Phenol degradation in heterogeneous catalytic oxidation using Co-MCM48 and Co-Natural Zeolite Catalyst*, Proceeding of Water Congress, Busan-Korea, 2012.

13. Yao, Y., Peng, W., Sun, H., Saputra, E., Wang, S., *Synthesis and Catalytic Performance of Magnetic $CoFe_2O_4$-Graphene Hybrids*, *5th International Symposium on Carbon for Catalysis,* CARBOCAT-V, June 28-30, 2012, Brixten-Italy.

14. Saputra, E., Utama, P. S., Muhammad, S., Sun, H., Ang, H. M., Tadé, M. O., Wang, S., *Catalytic oxidation of toxic organic in aqueous solution for wastewater treatment : a review*, Proceeding of TIChE International Conference, Songkhla-Thailand, 2011.

15. Muhammad, S., Saputra, E., Tade, M. O., Wang, S., *Phenol degradation on heterogeneous catalytic oxidation by using Cobalt-Natural Zeolite Catalyst*, Proceeding of Annual International Conference Syiah Kuala University, Banda Aceh-Indonesia, 2011.

Content

Chapter 1 Introduction

1.1 Wastewater management

Worldwide attention to the problem of clean water is increasing day by day. This is because of the increasing need for clean water with the increase in population and economy[1]. The main concern in this case is not due to depletion of fresh water, but the damage done by industrial and human activities. Thus, fresh water is one of the most challenges for health, agriculture, energy and urbanization [2].

Water resources available today are not abundant as it seems before, because only a very limited amount of available water resources can be used without any treatment. Based on current estimation, the total volume of water in the Earth is about 1.4 billion cubic kilometers (km^3). However, almost 97.5% or 1.36 billion km^3 are saline water and only 2.5% is fresh water. Approximate 69% of the total fresh water are in the form of ice or snow found in Antarctica and in the mountainous regions. Only a small fraction at about 0.26% can be used for human purposes, which are located in lakes, reservoirs and rivers (**Figure 1.1**). Furthermore, the use of fresh water can be divided into three main activities, agriculture, industry and domestics. Agriculture is the biggest user at around 70% of the total fresh water, followed by industry at 25% and 5% by domestics [3]. In agriculture, water is used for irrigations to maximize food supply for humanity, so that the intensive development of irrigation can be found in almost every country [4]. While in industry, water is used for various purposes such as cooling, transport and cleaning, as solvents, as well as the raw materials for the

production of products. Thus agriculture and industry are major polluters of natural bodies of water [5].

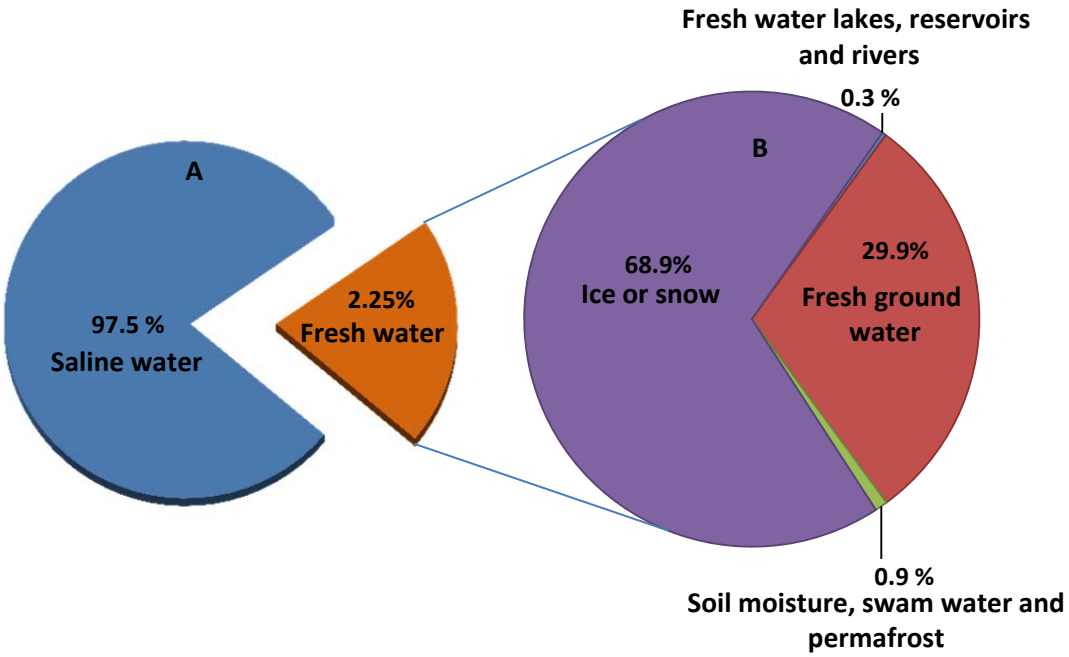

Figure 1.1 Total volume of water in the Earth. (A) total global water, (B) total global fresh water [5].

In most cases, the main contaminants originated from agriculture are pesticides (insecticides and herbicides) [6], while from the industry they are by-products of the activities [7]. Since only a small amount of water is available for human needs, therefore it is important to preserve water resources for future generations by the ways of not being discharged of pollutants into water bodies.

In order to manage environmental pollution, many countries have designed environmental regulations regarding the maximum threshold allowed for a variety of toxic organics that can be disposed of in the environment, for instance, 0.5 mg/L of phenol in water stream for Australia wastewaters [8, 9]. Thus, the environment can be protected and maintained properly. However, even with the strict regulations the water resources are still a major problem. Therefore, it is important to develop a

waste treatment technology that can destroy pollutants into non-toxic compounds or biodegradable end products.

In general, contaminants are categorized into two broad classes which are organic and inorganic. Some organic pollutants in water include a wide spectrum of chemicals such as pesticides, food processing wastes, volatile organic compounds (VOCs), dense non-aqueous phase liquid, petroleum hydrocarbon, detergents, dyes, acidity caused by industrial discharge, etc. [10]. As seen, there are so many different types of organic waste in wastewater, however one of the most important classes is phenol and derivatives due to their strong toxicity to many living organisms even at low concentrations [11]. These pollutants have been considered on the EPAs priority list since 1976 [12]. Phenol and its derivatives can be found from many industries as by-products such as petroleum refining, petrochemical, pharmaceutical, plastic and pesticide chemical industries, etc. [13, 14].

Phenol is a monohydroxy derivative of benzene, colourless, crystalline substance. The compound has a molecular formula of C_6H_5OH, and a molecular weight of 94.1 g/mol. The chemical structure of phenol can be seen in **Figure 1.2**. Phenol's solubility in water is variable between 0-65 ^oC, but it is highly soluble in most organic solvents [15]. Furthermore, colorless and easily soluble in water causes this compound difficult to detect in water that has been contaminated. Based on data from EPA the phenol wastes discharged into the environment has increased in 2000 and 2005 and was ranked 21 (**Table 1.1**) [16].

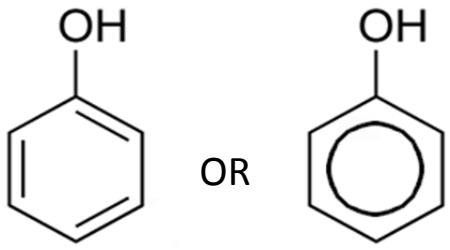

Figure 1.2 Phenol structure

Thus water pollution is a problem that continues to emerge from the industry and human activities despite being restricted by environmental regulations. For this reason, the phenol and derivatives are usually used as a model compound for studies of wastewater treatment, as in this study. Since, only a small amount of water available for human needs, therefore it is important to preserve water resources for future generations by way of advanced process in an appropriate manner before being discharged into water bodies. One of the promising methods for degradation of organic pollutants in wastewater is advanced oxidation process (AOP) being able to completely degrade organic compounds into simple compounds, CO_2 and H_2O. Advanced oxidation processes (AOPs) using chemicals as an oxidant is most suitable to degrade toxic organics in aqueous solutions such as phenol and derivatives due to lower operating costs, no need of special equipment, less energy consumption, and high conversion of organic pollutants.

Table 1.1 Annual release of toxic phenol-like pollutants in the USA [16].

Compound	Emission in 2000, ton.year^{-1}	Emission in 2005, ton.year^{-1}	Overall ranking
Phenol	21.3	45.8	21
2,4-dinitrophenol	10.6	0.20	143
Catechol	8.3	18.1	32
hydroquinone	1.9	4.9	66
Quinone	0.64	0.0	362
pentachlorophenol	0.31	0.24	134
p-cresol	0.18	0.12	157
Chlorophenol	0.045	0.025	192
2-nitrophenol	0.025	0.027	191
2,4,5-trichlorophenol	0.023	1.6	97
2,4-dichlorophenol	0.023	0.012	205
m-cresol	0.019	0.247	132
4-nitrophenol	0.007	0.212	139
o-cresol	0.006	0.056	177

1.2 Aim and scope of research

The main objective of the research is to synthesize different types of manganese-based catalyst for wastewater treatment. The catalysts will be used in heterogeneous catalytic oxidation to degrade phenol, a model organic pollutant in wastewater treatment. To achieve the goals of this research, several stages of research conducted with specific objectives are listed below.

1. To synthesize catalysts based on transition metal of Mn, on a support or without a support.
2. To investigate the activity and stability of the synthesised catalysts.
3. To investigate various processes with catalyst, oxidant in heterogeneous catalytic oxidation of organic compounds for wastewater treatment and to identify their synergistic effect.
4. To identify the parameters of organic pollutant degradation particularly the effects of catalyst amount, organic pollutant concentration, oxidant concentration, and temperature.
5. To determine the kinetic constant and activation energy of the catalytic reaction of phenol degradation in aqueous solution.

1.3 Thesis Organization

The thesis is divided into nine chapters, including introduction, literature review, results and discussion, conclusions and suggestions.

Chapter 1 — *Introduction* — presents an introduction consisting of the background of the research including several issues in water and wastewater. This chapter also presents Aim and Scope of Research with some specific objectives and organization of the thesis.

Chapter 2 — *Literature Review* — presents the theoretical view of the research based on the studies of other researchers particularly about the various oxidation techniques for the treatment of phenol in waste water and catalyst preparation and synthesis with a variety of methods.

Chapter 3 — *Catalytic Oxidation of Toxic Organics in Aqueous Solutions Using MnO_2 and Peroxymonosulfate. Catalysis Communications,* ***26*** *(2012) 144-148 and Environmental Science & Technology* ***47*** *(2013) 5882-5887* — describes the study of catalytic oxidation of phenol in aqueous solution using α-MnO_2 catalyst with different phase. The study shows that the α-MnO_2 catalysts have different activities in activation of peroxymonosulfate, which depend on structure and morphology. Crystalline structure of catalyst is more important than porous structure in influencing the activity of catalyst. In addition, this chapter also describes the study of the removal of phenol from aqueous solution in heterogeneous catalytic system using different crystallographic phase of MnO_2 (α-, β-, γ-MnO_2) as catalysts for environmentally benign process. The kinetic rate and activation energy of phenol oxidation are also presented.

Chapter *4* — *Manganese Oxides at Different Oxidation States for Heterogeneous Activation of Peroxymonosulfate for Phenol Degradation in Aqueous Solution. Applied Catalysis B: Environmental* ***142-143*** *(2013) 729-735* — describes the study of a series of manganese oxide with different oxidation states for phenol degradation using peroxymonosulfate. The study revealed that the reactivity of Mn oxide catalysts associated with the capacity of manganese to form various oxidation states (redox reaction and oxygen mobility) in the oxide lattice. The kinetic study of heterogeneous catalytic oxidation of phenol has also been presented in this chapter.

Chapter 5 — *Synthesis of Mn_3O_4, Co_3O_4 and Fe_3O_4 Nanoparticles and Their Catalytic Performances in Oxidation of Phenolic Contaminants in Aqueous Solutions. Journal of Colloid and Interface Science* ***407*** *(2013) 467-473* — describes the study of the removal of phenol from aqueous solution in heterogeneous catalytic systems using *Mn_3O_4, Co_3O_4 and Fe_3O_4* catalysts. The study revealed that *Mn_3O_4, Co_3O_4* are

effective catalysts for generating suphate radicals in the presence peroxymonosulfate. The kinetic rate and activation energy of phenol oxidation are also presented.

Chapter 6 — *Synthesis of α-Mn_2O_3@α-MnO_2 Core/Shell Nanocomposite and Catalytic Oxidation of Phenoloc Contaminats in Aqueous Solutions* — describes the study of a Core/Shell Nanocomposite catalyst for phenol degradation using peroxymonosulfate. The study shows that the catalyst has high activity for oxone activation in producing sulfate radicals for phenol degradation. The kinetic study of heterogeneous catalytic oxidation of phenol has also been presented in this chapter.

Chapter 7 — *Carbon Supported Manganese Catalysts for phenol degradation in aqueous solutions* — describes the study of the removal of phenol from aqueous solution in heterogeneous catalytic system using Mn/Carbon catalysts. This chapter investigated the utilization of carbon materials as a catalyst support for environmentally benign process. The kinetic rate and activation energy of phenol oxidation are also presented.

Chapter 8 — *Metal Free Catalytic Degradation of Aqueous Contaminants by Activated Carbon. RSC Advances (2013), in press and 5th international syposium on carbon for catalysis, CARBOCAT-V, 2012, Brixten-Italy* — describes the study of activated carbon catalysts for phenol degradation using peroxymonosulfate. The study revealed that activated carbon could activate PMS, which previously could only be achieved by metals ions, heat, and light. The kinetic study of heterogeneous catalytic oxidation of phenol has also been presented in this chapter.

Chapter 9 — Conclusions and recommendations for future work — this chapter presents the summary of the research results and some suggestions for further research in this area. A lot of challenging issues are addressed for development of heterogeneous catalytic oxidation technology.

Reference

1. Jackson, R.B., S.R. Carpenter, C.N. Dahm, D.M. McKnight, R.J. Naiman, S.L. Postel, and S.W. Running, *Water in a Changing World.* Ecological Applications, 2001. **11**(4): p. 1027-1045.

2. von Schirnding, Y., *Health and sustainable development: can we rise to the challenge?* The Lancet, 2002. **360**(9333): p. 632-637.

3. Abdel-Rahman, H.A. and I.M. Abdel-Magid, *Water Conservation in Oman.* Water International, 1993. **18**(2): p. 95-102.

4. Hanjra, M.A. and M.E. Qureshi, *Global water crisis and future food security in an era of climate change.* Food Policy, 2010. **35**(5): p. 365-377.

5. Shiklomanov, I., A., *World water resources: Anew appraisal and assessment for the 21st century.* UNESCO, 1998: p. 4.

6. Larson, S.J., P.D. Capel, D.A. Goolsby, S.D. Zaugg, and M.W. Sandstrom, *Relations between pesticide use and riverine flux in the Mississippi River basin.* Chemosphere, 1995. **31**(5): p. 3305-3321.

7. Vargas, M.-C. and N.E. Ramírez, *Phenol oxidation of petrol refinery wastewater catalyzed by laccase* CT&F - Ciencia, Tecnología y Futuro, 2002. **2**: p. 23-30.

8. Matheswaran, M. and I.S. Moon, *Influence parameters in the ozonation of phenol wastewater treatment using bubble column reactor under continuous circulation.* Journal of Industrial and Engineering Chemistry, 2009. **15**(3): p. 287-292.

9. M. Bosnic, J.B. and, and R.P. Daniels, *Pollutants in tannery effluents.* United Nations Industrial Development Organization 2000: p. 1-26.

10. Cheremisinoff, N.P., *Handbook of water and wastewater treatment technologies*. 2001, Butterworth-Heinemann: Oxford.

11. Dohnal, V. and D. Fenclova, *Air-water partitioning and aqueous solubility of phenols.* Journal of Chemical & Engineering Data, 1995. **40**(2): p. 478-483.

12. Keith, L. and W. Telliard, *ES&T Special Report: Priority pollutants: I-a perspective view.* Environmental Science & Technology, 1979. **13**(4): p. 416-423.

13. Fortuny, A., C. Bengoa, J. Font, and A. Fabregat, *Bimetallic catalysts for continuous catalytic wet air oxidation of phenol.* Journal of Hazardous Materials, 1999. **64**(2): p. 181-193.

14. Christoskova, S.G., M. Stoyanova, and M. Georgieva, *Low-temperature iron-modified cobalt oxide system: Part 2. Catalytic oxidation of phenol in aqueous phase.* Applied Catalysis A: General, 2001. **208**(1–2): p. 243-249.

15. Bruce, R.M., J. Santodonato, and M.W. Neal, *Summary review of the health effects associated with phenol.* Toxicology and Industrial Health, 1987. **3**(4): p. 535-568.

16. Vidal, E., S., Aguilera, E., C., *Coupled photochemical-biological system to treat biorecalcitrant wastewaters.* Doctor Dissertation, 2007. Department of Chemical Engineering, University of Barcelona, Marti i Franques.

Chapter 2

Literature Review

Abstract

Over the last decades, water treatment plays an important role in our lives, because of the fresh water crisis and the increasing awareness of health and human ecological systems as a result of industrial waste pollution. Industrial activities generate large amounts of hazardous substances which are discharged into the environment. It is important to dispose of wastewater in a proper way after treatment to comply with environmental regulations. The organics containing wastewater from chemical and related industries cannot be treated by conventional processes because degradation of these pollutants is often very slow or ineffective and not environmentally compatible. Therefore, various efficient wastewater treatment technologies have been developed as an alternative to the conventional processes to degrade wastes into non-toxic or biodegradable end products. This chapter will focus on the evaluation of water treatment technologies that have been proven effective in removal of organic compounds into simple compounds, CO_2 and H_2O. In this chapter, we will also explain the advantages and limitations of the technologies for degradation of organics. In addition, some conventional processes and recent advances in the preparation and synthesis of solid catalysts will be reviewed. Finally, a short summary will be given in the last section.

2.1 Introduction

One of the greatest challenges in the twenty-first century is the shortage of fresh water supply for millions of living beings around the world. The main concern in this case is not due to the depletion of the fresh water but the damage done by industrial and human activities. Wastewater from various industrial processes and households contains many organic compounds. Most of the organic compounds are toxic to the environment and human beings. One of the most important classes of water pollutants is phenol and its derivatives due to their strong toxicity to many living organisms even at low concentrations [1]. These pollutants have been considered on the EPAs priority list since 1976 [2]. Phenol and its derivatives can be found from many industries as by products such as petroleum refining, petrochemical, pharmaceutical, plastic and pesticide chemical industries [3, 4]. In many countries, the maximum threshold allowed for phenol in water streams is less than 1 mg/L, for instance 0.5 mg/L for Australia wastewaters [5, 6]. Therefore, the wastewaters have to be treated before discharged into the environment in order to comply with environmental regulations.

Among the variety of physical, and biological technologies for water treatment, each has inherent limitation in applicability, effectiveness and cost [7]. Physical processes, such as adsorption, only transfer of pollutants from the liquid to the solid phase, but the pollutants are still present and not degraded to organic compounds which are less toxic [8, 9]. Furthermore, the biological processes are very sensitive to the process conditions, and also generate large amounts of sludge that may require further treatment and disposal. In addition, some organic compounds can be a severe problem in the biological treatment system because of their resistance to biodegradation and/or toxic effects on microbial processes [10, 11].

Some well-known water treatment technologies, such as wet air oxidation, supercritical water oxidation, catalytic wet air oxidation, have been widely used for toxic organic degradation in industrial wastewater. These technologies are viable for highly concentrated effluents (COD concentration > 40,000 mg/L), however they are limited by the solubility of oxygen in water and high operation cost [12, 13]. Other

technologies of AOPs (Advanced oxidation processes), such as cavitation, photocatalytic oxidation, Fenton chemical oxidation, can be operated at ambient conditions and have potentially either partially or fully degrade the toxic organics, bio-refractory compounds, and pesticides etc. [14-16].

AOPs are based on the generation of reactive species (hydroxyl radicals, $OH^{\bullet}$), that have an oxidation potential of 2.33 V and exhibit faster of oxidation compared with conventional oxidants such as potassium permanganate. Hydroxyl radicals can react with most organics and inorganics into simple compounds, CO_2 and H_2O. Chemical oxidation processes constitute the use of oxidizing agents, such as hydrogen peroxide and ozone, for generating hydroxyl radical. Hydrogen peroxide (H_2O_2) is a more powerful oxidant compared to ozone and its application in the treatment of various inorganic and organic pollutants is well established. However, the use of individual oxidant is not efficient in oxidizing more complex and recalcitrant materials due to mass transfer resistance between the pollutant and the oxidizing agents. Improvements can be achieved by using transition metal salts (homogeneous catalysts) or energy that can activate H_2O_2 to form hydroxyl radicals. Apart from hydroxyl radicals, sulphate radicals have also been recently suggested as an alternative due to their higher oxidation potential.

Homogeneous catalysts are commonly more efficient compared to solid or heterogeneous catalysts because every single catalytic entity can act as a single active site. This characteristic makes the catalyst intrinsically more active and selective [17]. However, recovery needs further process for separation of the homogeneous catalyst. Moreover, most of the dissolved metal catalysts are harmful to the environment. This disadvantage can be overcome by using heterogeneous catalysts, in which the catalysts will be easily recoverable and reusable [18]. Because of these advantages, many researchers focus on the study of solid catalysts as well as on the improvement of existing and development of new catalysts [19-21].

Catalysis is a well-established scientific discipline, dealing not only fundamental principles or mechanism of catalytic reactions but also with preparation, synthesis and modification of various catalysts [22]. Up to now, catalysts have been played a

key role in the production of chemicals and materials. It can be seen from the fact that more than 80% of today's large-scale chemical processes, such as chemical, petrochemical and biochemical industries, as well as in the production of polymers and in environmental protection, depend on catalysts [19, 23]. In development of new catalysts, preparation, synthesis, and modification processes can influence of physical and chemical properties of catalysts in particle size, surface area, phase, catalytic activities, and thermal durability etc. [24].

Thus, wastewater treatment has many facets that need to be attended to in order to cleanse the wastewater as pure as possible. Therefore, it is necessary to select the proper process which can increase the effectiveness and efficiency of toxic organic degradation and should be economical.

2.2 Wet Air Oxidation

Wet Air Oxidation (WAO) is the most successful technology which has been studied and applied in wastewater treatment. WAO is a hydrothermal treatment which is used to treat the organic toxic and non-biodegradable wastes either too dilute to be incinerated and too concentrated for biological treatment. The WAO technique was first patented in 1991 by Strehlener for the treatment of sulphite liquor. However, WAO technology was first successfully applied in industry in the late 1950s by Borregaard for the treatment of sulphite liquor [25]. WAO, involving oxidation at high temperature (125 - 320^{o}C), pressure (0.5-20 MPa), which use either air or pure oxygen as a source of oxidants [25-27]. For achieving the optimum results, WAO is preferred at chemical oxygen demand (COD) ranges between 20,000 and 200,000 mg/L[28]. During the oxidation process, the toxic organics which have high molecular compound, are converted to simple molecular compounds including carboxylic acids, acetaldehydes, alcohols, water and carbon dioxide during the oxidation process [26, 29]. If the toxic organics contain emission such as NO_x, SO_2, chlorine, dioxin and furans, then these emissions are usually reacted toNH_3, PO_4^{3-}, Cl^-, SO_4^{2-} ,respectively [30].

Based on mechanic reaction, the overall WAO system includes two steps. One is chemical reaction between organic compounds and dissolved oxygen in the liquid phase. Typically, the reaction mechanism follows the combination of two reactions occurring simultaneously [26, 27, 31].

1. First step, direct oxidation of organic compounds to end product

$$R - H + O_2 \xrightarrow{k_1} x\,CO_2 \quad (2.1)$$

2. Another oxidation of organic compounds with the formation of intermediates product of group of carboxylic acid

$$R - H + O_2 \xrightarrow{k_2} y\,H_2C_2O_4 \xrightarrow{k_3} z\,CO_2 \quad (2.2)$$

The global kinetic expression based on two reaction schemes above is shown below.

$$\frac{(R - H + H_2C_2O_4)}{(R - H + H_2C_2O_4)_0} = \frac{k_2}{k_1 + k_2 - k_3} e^{-k_3 t} + \frac{k_1 - k_3}{k_1 + k_2 - k_3} e^{-(k_3 + k_2)t} \quad (2.3)$$

The sequence of reaction steps based on free radical reaction could be divided into three steps, which are initial, propagation, termination reactions. The first step is initiation in which free radicals are produced by the bimolecular reaction of oxygen with the organic compounds. Another reaction is propagated by the further reactions of other organic, inorganic radicals and oxygen, as shown below [32].

Initiation reaction; $R - H + O_2 \rightarrow R^{\bullet} + HO_2^{\bullet}$ (2.4)

Propagation reaction; $R^{\bullet} + O_2 \rightarrow ROO^{\bullet}$ (2.5)

$R - H + ROO^{\bullet} \rightarrow ROOH^{\bullet} + R^{\bullet}$ (2.6)

Termination reaction; $2\,ROO^{\bullet} \rightarrow ROOR^{\bullet} + O_2$ (2.7)

The other one is a physical step which is mass transfer of oxygen from the gas phase to the liquid and the mass transfer of carbon dioxide from the liquid to the gas. In general, the gases diffuse rapidly into gas phase. Therefore, the only significant influence is mass transfer of oxygen which is located at gas-liquid phase. The equation rate of mass transfer of a component between gas-liquid phase can be seen below [33, 34].

$$r_{t,i} = k_l a_i \left(\frac{Y_i \Phi_i P}{\gamma_i FP_i H_{i/w}} - X_i \right) \quad (2.8)$$

$$p\ v = H\ (x)(\Phi) \quad (2.9)$$

In some cases, the WAO technology could achieve 99+% conversion of toxic organics. For example, in the cases of oxidation of phenol almost 100% waste can be removed [28], however this technique cannot degrade wastewater completely into water and carbon dioxide. Therefore, the WAO often requires additional treatment process in order to achieve complete removal of toxic organics e.g. biological process is often used for final treatment. The basic treatment system of a WAO plant can be seen in **Figure 2.1**, which consists of a high pressure feed pump, an air compressor, a heat exchanger, a reactor and a separator. The reactor is usually a co-current bubble column reactor with or without internal baffling, which has a geometry ratio of a height-to-diameter in the range of 5-20 [35, 36].

The waste is pumped by a high pressure feed pump to the reactor continuously through a heat exchanger. The oxygen for oxidation is given by an air compressor and is combined with the waste in the mixing point. Further, the mix effluents pass through a heat exchanger where the fluid is heated to near reaction temperatures. After heating, the fluid flows to the lower section of reactor where the exothermic reaction takes place. The common residence time of the fluid in the reactor is 20 to 240 minutes [29]. The usual oxygen flow rate is less than 110% of the inlet COD flow rate [37]. After reaction, the effluent then passes through a vertical column separator for separating of the liquid and gas. Typically, the WAO unit is combined with conventional biological facilities where a post-treatment is carried out before returning into the environment.

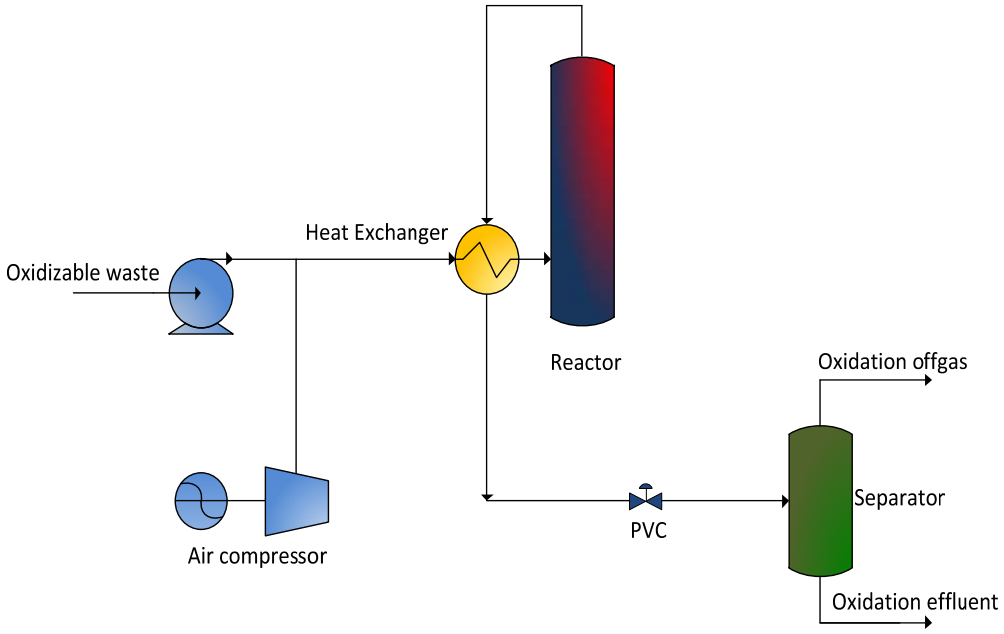

Figure 2.1 Basic Wet Air Oxidation (WAO) process flow sheet

The WAO waste treatment has wide range application spectrum, therefore more than 200 WAO treatment plants have been installed around the world. Wastewater including sludge waste, petrochemical waste, textile waste, petroleum refining waste, spent caustic wastewaters containing phenolic compounds can be treated using WAO. The results of wet air oxidation of various pollutants in industrial wastewater are summarized in **Table 2.1**.

The major drawbacks of WAO are the high capital costs of the process which are almost entirely used for power to compress air and high pressure liquid pumping. WAO becomes economical when the concentration of oxidant material in the range 1-20 % by weight with water because the sufficient materials reach with oxygen to generate sufficient heat to keep the desired operation conditions in the reactor without external energy source [38].

Table 2.1 Wet air oxidation of organic compounds

Compounds	Treatment conditions	Removal	Refs.
Polyethylene glycols	T = 110-240 ^{o}C, P = 2-3 MPa	TOC, 80% (240 ^{o}C, 2 Mpa, 240 min) COD, 77% (240 ^{o}C, 2 Mpa, 120 min)	[39]
Alkylbenzene sulfonate	T = 200-240 ^{o}C P = 1.5 MPa	TOC, 60% (240 ^{o}C, 120 min) COD, 70% (240 ^{o}C, 120 min)	[40]
m-xylene	T = 225-240 ^{o}C P = 6.89-10.3 MPa	m-xylene > 99% (240 ^{o}C, 10.3 MPa, 66 min)	[41]
Lubricating oil	T = 200-350 ^{o}C P = 14-20 MPa	Greases, 99.5% (200 ^{o}C, 20 MPa, 40 min) COD, 91.1% (200 ^{o}C, 20 MPa, 40 min)	[42]
Cyanide	T = 225-250 ^{o}C P = 2-15 MPa	Cyanide, 99.99% (230 ^{o}C, 4 MPa, 120 min)	[43]
Fuel-oil	T = 200-350 ^{o}C P = 20 MPa	Oil, 99.9% (350 oC, 20 Mpa, 40 min) COD, 87.5% (200 ^{o}C, 20 MPa, 40 min)	[42]
Ammonium thiocyanate	T = 225-250 ^{o}C P = 2-15 MPa	liquor, 98% (230 ^{o}C, 43MPa)	[40]
Methyl alcohol, ethyl alcohol, diethyl malonate	T = 220 ^{o}C P = 3 MPa	TOC, 30-38% (120 min); COD, 29-38 (120 min)	[44]
Formaldehyde, dioxane	T = 220 ^{o}C P = 3 MPa	TOC, 43-54% (120 min); COD, 58-61 (120 min)	[44]
Black liquor	T = 187-227 ^{o}C	TOD, 93% (227 ^{o}C, 213 min)	[45]
Phenol	T = 150-180 ^{o}C P = 0.3-1.15 MPa	Phenol, 99.9%; COD > 90	[36]
Bleaching earth	T = 140-200 ^{o}C P = 0.1-0.5 MPa	Bleaching earth, 99.9% (200 ^{o}C, 0.5 MPa, 120 min)	[46]
Propionic acid	T = 150-315 ^{o}C P = 7-13 MPa	Propionic acid, 95% (260 ^{o}C, 3.5 MPa)	[47]
Azo dye Orange II	T = 130-190 ^{o}C P = 0.5-1.5 MPa	Azo dye Orange II, 100% (190 ^{o}C, 1 MPa, 60 min)	[48]
Tetrachloroethylen	T = 225-275 ^{o}C P = 13.8-17.2 MPa	Tetrachloroethylen, 90% (275^{o}C, 13.8 MPa, 95ks)	[41]
PEG	T = 110-240 ^{o}C P = 2-3 MPa	TOC, 55% (240 ^{o}C, 60 min)	[49]
2,4-dinitro-toluen	T = 275-320 ^{o}C	2,4-dinitro-toluen, 99.74% (275 ^{o}C)	[50]
Monoazo dye Orange II, $C_{16}H_{11}N_2NaO_4S$	T = 180-240 ^{o}C P = 1 MPa	TOC, 70% (230 ^{o}C, 90 min)	[51]
Basilen Brilliant Blue P-3R	T = 200 ^{o}C P = 3.3 MPa	TOC, 20% (120 min); COD, 35% (120 min)	[52]
Acenaptene	T = 275-320 ^{o}C	Acenaptene, 99.99% (275 ^{o}C)	[50]
Acrolein	T = 275-320 ^{o}C	Acrolein, 99,05% (275 ^{o}C)	[50]
Acrylonitrile	T = 275-320 oC	Acrylonitrile, 99% (275 ^{o}C)	[50]
Tert-butyl alcohol	T = 220 ^{o}C, P = 3 MPa	TOC, 915 (120 min) COD, 83% (120 min)	[44]

2.3 Supercritical Water Oxidation

Supercritical Water Oxidation (SCWO) is a technology that takes advantage of the special properties of supercritical condition of water with the temperature and pressure above critical point ($T_c > 374$ ℃, $P_c > 22.1$ MPa). In this region (**Figure 2.2**), the values of density, dielectric constant and ionic of water decrease, consequently, the solubility of gases and organic compounds become dramatically increased while inorganic compounds become nearly insoluble [53, 54]. During the SCWO process, the organic compounds will react with an oxidant, mostly O_2, and produces a simple compound. In the single-phase reaction, carbon dioxide and water is a final product from SCWO process. The hetero-atoms such as sulphur, chlorine or phosphorus are transformed into the mineral acids, HCl, H_2SO_4, or H_3PO_4. When organic waste contains nitrogen, it will convert to molecular nitrogen (N_2). Meanwhile, for incomplete reaction, it leads to the formation of nitrous oxide (N_2O), ammonia (NH_3), nitrogen dioxide (NO_2), nitric acid (HNO_3) and hydrazine (N_2H_4) [54, 55].

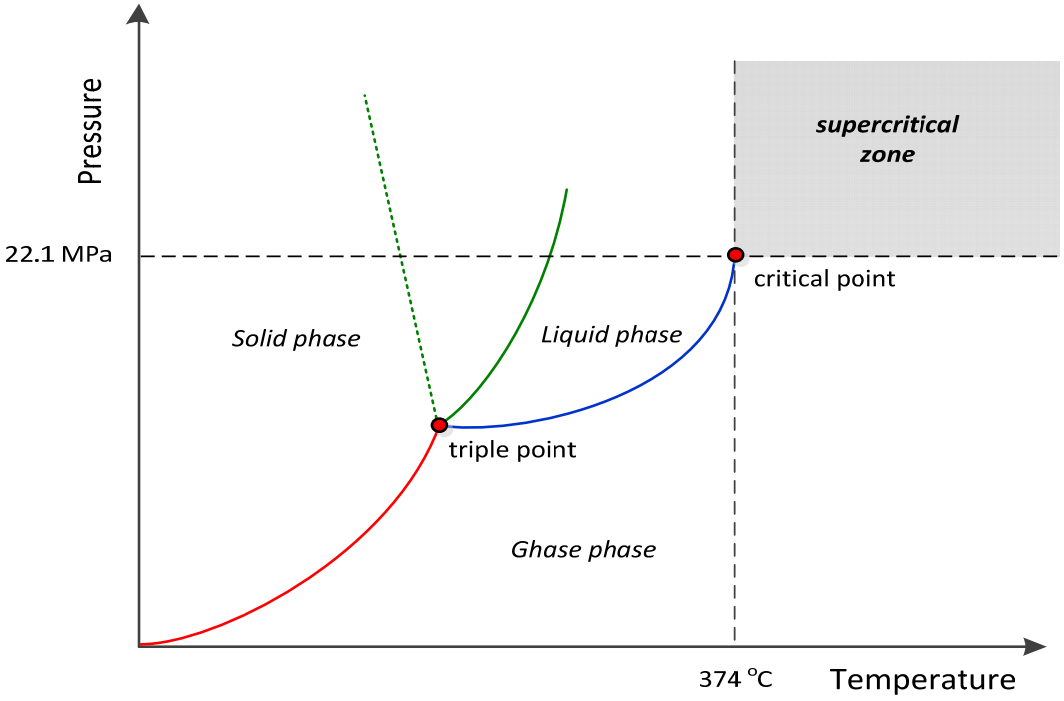

Figure 2.2 Phase diagram of water [56]

Typical process conditions of SCWO are at a temperature of 500-700 ^{o}C and a pressure of 24-50 MPa. Commonly, the rate of reaction for complete removal occurs several minutes only or less [53, 54, 57]. Further, the effluent of SCWO can be discharged into the water body without requires additional treatment process. The SCWO technology for wet oxidation of organic substances was first patented in late 1970 and research on SCWO has been growing rapidly in 1980s [58, 59]. Currently, there are many SCWO technologies that have been set up around the world and this technology has been successfully applied for removing of a wide variety of organic wastes. Some applications involving the SCWO includes sludge, dyes, sewage, fuels as solvent, cutting and/or contaminated oils, soils, ground water, polycyclic aromatic hydrocarbons, chloride hydrocarbons, PCBs, paint, oil, wastewater from chemical, petroleum waste, pulp and paper, textile, medical waste, chemical warfare agents, waste from solid rocket propellants, human waste, recycle of vital materials in space application and ship board hazardous materials [38, 60-77].

The basic treatment system of a SCWO plant is shown in **Figure 2.3**. The aqueous contaminant is pumped through feed heater by a high pressure pump that can deliver the feed between 24 and 50 MPa. Further, the contaminant is combined with pressurised O_2 and then heated to the reactor temperature condition. After heating, the fluid flows to the top section of the reactor where the exothermic reaction takes place. After reaction in the reactor, the outlet stream is cooled down by exchanging heat in the feed heater and the heat recovery, and then the fluid flows to the vertical separator through the pressure release valve. Two streams are obtained in the gas separator which is CO_2, unreacted O_2 and N_2.

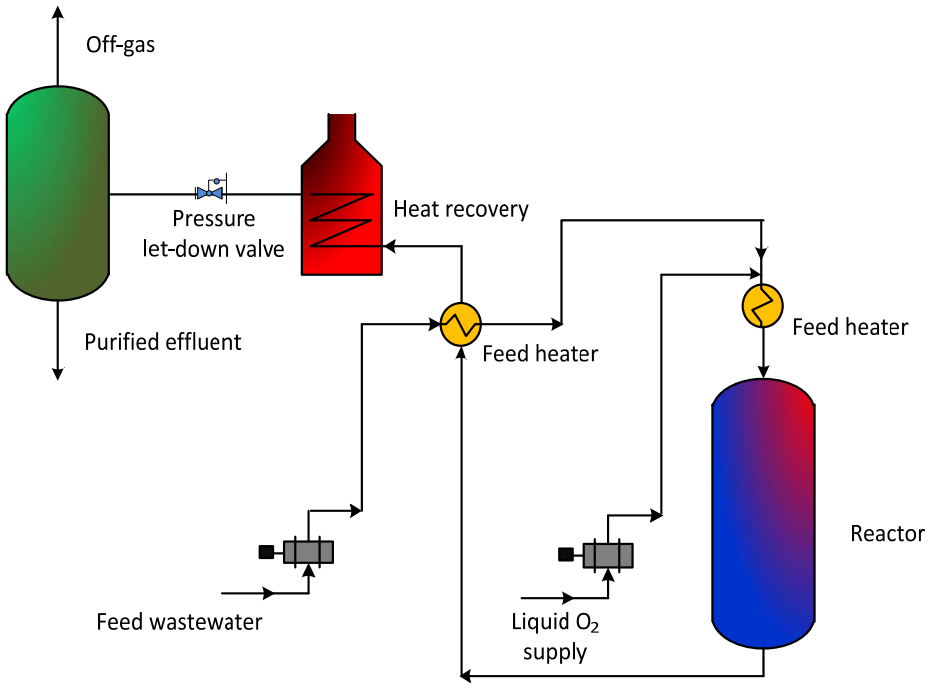

Figure 2.3 Basic flow diagram Supercritical Water Oxidation (SCWO) [78]

In case of SCWO, the rate of reaction is complex even for simple molecules. According to Kruse and Dinjus [79] for investigating the rate of reaction in supercritical conditions, physicochemical and transport properties have significant roles which could affect reaction. These properties are miscibility, dielectric constant, ionic product, diffusion, viscosity, collision frequencies, dipole moment, and hydrogen bonds. When the reaction occurs, all of properties of reactant as mentioned above will affect the reaction. Although, the rate of reaction is not simple, for engineering purpose, it is often sufficient to develop a global rate of reaction models to express the reduction of organic compounds waste in SCWO [80-83]. The following **Table 2.2** provides a summary showing that the global rate of reaction is the simple and suitable model for studying rate of degradation of almost all types of pollutants.

Table 2.2 Reaction rate models of various pollutants in SCWO system

Pollutants	Treatment conditions	Removal	Rate of reaction model	Refs.
Municipal solid waste	T = 400-550 ^{o}C, P = 28 MPa	Dog food, 99.99+ % (550 ^{o}C, 30 min)	First-order kinetic, R^2 = 0.999)	[83]
Municipal sewage sludge	T = 400-500 ^{o}C P = 30 MPa	Sewage sludge, 99.99+ % (500 ^{o}C, 1 min)	First-order kinetic, R^2 = 0.965	[84]
Alcohol distillery	T = 400-500 oC P = 30 MPa	Alcohol distillery, 99.99+ % (500 ^{o}C, 1 min)	First-order kinetic, R^2 = 0.975	[84]
Phenol	T = 300-500 ^{o}C P = 25 MPa	Phenol, 82.9 % (300 ^{o}C, 67.7 s)	Pseudo-first order kinetic, R^2 = 0.979	[85]
Pyridine	T = 426-525 ^{o}C, P = 27.6 MPa	Pyridine, 95 % (523 ^{o}C, 6.57 s)	First-order kinetic, R^2 = 95	[86]
Olive oil mill	T = 380-500 ^{o}C P = 25 MPa	COD, 99.9 % (500 ^{o}C, 1 min)	First-order kinetic	[87]
LCD manufacturing wastewater	T = 396-615 ^{o}C P = 25-29 MPa	COD, 99.99 % (615 ^{o}C, 10 s)	First-order kinetic, R^2 = 95	[88]
Oily wastwater	T = 380-430 ^{o}C P = 22.5-40 MPa	COD, 97.7 % (430 ^{o}C, 40 MPa, 150 s)	First-order kinetic, R^2 = 0.9857	[89]
Oily sludge	T = 390-450 ^{o}C P = 23-27 MPa	COD, 92 % (450 ^{o}C, 25 MPa, 10 min)	Zero-order kinetic, R^2 = 95	[90]
Aroclor 1248	T = 450-550 ^{o}C P = 25.3 MPa	Aroclor 1248, 99.95 % (550 ^{o}C, 54,4 s)	Second-order kinetic	[91]
Dyehouse	T = 400-600 ^{o}C P = 25 MPa	TOC, 100 % (550 ^{o}C, 10 s)	First-order kinetic, R^2 = 95	[62]
Orange 25	T = 400-600 ^{o}C P = 25 MPa	TOC, 98,5 % (550 ^{o}C, 6.1 s)	First-order kinetic, R^2 = 95	[72]
2-Chlorophenol	T = 300-420 ^{o}C P = 19-30 MPa	2-Chlorophenol, 99% (380 oC, 28.17 MPa, 58.6 s)	First-order kinetic, R^2 = 95	[82]
O-cresol	T = 350-500 ^{o}C P = 25.3 MPa	O-cresol, 98.3 % (499.7 ^{o}C, 25.3 MPa, 4.3 s)	First-order kinetic, 95% confidence interval	[92]
Aliphatic nitro methane	T = 390-430 ^{o}C P = 22.5-32.5 MPa	nitro methane, 99.3 % (391 ^{o}C, 27.5 MPa, 490 s)	First-order kinetic	[93]
Aliphatic nitro ethane	T = 390-430 ^{o}C P = 22.5-32.5 MPa	nitro methane, 75.34 % (391 ^{o}C, 27.5 MPa, 290 s)	First-order kinetic	[93]
Aliphatic nitro propane	T = 390-430 ^{o}C P = 22.5-32.5 MPa	nitro methane, 50.34 % (391 ^{o}C, 27.5 MPa, 160 s)	First-order kinetic	[93]
2,4-Dichlorophenol	T = 380-420 ^{o}C P = 23-28 MPa	2,4-Dichlorophenol, 99.99 % (420 ^{o}C, 23 MPa, 90 s)	First-order kinetic, 95% confidence interval	[80]

Compared with WAO and incineration technology, the installing cost of SCWO is approximately 15% and 10% less than WAO and incineration. In this comparison, the initial concentration of effluent was 50000 ppm and the water flow rate was 10 gpm. For the operating cost, SCWO system is approximately more than 50% less expensive

than incineration [94]. This indicates that SCWO treatment is better alternatives for wastewater treatment. The comparison of costs is shown in **Table 2.3**.

Table 2.3 Comparison of installed and operating cost for alternative treatment technologies [94].

Method of treatment	Total Cost, $ million	Operating Cost, $/gal
Catalytic supercritical water oxidation (air as the oxidant)	1.65	0.09-0.4
Incineration	1.92	0.26-1.17
Supercritical water oxidation (air as the oxidant)	2.01	0.18-0.46
Wet air oxidation (oxygen as the oxidant)	2.35	n/a
Fluidized bed thermal oxidation	6.35	n/a

2.4 Catalytic Wet Air Oxidation

Catalytic Wet Air Oxidation (CWAO) technology is a further development of Wet Air Oxidation (WAO) process to achieve "Zero Discharge". The use of a catalyst in CWAO, the Zero Discharge is possible to reach because the intermediate products, such as acetate acid and ammonia are very difficult to convert in the absence of a catalyst, but they could be react under a catalyst into CO_2 and H_2O [95]. Compared with WAO, CWAO has several advantages, low energy requirements, reduced gas emission, low operating condition and low footprint requirements [96]. The first development of CWAO to commercial application was started by DuPont in the mid-fifties in the United State. The process used a heterogeneous system with Mn-Zn-Cr as a catalyst at temperatures in the range of 120-200 ^{o}C [97]. While, in Japan, CWAO technologies have been developed since mid-eighties using precious metals deposited either on titania or titania-zirconia [98]. Typical process conditions of CWAO are at a temperature of 80-180 ^{o}C and a pressure of 1-5 MPa [99].

The basic flow diagram of a CWAO plant can be seen in **Figure 2.4.** As can be seen, CWAO technology consists mainly of a fixed bed column reactor, a high pressure pump, an air compressor, a heat-exchanger and a gas/liquid separator. CWAO uses air as an oxidant, which is mixed with the aqueous contaminants and passed over a catalyst at required temperature and pressure. The effluent from outlet reactor was cooled through heat exchanger. A high pressure separator was used to separate two-

phase mixture into gas and liquid phase. The off gas as top outlet separator was passed to chimney. A catalytic unit for the treatment of the off gas is also typically necessary. CWAO technology is particularly cost-effective for effluents that are highly concentrated having a range COD of 10,000 to 100,000 mg/L [100, 101] . The type of a reactor is commonly a trickle bed reactor suitable for CWAO because this reactor will provide a plug flow pattern and high liquid-solid interfacial area improving the effectiveness of mass transfer and reaction [102].

The catalytic agents that have been employed in CWAO can be classified into three classes: metal, metal oxides and metal salts. Metal salts and their complexes, which are well known as homogeneous catalytic oxidation, are commonly more efficient compared to that of solid catalysts or heterogeneous catalytic oxidation. However, recovery needs a more process for separation of the catalyst [103]. Moreover, most of the dissolved metal catalysts are harmful to the environment. This disadvantage can be overcome by using heterogeneous catalysts, in which the catalysts will be easily recoverable and reusable [104, 105]. Nevertheless, heterogeneous catalysts have several crucial issues related to chemical and physical stability of catalysts in terms of leaching, loss of surface area of the support and catalyst deactivation.

Several characteristics of the catalyst for water-phase oxidation which have to be met in order to be applied in industry are [106];

1. Exhibiting high oxidation rate or activity; in many cases, the reaction is diffusion limited and under such condition the rate should be enhanced by better contact between the phases.
2. Resistance for poisoning and stability in prolonged use at elevated temperature.
3. Mechanical stability and resistance to attrition.
4. Non-selectivity in most cases.
5. Physical and chemical stability in various conditions.

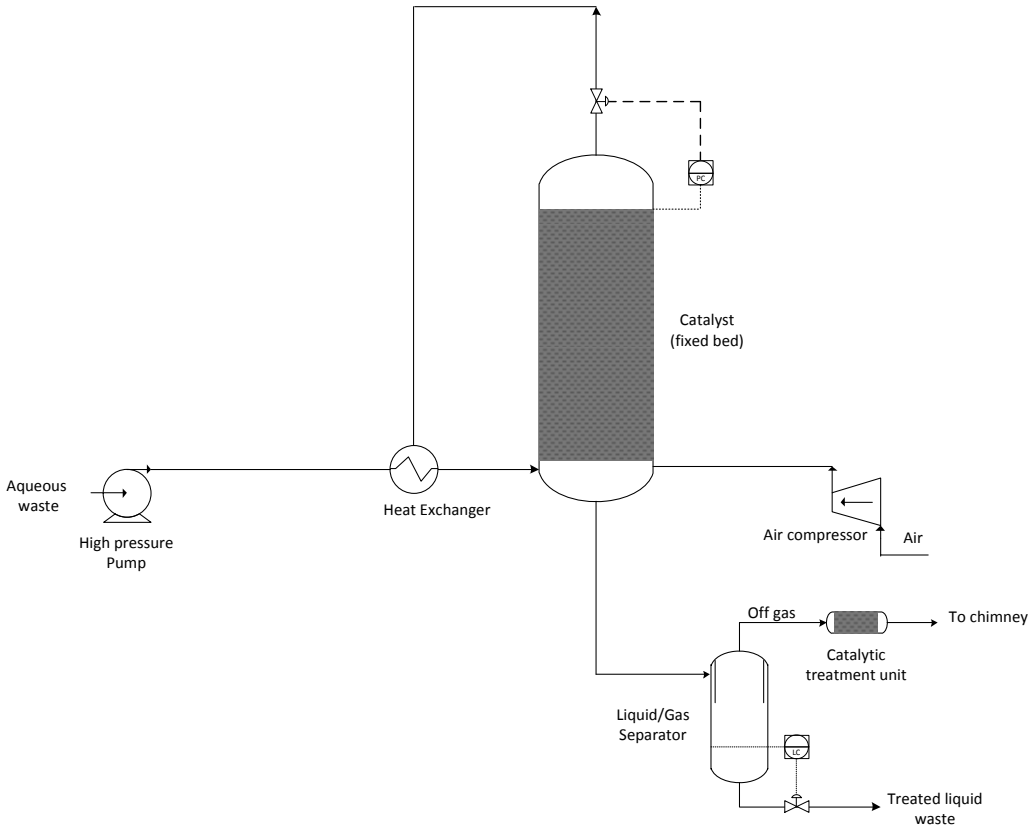

Figure 2.4 Basic flow diagram of Catalytic Wet Air Oxidation (CWAO) [95]

In the heterogeneous catalytic reaction, commonly several steps will determine rate of degradation reaction, the overall process can be decomposed into seven independent steps [107-109]:

1. Film diffusion or interphase diffusion.
2. Pore diffusion or intraparticle diffusion.
3. Adsorption of a least one of the reactants.
4. Reaction in the adsorbed phase.
5. Desorption of the product(s).
6. Intraparticle diffusion.
7. Diffusion of the products through the external boundary layer into the bulk fluid phase.

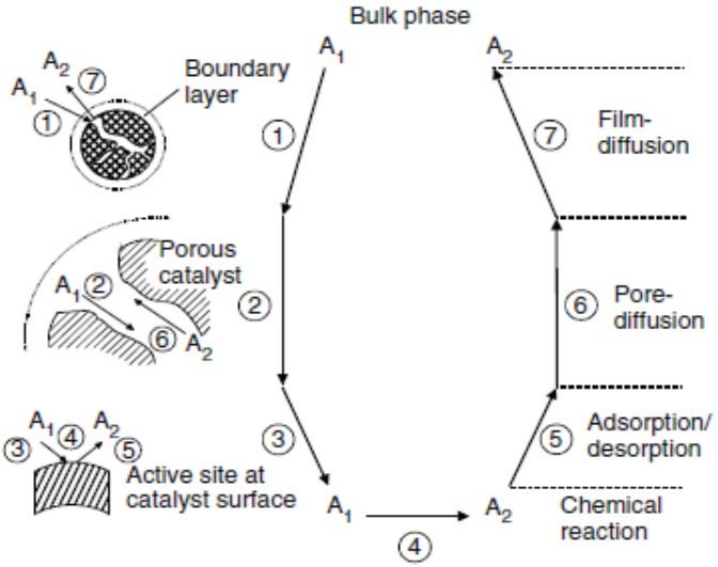

Figure 2.5 Steps in heterogeneous catalytic reaction [109]

In Adsorption, surface reactions, as well as desorption are sequential steps, these constitute the chemical transformation. Interphase and intraparticle diffusion also occur in a serial manner. The net kinetics for overall reaction from steps 1 to 7 is usually called effective kinetics. In the most of catalytic reaction, the rate of reaction is highly relying on the molecular transport (steps 1-3) rather than the reaction itself [109]. Therefore, intensive research is needed on the development and engineering of catalysts.

The heterogeneous catalyst that have been employed in CWAO technique can be divided in three main group which are supported noble metals, metal oxides, and active carbon without any deposited active phase. Pd, Pt, Ir, Rh and Ru are noble metals which have been effective in the treatment of different pollutants such as phenol, substitute phenol, carboxylic acid, Kraft bleaching effluents and olive oil mill wastewater [110-114]. Among the noble metals catalyst used for the CWAO of phenol, Ru is one the most active catalyst based on the removal of phenol and TOC conversion [115]. Although noble metals show excellent catalytic activities, the major drawbacks of these metals are expensive and vulnerable to poisoning by halogen-, sulphur-, and phosphorus-containing compounds, affecting tremendously the economics of corresponding processes [116]. Studies on the CWAO of phenol using

noble metal catalysts are listed in **Table 2.4**. The activity order of CeO_2 supported noble metals for CWAO of phenol as shown below [113].

$$Ru/CeO_2 > Pd/CeO_2 > Pt/CeO_2$$

Table 2.4 Summary of CWAO of phenol over noble metal catalysts [116].

Nobel Metal	Support	Reactor	T (^oC)	P MPa
Ru	TiO_2	Fixed-bed reactor	55-250	0-1.0
Ru	ZrO_2, graphite, AC	Stirred-tank reactor	140	2.0
Ru, Pd, Pt	CeO_2	Stirred-tank reactor	120-230	-
Pt	CeO_2, Ce_xZr_{1-x}	Stirred-tank reactor	160	2.0
Pt, Pt-Ce	γ -Al_2O_3	Stirred-tank reactor	155-200	5.05
Pt, Pd, Ru	CNF	Fixed-bed reactor	180-240	1.0
Pt	Graphite, TiO_2, Al_2O_3 AC	Stirred-tank reactor	120-170	1.7
Ru-CeO_2	γ -Al_2O_3	Fixed-bed reactor	155-200	5.05
Ru, Ru-CeO_2	C	Stirred-tank reactor	160	2.0
Ru	CeO_2, ZrO_2- CeO_2	Fixed-bed reactor	140	4

The other broad family of catalysts used in CWAO is the pure or mixed metal oxides. Metal oxide catalysts are mainly one or several of Cu, Mn, Co, Cr, V, Ti, Ni, Bi, Zn and other metals. These metals can be classified according their physico-chemical properties. The most stable oxides in the high oxidation state ($\Delta H^{\circ}_{298} > 15.5 \frac{kJ}{mol}$ of O) are of metals such as Ti, V, Cr, Mn, Zn and Al. The second is the group which have intermediate stability of high oxidation state oxides ($\Delta H^{\circ}_{298} = 9.5 - 15.5 \frac{kJ}{mol}$ of O) which are Fe, Co, Ni, and Pb. In terms of electrical conductivity, metals oxides can be divided into three groups which are n-type metal oxides, p-type metal oxides and insulator. Among them the p-type metal oxides have the highest activity for catalytic oxidation due to the electron deficient lattice. The n-type and insulator have low electron mobility, and therefore their catalytic activity is generally poor [117]. Catalytic activity of metal oxide catalysts during phenol oxidation shows the following order [118].

$$CuO > CoO > Cr_2O_3 > NiO > MnO_2 > Fe_3O_3 > YO_2 > Cd_2O_3 > ZnO > TiO_2 > Bi_2O_3$$

Studies on the CWAO of phenol over various metal oxide catalysts are summarized in **Table 2.5**.

Table 2.5 Summary of studies on CWAO of phenol over metal oxides catalysts [116].

Nobel Metal	Support	Reactor	T (^{o}C)	P MPa
Cu, Ni, Co, Fe, Mn	γ-Al_2O_3	Stirred-tank reactor	150	5.05
1-25 wt% CuO	γ -Al_2O_3	Stirred-tank reactor	150	5.05
Cu, Ni, Co, Fe, Mn	$Ce_{0.65}Zr_{0.35}O_2$	Stirred-tank reactor	150	5.05
$CuCeO_x$	-	Stirred-tank reactor	150	0.73
Cu	MCM-41	Stirred-tank reactor	150	2.0
CeO_2	-	Stirred-tank reactor	95-180	0.5-1.0
CeO_2	γ -Al_2O_3, SiO_2, TiO_2, CeO_2, $AlPO_4$-5	Stirred-tank reactor	140-180	1.5
CeO_2	γ -Al_2O_3	Stirred-tank reactor	180	0.5-2.0
Cu, Mn, Co, Cr, Fe, Mo, Ni	γ -Al_2O_3, CeO_2	Stirred-tank reactor	140-180	1.5
$MnCeO_x$	-	Stirred-tank reactor	110	0.5
Fe	AC	Fixed-bed reactor	100-127	0.8

The last type of catalyst used in CWAO is active carbon. The most remarkable characteristics of activated carbons are their high surface area and porosity compared to other materials such as Al_2O_3, TiO_2, CeO_2 and the presence of oxygen surface groups, which affects the catalytic activity. There are several particularities which should be considered when an activated carbon is used as a catalyst in CWAO processes. The condition of CWAO process should be performed at temperature and pressure less than 423 K and 10 atm (mild conditions), in order to minimize oxidation of the activated carbon [119]. Studies on the CWAO of phenolic using activated carbon catalysts are listed in **Table 2.6**.

Table 2.6 Summary of studies on CWAO of phenolic over activated carbon catalysts [120].

Substrate	Operating conditions	Origin	S_A (m^2/g)	X (%)	X_{COD} (%)
Phenol (5 g/L)	TBR 120-160 °C, 0.1-0.9 MPa τ = 0.05-0.6 h, 7 g of AC	Wood Wood Coco Mineral	1000 1000 600 960	>99 40 15 8	85
Phenol (0.27-7 g/L)	Slurry batch reactor 100-160 °C, 0.35-0.95 MPa τ = 6 h, 1-4 g of AC	Wood	1000	50-99	
Phenol (1 and 5 g/L)	Fixed bed reactor (upflow) 160 °C, 1.6 MPa, pH = 3.5 τ = 0.03-0.3 h, 3.5-7 g of AC	IndReact Centaur RTA180	745 931 1333	>99 >99 88	85
Phenol 2-amino phenol Salicylic acid 5-sulfo salicylic acid (all 5g/L)	TBR 125-175 °C, 1-7 MPa VLHSV = 1-20 h^{-1}	Charcoal	1049	>99 >99 40 40	
Phenol (5 g/L)	Slurry batch reactor 110-160 °C, 3-5 MPa t_R = 3 h, 0.1-1 g of AC	Chezacarb Charcoal	950 1049	>99	
Phenol (5 g/L)	TBR 110-160 °C, 5-8 MPa F_{AIR}/F_L = 400m^3/m^3 τ = 2.0 h, Liquid holduap = 0.05-0.065	CBC	70.1	>99	85
Phenol (20 g/L)	Fixed bed reactor (upflow) 400 °C, 25 MPa τ = 2.6 s, 0.9 g of AC	Coconut Bamboo Coke Graphite Fibre	430 42.7 12.4 0.003 0.6	63 30 38 22 40	50 18 28 17 29

Heterogeneous catalysts are capable of activation of an oxidant into active radicals. The catalyst directly activates reactant molecules, facilitating their decomposition into radicals. The catalytic cycle would follow the reduction-oxidation reactions as shown below [121].

$$ROOH + M^{n+} \longrightarrow ROOH^{\bullet} + M^{(n-1)+} + H^{+} \quad (2.10)$$

$$ROOH + M^{(n-1)+} \longrightarrow RO^{\bullet} + M^{n+} + OH^{-} \quad (2.11)$$

The solid catalysts enhance the free radical propagation through the formation of alkyl peroxy radical (2.10) and then the decomposition of hydroperoxide (2.11). The efficiency of the catalyst is related to the redox potential of the $M^{n+}/M^{(n-1)+}$ couple. Catalyst may also involve an oxygen-transfer mechanism in which the role of

catalyst is to transfer an oxygen atom to aqueous reactant molecule through complexation and activation [122].

To date, the main disadvantage of CWAO technology is the problem of the catalyst deactivation which occurred during reaction process. This may occur mainly due to active phase leaching or formation of carbonaceous deposits, during the oxidation process. Among the most promising catalysts, activated carbon offers a less expensive alternative with a proven activity in the abatement of several phenols like compounds.

2.5 Advanced Oxidation Processes (AOPs)

Advanced oxidation processes (AOPs) are defined as near ambient temperature and pressure water treatment processes which are based on generation of very reactive species, such as hydroxyl radical ($OH^{\bullet}$) that has a high standard oxidation potential and reacts non-selectively. The concept of this technique was first introduced by Glaze et al. [123]. The redox potential of hydroxyl radical (2.08) is the highest after fluorine (3.03), followed by that of atomic oxygen (2.42), H_2O_2 (1.77), and then permanganate (1.67). Thus, hydroxyl radicals have emerged as effective species to completely degrade organic compounds in aqueous media. The complete mineralization of an organic pollutant will produce H_2O, CO_2 as seen in the mechanism reaction below.

$$C_aH_bX + mOH \longrightarrow aCO_2 + \frac{b}{2}H_2O + X^{n^-} \qquad (2.12)$$

All the carbon and hydrogen atom are completely oxidized to CO_2 and H_2O, while the X gives X^{n^-}. X^{n^-} is an inorganic ion which is depending with the molecular composition of that pollutant. Recently, sulphate radicals ($SO_4^{-\bullet}$) have been proposed as an alternative to hydroxyl radical for organic degradation due to higher oxidizing potential (1.82 V) and in many cases more efficiency of oxidation than that of hydrogen peroxide [124, 125].

2.5.1 Cavitation

First reported in 1895 by Thornycroft and Barnaby, cavitation is defined as the phenomena of the formation, growth and subsequent collapse of micro-bubbles or cavities occurring in extremely small interval of time (milliseconds), releasing large magnitudes of energy [126-128]. Cavitation events occur at multiple locations in the reactor simultaneously and hence the overall effects are spectacular. There are some important effects of cavitation during the events occur, namely the generation of hot spots, release of highly reactive free radicals, continuous cleaning as well as increase in the surface area of the solid catalyst and also enhancement in the mass transfer rates due to turbulence generated as a result of acoustic streaming [129-131]. The ambient conditions of the reaction system can greatly influence the intensity of cavitation, which directly affects the rate of reaction or yield. These conditions include the temperature of reaction, pressure of hydrostatic, irradiation frequency, acoustic power, and ultrasonic intensity. There are other factors which significantly influence the cavitational intensity, namely the presence and nature of dissolved gases, sample preparation, choice of buffer and solvent [130]. The cavitation technique can be divided into several types based on the mode of generation, which are hydrodynamic cavitation, acoustic cavitation, optic and particle cavitation. Among the types of cavitation, hydrodynamic and acoustic cavitation has been proven as efficient technique in bringing about the desired chemical changes. Others, optic and particle cavitation are typically used for single bubble cavitation, which fails to induce chemical change in the bulk solution [12]. In the case of caustic cavitation, cavitation is affected using the high frequency sound waves in the range of 16 kHz-100MHz, usually ultrasound. Alternate compression and rarefaction cycles of the sound waves results in various phase of cavitation such as generation of the cavity/bubble, growth phase and finally collapse phase releasing large amount of energy locally [127]. The most common device used for acoustic cavitation can be shown in **Figure 2.6.**

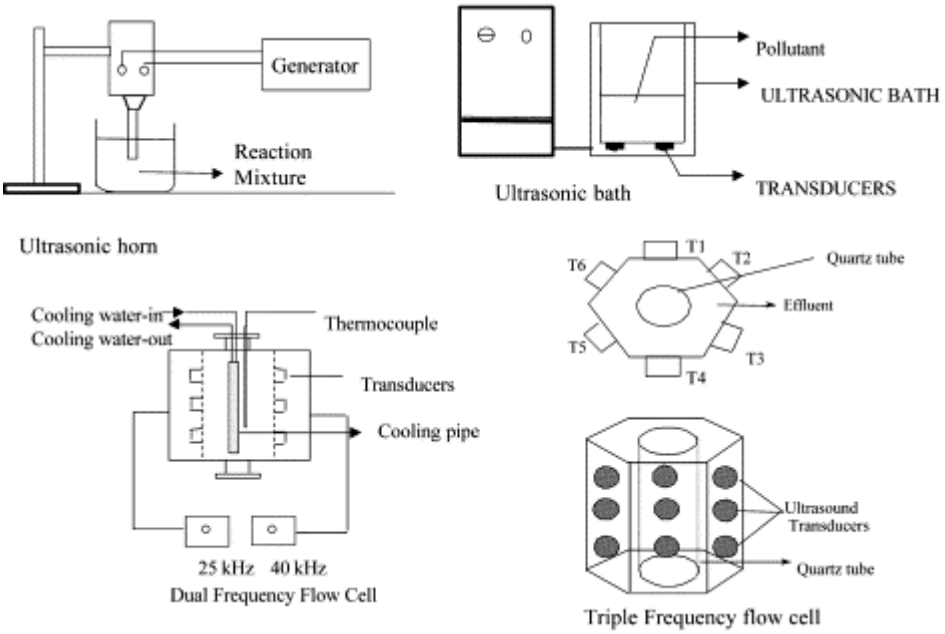

Figure 2.6 Schematic representation of the equipment based on acoustic cavitation [12].

Typically, the devices with higher dissipation area give larger efficiency at similar levels of the supplied input energy. It is also has been reported that using a device with multiple frequencies transducers is more beneficial compared with the use of a single frequency [132, 133]. Moreover, another technique with promising future has been developed for large-scale applications is ultrasonic horns vibrating in radial directions, which also gives additional benefit of better energy dissipation due to larger irradiating area [134], however more investigation is needed in terms of testing this device for operation at high frequency and high power dissipation.

The other technique is hydrodynamic cavitation, as an alternative process, is the use of hydraulic devices to generate cavitation by the passage of the liquid through a constriction such as valve, orifice and plate venturi [135]. When the liquid passes through the orifice, the kinetic energy/velocity of the liquid is increased at the expense of the pressure. Some of the equipment used for the generation of hydrodynamic cavitation can be seen in **Figure 2.7**.

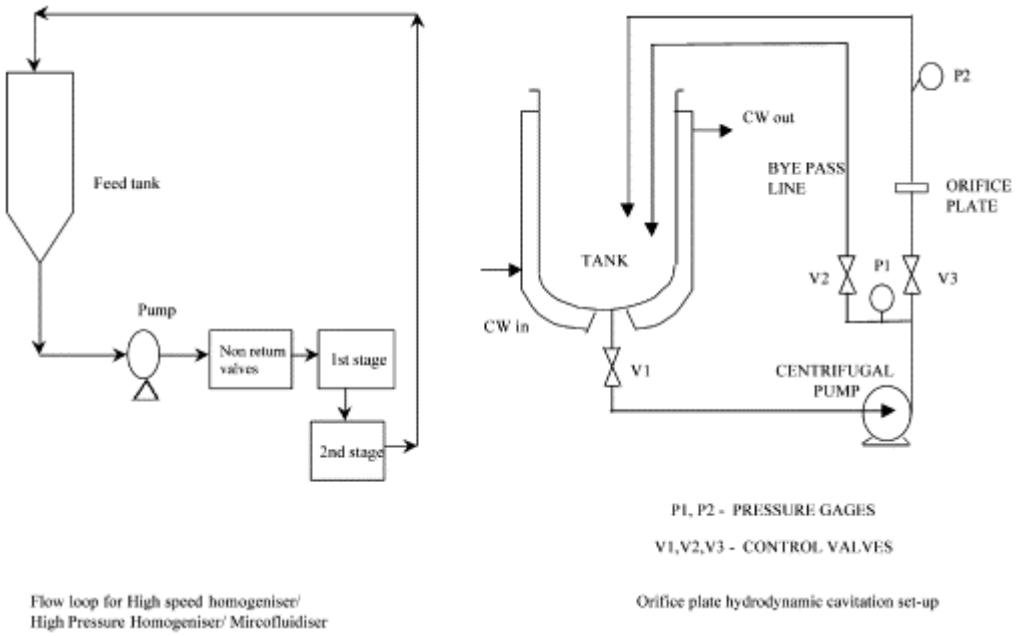

Figure 2.7 Schematic representation of the equipment based on hydrodynamic cavitation [12].

The cavitation intensities generated in the hydrodynamic equipment is lower compared to the acoustic equipment. Design of a reactor, in terms of the operating and geometric conditions, must be customised to the particular application. There are not many publications that describe the use of hydrodynamic cavitation in the area of wastewater treatment [136]. However, hydrodynamic cavitation technologies offer a simple process, higher energy efficient, low cost for reactor maintenance, and relative flexible for scale-up as compared to acoustic techniques [137].

2.5.2 Photocatalytic oxidation

Photocatalytic oxidation (PCO) processes are gaining importance in the area of wastewater treatment, since these techniques result in high total organic carbon removal with operation at mild conditions of temperature and pressure. A photocatalyst is defined as a species that induces photochemical reactions, as a result of activations of a semiconductor material, for instance TiO_2, by the radiation of ultra violet light (UV-light) with a specific wave length. The activation is achieved with

the absorption of photons by a semiconductor material promoting the electrons from its valence band to conduction band, thereby creating a hole and an electron (**Figure 2.8**). The holes will act as oxidizing agent, while the electron is reducing agent [138]. Furthermore, the hole will react with water to produce the powerful oxidizing agents (hydroxyl radical, $OH^{\bullet}$) which are responsible for removal of hazardous components from aqueous solution [139]. The mechanism of the reduction and oxidation reaction is shown in the following equations [140].

$$TiO_2 \xrightarrow{hv} TiO_2\,(e_{cb}^- + hole_{cb}^+) \quad (2.13)$$

$$TiO_2\,(e_{cb}^- + hole_{cb}^+) \xrightarrow{recomb} TiO_2 + \text{heat} \quad (2.14)$$

$$H_2O \longrightarrow OH^- + H^+ \quad (2.15)$$

$$hole_{vb}^+ + OH_{ads}^- \longrightarrow OH^{\bullet} \quad (2.16)$$

$$O_2 + e_{cb}^- \longrightarrow O_2^{-\bullet} \quad (2.17)$$

$$O_2^{-\bullet} + 2OH_{aq}^+ \longrightarrow H_2O_2 + O_2 \quad (2.18)$$

$$OH^{\bullet} + \text{Organic compound} + O_2 \longrightarrow \text{products } (CO_2, H_2O_2, \text{etc.}) \quad (2.19)$$

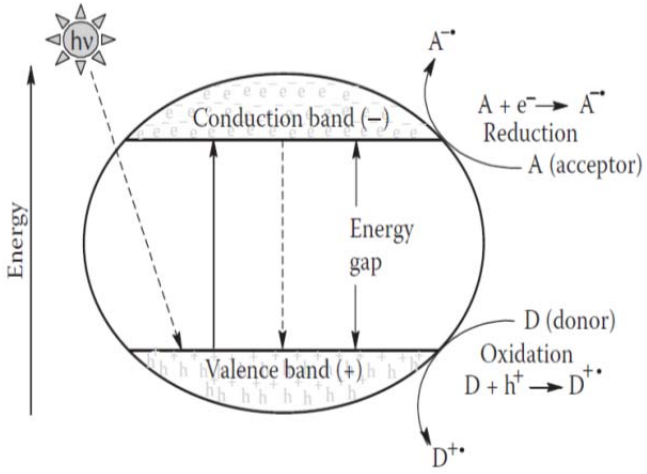

Figure 2.8. Illustration of the oxidation and reduction reactions in a semiconductor exposed to UV light [141].

Semiconductor materials such as titanium dioxide, zinc oxide, cadmium sulphide, bismuth oxide, ferric oxide, and tungsten oxide have been investigated in different studies for degradation of organic pollutants in aqueous solution [142-145]. However, among the semiconductors used in photocatalysis, titanium dioxide only has the best photocatalytic performance with maximum quantum yields. In addition, Degussa P-25 catalyst is the most active form among the several of TiO_2 that are available and usually give better degradation efficiencies [12]. However, photocatalytic oxidation is expensive to run because it is slow rate of degradation leading to high power consumption (electrical energy) and in some cases leading to incomplete mineralization of organics [146].

Generally, the rate of photocatalytic degradations is influenced by several factors, such as illuminations intensity, photocatalyst type, pH value, oxygen concentration, presence of inorganic ions, and the concentration of organic reactant. Among them, the pH value has a dominant effect on the photocatalytic reaction because many properties are strongly pH dependent, such as the semiconductor's surface state, the dissociation of organic contaminants, and the flat-band potential [147]. The rate of photocatalytic degradation has been modelled by different kinetic models. Langmuir-Hinshelwood (L-H) kinetics seems to describe many of reactions fairly well. The L-H expression in low solute concentration can be reduced to a pseudo first order equation, as can be seen below [148].

$$-\frac{dC}{dt} = K_1 K_2 C = kC \qquad (2.20)$$

Where k is a pseudo first-order rate constant of organic pollutant, C is the bulk solution concentration of pollutants at various time (t). This equation has been applied to many photocatalytic reactions. **Table 2.7** lists the aqueous toxic organics that can be mineralized using PCO.

Table 2.7 List of the aqueous pollutants mineralized by photocatalysis [12]

Class of organics	Examples
Haloalkanes/haloalkenes	Chloroform, trichloroethylene, perchloroethylene, tribromomethane, dicloromethane, CCl_4
Aliphatic alcohols	Methanol, ethanol, 1-octanol, 2-propanol
Aliphatic carboxylic acids	Formic, glycolic, citric
Amines	Alkylamines, alkanolamines, heterocyclic and aromatic N-compounds
Aromatics	Toluene
Halophenols	2-,4-chlorophenol and 2,4-dichlorophenol
Aromatic carboxylic acids	Malic, chlorobenzoic acids, phenoxy acetic acid, 2,4-dicholorophenoxyacetic acid
Amides	Benzamide, 4-hydroxybenzamide
Surfactants	Sodium dodecyl benzene sulfonate, trimethyl phosphate
Herbicides	Atrazine, S-trizine herbicides, bentazone
Pesticides/fungicides	Fenitrothion, metalaxyl
Dyes	Methylene blue, Rhodamine B, methyl orange, fluorescin, SBB dye, reactive black 5
Sulphides	Trimethylene sulphide, propylene sulphide, thiophene, methy disulphide

2.5.3 Fenton chemistry

The Fenton process was discovered about 100 years ago by Fenton, but its application as an oxidizing technique for degradation of organic pollutants was not applied until the late 1960s [13]. Fenton reaction involves hydrogen peroxide and ferrous ions (Fe^{2+}) in aqueous acidic medium. Furthermore, hydrogen peroxide decomposes into hydroxyl radical and hydroxyl ion and the oxidation of Fe^{2+} to Fe^{3+}. The Fe^{3+} ions may further catalyze hydrogen peroxide and generates again hydroxyl radicals. Hydroxyl radicals will oxidize organic pollutants by abstraction of protons producing organic radical ($R^{\bullet}$), which can be further oxidized into H_2O and CO_2. The Fenton's reaction is as follow [149].

$$Fe^{2+} + H_2O_2 \longrightarrow Fe^{3+} + OH^- + OH^{\bullet} \quad (2.21)$$

$$OH^{\bullet} + Fe^{2+} \longrightarrow Fe^{3+} + OH^- \quad (2.22)$$

$$Fe^{3+} + H_2O_2 \leftrightarrow Fe\cdots OOH^{2+} + H^+ \quad (2.23)$$

$$Fe\cdots OOH^{2+} \longrightarrow Fe^{2+} + HO_2^{\bullet} \quad (2.24)$$

$$HO_2^{\bullet} + Fe^{2+} \longrightarrow Fe^{3+} + HO_2^{-} \quad (2.25)$$

$$Fe^{3+} + HO_2^{\bullet} \longrightarrow Fe^{2+} + O_2 + H^{+} \quad (2.26)$$

$$OH^{\bullet} + H_2O_2 \longrightarrow H_2O + HO_2^{\bullet} \quad (2.27)$$

$$RH + OH^{\bullet} \longrightarrow R^{\bullet} + H_2O \longrightarrow \text{further oxidation} \quad (2.29)$$

Some investigations showed that the Fenton's reagent has successfully used for the remediation of colour from textile industries, diesel-contaminated soil, and removal of organics such as phenol, alcohol, ketones, chlorophenol, benzene, nitrobenzene, dichlorophenol, and poly aromatic hydrocarbon [150-154]. However, common problems that are often encountered in the process are acidic condition, large quantity of chemical reagents, very slow catalysis of the ferrous ions generation and large production of ferric hydroxide sludge [155].

2.5.4 Chemical oxidation methods

There has been considerable interest in the use of chemical oxidants for destruction of organic contaminants present in the wastewater. This technique is fairly simple and widely used for the remediation of soil and ground water [156, 157]. An oxidant can be defined a substance that can remove electrons from other reactants in a redox chemical reaction. In general, the ability of a chemical compound oxidizing the organic pollutants in the water can be affected by oxidation reduction potential of the oxidant itself. In the wastewater treatment applications, there are several commonly oxidants, some of them are presented in **Table 2.8** below [158]. In general, a oxidant which has a high redox potential, can achieve the faster rate of the oxidation reaction [159].

Table 2.8 Standard reduction potential of some oxidants in acidic media

Oxidant	Redox Potential E^o (eV)
Fuorine (F_2)	3.03
Hydroxyl radical ($OH^•$)	2.80
Atomic Oxygen	2.42
Ozone (O_3)	2.07
Hydrogen peroxide (H_2O_2)	1.77
Potassium permanganate (KmnO4)	1.67
Hypobromous acid (HbrO)	1.59
Chlorine dioxide (ClO_2)	1.50
Hypochlorous acid (HClO)	1.49
Chlorine (Cl_2)	1.36
Bromine (Br_2)	1.09

Some of the popular oxidants commonly used in wastewater treatment processes include ozone, hydrogen peroxide, potassium permanganate, and peroxymonosulfate [160, 161].

Ozone is the triatomic state of oxygen which simply means that the ozone molecule contains three oxygen atoms having the chemical symbol of O_3. At ambient conditions, it always exists in the gas phase. Ozone is the most powerful known oxidizing agent (2.07 eV) and can react with most species containing multiple bonds such as C=C, C=N, and N=N [12]. In practical scale, ozone has been widely applied and can be used for treatment of effluents from various industries relating to dye manufacture, pulp and paper production, shale oil processing, production of pesticides, textile dyeing, pharmaceutical production [162-167]. The solubility of ozone depends on the water temperature. In the temperature range of 0 to 60 ^oC, solubility of ozone is 10 to 15 times higher compared with oxygen [168]. Because ozone is very reactive in an aqueous environment, ozone can oxidize materials between 10 to 1000 times faster than most oxidants used in water treatment [169]. However, the molecule is unstable thus it cannot be compressed and stored. Therefore, ozone must be generated close to the point of application and used immediately. Usually the decomposition rate of ozone follows a pseudo first-order kinetic model [170]:

$$-(\frac{d[O_3]}{dt})_{pH} = k'[O_3] \quad (2.30)$$

Where k' is a pseudo first-order constant at given pH value. Molecular ozone can oxidize water impurities via direct, selective reactions or can undergo decomposition via a chain reaction mechanism resulting in the production of free hydroxyl radicals (**Figure 2.9**). The decomposition proceeds through the five-step chain reaction, as shown in **Table 2.9** [170]:

Table 2.9 Ozone decomposition proceeds

Reaction	Rate constant ($M^{-1}s^{1-}$)
$O_3 + H_2O \longrightarrow 2HO^{\bullet} + O_2$	1.1×10^{-4}
$O_3 + OH^{-} \longrightarrow O_2^{\bullet -} + HO_2^{\bullet}$	70
$O_3 + HO^{\bullet} \longrightarrow O_2 + HO_2^{\bullet} \leftrightarrow O_2^{\bullet -} + H^{+}$	-
$O_3 + HO_2^{\bullet} \leftrightarrow 2O_2 + HO^{\bullet}$	1.6×10^{9}
$2HO_2^{\bullet} \longrightarrow O_2 + H_2O_2$	-

Ozone reacts in aqueous solution with various organic and inorganic compounds, either by a direct reaction of molecular ozone or indirect reaction through hydroxyl radicals induced by the ozone decomposition in water. In general, the decomposition of ozone is significantly influenced by the pH of the solution because it can affect the formation of hydroxyl radicals ($OH^{\bullet}$). The hydroxyl radical is the most important intermediate because it leads to an indirect attack on organic compounds, which is faster than a direct attack by molecular ozone. Direct reaction usually occurs at pH less than 3, while the combined reaction occurs at pH between 7 and 10, and indirect at a pH above 10 [147, 170, 171].

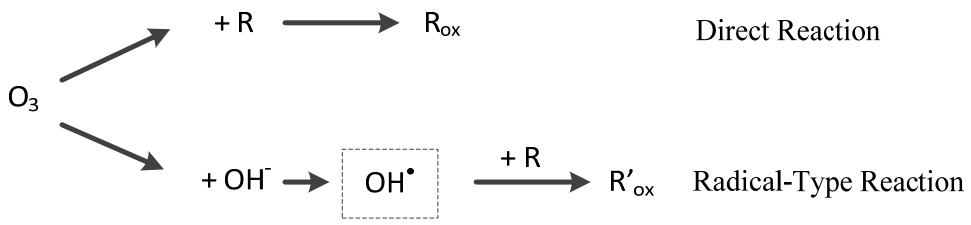

Figure 2.9 Reactivity of ozone in an aqueous solution [172].

Hydrogen peroxide is another oxidant that has been well-known as a strong oxidant which is effective in degradation of organic contaminants or in the treatment wastewater requiring less stringent oxidation condition [173], which was found by Thenard in 1818 as the product of the reaction of barium peroxide with nitric acid [174]. Hydrogen peroxide is a versatile oxidant that is effective over the whole pH range, which has a standard reduction potential of 2.8 eV in acidic media, and would be able to oxidize almost all organic compounds to carbon dioxide and water, except for some of the simplest organic compounds, such as acetic, maleic and oxalic acids, acetone or simple chloride derivatives [175]. Hydrogen peroxide is an oxidant which has environmentally benign profile, because it can decompose to water and oxygen only. Therefore, H_2O_2 is widely used as a bleaching agent in textile industry, pulp and paper, and home laundry application. However, there are some major problems encountered with the application of hydrogen peroxide alone for wastewater application which are: hydrogen peroxide is unstable and has a tendency to decompose, so that stabilizing agents have to be added, very sensitive to rise in temperature, and limited effectiveness due to mass transfer limitations [150, 176, 177].

Furthermore, another oxidant which is different with all oxidants, which do not rely on generating hydroxyl radicals to oxidize organic pollutants in AOPs, is potassium permanganate. Permanganate (MnO_4^-) compounds is one of the most famous oxidants utilized to oxidize inorganic and organic pollutants such as cyanide, hydrogen sulfide, and phenols. Permanganate has also been used to oxidize iron, manganese, and compounds associated with taste and odor. Permanganate obtained from potassium permanganate, which can be stored dry in crystalline form [178]. In addition, reactive species of permanganate depend on the reaction conditions, such as pH. For instance in acidic medium, potassium permanganate will generate several active radicals such as $HMnO_4$, $H_2MnO_4^+$, $HMnO_3$, and Mn_2O_7 which react with toxic organic into less toxic compounds [179], while in basic medium, the reactive species is MnO_4^{2-} [180]. A study has reported that pH has an impact in generating reactive species and it can be seen from the intermediate products of oxidation of benzaldehyde in aqueous solution. At pH 4 half products dominated by formic acid,

whereas at pH 6 to 8 the dominated species are oxalic acid and glyoxylate and then the organic acids are subsequently oxidized to carbon dioxide [181]. The drawback of this system is the formation of precipitation in form of magnesium oxide in end products which requires additional removal process [182].

Moreover, another popular oxidatant has come forth recently for degradation of non-biodegradable compounds, which is peroxymonosulphate. Peroxymonosulphate is a triple salt consisting of $2KHSO_5 \bullet KHSO_4 \bullet K_2SO_4 \bullet KHSO_5$, which is best known under the commercial name of Oxone® (DuPont). In aqueous solution, the active component of oxone® which is potassium peroxymonosulfate ($KHSO_5$) leads to the formation of $SO_4^{\bullet -}$ and $SO_5^{\bullet -}$ radicals which are known as sulfate radicals. The active component of oxone has a short oxygen-oxygen bond (1.460 Å) compared with H_2O_2 (1.497 Å) with a hydrogen atom on left side and SO_3 group on right side, which is capable of providing a sulfate group [183]. The schematic representation of $KHSO_5$ structure can be seen in **Figure 2.10**.

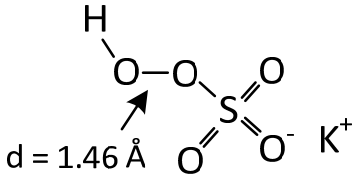

Figure 2.10 Schematic representation of $KHSO_5$ structure [184].

Peroxymonosulfate is known to be among the strongest oxidant, which has standard reduction potential (E^0) of HSO_5^-/HSO_4^- = 1.82 V and generally oxidizes faster than hydrogen peroxide which has standard reduction potential (E^0) of H_2O_2/H_2O = 1.76 V [185]. In addition, the oxidant is stable at pH < 6 and at pH 12. At pH 9, peroxymonosulfate will reach a point of minimum stability where concentration of HSO_5^- and SO_5^{2-} are equal. While at pH less than 1, HSO_5^- hydrolyzes to hydrogen peroxide [183]. Based on half-life, a sulfate radical has a longer half-life than the hydroxyl radical, because the tendency of the sulfate radical is for electron transfer reactions, while the hydroxyl radicals can participate in a variety of reactions with equal tendency [186, 187]. In addition, the sulfate radical ($SO_4^{\bullet -}$) has stability and

high oxidation efficiency, thus making them very effective for degradation of organic and inorganic compounds such as cyanide, the reduced sulphur compounds, ketone, phenolic and aldehydes. The advantage of this system is that the oxidation process may not require pH adjustment because peroxymonosulfate provokes pH dropping, which can be controlled by optimizing experimental parameter [188].

All oxidant as mentioned above are strong oxidants that can be used to degrade organic contaminants present in aqueous solution. However, the use of individual oxidant is not that efficient in oxidizing more complex and recalcitrant materials due to mass transfer resistance between the pollutant and the oxidizing agents [12]. Therefore, these oxidants require some other metal salts or energy which is capable of dissociating oxidant to generate radical species [141].

Recently, many investigations have reported that sulphate radicals are superior to hydroxyl radicals in oxidation for water treatment. In most previous investigations, Co^{2+}/peroxymonosulphate (oxone®, HSO_5^-) has been found to be an effective route of AOP for sulphate radical production and oxidation of various organics [189-194] [189]. Anipsitakis and Dionysiou [124] investigated homogeneous activation of oxone® by several metal ions, Fe^{2+}, Fe^{3+}, Co^{2+}, Mn^{2+}, Ni^{2+}, Ru^{3+}, Ce^{3+}, and Ag^{+}, for 2,4-dichlorophenol degradation. They found that Co^{2+} is the best metal catalyst for the activation of peroxymonosulfate. They also found that Co^{2+}, Ru^{3+}, and Fe^{2+} interact with PMS to produce freely diffusible sulfate radicals while Mn^{2+}, Ni^{2+}, and Ce^{3+} with oxone® generate caged or bound to the metal sulfate radicals. The radical generation and organic degradation processes can be described as shown below.

$$Co^{2+} + HSO_5^- \rightarrow Co^{3+} + SO_4^{-\bullet} + OH^- \quad (2.31)$$

$$Co^{3+} + HSO_5^- \rightarrow Co^{2+} + SO_5^{-\bullet} + H^+ \quad (2.32)$$

$$SO_4^{-\bullet} + H_2O \rightarrow SO_4^{2-} + OH^\bullet + H^+ \quad (2.33)$$

$$SO_4^{-\bullet} + \text{Organics} \rightarrow \text{several steps} \rightarrow CO_2 + H_2O + SO_4^{2-} \quad (2.34)$$

However, a major issue in using Co metal ions is the toxicity which can cause health problems to humans, such as asthma and pneumonia, and secondary pollution [195]. Therefore, alternative catalysts with less toxicity and environmental benign for peroxymonosulphate activation are highly required. In the past few years, several heterogeneous Co catalysts have been tested in our lab and reported for oxone® activation, such as Co_3O_4 [155], Co exchanged zeolites [125], supported Co_3O_4 [14, 196-200], and $CoFe_2O_4$ [201, 202] for phenolic degradation and proposed that both CoO and Co_2O_3 contained in Co_3O_4 are responsible for oxone® activation.

In the past decade, manganese oxides have attracted much attention because of their physical and chemical properties and wide potential applications as heterogeneous catalysts [203-205], adsorbents [206-208], enhanced luminescence [209, 210], battery materials [211-213], biolabeling [214, 215] and supercapacitor [216, 217]. In the most previous investigations in water treatment, MnO_x was usually used for Fenton-like reaction for production of hydroxyl radicals from H_2O_2 and oxidation of organic compounds. Manganese oxide has several different phases and oxidation states, such as MnO, MnO_2, Mn_2O_3 and Mn_3O_4, with varying structures. Using nano structured manganese oxide instead of supported Co oxide will be a promising for advance oxidation process. For this purpose, the use manganese oxides are an alternative to be developed because of their widely presence in nature and low toxicity to the environment.

2.6 Preparation and Synthesis of Solid Catalysts

2.6.1 Solid synthesis

Developments of new methods to obtain more efficient catalysts have increased. There are various methods that are commonly used in making catalysts, one of which is solid to solid method. The solid to solid route is a direct reaction of corresponding solid compounds in certain circumstances to obtain the desired material. In general there are two popular methods that can be used in the solid state reaction which are ceramic method and mechanical milling. Both techniques will be described further below.

2.6.1.1 Ceramic method

Many inorganic solid materials have been synthesized by reacting solid with another solid. The most common and widely used method for preparation of solid materials is the ceramic method, which is a direct reaction of two non-volatile solids to form the desired product at high temperature. This method is widely used in industry and the laboratory, and can be used to synthesize the whole range of materials such as mixed metal oxides [218]. Since, solid-state does not react at low temperature, therefore high temperature (>1000 ^{o}C) is necessary to complete the reaction [219]. Thus, thermodynamics and kinetics are very important factors in solid-state reaction. In order to get better understanding about ceramic method, it is considered the thermal reaction of two single crystals compound, A and B, with a contact across one face (**Figure 2.11**).

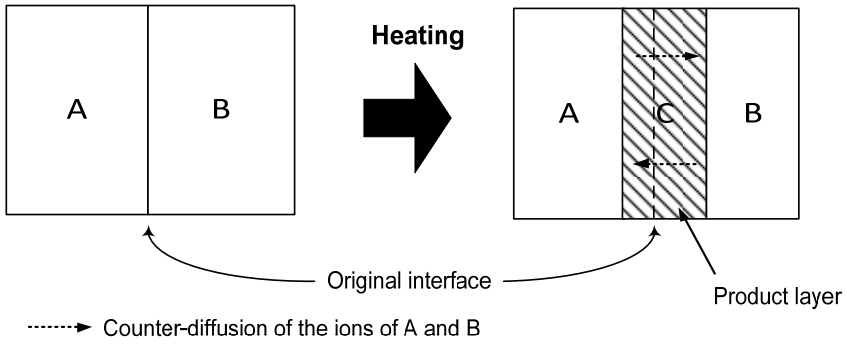

Figure 2.11 Schematic illustration of a solid to solid reaction [220, 221]

It is seen from **Figure 2.11,** the first stage of reaction occurs at the interface between A and B, when no melt is formed during the reaction, to form nuclei of product phase. Nucleation is commonly difficult when phase of product is different from the one of the reactant phases due to structural reorganization of the lattice. Next, the reactants diffuse from the bulk to the product phase. After the nuclei of product C have formed, there are two reaction interfaces at this stage: one between A and C interface, and another is C and B interface. At the growth stage of product layer, counter diffusion of reactant ions (A and B) have to occur through the product layer C towards the new reaction interface. Further reaction causes the growth of the product layer, which results in a longer distance for diffusion paths, as consequently the rate of reaction

gradually becomes slower with the time. This phenomenon occurs because the product layer between A and B acts as a barrier. It is difficult for ions to move to adjacent sites because they are normally regarded as being trapped in their respective lattice sites. Therefore, the high temperatures are required in order that the ions have sufficient energy to diffuse through the crystal lattice [221]. The rule of thumb suggests that a temperature of about two-thirds of the melting temperature of the reactant is required to enable the solid-state reaction. In the ceramic method, diffusion is often the limiting step in the whole reaction step. Therefore, using small particle size could maximise the surface contact area and minimise the distance that the reactants have to diffuse [222].

Although the ceramic method is a simple technique and has been used widely, this technology has some drawbacks such as large energy consumption due to high temperature reaction, the desired product may be unstable or decompose at high temperatures, chemical inhomogeneity, coarser particle size, and introduction of impurities during ball milling, and also difficult to process further purification for end product due to solid phase product [223-225].

In a manganese-cobalt-based material, the starting reactants usually used are metal oxides. To assist researchers in developing new material a phase diagram is usually used as a practical reference in material synthesis for particular interest, such as $Co_{3-x}Mn_xO_4$ spinel phase diagram, as can be seen in **Figure 2.12**. Typically, starting materials, Co_3O_4 and Mn_3O_4 in different proportions are mixed together. The mixed oxide-based material were pressed into pellet at 3500 kg/cm^2, and heated at 1000 ^oC in air with flow rate 6 to 8 cc/sec. After the heat, they were cooled and crushed and ground into powder. Using this method, a single phase cubic spinel could be synthesized in the composition range $x \leq 0.1$ [226]. For application, $Co_{3-x}Mn_xO_4$ spinel catalyst is widely used in Fischer-Tropsch process for synthesis of gaseous, liquid, and solid (waxes) hydrocarbons from carbon monoxide and hydrogen reaction [227-229].

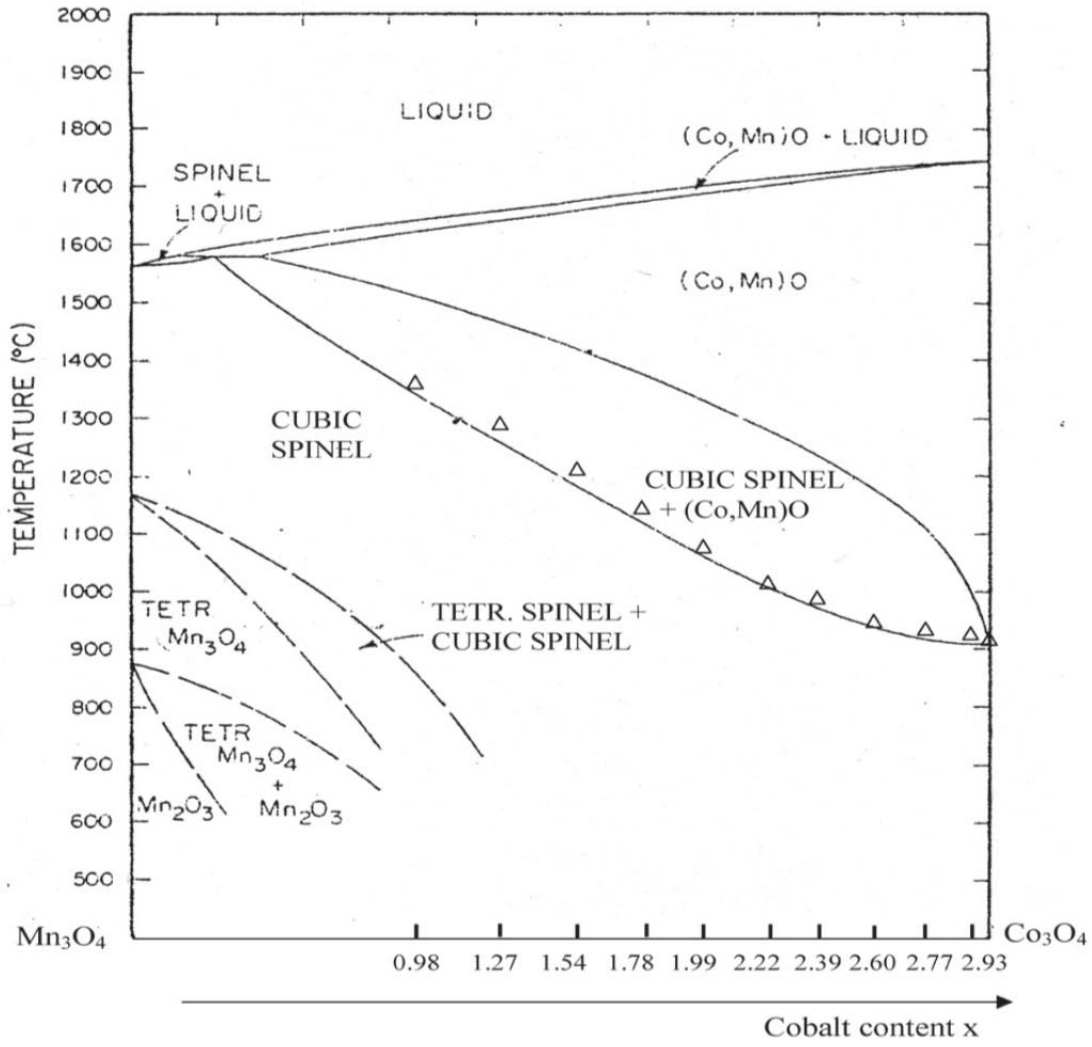

Figure 2.12 Diagram showing phase relations in the system manganese oxide-cobalt oxide under air [230].

2.6.1.2 Mechanical Milling Method

Mechanical milling has been used long time ago in producing ultra-fine powders in the range of a sub-micron to a nanometer with a high concentration of lattice defects. The synthesis of materials using high energy ball milling of powders was first developed by John Benjamin in 1970 [231]. The aim of milling is to reduce the particle size and blending of particle in new phases. Typically, this technique uses mechanical action from the balls and then transfers the kinetic energy into the powder during milling processes. The balls may roll down the surface of the chamber in a

series of parallel layers or the balls may fall freely and impact the powder and balls beneath them. The basic process of mechanical milling is presented in **Figure 2.13**. These actions would increase the surface area, surface energy and number defects of material. The increased surface energy can result in mechano-chemical activation if alterations in structure, chemical composition or chemical reactivity occurred throughout milling [232, 233].

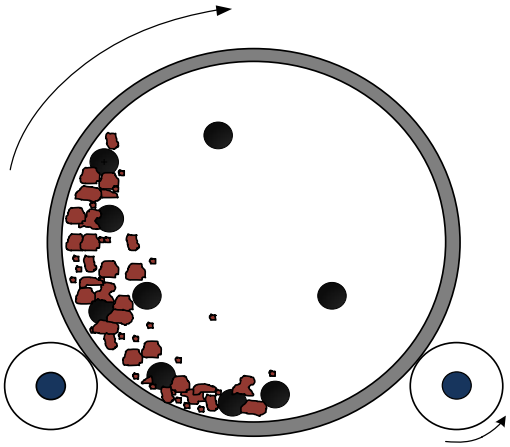

Figure 2.13 Schematic illustration of the high-energy ball milling

In general, there are several important parameters influencing significantly in the success of catalyst synthesis using mechanical mill process, such as size of milling ball, number of milling balls, temperature during milling, milling speed and time [234-236]. The large size and high density of milling balls is useful since the larger density of the balls will transfer more impact kinetic energy to powder particle. Furthermore, the number of milling balls has linear correlation with yield due to the linear correlation between mass (m), moment of inertia I and kinetic energy of the system $E_{kinetic}$ (Eqn. 1) [237].

$$E_{kinetic}\ (\text{rot or osc}) = 0.5I\omega^2 = 2\pi^2 I v^2 \qquad (2.35)$$

Where I, ω, and v are the moment of inertia, angular velocity and angular frequency, respectively. The temperature during milling will affect the phase of final product because heat treatment can facilitate a solid diffusion and defects of lattice in the material. Moreover, at higher temperature, milling process produced a fully

amorphous phase product, while a partially amorphous phase was produced on milling at lower temperature [238]. In addition, mill speed and time will affect specific surface area of final product. with using same speed of milling, fine particle will be obtained in short time of milling process, while specific surface area will decrease with increasing the milling time due to change of powder phase [239].

There are many solid state mechano-chemical studies on the synthesis of alloys, transition-metal nano powder, and nano-phase material [240-244]. Of course, many materials have been synthesized using this method for a wide range of applications, such as Mn-Zn spinel ferrites, Mn-Fe, Ni-Fe, $LaMnO_3$, $La_{0.7}Ca_{0.3}MnO_3$, $LiMnO_4$, graphene nanosheet, carbon scrolls, carbon nanotubes, and activated carbon [245-255]. For example, β-MnO_2 nano-crystalline catalyst was synthesized with starting material manganese salt. Further, the starting material is placed in high-energy ball milling which is equipped with 2 balls for 16 hours. After the process, the average particle was obtained in the range of 88-500 nm and surface area between 61.5-4 m^2g^{-1} [256].

The solid state mechanochemical process is relatively promising because it is a simple and effective method to prepare materials for various purposes. However, there are several disadvantages which have to overcome during the ball milling, such that the particles produced tend to be non-uniform size and shape, and have a wide range distribution of particle sizes. In addition, the products are easily contaminated due to erosion of the milling material [257-259].

2.6.2 Liquid to solid synthesis

Liquid to solid synthesis is one route for the preparation of heterogeneous catalysts. This method has a major difference compared to solid to solid method, in which it do not require high temperature heating or high mechanical energy for preparation stages into the catalyst. Synthesis of solid catalysts in solution state is powerful because the nucleation and growth process can be easily controlled by adjusting the reaction parameters, such as the concentrations of reactants, the mole ratio between surfactant

and precursors, the reaction time and temperature [260]. There are several methods concerning this route that will be described further below.

2.6.2.1 Precipitation and co-precipitation method

The synthesis of materials using precipitation routes was first introduced by Marcilly [261]. The aim of this technique is to precipitate an insoluble compound from a liquid solution. The term precipitation is usually reserved for preparation of individual component precipitates, while co-precipitation for multicomponent precipitates. The precipitate usually composed of fine particles or very small particles. For instance, manganese or cobalt-based fine particle can be synthesized using the reaction of aqueous solution of inorganic manganese salt or cobalt salt ($Mn(NO_3)_2$, $MnCl_3$, $MnSO_4$, CoCl) with an alkali solution (NaOH, NH_4OH, $(NH_2)_2.H_2O$) or sodium carbonate [262-267]. Usually, products of precipitation, such as metal hydroxides, need to be calcined to obtain the metal oxide as heterogeneous catalysts.

Most precipitates are crystalline or amorphous precipitates. Getting one of precipitates is depending on the precipitation conditions. If the supersaturation setting is very high, the aggregation rate can exceed the orientation rate and the solid obtained is amorphous [268, 269]. Further, by ripening in the presence of the mother liquor, the amorphous solid can be turning to crystalline [270].

Precipitation involves three distinct processes, namely supersaturation, nucleation and growth. Supersaturation solution can be obtained in several ways, including raising the concentration of the solution by evaporation (A to C), lower temperature (A to B) or raising the pH. More details on the three parameters that affect supersaturation are presented in **Figure 2.14** [270]. Typically, this last approach is more commonly used in the preparation of metal hydroxides by adding the solution containing active component to the precipitating solution, or vice versa [271]. However, this approach has the disadvantage of lack of control on particle size, and morphology. This occurs due to the rapid change of the concentration of the mother liquor and disconnected nature of the precipitate formation [272-274].

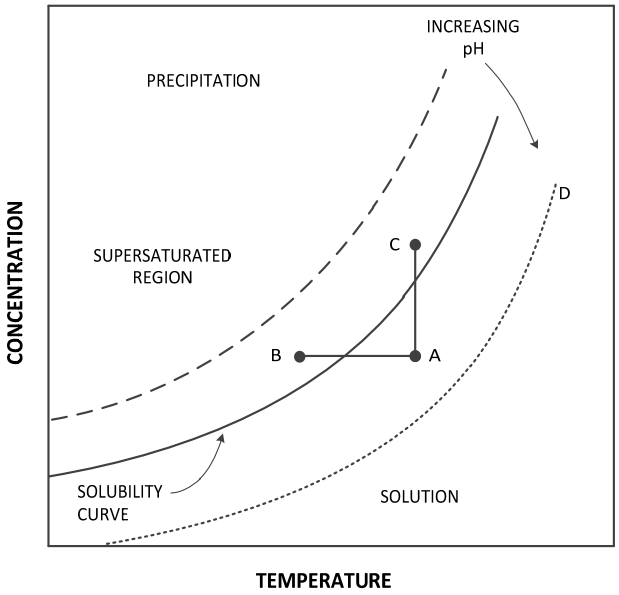

Figure 2.14 Supersaturation dependence on concentration, temperature and pH [270].

Therefore, another method of homogenous precipitation has been developed to overcome this disadvantage. By this technique, a better control is possible to obtain precipitate simultaneously and uniformly throughout the solution. This can be occurred by using the controlled release of the reaction-participating ligands with another source of chemical in the solution [273]. For example, urea or $NH_3 \cdot H_2O$ as the ligand source slowly decompose to yield ammonia by heating at 60 ^oC. Using this method, Fe_3O_4@MnO_2 as shown in **Figure 2.15** with narrow size distribution has been synthesized [71].

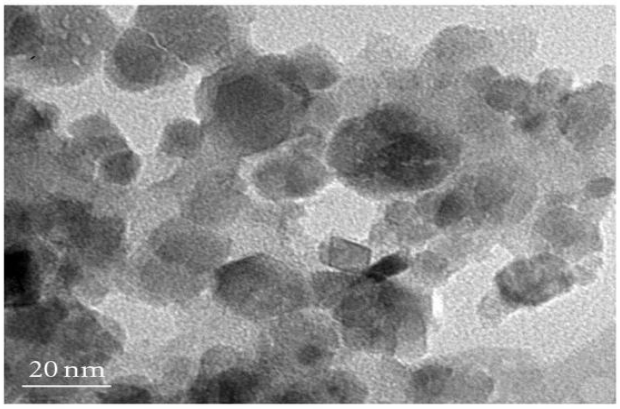

Figure 2.15 Transmission electron images of Fe_3O_4@MnO_2 core-shell particles prepared by the homogeneous precipitation [71].

2.6.2.2 Sol-gel method

The sol-gel process is a very useful technique for preparing many materials in a variety of shapes and forms. Applying the sol-gel process, it is possible to fabricate ultrafine oxide material at relatively low temperatures. In general, the sol-gel process involves the transition of a system from a liquid "sol" (colloidal) into a solid "gel" phase. The term sol refers to a stable colloidal suspension of solid particles in liquids. The particle, which can be crystalline or amorphous and particle aggregation, is prevented by electrostatic repulsion. The sol particles are connected by covalent bonds, Van der Waals force or hydrogen bonds. A gel can be interpreted to be consisting of continuous solid and liquid phases of colloidal dimensions [275].

The sol-gel technique has the drawback similar to precipitation method because the stoichiometry of the precipitates may not be exact if one or more ions left in solution. In the sol gel process, the reactants are never precipitate out. After the sol is formed, which then interact to form a continuous network of connected particles called gel. This homogeneous gel is then dried by evaporating the interstitial liquid and gives rise to capillary forces causing the gel shrink to form the product known as a xerogel [222]. The main steps in sol-gel process outlined above can be seen in **Figure 2.16**.

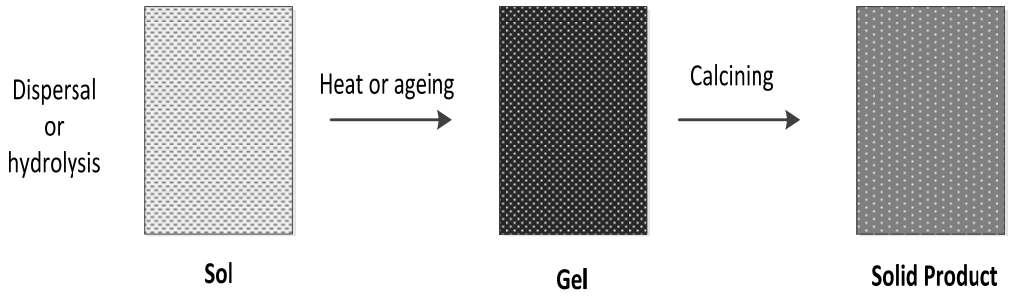

Figure 2.16 Step in the sol-gel synthesis route [222].

In the sol-gel method, the starting materials for the preparations of metal oxides usually use a class of metal organic compounds known as metal alkoxides [276], which have the following general formula:

$$M(OR)_n \tag{2.36}$$

Where M is a metal such as Si, Ti, Al, Zr, while R is an alkyl group such as $-CH_3$, $-C_2H_5$, or $-C_4H_9$ [277, 278]. The metal organics are generally dissolved in a solvent, usually an alcohol (methanol, ethanol, or iso-proponal) [279-281] and addition of water causes hydrolysis of metal alkoxides because a hydroxyl ion becomes attached to the metal atom, as in the following reaction:

$$M(OR)_n + n\ H_2O \longrightarrow M(OH)_n + n\ ROH \tag{2.37}$$

This is followed with a series of condensation reaction between hydroxide group, and the complete reaction is shown by the following reaction:

$$M(OH)_n \longrightarrow MO_{\frac{n}{2}} + \frac{n}{2} H_2O \tag{2.38}$$

Based on the reactions above, it can be seen that sol-gel technique can produce mixed gels easily by mixing of their alkoxides solutions prior to hydrolysis [277, 282]. In theory, almost all metal oxides can be synthesized via a sol-gel method, such as TiO_2, Fe_2O_3, Fe_3O_4, SnO_2, ZrO_2, CeO_2-ZrO_2, $BaTiO_3$, $BaZrO_3$, $BaTi_{0.5}Zr_{0.5}O_3$, $Y_3Al_5O_{12}$ [283-288]. In addition, α, β and γ-MnO_2 and Co_3O_4 nano size with uniform size diameter also can be prepared by a sol-gel process [289-292]. For example,

manganese acetate was dissolved in n-propyl alcohol and citric acid. Further, the pH was adjusted with ammonium hydroxide to get a base solution at 8.5. This solution was heated at 80 ^{o}C to induce etherification and distill out excess n-propyl alcohol. When the solution changed to a transparent viscous sol, then dried in air at 80 C for 2 hours and calcined at 400 ^{o}C. Applying this method, α-MnO_2 particle of nanowires shape with a narrow size distribution have been prepared [289]. Thus all porous oxide materials used in heterogeneous catalysis as catalyst supports or precursors of catalyst supports can be synthesized using this method.

2.6.2.3 Hydrothermal and solvothermal methods

The hydrothermal term came from the geology science, where it refers to any heterogeneous reaction in the presence of aqueous solvents or mineralizers under high temperature and pressure in order to dissolve and recrystallize under ordinary conditions [293, 294]. The hydrothermal synthesis has been an interesting technique to prepare materials with different nanostructures, such as nanowires, nanorods, nanobelts, and nanoflowers [295-298]. The solvothermal method is almost identical to the hydrothermal method except the solvent used. If water is used as the solvent, the method is called “hydrothermal synthesis”. The synthesis under hydrothermal conditions is usually performed below the supercritical temperature of water (374 ^{o}C) in a closed bomb [299, 300]. The high-pressure acid-digestion vessel that is usually used in a hydrothermal process can be seen in **Figure 2.17**.

In the solvothermal, the temperature can be elevated much higher than that in hydrothermal technique, since variety of organic solvent with high boiling point can be chosen. There are several solvents that are usually used in solvothermal such as glycol, ammonia, urea and some organic solvents. The solvothermal route takes the benefits of both the sol-gel and hydrothermal technique [301, 302]. Thus solvothermal synthesis allows for the precise control over the size, shape distribution, and the crystallinity of the products. These characteristics can be altered by changing certain experimental parameters, including reaction temperature, reaction time, solvent type, surfactant and precursor.

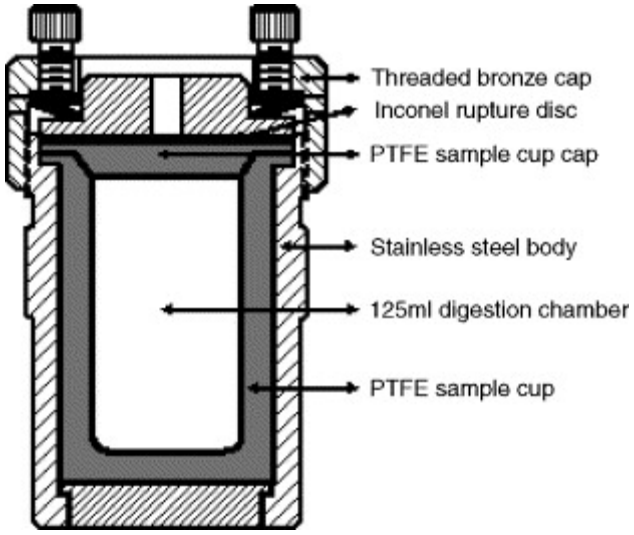

Figure 2.17 High-pressure acid-digestion vessel (Parr Instrument Co. Model 4748) [303].

preparationof fine particles of organic metal oxide by using the hydrothermal technique is believed to occur in two-step process [304]. First, the metal salt solution will be hydrolyzed to metal hydroxides. After that, the hydroxides will dehydrate, yielding the metal oxide desired. The rate of the overall reaction is affected by the temperature, pressure, water, and the dielectric constant of the solvent. The hydroxide of the metal salt is favored by a high dielectric constant, while the dehydration of the metal hydroxide is favored by a low dielectric constant [304, 305].

In preparing manganese oxide or cobalt oxide, there are several precursors that can be used as starting materials such as manganese nitrate, manganese oxalates, manganese acetates, and cobalt nitrate. Usually the hydrothermal method is carried out as follows. An amount of precursors is added to distilled water, stirred at room temperature to form a homogeneous solution. Then the solution is transferred into a Teflon-lined autoclave and hydrothermally treated at 90-200 ^{o}C for several hours. The autoclaves are quenched and the crystalline powder products are washed and dried [296, 306, 307]. Using the hydrothermal synthesis, a number of manganese

nanoparticle have prepared as summarized in **Table 2.10**. The particle size clearly depends on the reaction temperature and starting materials used.

Table 2.10. Synthesis condition and diameter crystalline size of hydrothermal crystallized manganese-based materials.

Sample	Starting material	Oxidant	Solvent	T/°C	Diameter, nm	Morphology	Ref.
δ-MnO_2	$MnSO_4.H_2O$	$KMnO_4$	H_2O	160	-	nanorods	[290]
β-MnO_2	$Mn(NO_3)_2$	-	H_2O	170	-	nanowire	[306]
α-MnO_2	$MnSO_4.H_2O$	$KClO_3$	H_2O	150	150-200	Sea urchin	[308]
γ-MnO_2	$MnSO_4.H_2O$	$(NH_4)S_2O_8$	H_2O	90	20-40	nanowire	[307]
Na-OMS-2	$MnSO_4 \cdot H_2O$, Na_2-Cr_2O_7	-	H_2SO_4, H_2O	100	200	nano-urchins	[309]
Pyrolusite	$MnSO_4 \cdot H_2O$, Na_2-Cr_2O_7	-	H_2SO_4, H_2O	180	2-4	3D urchinlike	[309]
OMS-2	$MnSO_4 \cdot H_2O$, $K_2Cr_2O_7$	-	H_2SO_4, H_2O	120	2	nanorods	[310]
OMS-7	$MnSO_4 \cdot H_2O$	$KMnO_4$	H_2O	180	150-250	rodlike	[311]
OMS-2	$MnSO_4 \cdot H_2O$	$KMnO_4$	H_2O	120	150-250	wirelike	[311]
H-KOMS-2	$MnSO_4 \cdot H_2O$	$KMnO_4$	H_2O	120	150-250	nanowire	[311]
K-OMS-2	$MnSO_4 \cdot H_2O$	$KMnO_4$	H_2O	120	150-250	nanobelts	[311]
$Mn_xZn_yFe_{3-x-y}O_4$	$Mn(NO_3)_2.xH_2O$, $Fe(NO_3)_3.9H_2O$, and $Zn(NO_3)$	-	H_2O	95	11	-	[312]
γ-MnS	$Mn(CH_3COO)_2$, thioacetamide	-	H_2O	60	-	wurtzite	[313]
α-MnS	$MnCl_2 \cdot 4H_2O$, $N_2H_4 \cdot H_2O$, Na_2S	-	H_2O	180	170–200	nanooctahedrons	[314]
$SmMnO_3$	$MnCl_2$, $Sm(NO_3)_3$, KOH	$KMnO_4$	H_2O	240	-	orthorhombic	[315]
$DyMnO_3$	$MnCl_2$, $Dy(NO_3)_3$, KOH	$KMnO_4$	H_2O	240	-	orthorhombic	[315]
$TbMnO_3$	$MnCl_2$, Tb_4O_7 KOH	$KMnO_4$	H_2O	240	-	-	[315]

2.6.2.4 Electrochemical method

Electrochemical synthesis is a well-known and promising technique for preparing metal oxide, hydroxides and ceramic thin film because it provides several benefits, such as low energy consumption, low cost, high purity, as well as high degree of stability of the synthesized nanoparticles [316-319]. The electrochemical synthesis of

oxide particle requires an electrolytic cell, generally consisting of two electrodes, which are anodic (redox change) and cathodic (base generation). In anodic oxidation, a metal ion or complex in a lower oxidation state is oxidized to a higher oxidation state anodically at the electrode surface. The pH value of the solution or electrolyte is adjusted so that the initial oxidation state is stable, and then the electrogenerated higher oxidation state experiences hydrolysis to a metal oxide or hydroxide [317, 320]. The reaction of anodic oxidation scheme can be seen below.

$$M^{2+} \longrightarrow M^{(z+\Delta)} + \Delta e^{-} \tag{2.39}$$

$$M^{(z+\Delta)} + (z+\Delta)\ OH^{-} \longrightarrow M(OH)_{z+\Delta} \longrightarrow MO_{\left(\frac{z+\Delta}{2}\right)} + \frac{(z+\Delta)}{2}\ H_2O \tag{2.40}$$

In the cathodic method, cathodic currents are used to generate a base at an electrode surface, and the electrogenerated base then hydrolyses metal ions or complexes. The pH value at the electrode surface is considerably higher than that of the bulk solution [321]. One example of base electrogeneration can be seen below.

$$2H_2O + 2e^{-} \rightarrow H_2 + 2OH^{-} \tag{2.41}$$

$$NO_3^{-} + H_2O + 2e^{-} \rightarrow NO_2^{-} + 2OH^{-} \tag{2.42}$$

$$\text{metal ion} \xrightarrow{\text{base}} \text{metal hydroxide} \longrightarrow \text{metal oxide} \tag{2.43}$$

Manganese dioxide (MnO_2) nanowires with an average particle size of 30-70 nm have been prepared by the cathodic electrodeposition technique. The electrochemical cell uses the cathodic substrate centered between two co-planar graphite counter electrodes. Cathodic deposits were obtained on a steel electrode (316 L, 100 mm x 50 mm x 0.5 mm) by the galvanostatic mode deposition at the current density of 2 mA cm^{-2} (deposition time was 10 min) and without stirring using an Autolab 302 electrochemical workstation system [319].

2.6.2.5 Impregnation method

Impregnation method is used for preparing catalysts that species in solution are deposited on the high-surface of the support. The most attractive feature of this technique is its simplicity in practical execution on both laboratory and industrial scales [322, 323]. Furthermore, by using impregnation technique, the metal species can be easily dispersed on the support. Usually, the synthesis of catalysts using the impregnation technique involves three steps: First, contacting the support with the aqueous precursors for a certain period of time. After that, the support is dried to remove the imbibed liquid. Finally, the catalyst is activated by calcination, reduction or other appropriate treatment [270, 324]. Using this method, Ag/TiO_2 as shown in **Figure 2.18** with highly dispersion on the catalyst has been synthesized.

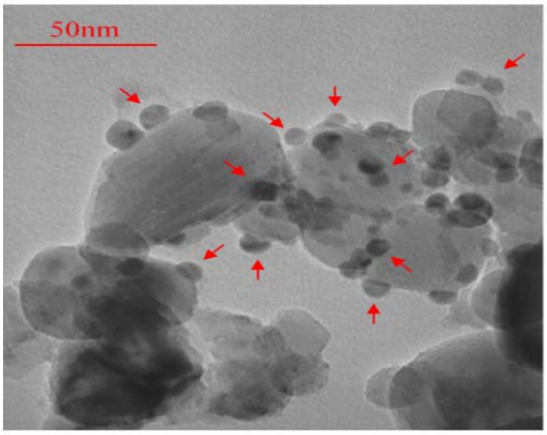

Figure 2.18 TEM image of distribution of Ag species on TiO_2 support [325].

In practice, two methods of contacting may be distinguished in catalyst synthesis using impregnation technique, depending on the total amount of solution that used. Incipient wetness impregnation methods, also called dry impregnation, are a procedure whereby a certain volume of the metal-containing solution is added to a catalyst support containing the same or less pore volume as the volume of the solution that was added [326-328]. If excess volume of solution is used, the technique is referred to as wet impregnation or dipping [14, 329].

Manganese oxide nanoparticles and its supported Co_3O_4 nano particles have been prepared according to the wet impregnation to investigate their effects on stability, activity of the catalysts for phenol degradation in aqueous solution. This catalyst has a significant synergistic effect in reaction because a highly dispersion can be obtained [330].

2.6.2.6 Ion exchange method

Term of ion exchange is used to describe all processes where ionic species from aqueous solution are attracted electrostatically by charge sites on the support surface [331]. Ion exchange is the reversible interchange of ions between a solid and a liquid in which there is no permanent change in the structure of the solid, which is the ion-exchange material [332]. The method of ion exchange allows for the introduction, in a controlled way, of a precursor from aqueous solution onto the support and is usually followed by drying, calcination and reduction [333].

In preparing the catalyst, the most common material suitable for ion exchange method, include zeolite, cationic clay, and double layered hydroxides [334-336]. These are ideal ion exchangers because they have crystalline lattice bearing electric charges which is a prerequisite for stability of the crystalline structure [337].

Zeolites are cationic exchangers. One of most important properties of zeolites is having a high ion exchange capacity, crystalline structure, and uniform pore sizes. The structure of zeolite is a 3 dimensional framework structure composed of Al_2O_3 tetrahedrons (trivalent cations, Al^{3+}) and SiO_4 (quadrivalent, Si_4^{+}) as the building block, which are connected with one another by sharing an oxygen atom. The anionic framework charge is filled by cations, and these cations are often accessible to ion-exchange through the zeolite pore system [338].

Preparation of zeolite supported metals by ion exchange technique is simple. A fixed amount of zeolite sample were added to Mn (II) nitrate solution in solid to liquid ratio of 1:67 and stirred for 5 hours at 85 ^{o}C, and then the mixture was aged for 16 hours. The solution was filtered and washed with de-ionized water. The collected solid was

dried and then calcined. Using this method Mn-containing catalyst has been synthesized [339]. Although ion exchange technique is usually used to prepare zeolite supported metals, there are virtually no advantages to the method except familiarity [338].

2.6.3 Gas to solid synthesis

A wide variety of gas-phase techniques have been developed for the fabrication of solid catalysts for a variety of applications. Currently, some different techniques, inert-gas condensation (IGC) and chemical vapor deposition (CVD) have been employed for developing catalysts which have nanoparticle size and uniform morphology [340, 341]. To date, intensive research activities to improve the synthesis methods and conditions, product quality and productivity are still continuing [342]. Both methods IGC and CVD routes will be explained further below.

2.6.3.1 Inert gas condensation method

The inert gas condensation (IGC) is the most commonly used technique of gas to solid synthesis involving the condensation of a vapour phase produced by the heating of a solid or liquid starting material. This method has been widely used in the synthesis of ultrafine metal particles since the 1930s [343]. The process is commonly used to synthesize nanoparticles and thin film material and consists of three main steps [344, 345]:

a. Generating a vapor phase by evaporation or sublimation of the material
b. A rapid controlled condensation, and
c. Formation of the particle and/or film by nucleation and growth.

A model of a typical apparatus used is shown in **Figure 2.19**. It consists of an ultrahigh vacuum chamber, which is equipped with a liquid nitrogen-cooled finger, scraper and collector. The vacuum chamber is first pumped to a vacuum by a turbo-molecular pump ($< 10^{-5}$ Pa). In the case of nano material synthesis, the chamber is

then back-filling with a low-pressure high-purity inert gas, at pressure of typically a few hundred Pa. The starting material, mostly a metal, is vaporized by resistive heating in a crucible. Some alternative energy sources can be used such as radiofrequency heating, sputtering, electron beam heating, laser/plasma heating or ion sputtering [343, 346-348].

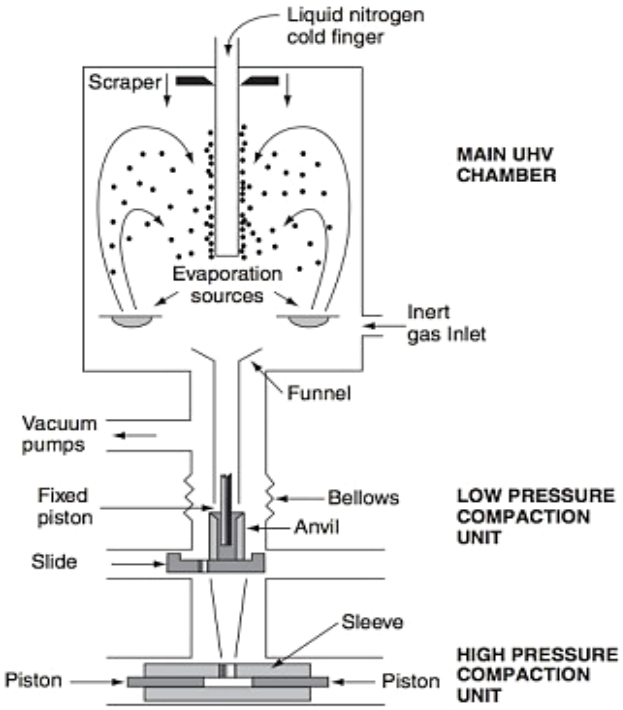

Figure 2.19 Schematic of the gas condensation chamber for the synthesis of nanostructured materials [347].

In the fabrication process of fine particles, the metal atoms are evaporated, as a result of heating, collide with the inert gas atoms inside the chamber. Vapor from the hot source migrates into a cooler gas by a combination of convective flow and diffusion. The vaporized species then lose their energy kinetics via collusion with inert gas molecules. At high supersaturation, the vapors rapidly nucleate, forming large number of clusters that grow via coalescence, agglomeration and result in the formation of particles. The formed powder particles are collected on the surface of the cold finger [345, 349, 350]. The advantage of IGC technique is the products have high quality crystalline structure due to particle formation in a quasi-thermal equilibrium state. However, the product cannot be obtained continuously due to semi-

batch process leading to low production rates. Further, the technique also cannot be used for producing multicomponent materials [343, 351].

Metal oxide nanoparticles such as manganese oxides have also been produced by the controlled oxidation of metal nanoparticles synthesized by evaporation of the metal. Manganese oxide-base catalysts, β-Mn, MnO, Mn_3O_4, Mn_5O_8, Mn_2O_3 nanoparticles, have been prepared by this technique with average particle size of about 43 nm [352, 353].

2.6.3.2 Chemical vapor deposition method

Chemical vapor deposition (CVD) is a chemical process, in which volatile compounds react and/ or decompose on the substrate surface to produce the desired deposit. Frequently, volatile by-products are also produced, which are removed by gas flow through the reaction chamber. CVD technique is a widely used route to produce high-purity, high-performance materials, which first patented by de Lodyguine in 1893 [354-356].

The starting materials used in CVD process are usually metal precursors such as metal hydrides, metal chlorides, and metal compounds [357-359]. In the case of metal compounds, the process is generally referred to as metal-organic chemical vapor deposition (MOCVD) [360]. The starting materials are introduced into a reactor with the aid of a carrier gas, heated by irradiation of UV light or electrical plasma in a process chamber and then decompose.

There are a number of CVD processes used for the formation of nanoparticles such as the classical (thermally activated/pydrolytic), metal-organic, plasma-assisted, and photo CVD methodologies [355, 361]. Among them, thermal CVD is the most generally used technique. The advantages of this methodology are producing uniform, pure, high yield, and reproduce nanoparticles and films [362-364]. Of course, nanostructured particles of manganese oxide have been synthesized using this method by some arrangement of the equipment. The equipment was used to produce the MnO_x nanostructured consisting of the following three parts; a precursor

evaporator, a hot-wall reactor, and a particle trap (collector), as can be seen in **Figure 2.20**. The precursor was stored in a bubbler placed in an oil bath at 90 °C. The sorbent precursor was introduced into the system by bubbling argon. The bubbler was wrapped with heating tape (90 °C) to prevent any losses due to condensation. An additional inlet was connected to the reactor to supply air. All the precursor and carrier gases (air and argon) passed through an alumina tube placed in the hot-wall reactor (electric furnace). The synthesis temperature was controlled by a temperature controller and was varied from 500 to 1500 °C. After synthesis, the nanoparticles were collected outside the reactor tube, where the temperature was held at room temperature using a water-cooled jacket [365]. Using this method, MnO_2, Mn_2O_3, Mn_2O_3/Mn_3O_4, and Mn_3O_4, as shown in **Figure 2.21** with particle size from 10 to 30 nm, have been synthesized.

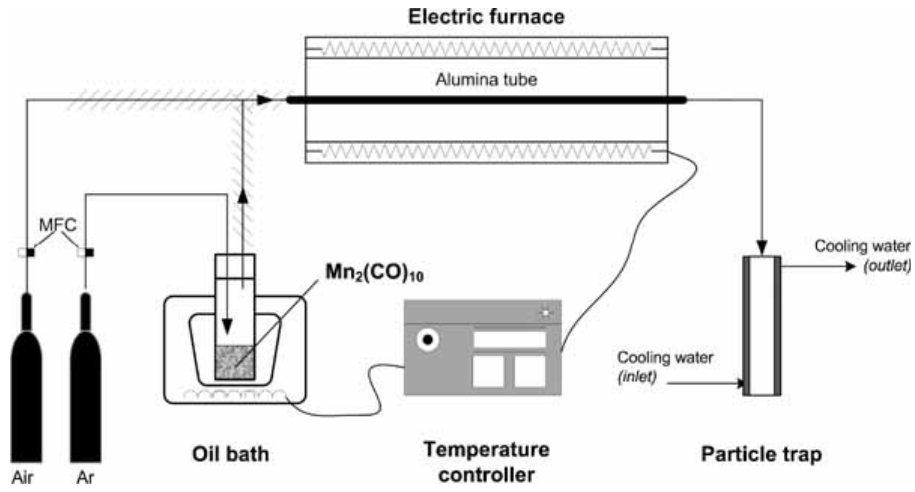

Figure 2.20 Schematic diagram of the CVD technique apparatus [365].

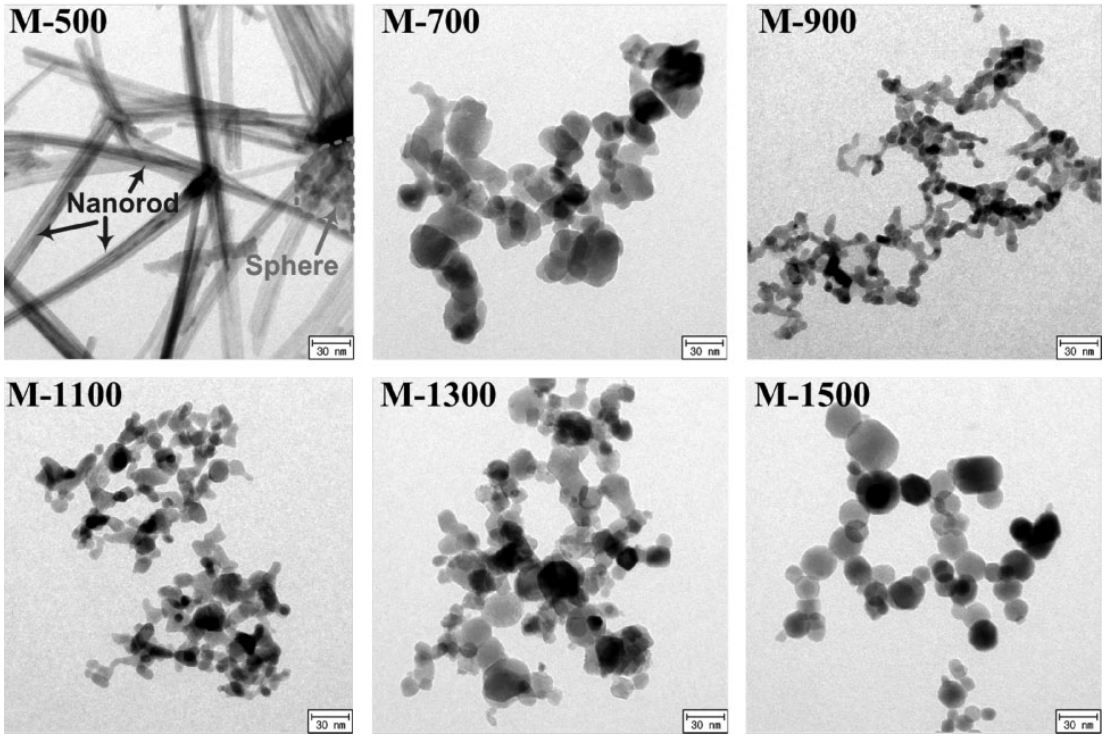

Figure 2.21 Transmission electron images of MnO_x particles prepared by the CVD technique [365].

2.7 Summary

Among all the water treatment technologies described above, advanced oxidation processes (AOPs) are the promising technology that can be used as an effective process to completely degrade organic compounds and also can be operated at ambient conditions. Cavitation is defined as the phenomena of the formation, growth and subsequent collapse of micro-bubbles or cavities occurring in extremely small interval of time. This technology has been shown to be feasible on a small scale, but the commercialization of cavitation technology is still a challenge, due to the high energy requirement of the process. Photocatalytic oxidation is based on the activation of semiconductor materials by the action of radiation with an appropriate wavelength. Photocatalytic oxidation technique has been proven for removal of toxic organics in aqueous solution, but this technique is expensive to run because it is slow rate of degradation leading to high power consume (electrical energy). Fenton chemistry is a

promising technique, using ferrous ions (Fe^{2+}) in aqueous acidic medium, and can degrade organic pollutants completely. However, a common problem that is often encountered in the process is requiring acidic condition, large quantity of chemical reagents, very slow catalysis of the ferrous ions generation and large production of ferric hydroxide sludge. Chemical oxidation processes constitute the use of oxidizing agents, such as hydrogen peroxide and ozone, for generating hydroxyl radicals. Hydrogen peroxide (H_2O_2) is the most powerful oxidant compared to ozone and its application in the treatment of various inorganic and organic pollutants is well established. However, the use of individual oxidant is not that efficient in oxidizing more complex and recalcitrant materials due to low rate of reaction. Further, combining the use of oxidants with a suitable catalyst will effectively enhance rate of reaction. Apart from hydroxyl radicals, sulphate radicals have also been suggested as an alternative because it has standard reduction potential (E^0) of HSO_5^-/HSO_4^- = 1.82 V and generally oxidizes faster than hydrogen peroxide which has standard reduction potential (E^0) of H_2O_2/H_2O = 1.76 V. Heterogeneous catalyst is quite promising to be applied because no need for process separation unit. Heterogeneous catalysts used in the water treatment process are generally from noble metals or metal oxides in supported or unsupported mode. One that should be considered is the use of environmentally benign materials and easy to obtain. For this purpose, the use of Mn oxide is an alternative to be developed because Mn oxides are widely presence in nature and has low toxicity to the environment. Thus, advanced oxidation processes (AOPs) using chemicals as an oxidant is the most suitable to degrade toxic organics in aqueous solutions such as phenol and derivatives due to lower operating costs, no special equipment, less energy consumption, and high conversion of organic pollutants.

Reference

1. Dohnal, V. and D. Fenclova, *Air-water partitioning and aqueous solubility of phenols.* Journal of Chemical & Engineering Data, 1995. **40**(2): p. 478-483.

2. Keith, L. and W. Telliard, *ES&T Special Report: Priority pollutants: I-A perspective view.* Environmental Science & Technology, 1979. **13**(4): p. 416-423.

3. Fortuny, A., C. Bengoa, J. Font, and A. Fabregat, *Bimetallic catalysts for continuous catalytic wet air oxidation of phenol.* Journal of Hazardous Materials, 1999. **64**(2): p. 181-193.

4. Christoskova, S.G., M. Stoyanova, and M. Georgieva, *Low-temperature iron-modified cobalt oxide system: Part 2. Catalytic oxidation of phenol in aqueous phase.* Applied Catalysis A: General, 2001. **208**(1-2): p. 243-249.

5. Matheswaran, M. and I.S. Moon, *Influence parameters in the ozonation of phenol wastewater treatment using bubble column reactor under continuous circulation.* Journal of Industrial and Engineering Chemistry, 2009. **15**(3): p. 287-292.

6. M. Bosnic, J.B. and, and R.P. Daniels, *Pollutants in tannery effluents.* United Nations Industrial Development Organization, 2000: p. 1-26.

7. Isaev, A.B., Z.M. Aliev, and D.S. Alieva, *Influence of the dissolved oxygen under pressure to electrochemical oxidation toluene and acetone aqueous mixtures.* Electrochemistry Communications, 2007. **9**(6): p. 1400-1403.

8. Ahmaruzzaman, M., *Role of fly ash in the removal of organic pollutants from wastewater.* Energy & Fuels, 2009. **23**(3): p. 1494-1511.

9. Scott, J.P. and D.F. Ollis, *Integration of chemical and biological oxidation processes for water treatment: Review and recommendations.* Environmental Progress, 1995. **14**(2): p. 88-103.

10. Stasinakis, A., S, *Use of selected advanced oxidation processes (AOPs) for wastewater treament- a mini review.* Global NEST Journal, 2008. **10**(3): p. 376-385.

11. Dias, A.M.A., Moita, I., Alves, M. M., Ferreira, E. C., Páscoa, R. and Lopes, J. A., *Activated sludge process monitoring through in situ near-infrared spectral analysis.* Water Science & Technology, 2008. **57**(10): p. 1643-1650.

12. Gogate, P.R. and A.B. Pandit, *A review of imperative technologies for wastewater treatment I: oxidation technologies at ambient conditions.* Advances in Environmental Research, 2004. **8**(3–4): p. 501-551.

13. Huang, C.P., C. Dong, and Z. Tang, *Advanced chemical oxidation: Its present role and potential future in hazardous waste treatment.* Waste Management, 1993. **13**(5–7): p. 361-377.

14. Saputra, E., S. Muhammad, H. Sun, H.M. Ang, M.O. Tadé, and S. Wang, *Red mud and fly ash supported Co catalysts for phenol oxidation.* Catalysis Today, 2012. **190**(1): p. 68-72.

15. Mijangos, F., F. Varona, and N. Villota, *Changes in solution color during phenol oxidation by Fenton reagent.* Environmental Science & Technology, 2006. **40**(17): p. 5538-5543.

16. Wei, T.-Y., Y.-Y. Wang, and C.-C. Wan, *Photocatalytic oxidation of phenol in the presence of hydrogen peroxide and titanium dioxide powders.* Journal of Photochemistry and Photobiology A: Chemistry, 1990. **55**(1): p. 115-126.

17. Miyamura, H., R. Matsubara, Y. Miyazaki, and S. Kobayashi, *Aerobic oxidation of alcohols at room temperature and atmospheric conditions catalyzed by reusable gold nanoclusters stabilized by the benzene rings of polystyrene derivatives.* Angewandte Chemie, 2007. **119**(22): p. 4229-4232.

18. Cole-Hamilton, D.J., *Homogeneous catalysis-new approaches to catalyst separation, recovery, and recycling.* Science, 2003. **299**(5613): p. 1702-1706.

19. Rinaldi, R. and F. Schuth, *Design of solid catalysts for the conversion of biomass.* Energy & Environmental Science, 2009. **2**(6): p. 610-626.

20. Centi, G. and S. Perathoner, *Integrated design for solid catalysts in multiphase reactions.* ChemInform, 2003. **34**(45).

21. Ying, J.Y., *Design and synthesis of nanostructured catalysts.* Chemical Engineering Science, 2006. **61**(5): p. 1540-1548.

22. Sinfelt, J.H., *Role of surface science in catalysis.* Surface Science, 2002. **500**(1–3): p. 923-946.

23. Deutschmann, O., H. Knözinger, K. Kochloefl, and T. Turek, *Heterogeneous catalysis and solid catalysts*, in *Ullmann's Encyclopedia of Industrial Chemistry*. 2000, Wiley-VCH Verlag GmbH & Co. KGaA.

24. Acres, G.J.K., A.J. Bird, J.W. Jenkins, and F. King, *The design and preparation of supported catalysts*, in *Catalysis*, C. Kemball and D.A. Dowden, Editors. 1981, The Royal Society of Chemistry. p. 1-30.

25. Mishra, V.S., V.V. Mahajani, and J.B. Joshi, *Wet Air oxidation.* Industrial & Engineering Chemistry Research, 1995. **34**(1): p. 2-48.

26. F, L., *A review of industrial catalytic wet air oxidation processes.* Catalysis Today, 1996. **27**(1–2): p. 195-202.

27. Li, L., P. Chen, and E.F. Gloyna, *Generalized kinetic model for wet oxidation of organic compounds.* AIChE Journal, 1991. **37**(11): p. 1687-1697.

28. Portela Miguélez, J.R., J. López Bemal, E. Nebot Sanz, and E. Martínez de la Ossa, *Kinetics of wet air oxidation of phenol.* Chemical Engineering Journal, 1997. **67**(2): p. 115-121.

29. Kolaczkowski, S.T., P. Plucinski, F.J. Beltran, F.J. Rivas, and D.B. McLurgh, *Wet air oxidation: A review of process technologies and aspects in reactor design.* Chemical Engineering Journal, 1999. **73**(2): p. 143-160.

30. Maugans, C., B., and Ellis, C., *Wet air oxidation: A review of commercial sub-critical hydrotermal treatment.* IT3'02 Conference, New Orlens, Louisiana, 2002.

31. Mantzavinos, D., R. Hellenbrand, A.G. Livingston, and I.S. Metcalfe, *Reaction mechanisms and kinetics of chemical pretreatment of bioresistant organic molecules by wet air oxidation.* Water Science and Technology, 1997. **35**(4): p. 119-127.

32. Arslan-Alaton, I. and J.L. Ferry, *Application of polyoxotungstates as environmental catalysts: wet air oxidation of acid dye Orange II.* Dyes and Pigments, 2002. **54**(1): p. 25-36.

33. Akita, K. and F. Yoshida, *Bubble size, interfacial area, and liquid-phase mass transfer coefficient in bubble columns.* Ind. Eng. Chem., Process Des. Develop., 1974. **13**(1): p. 84-91.

34. Himmelblau, D.M., *Solubilities of Inert Gases in Water. 0° C. to Near the Critical Point of Water.* Journal of Chemical & Engineering Data, 1960. **5**(1): p. 10-15.

35. Luck, F., *A review of industrial catalytic wet air oxidation processes.* Catalysis Today, 1996. **27**(1–2): p. 195-202.

36. Joglekar, H.S., S.D. Samant, and J.B. Joshi, *Kinetics of wet air oxidation of phenol and substituted phenols.* Water Research, 1991. **25**(2): p. 135-145.

37. Debellefontaine, H. and J.N. Foussard, *Wet air oxidation for the treatment of industrial wastes. Chemical aspects, reactor design and industrial applications in Europe.* Waste Management, 2000. **20**(1): p. 15-25.

38. Tester Jefferson, W., H.R. Holgate, J. Armellini Fred, A. Webley Paul, R. Killilea William, T. Hong Glenn, and E. Barner Herbert, *Supercritical water oxidation technology*, in *Emerging Technologies in Hazardous Waste Management III*. 1993, American Chemical Society. p. 35-76.

39. Mantzavinos, D., A.G. Livingston, R. Hellenbrand, and I.S. Metcalfe, *Wet air oxidation of polyethylene glycols; mechanisms, intermediates and*

implications for integrated chemical-biological wastewater treatment. Chemical Engineering Science, 1996. **51**(18): p. 4219-4235.

40. Patterson, D.A., I.S. Metcalfe, F. Xiong, and A.G. Livingston, *Wet air oxidation of linear alkylbenzene sulfonate 2. effect of pH.* Industrial & Engineering Chemistry Research, 2001. **40**(23): p. 5517-5525.

41. Willms, R.S., A.M. Balinsky, D.D. Reible, D.M. Wetzel, and D.P. Harrison, *Aqueous-phase oxidation: The intrinsic kinetics of single organic compounds.* Industrial & Engineering Chemistry Research, 1987. **26**(1): p. 148-154.

42. López Bernal, J., J.R. Portela Miguélez, E. Nebot Sanz, and E. Martínez de la Ossa, *Wet air oxidation of oily wastes generated aboard ships: kinetic modeling.* Journal of Hazardous Materials, 1999. **67**(1): p. 61-73.

43. Laughlin, R.G.W., T. Gallo, and H. Robey, *Wet air oxidation for hazardous waste control.* Journal of Hazardous Materials, 1983. **8**(1): p. 1-9.

44. Imamura, S., *Catalytic and noncatalytic wet oxidation.* Industrial & Engineering Chemistry Research, 1999. **38**(5): p. 1743-1753.

45. Foussard, J.-N., H. Debellefontaine, and J. Besombes-Vailhe, *Efficient elimination of organic liquid wastes: Wet air oxidation.* Journal of Environmental Engineering, 1989. **115**(2): p. 367-385.

46. Kalam, A. and J. Joshi, *Regeneration of spent earth by wet oxidation.* Journal of the American Oil Chemists' Society, 1988. **65**(9): p. 1536-1540.

47. Day, D.C., R.R. Hudgins, and P.L. Silveston, *Oxidation of propionic acid solutions.* The Canadian Journal of Chemical Engineering, 1973. **51**(6): p. 733-740.

48. Raffainer, I.I. and P. Rudolf von Rohr, *Promoted wet oxidation of the azo dye orange II under mild conditions.* Industrial & Engineering Chemistry Research, 2001. **40**(4): p. 1083-1089.

49. Mantzavinos, D., E. Lauer, R. Hellenbrand, A.G. Livingston, and I.S. Metcalfe, *Wet oxidation as a pretreatment method for wastewaters contaminated by bioresistant organics.* Water Science and Technology, 1997. **36**(2–3): p. 109-116.

50. Wilhelmi, A.R., Knoop, P. V., *Wet air oxidation-An alternative to inceneration.* Chem. Eng. Progress, 1979. **75**(8): p. 46.

51. Đonlagić, J. and J. Levec, *Does the catalytic wet oxidation yield products more amenable to biodegradation.* Applied Catalysis B: Environmental, 1998. **17**(1–2): p. L1-L5.

52. Chen, G., L. Lei, and P.-L. Yue, *Wet oxidation of high-concentration reactive dyes.* Industrial & Engineering Chemistry Research, 1999. **38**(5): p. 1837-1843.

53. Lavric, E.D., H. Weyten, J. De Ruyck, V. Pleşu, and V. Lavric, *Delocalized organic pollutant destruction through a self-sustaining supercritical water oxidation process.* Energy Conversion and Management, 2005. **46**(9–10): p. 1345-1364.

54. Kritzer, P. and E. Dinjus, *An assessment of supercritical water oxidation (SCWO): Existing problems, possible solutions and new reactor concepts.* Chemical Engineering Journal, 2001. **83**(3): p. 207-214.

55. Twigg, *Catalyst handbook / edited by Martyn V. Twigg*.

56. Wagner, W. and A. Pruss, *The IAPWS formulation 1995 for the thermodynamic properties of ordinary water substance for general and scientific use.* Journal of Physical and Chemical Reference Data, 2002. **31**(2): p. 387-535.

57. Kodra, D. and V. Balakotaiah, *Autothermal oxidation of dilute aqueous wastes under supercritical conditions.* Industrial & Engineering Chemistry Research, 1994. **33**(3): p. 575-580.

58. Thiel, R., Dietz, K., Kerres, H., Rosenbaum, Steiner, S., *Process for wet oxidation of organic subtances.* U.S. Patent No. 4141829, 1979.

59. Minok, K., W.K. Lee, and C.H. Lee, *New reactor system for supercritical water oxidation and its application on phenol destruction.* Chemical Engineering Science, 1997. **52**(7): p. 1201-1214.

60. Goto, M., T. Nada, A. Ogata, A. Kodama, and T. Hirose, *Supercritical water oxidation for the destruction of municipal excess sludge and alcohol distillery wastewater of molasses.* The Journal of Supercritical Fluids, 1998. **13**(1–3): p. 277-282.

61. A, S., *Production of useful organic matter from sludge using hydrothermal treatment.* Water Research, 2000. **34**(3): p. 945-951.

62. Söğüt, O.Ö. and M. Akgün, *Treatment of dyehouse waste-water by supercritical water oxidation: a case study.* Journal of Chemical Technology & Biotechnology, 2010. **85**(5): p. 640-647.

63. Fassbender, A.G., Richland, W., *Sewage Treatment Methode.* U.S. Patent No. 5433868, 1995.

64. Portela, J.R., E. Nebot, and E. Martínez de la Ossa, *Generalized kinetic models for supercritical water oxidation of cutting oil wastes.* The Journal of Supercritical Fluids, 2001. **21**(2): p. 135-145.

65. D.M. Harradine, S.J.B., P.C. Dell'orco, R.B. Dyer, B.R. Foy, J.M. Robinson, J.A. Sanchez, T. Spontarelli, and J.D. Wander, *Oxidation chemistry of energetic materials in supercritical water.* Hazardous Waste and Hazardous Materials, 1993. **10**(2): p. 233-246.

66. Kronholm, J., T. Kuosmanen, K. Hartonen, and M.-L. Riekkola, *Destruction of PAHs from soil by using pressurized hot water extraction coupled with supercritical water oxidation.* Waste Management, 2003. **23**(3): p. 253-260.

67. Mota, A., L., N, Albuquerque, L., F., Beltrame, L., T., C, Chiavone-Filho, O., Machulek Jr, A., Nascimento, C., A., O., *Advanced oxidation processes and their application in the petroleum industry: A review.* Brazilian Journal of Petroleum and Gas, 2008. **2**(3): p. 122-142.

68. Johnston, L., E., *Decontamination and disposal of PCB wastes.* Environmetal Health Perspectives, 1985. **60**: p. 339-346.

69. Qi, X.-H., Y.-Y. Zhuang, Y.-C. Yuan, and W.-X. Gu, *Decomposition of aniline in supercritical water.* Journal of Hazardous Materials, 2002. **90**(1): p. 51-62.

70. Blaney Carol, A., L. Li, F. Gloyna Earnest, and U. Hossain Shafi, *Supercritical water oxidation of pulp and paper mill sludge as an alternative to incineration*, in *Innovations in Supercritical Fluids*. 1995, American Chemical Society. p. 444-455.

71. Han, C., S. Qin, M. Li, L. Xing, S. Li, and G. Jing. *Oxidation of oilfield sludge in supercritical water*. in *Bioinformatics and Biomedical Engineering , 2009. ICBBE 2009. 3rd International Conference on*. 2009.

72. Söğüt, O.Ö. and M. Akgün, *Treatment of textile wastewater by SCWO in a tube reactor.* The Journal of Supercritical Fluids, 2007. **43**(1): p. 106-111.

73. Ruamchat, T., R. Hayashi, S. Ngamprasertsith, and Y. Oshima, *A novel on-site system for the treatment of pharmaceutical laboratory wastewater by supercritical water oxidation.* Environmental sciences, 2006. **13**(5): p. 297-304.

74. Kiddle, J.J. and S.P. Mezyk, *Reductive destruction of chemical warfare agent simulants in water.* The Journal of Physical Chemistry B, 2004. **108**(28): p. 9568-9570.

75. Spritzer, M.H., D.A. Hazlebeck, and K.W. Downey, *Supercritical water oxidation of chemical agents, and solid propellants.* Journal of Energetic Materials, 1995. **13**(3-4): p. 185-212.

76. Webley, P.A., *Oxidation kinetics of model compounds of metabolic waste in supercritical water*. 1990.

77. LaJeunesse, C.A., Haroldsen, B. L., Rice, S. F., Brown, B. G., *Hydrothermal oxidation of navy shipboard excess hazardous materials.* Sandia Report, 1997. **SAND97-8212**.

78. Dixon, D., Johnston, K., Richard, L., *Supercritical fluid.* in AccessScience, ©McGraw-Hill Companies, 2008.

79. Kruse, A. and E. Dinjus, *Hot compressed water as reaction medium and reactant: Properties and synthesis reactions.* The Journal of Supercritical Fluids, 2007. **39**(3): p. 362-380.

80. Lee, H.-C., J.-H. In, J.-H. Kim, K.-Y. Hwang, and C.-H. Lee, *Kinetic analysis for decomposition of 2,4-Dichorophenol by supercritical water oxidation.* Korea J. Chem. Eng, 2005. **22**(6): p. 882-888.

81. Thornton, T.D. and P.E. Savage, *Kinetics of phenol oxidation in supercritical water.* AIChE Journal, 1992. **38**(3): p. 321-327.

82. Li, R., P.E. Savage, and D. Szmukler, *2-Chlorophenol oxidation in supercritical water: Global kinetics and reaction products.* AIChE Journal, 1993. **39**(1): p. 178-187.

83. Mizuno, T., M. Goto, A. Kodama, and T. Hirose, *Supercritical water oxidation of a model municipal solid waste.* Industrial & Engineering Chemistry Research, 2000. **39**(8): p. 2807-2810.

84. Goto, M., T. Nada, A. Kodama, and T. Hirose, *Kinetic analysis for destruction of municipal sewage sludge and alcohol distillery wastewater by supercritical water oxidation.* Industrial & Engineering Chemistry Research, 1999. **38**(5): p. 1863-1865.

85. Portela, J.R., E. Nebot, and E. Martínez de la Ossa, *Kinetic comparison between subcritical and supercritical water oxidation of phenol.* Chemical Engineering Journal, 2001. **81**(1–3): p. 287-299.

86. Crain, N., S. Tebbal, L. Li, and E.F. Gloyna, *Kinetics and reaction pathways of pyridine oxidation in supercritical water.* Industrial & Engineering Chemistry Research, 1993. **32**(10): p. 2259-2268.

87. Rivas, F.J., O. Gimeno, J.R. Portela, E.M. de la Ossa, and F.J. Beltrán, *Supercritical water oxidation of olive oil mill wastewater.* Industrial & Engineering Chemistry Research, 2001. **40**(16): p. 3670-3674.

88. Veriansyah, B., T.-J. Park, J.-S. Lim, and Y.-W. Lee, *Supercritical water oxidation of wastewater from LCD manufacturing process: kinetic and formation of chromium oxide nanoparticles.* The Journal of Supercritical Fluids, 2005. **34**(1): p. 51-61.

89. Suqin, L. and X. Yunfei. *Treatment of oily wastewater generated from steel production by supercritical water oxidation*. in *Advanced Management Science (ICAMS), 2010 IEEE International Conference on*. 2010.

90. Cui, B., F. Cui, G. Jing, S. Xu, W. Huo, and S. Liu, *Oxidation of oily sludge in supercritical water.* Journal of Hazardous Materials, 2009. **165**(1–3): p. 511-517.

91. Anitescu, G., Tavlarides, Lawrence L., *Oxidation of aroclor 1248 in supercritical water: A global kinetic study.* Industrial & Engineering Chemistry Research, 2000. **39**(3): p. 583-591.

92. Martino, C.J., P.E. Savage, and J. Kasiborski, *Kinetics and products from o-cresol Oxidation in supercritical water.* Industrial & Engineering Chemistry Research, 1995. **34**(6): p. 1941-1951.

93. Anikeev, V., A. Ermakova, and M. Goto, *Decomposition and oxidation reactions of aliphatic nitro compounds in supercritical water.* Kinetics and Catalysis, 2005. **46**(6): p. 821-825.

94. Aki, S.N.V.K. and M.A. Abraham, *An economic evaluation of catalytic supercritical water oxidation: Comparison with alternative waste treatment technologies.* Environmental Progress, 1998. **17**(4): p. 246-255.

95. Spivey, J., *Catalysis, Volume 18, A Review of Recent Literature* 2005. 198-pp.

96. Bhargava, S., J. Tardio, H. Jani, D. Akolekar, K. Föger, and M. Hoang, *Catalytic wet air oxidation of industrial aqueous streams.* Catalysis Surveys from Asia, 2007. **11**(1): p. 70-86.

97. F, L., *Wet air oxidation: past, present and future.* Catalysis Today, 1999. **53**(1): p. 81-91.

98. Roy, S., M. Vashishtha, and A.K. Saroha, *Catalytic wet air oxidation of oxalic acid using platinum catalysts in bubble column reactor: A review.* Journal of Engineering Science and Technology Review, 2010. **3**(1): p. 95-107.

99. Zhang, Y., D. Li, Y. Chen, X. Wang, and S. Wang, *Catalytic wet air oxidation of dye pollutants by polyoxomolybdate nanotubes under room condition.* Applied Catalysis B: Environmental, 2009. **86**(3–4): p. 182-189.

100. Perathoner, S. and G. Centi, *Wet hydrogen peroxide catalytic oxidation (WHPCO) of organic waste in agro-food and industrial streams.* Topics in Catalysis, 2005. **33**(1): p. 207-224.

101. Zou, L.Y., Y. Li, and Y.-T. Hung, *Wet air oxidation for waste treatment advanced physicochemical treatment technologies*, L.K. Wang, Y.-T. Hung, and N.K. Shammas, Editors. 2007, Humana Press. p. 575-610.

102. WU, Q., P.L. YUE, and X. HU, *Continuous catalytic wet air oxidation of phenol in a trickle bed reactor.* SUSTAINABLE ENERGY AND ENVIRONMENTAL TECHNOLOGIES Proceedings of the Third Asia-Pacific Conference, 2000.

103. Gallezot, P., S. Chaumet, A. Perrard, and P. Isnard, *Catalytic wet air oxidation of acetic acid on carbon-supported ruthenium catalysts.* Journal of Catalysis, 1997. **168**(1): p. 104-109.

104. Imamura, S., A. Doi, and S. Ishida, *Wet oxidation of ammonia catalyzed by cerium-based composite oxides.* Industrial & Engineering Chemistry Product Research and Development, 1985. **24**(1): p. 75-80.

105. Esplugas, S., J. Giménez, S. Contreras, E. Pascual, and M. Rodríguez, *Comparison of different advanced oxidation processes for phenol degradation.* Water Research, 2002. **36**(4): p. 1034-1042.

106. Matatov-Meytal, Y.I. and M. Sheintuch, *Catalytic abatement of water pollutants.* Industrial & Engineering Chemistry Research, 1998. **37**(2): p. 309-326.

107. Herrmann, J.-M., *Heterogeneous photocatalysis: fundamentals and applications to the removal of various types of aqueous pollutants.* Catalysis Today, 1999. **53**(1): p. 115-129.

108. Fogler, H.S., *Elements of chemical reaction engineering / H. Scott Fogler*.

109. Dittmeyer, R. and G. Emig, *Simultaneous heat and mass transfer and chemical reaction*, in *Handbook of Heterogeneous Catalysis*. 2008, Wiley-VCH Verlag GmbH & Co. KGaA.

110. Gomes, H.T., J.L. Figueiredo, and J.L. Faria, *Catalytic wet air oxidation of olive mill wastewater.* Catalysis Today, 2007. **124**(3–4): p. 254-259.

111. Pintar, A., M. Besson, and P. Gallezot, *Catalytic wet air oxidation of Kraft bleach plant effluents in a trickle-bed reactor over a Ru/TiO_2 catalyst.* Applied Catalysis B: Environmental, 2001. **31**(4): p. 275-290.

112. Minh, D.P., G. Aubert, P. Gallezot, and M. Besson, *Degradation of olive oil mill effluents by catalytic wet air oxidation: 2-Oxidation of p-hydroxyphenylacetic and p-hydroxybenzoic acids over Pt and Ru supported catalysts.* Applied Catalysis B: Environmental, 2007. **73**(3–4): p. 236-246.

113. Barbier, J., L. Oliviero, B. Renard, and D. Duprez, *Role of ceria-supported noble metal catalysts (Ru, Pd, Pt) in wet air oxidation of nitrogen and oxygen containing compounds.* Topics in Catalysis, 2005. **33**(1): p. 77-86.

114. Lee, D.-K. and D.-S. Kim, *Catalytic wet air oxidation of carboxylic acids at atmospheric pressure.* Catalysis Today, 2000. **63**(2–4): p. 249-255.

115. Pintar, A., J. Batista, and T. Tišler, *Catalytic wet-air oxidation of aqueous solutions of formic acid, acetic acid and phenol in a continuous-flow trickle-bed reactor over Ru/TiO$_2$ catalysts.* Applied Catalysis B: Environmental, 2008. **84**(1–2): p. 30-41.

116. Kim, K.-H. and S.-K. Ihm, *Heterogeneous catalytic wet air oxidation of refractory organic pollutants in industrial wastewaters: A review.* Journal of Hazardous Materials, 2011. **186**(1): p. 16-34.

117. Pirkanniemi, K. and M. Sillanpaa, *Heterogenous water phase catalysis as an environmental applicatian: a riview.* Chemosphere, 2002. **48**(2002): p. 1047-1060.

118. Kochetkova, R.P., A.F. Babikov, L.I. Shpilevskaya, I.P. Shiverskaya, S.A. Éppel, and F.K. Shmidt, *Liquid phase catalytic oxidation of phenol.* Chemistry and Technology of Fuels and Oils, 1992. **28**(4): p. 225-229.

119. Mvndale, V.D., H.S. Joglekar, A. Kalam, and J.B. Joshi, *Regeneration of spent activated carbon by wet air oxidation.* The Canadian Journal of Chemical Engineering, 1991. **69**(5): p. 1149-1159.

120. Stüber, F., J. Font, A. Fortuny, C. Bengoa, A. Eftaxias, and A. Fabregat, *Carbon materials and catalytic wet air oxidation of organic pollutants in wastewater.* Topics in Catalysis, 2005. **33**(1): p. 3-50.

121. Zhang, Q. and K.T. Chuang, *Alumina-supported noble metal catalysts for destructive oxidation of organic pollutants in effluent from a softwood kraft pulp mill.* Industrial & Engineering Chemistry Research, 1998. **37**(8): p. 3343-3349.

122. Cavani, F. and F. Trifiró, *Classification of industrial catalysts and catalysis for the petrochemical industry.* Catalysis Today, 1997. **34**(3–4): p. 269-279.

123. Glaze, W.H., J.-W. Kang, and D.H. Chapin, *The chemistry of water treatment processes involving ozone, hydrogen peroxide and ultraviolet radiation.* Ozone: Science & Engineering, 1987. **9**(4): p. 335-352.

124. Anipsitakis, G.P. and D.D. Dionysiou, *Radical generation by the interaction of transition metals with common oxidants.* Environmental Science & Technology, 2004. **38**(13): p. 3705-3712.

125. Shukla, P., S. Wang, K. Singh, H.M. Ang, and M.O. Tadé, *Cobalt exchanged zeolites for heterogeneous catalytic oxidation of phenol in the presence of peroxymonosulphate.* Applied Catalysis B: Environmental, 2010. **99**(1–2): p. 163-169.

126. Lorimer, J.P. and T.J. Mason, *Sonochemistry. Part 1-The physical aspects.* Chemical Society Reviews, 1987. **16**: p. 239-274.

127. Suslick, K.S., *Sonochemistry.* Science, 1990. **247**(4949): p. 1439-1445.

128. Thorneycroft, J.a.B., S.W., *Torpedo-boat destroyers.* Inst. Civil Eng., 1895. **122**(51).

129. Adewuyi, Y.G., *Sonochemistry: Environmental science and engineering applications.* Industrial & Engineering Chemistry Research, 2001. **40**(22): p. 4681-4715.

130. Thompson, L.H. and L.K. Doraiswamy, *Sonochemistry: Science and Engineering.* Industrial & Engineering Chemistry Research, 1999. **38**(4): p. 1215-1249.

131. Shah, Y., *Cavitation reaction engineering / Y.T. Shah, and A.B. Pandit, and V.S. Moholkar*.

132. Hua, I., R.H. Hochemer, and M.R. Hoffmann, *Sonochemical degradation of p-nitrophenol in a parallel-plate near-field acoustical processor.* Environmental Science & Technology, 1995. **29**(11): p. 2790-2796.

133. Sivakumar, M., P.A. Tatake, and A.B. Pandit, *Kinetics of p-nitrophenol degradation: effect of reaction conditions and cavitational parameters for a multiple frequency system.* Chemical Engineering Journal, 2002. **85**(2–3): p. 327-338.

134. Dahlem, O., V. Demaiffe, V. Halloin, and J. Reisse, *Direct sonication system suitable for medium-scale sonochemical reactors.* AIChE Journal, 1998. **44**(12): p. 2724-2730.

135. Gogate Parag, R. and B. Pandit Aniruddha, *Hydrodynamic cavitation reactors: A state of the art review*, in *Reviews in Chemical Engineering*. 2001. p. 1.

136. Suslick, K.S., M.M. Mdleleni, and J.T. Ries, *Chemistry induced by hydrodynamic cavitation.* Journal of the American Chemical Society, 1997. **119**(39): p. 9303-9304.

137. Gogate, P.R., I.Z. Shirgaonkar, M. Sivakumar, P. Senthilkumar, N.P. Vichare, and A.B. Pandit, *Cavitation reactors: Efficiency assessment using a model reaction.* AIChE Journal, 2001. **47**(11): p. 2526-2538.

138. Cabrera, M.a.I., A.C. Negro, O.M. Alfano, and A.E. Cassano, *Photocatalytic reactions involving hydroxyl radical attack.* Journal of Catalysis, 1997. **172**(2): p. 380-390.

139. Romero, M., J. Blanco, B. Sánchez, A. Vidal, M. Sixto, A.I. Cardona, and E. Garcia, *Solar photocatlytic degradation of water and air pollutants: challenges and perspectives.* Solar Energy, 1999. **66**(2): p. 169-182.

140. Turchi, C.S. and D.F. Ollis, *Photocatalytic degradation of organic water contaminants: Mechanisms involving hydroxyl radical attack.* Journal of Catalysis, 1990. **122**(1): p. 178-192.

141. Rakshit, A., K. Anil, P. Punjabi, and A. Suresh, *Advanced oxidation processes*, in *Wastewater Treatment*. 2012, CRC Press. p. 61-106.

142. Davis, A.P. and C.P. Huang, *The removal of substituted phenols by a photocatalytic oxidation process with cadmium sulfide.* Water Research, 1990. **24**(5): p. 543-550.

143. Richard, C. and P. Boule, *Is the oxidation of salicylic acid to 2,5-dihydroxybenzoic acid a specific reaction of singlet oxygen?* Journal of Photochemistry and Photobiology A: Chemistry, 1994. **84**(2): p. 151-152.

144. Weidong, H., Q. Wei, W. Xiaohong, D. Xianbo, C. Long, and J. Zhaohua, *The photocatalytic properties of bismuth oxide films prepared through the sol–gel method.* Thin Solid Films, 2007. **515**(13): p. 5362-5365.

145. Kormann, C., D.W. Bahnemann, and M.R. Hoffmann, *Environmental photochemistry: Is iron oxide (hematite) an active photocatalyst? A comparative study: α-Fe_2O_3, ZnO, TiO_2.* Journal of Photochemistry and Photobiology A: Chemistry, 1989. **48**(1): p. 161-169.

146. Babay, P.A., Emilio, Carina A., Ferreyra, Rosana E., Gautier, Eduardo A., Gettar, Raquel T., Litter, Marta I., *Kinetics and mechanisms of EDTA photocatalytic degradation with TiO_2 under different experimental conditions.* International Journal of Photoenergy, 2001. **3**(4): p. 193-199.

147. Munter, R., *Advanced oxidation processes - current status and prospect.* Proc. Estonian Acad. Sci. Chem, 2001. **50**(2): p. 59-80.

148. Khezrianjoo, S. and H. Revanasiddappa., *Langmuir-Hinshelwood kinetic expression for the photocatalytic degradation of metanil yellow aqueous solutions by ZnO catalyst.* Chemical Sciences Journal,, 2012. **2012**(CSJ-85): p. 1-7.

149. Neyens, E. and J. Baeyens, *A review of classic Fenton's peroxidation as an advanced oxidation technique.* Journal of Hazardous Materials, 2003. **98**(1–3): p. 33-50.

150. Kuo, W.G., *Decolorizing dye wastewater with Fenton's reagent.* Water Research, 1992. **26**(7): p. 881-886.

151. Watts, R.J. and S.E. Dilly, *Evaluation of iron catalysts for the Fenton-like remediation of diesel-contaminated soils.* Journal of Hazardous Materials, 1996. **51**(1–3): p. 209-224.

152. Kwon, B.G., D.S. Lee, N. Kang, and J. Yoon, *Characteristics of p-chlorophenol oxidation by Fenton's reagent.* Water Research, 1999. **33**(9): p. 2110-2118.

153. Martens, D.A. and W.T. Frankenberger, *Enhanced degradation of polycyclic aromatic hydrocarbons in soil treated with an advanced oxidative process - Fenton's Reagent.* Journal of Soil Contamination, 1995. **4**(2): p. 175-190.

154. Zazo, J.A., J.A. Casas, A.F. Mohedano, M.A. Gilarranz, and J.J. Rodríguez, *Chemical pathway and kinetics of phenol oxidation by Fenton's reagent.* Environmental Science & Technology, 2005. **39**(23): p. 9295-9302.

155. Liang, H., Y.Y. Ting, H. Sun, H.M. Ang, M.O. Tadé, and S. Wang, *Solution combustion synthesis of Co oxide-based catalysts for phenol degradation in aqueous solution.* Journal of Colloid and Interface Science, 2012. **372**(1): p. 58-62.

156. Yan, Y.E. and F.W. Schwartz, *Oxidative degradation and kinetics of chlorinated ethylenes by potassium permanganate.* Journal of Contaminant Hydrology, 1999. **37**(3–4): p. 343-365.

157. Kakarla and Watts, *Depth of fenton-like oxidation in remediation of surface soil.* Journal of Environmental Engineering, 1997. **123**(1): p. 11-17.

158. Hunsberger, J.F., *Standart reduction potentials; In R.C. Weast (ED), Handbook of Chemistry and Physic. 58 ed. Ohio: CRC Press, Ohio.* 1997.

159. Vogelpohl, A., and Kim, S., *Advanced oxidation process (AOPs) in wastewater treatment.* J. Ind. Eng. Chem, 2004. **10**(1): p. 33-40.

160. Saputra, E., Utama, P, S., Muhammad, M., Ang., M, O Tadé, M., Wang, S., *Catalytic oxidation of toxic organics in aqueous solution for wastewater treatment: A review.* TIChE International Conference, 2011: p. 1-4.

161. Anipsitakis, G.P., Stathatos, Elias, Dionysiou, Dionysios D., *Heterogeneous activation of oxone using Co_3O_4.* The Journal of Physical Chemistry B, 2005. **109**(27): p. 13052-13055.

162. Hsu, Y.-C., J.-T. Chen, H.-C. Yang, J.-H. Chen, and C.-F. Fang, *Ozone decolorization of mixed-dye solutions in a gas-induced reactor.* Water Environment Research, 2001. **73**(4): p. 494-503.

163. Kreetachat, T., M. Damrongsri, V. Punsuwon, P. Vaithanomsat, C. Chiemchaisri, and C. Chomsurin, *Effects of ozonation process on lignin-derived compounds in pulp and paper mill effluents.* Journal of Hazardous Materials, 2007. **142**(1–2): p. 250-257.

164. Kulik, N., Trapido, M., Veressinina, Y., Munter, R, *Oil shale semicoke leachate pre-treatment by means of advanced oxidation.* International Conference Ozone and UV, Berlin, 2006: p. 41-46.

165. Ormad, M.P., N. Miguel, A. Claver, J.M. Matesanz, and J.L. Ovelleiro, *Pesticides removal in the process of drinking water production.* Chemosphere, 2008. **71**(1): p. 97-106.

166. Perkowski, J., L. Kos, and S. Ledakowicz, *Application of ozone in textile wastewater treatment.* Ozone: Science & Engineering, 1996. **18**(1): p. 73-85.

167. Carballa, M., G. Manterola, L. Larrea, T. Ternes, F. Omil, and J.M. Lema, *Influence of ozone pre-treatment on sludge anaerobic digestion: Removal of pharmaceutical and personal care products.* Chemosphere, 2007. **67**(7): p. 1444-1452.

168. Battino, R., Rettich, T., R., Tominaga, T., *The solubility of oxygen and ozone in liquids.* J. Phys. Chem. Ref. Data, 1983. **12**(2): p. 164-177.

169. Hoigné, J. and H. Bader, *Rate constants of reactions of ozone with organic and inorganic compounds in water-I: Non-dissociating organic compounds.* Water Research, 1983. **17**(2): p. 173-183.

170. Kasprzyk-Hordern, B., M. Ziółek, and J. Nawrocki, *Catalytic ozonation and methods of enhancing molecular ozone reactions in water treatment.* Applied Catalysis B: Environmental, 2003. **46**(4): p. 639-669.

171. Silva, L.M.d. and W.F. Jardim, *Trends and strategies of ozone application in environmental problems.* Química Nova, 2006. **29**: p. 310-317.

172. Forero, J.E., J.J. DUQUE, F. RIOS, and J. DÍAZ, *Ozone for phenol treatment in industrial wastewater* CT&F - Ciencia, Tecnología y Futuro, 2001. **2**: p. 17-26.

173. Ayling, G.w., and H. M., Castrantas, *Waste treatment with hydrogen peroxide.* Chemical Engineering (New York), 1981. **88**(24): p. 79-82.

174. Jones, C.W., *Applications of hydrogen peroxide and derivatives*. 1999, Royal Society of Chemistry. p. 1-35.

175. Pera-Titus, M., V. García-Molina, M.A. Baños, J. Giménez, and S. Esplugas, *Degradation of chlorophenols by means of advanced oxidation processes: A general review.* Applied Catalysis B: Environmental, 2004. **47**(4): p. 219-256.

176. Landon, P., P.J. Collier, A.J. Papworth, C.J. Kiely, and G.J. Hutchings, *Direct formation of hydrogen peroxide from H_2/O_2 using a gold catalyst.* Chemical Communications, 2002. **0**(18): p. 2058-2059.

177. Venkatadri, R., and R. W., Peters, *Chemical oxidation technologies: Ultraviolet light/hydrogen peroxide, Fenton's reagent, and titanium dioxide-assisted photocatalysis.* Hazardous Waste and Hazardous Materials, 1993. **10**(2): p. 107-149.

178. Vella, P.A., G. Deshinsky, J.E. Boll, J. Munder, and W.M. Joyce, *Treatment of low level phenols (μg/L) with potassium permanganate.* Research Journal of the Water Pollution Control Federation, 1990. **62**(7): p. 907-914.

179. Lamani, S.D., Nandibewoor, S.T, *Oxidation of tricyclic antidepressant agent, amitriptyline, by permanganate in sulphuric acid medium: Kinetic and mechanistic approach.* J Thermodyn Catal, 2011. **2**(2): p. 1-7.

180. Dash, S., S. Patel, and B.K. Mishra, *Oxidation by permanganate: Synthetic and mechanistic aspects.* Tetrahedron, 2009. **65**(4): p. 707-739.

181. Wiberg, K.B. and F. Freeman, *Kinetics of the base-catalyzed permanganate oxidation of benzaldehyde.* The Journal of Organic Chemistry, 1999. **65**(2): p. 573-576.

182. Seol, Y., H. Zhang., and F. W., Schwartz, *A review of in situ chemical oxidation and heterogeneity.* Environmental & Engineering Geoscience, 2003. **9**(1): p. 37-49.

183. Meunier, B., *Metalloporphyrins as versatile catalysts for oxidation reactions and oxidative DNA cleavage.* Chemical Reviews, 1992. **92**(6): p. 1411-1456.

184. Flanagan, J., W.P. Griffith, and A.C. Skapski, *The active principle of Caro's acid, HSO_5-: X-ray crystal structure of $KHSO_5.H_2O$.* Journal of the Chemical Society, Chemical Communications, 1984. **0**(23): p. 1574-1575.

185. Betterton, E.A., Hoffmann, M. R., *Kinetics and mechanism of the oxidation of aqueous hydrogen sulfide by peroxymonosulfate.* Environmental Science and Technology, 1990. **24**(12): p. 1819-1824.

186. Liang, C., C.J. Bruell, M.C. Marley, and K.L. Sperry, *Persulfate oxidation for in situ remediation of TCE. II. Activated by chelated ferrous ion.* Chemosphere, 2004. **55**(9): p. 1225-1233.

187. Neta, P., V. Madhavan, H. Zemel, and R.W. Fessenden, *Rate constants and mechanism of reaction of SO_4- with aromatic compounds.* Journal of the American Chemical Society, 1977. **99**(1): p. 163-164.

188. Chen, X., X. Qiao, D. Wang, J. Lin, and J. Chen, *Kinetics of oxidative decolorization and mineralization of acid Orange 7 by dark and photoassisted Co^{2+}-catalyzed peroxymonosulfate system.* Chemosphere, 2007. **67**(4): p. 802-808.

189. Anipsitakis, G.P. and D.D. Dionysiou, *Degradation of Organic Contaminants in Water with Sulfate Radicals Generated by the Conjunction of Peroxymonosulfate with Cobalt.* Environmental Science & Technology, 2003. **37**(20): p. 4790-4797.

190. Chan, K.H. and W. Chu, *Degradation of atrazine by cobalt-mediated activation of peroxymonosulfate: Different cobalt counteranions in homogenous process and cobalt oxide catalysts in photolytic heterogeneous process.* Water Research, 2009. **43**(9): p. 2513-2521.

191. Chen, X., X. Qiao, D. Wang, J. Lin, and J. Chen, *Kinetics of oxidative decolorization and mineralization of Acid Orange 7 by dark and photoassisted Co^{2+}-catalyzed peroxymono sulfate system.* Chemosphere, 2007. **67**(4): p. 802-808.

192. Fernandez, J., P. Maruthamuthu, A. Renken, and J. Kiwi, *Bleaching and photobleaching of Orange II within seconds by the oxone/Co^{2+} reagent in Fenton-like processes.* Applied Catalysis B-Environmental, 2004. **49**(3): p. 207-215.

193. Ling, S.K., S. Wang, and Y. Peng, *Oxidative degradation of dyes in water using Co^{2+}/H_2O_2 and Co^{2+}/peroxymonosulfate.* Journal of Hazardous Materials, 2010. **178**(1-3): p. 385-389.

194. Madhavan, J., P. Maruthamuthu, S. Murugesan, and M. Ashokkumar, *Kinetics of degradation of acid red 88 in the presence of Co^{2+}-ion/peroxomonosulphate reagent.* Applied Catalysis a-General, 2009. **368**(1-2): p. 35-39.

195. Başoğlu, A., S. Parlayan, M. Ocak, H. Alp, H. Kantekin, M. Özdemir, and Ü. Ocak, *Selective Recognition of Cobalt (II) Ion by a New Cryptand Compound with $N_2O_2S_2$ Donor Atom Possessing 2-Hydroxy-1-Naphthylidene Schiff Base Moiety.* Journal of Fluorescence, 2009. **19**(4): p. 655-662.

196. Sun, H., H. Liang, G. Zhou, and S. Wang, *Supported cobalt catalysts by one-pot aqueous combustion synthesis for catalytic phenol degradation.* Journal of Colloid and Interface Science, 2013. **394**(0): p. 394-400.

197. Yao, Y., Z. Yang, H. Sun, and S. Wang, *Hydrothermal Synthesis of Co3O4–Graphene for Heterogeneous Activation of Peroxymonosulfate for Decomposition of Phenol.* Industrial & Engineering Chemistry Research, 2012. **51**(46): p. 14958-14965.

198. Muhammad, S., E. Saputra, H. Sun, J.d.C. Izidoro, D.A. Fungaro, H.M. Ang, M.O. Tade, and S. Wang, *Coal fly ash supported Co3O4 catalysts for phenol degradation using peroxymonosulfate.* RSC Advances, 2012. **2**(13): p. 5645-5650.

199. Muhammad, S., E. Saputra, H. Sun, H.-M. Ang, M.O. Tadé, and S. Wang, *Heterogeneous Catalytic Oxidation of Aqueous Phenol on Red Mud-Supported Cobalt Catalysts.* Industrial & Engineering Chemistry Research, 2012. **51**(47): p. 15351-15359.

200. Shukla, P., H. Sun, S. Wang, H.M. Ang, and M.O. Tadé, *Co-SBA-15 for heterogeneous oxidation of phenol with sulfate radical for wastewater treatment.* Catalysis Today, 2011. **175**(1): p. 380-385.

201. Yang, Q., H. Choi, S.R. Al-Abed, and D.D. Dionysiou, *Iron-cobalt mixed oxide nanocatalysts: Heterogeneous peroxymonosulfate activation, cobalt*

leaching, and ferromagnetic properties for environmental applications. Applied Catalysis B-Environmental, 2009. **88**(3-4): p. 462-469.

202. Yao, Y., Z. Yang, D. Zhang, W. Peng, H. Sun, and S. Wang, *Magnetic $CoFe_2O_4$–Graphene Hybrids: Facile Synthesis, Characterization, and Catalytic Properties.* Industrial & Engineering Chemistry Research, 2012. **51**(17): p. 6044-6051.

203. Yang, X., F. Cheng, Z. Tao, and J. Chen, *Hydrolytic dehydrogenation of ammonia borane catalyzed by carbon supported Co core–Pt shell nanoparticles.* Journal of Power Sources, 2011. **196**(5): p. 2785-2789.

204. Zhang, M., Z. Yan, Q. Sun, J. Xie, and J. Jing, *Synthetic core-shell Ni@Pd nanoparticles supported on graphene and used as an advanced nanoelectrocatalyst for methanol oxidation.* New Journal of Chemistry, 2012. **36**(12): p. 2533-2540.

205. Li, P., C.-Y. Cao, Z. Chen, H. Liu, Y. Yu, and W.-G. Song, *Core-shell structured mesoporous silica as acid-base bifunctional catalyst with designated diffusion path for cascade reaction sequences.* Chemical Communications, 2012. **48**(85): p. 10541-10543.

206. Yao, Y., S. Miao, S. Yu, L. Ping Ma, H. Sun, and S. Wang, *Fabrication of Fe_3O_4/SiO_2 core/shell nanoparticles attached to graphene oxide and its use as an adsorbent.* Journal of Colloid and Interface Science, 2012. **379**(1): p. 20-26.

207. Park, M., S. Seo, S.J. Lee, and J.H. Jung, *Functionalized $Ni@SiO_2$ core/shell magnetic nanoparticles as a chemosensor and adsorbent for Cu^{2+} ion in drinking water and human blood.* Analyst, 2010. **135**(11): p. 2802-2805.

208. Emadi, M., E. Shams, and M.K. Amini, *Removal of Zinc from Aqueous Solutions by Magnetite Silica Core-Shell Nanoparticles.* Journal of Chemistry, 2013. **2013**: p. 10.

209. Zhang, H.-J., H.-M. Xiong, Q.-G. Ren, Y.-Y. Xia, and J.-L. Kong, *ZnO@silica core-shell nanoparticles with remarkable luminescence and stability in cell imaging.* Journal of Materials Chemistry, 2012. **22**(26): p. 13159-13165.

210. Ansari, A.A., M. Alam, J.P. Labis, S.A. Alrokayan, G. Shafi, T.N. Hasan, N.A. Syed, and A.A. Alshatwi, *Luminescent mesoporous $LaVO_4:Eu^{3+}$ core-shell nanoparticles: synthesis, characterization, biocompatibility and their cytotoxicity.* Journal of Materials Chemistry, 2011. **21**(48): p. 19310-19316.

211. Luo, Y., J. Luo, J. Jiang, W. Zhou, H. Yang, X. Qi, H. Zhang, H.J. Fan, D.Y.W. Yu, C.M. Li, and T. Yu, *Seed-assisted synthesis of highly ordered $TiO_2@\alpha$-Fe_2O_3 core/shell arrays on carbon textiles for lithium-ion battery applications.* Energy & Environmental Science, 2012. **5**(4): p. 6559-6566.

212. Zhang, H.P., L.C. Yang, L.J. Fu, Q. Cao, D.L. Sun, Y.P. Wu, and R. Holze, *Core-shell structured electrode materials for lithium ion batteries.* Journal of Solid State Electrochemistry, 2009. **13**(10): p. 1521-1527.

213. Lee, H. and J. Cho, *$Sn_{78}Ge_{22}$@Carbon Core−Shell Nanowires as Fast and High-Capacity Lithium Storage Media.* Nano Letters, 2007. **7**(9): p. 2638-2641.

214. Liu, F., Q. Zhao, H. You, and Z. Wang, *Synthesis of stable carboxy-terminated $NaYF_4$: Yb^{3+}, Er^{3+}@SiO2 nanoparticles with ultrathin shell for biolabeling applications.* Nanoscale, 2013.

215. Aldeek, F., C. Mustin, L. Balan, G. Medjahdi, T. Roques-Carmes, P. Arnoux, and R. Schneider, *Enhanced Photostability from CdSe(S)/ZnO Core/Shell Quantum Dots and Their Use in Biolabeling.* European Journal of Inorganic Chemistry, 2011. **2011**(6): p. 794-801.

216. Wang, Y., X. Jin, Y. Liu, J. Sun, and L. Gao, *Core-shell TiN@$SrTiO_3$ structure for grain boundary barrier layer capacitor.* Materials Letters, 2012. **74**(0): p. 191-193.

217. Wen, H., X. Wang, Z. Gui, and L. Li, *Modeling of the core-shell microstructure of temperature-stable $BaTiO_3$ based dielectrics for multilayer ceramic capacitors.* Journal of Electroceramics, 2008. **21**(1-4): p. 545-548.

218. Kolesnik, S. and B. Dabrowski, *Absence of room temperature ferromagnetism in bulk Mn-doped ZnO.* Journal of Applied Physics, 2004. **96**(9): p. 5379-5381.

219. Stein, A., S.W. Keller, and T.E. Mallouk, *Turning down the heat: Design and mechanism in solid-state synthesis.* Science, 1993. **259**(5101): p. 1558-1564.

220. Schubert, U. and N. Hüsing, *Synthesis of inorganic materials.* Wiley-VCH,Weinheim, Germany, 2000.

221. Trovarelli and A. Trovarelli, *Catalysis by ceria and related materials : Catalytic science series*. 2002.

222. Smart, L. and E.A. Moore, *Solid state chemistry*. Vol. 3rd Edition. 2005.

223. Kang, Y.C. and S.B. Park, *Zn_2SiO_4:Mn phosphor particles prepared by spray pyrolysis using a filter expansion aerosol generator.* Materials Research Bulletin, 2000. **35**(7): p. 1143-1151.

224. Fu, Y.-P. and C.-H. Lin, *Microwave-induced combustion synthesis of Ni–Zn ferrite powder and its characterization.* Journal of Magnetism and Magnetic Materials, 2002. **251**(1): p. 74-79.

225. Anil Kumar, P.S., Shrotri, J. J., Kulkarni, S. D., Deshpande, C. E., Date, S. K., *Low temperature synthesis of $Ni_{0.8}Zn_{0.2}Fe_2O_4$ powder and its characterization.* Materials Letters, 1996. **27**(6): p. 293-296.

226. Naka, S., M. Inagaki, and T. Tanaka, *On the formation of solid solution in $Co_{3-x}Mn_xO_4$ system.* Journal of Materials Science, 1972. **7**(4): p. 441-444.

227. Keyser, M.J., R.C. Everson, and R.L. Espinoza, *Fischer−Tropsch kinetic studies with cobalt−manganese oxide catalysts.* Industrial & Engineering Chemistry Research, 1999. **39**(1): p. 48-54.

228. Bridgwater, A.V., *Renewable fuels and chemicals by thermal processing of biomass.* Chemical Engineering Journal, 2003. **91**(2–3): p. 87-102.

229. Soled, S.L., I. Enrique, and R.A. F., *Copper promoted cobalt-manganese spinel catalyst and method for making the catalyst for Fischer-Tropsch synthesis.* United States Patent 5,162,284, 1992.

230. Bordeneuve, H., S. Guillemet-Fritsch, A. Rousset, S. Schuurman, and V. Poulain, *Structure and electrical properties of single-phase cobalt manganese oxide spinels $Mn_{3-x}Co_xO_4$ sintered classically and by spark plasma sintering (SPS).* Solid State Chemistry, 2009. **182**(2): p. 396-401.

231. Fogagnolo, J.B., M.H. Robert, and J.M. Torralba, *The effects of mechanical alloying on the extrusion process of AA 6061 alloy reinforced with Si_3N_4.* Journal of the Brazilian Society of Mechanical Sciences and Engineering, 2003. **25**: p. 201-206.

232. Kaupp, G., *Mechanochemistry: The varied applications of mechanical bond-breaking.* CrystEngComm, 2009. **11**(3): p. 388-403.

233. Stolle, A., T. Szuppa, S.E.S. Leonhardt, and B. Ondruschka, *Ball milling in organic synthesis: solutions and challenges.* Chemical Society Reviews, 2011. **40**(5): p. 2317-2329.

234. Rubinstein, M.H. and P. Gould, *Praticle size reduction in the ball mill.* Drug Development and Industrial Pharmacy, 1987. **13**(1): p. 81-92.

235. Zuo, K.-s., S.-q. Xi, and J.-e. Zhou, *Effect of temperature on mechanical alloying of Cu-Zn and Cu-Cr system.* Transactions of Nonferrous Metals Society of China, 2009. **19**(5): p. 1206-1214.

236. Abdellaoui, A.a.G., E., *Mechanical alloying in a planetary ball mill : Kinematic description* J. Phys. IV France, 1994. **04**(C3): p. 291-293.

237. Schneider, F., T. Szuppa, A. Stolle, B. Ondruschka, and H. Hopf, *Energetic assessment of the Suzuki-Miyaura reaction: a curtate life cycle assessment as an easily understandable and applicable tool for reaction optimization.* Green Chemistry, 2009. **11**(11): p. 1894-1899.

238. Suryanarayana, C., *Process variables in milling*, in *Mechanical Alloying And Milling*. 2004, CRC Press. p. 59-82.

239. Palaniandy, S. and N.H. Jamil, *Influence of milling conditions on the mechanochemical synthesis of $CaTiO_3$ nanoparticles.* Journal of Alloys and Compounds, 2009. **476**(1–2): p. 894-902.

240. Kim, J.W., J.-H. Shim, J.-P. Ahn, Y.W. Cho, J.-H. Kim, and K.H. Oh, *Mechanochemical synthesis and characterization of TiB_2 and VB_2 nanopowders.* Materials Letters, 2008. **62**(16): p. 2461-2464.

241. Portnoi, V., A. Leonov, A. Logacheva, and A. Logachev, *Mechanochemical synthesis and compaction of intermetallic alloys containing nanocrystalline substructure elements.* Bulletin of the Russian Academy of Sciences: Physics, 2012. **76**(1): p. 61-63.

242. Schouwink, P., V. D'Anna, M.B. Ley, L.M. Lawson Daku, B. Richter, T.R. Jensen, H. Hagemann, and R. Černý, *Bimetallic borohydrides in the system $M(BH_4)_2$–KBH_4 (M = Mg, Mn): On the structural diversity.* The Journal of Physical Chemistry C, 2012. **116**(20): p. 10829-10840.

243. F. Grigorieva, T., A. P. Barinova, and N. Z. Lyakhov, *Mechanochemical synthesis of intermetallic compounds.* Russian Chemical Reviews, 2001. **70**(1): p. 45-63.

244. Ďurišin, J., M. Orolínová, K. Ďurišinová, and V. Katana, *Mechanochemical method of nanocrystalline powder copper preparation.* Journal of Materials Science Letters, 1994. **13**(9): p. 688-689.

245. Antic, B., Kremenovic, A., Jovic, N., Pavlovic, M. B., Jovalekic, C., Nikolic, A. S., Goya, G. F., Weidenthaler, C., *Magnetization enhancement and cation valences in nonstoichiometric $(Mn,Fe)_{3-\delta}O_4$ nanoparticles* Journal of Applied Physics, 2012. **111**(7): p. 074309-6.

246. Arcos, D., Valenzuela, R., Vázquez, M., Vallet, Regı., *Chemical homogeneity of nanocrystalline Zn–Mn spinel ferrites obtained by high-energy ball milling.* Journal of Solid State Chemistry, 1998. **141**(1): p. 10-16.

247. Jeon, I.-Y., Y.-R. Shin, G.-J. Sohn, H.-J. Choi, S.-Y. Bae, J. Mahmood, S.-M. Jung, J.-M. Seo, M.-J. Kim, D. Wook Chang, L. Dai, and J.-B. Baek, *Edge-carboxylated graphene nanosheets via ball milling.* Proceedings of the National Academy of Sciences, 2012.

248. Li, J.L., Q.S. Peng, G.Z. Bai, and W. Jiang, *Carbon scrolls produced by high energy ball milling of graphite.* Carbon, 2005. **43**(13): p. 2830-2833.

249. Chen, Y., M.J. Conway, and J.D. Fitzgerald, *Carbon nanotubes formed in graphite after mechanical grinding and thermal annealing.* Applied Physics A: Materials Science & Processing, 2003. **76**(4): p. 633-636.

250. Shindo, K., T. Kondo, M. Arakawa, and Y. Sakurai, *Hydrogen adsorption/desorption properties of mechanically milled activated carbon.* Journal of Alloys and Compounds, 2003. **359**(1–2): p. 267-271.

251. Xu, F., S. Deng, J. Xu, W. Zhang, M. Wu, B. Wang, J. Huang, and G. Yu, *Highly active and stable Ni–Fe bimetal prepared by ball milling for catalytic hydrodechlorination of 4-chlorophenol.* Environmental Science & Technology, 2012. **46**(8): p. 4576-4582.

252. Alikina, G.B., Y. Bunina, R. Lukashevich, A. Mezentseva, N. Moroz, E. Orlovskaya, N. Sadykov, V. Uvarov, N. Zabolotnaya, G., *One-pot synthesis of mixed ionic-electronic conducting nanocomposites comprised of fluorite-like and perovskite-like phases as catalytic materials for SOFC.* Materials Research Society Symphosium Proceesings, 2005. **900**: p. 380-385

253. Zhang, Q. and F. Saito, *Mechanochemical synthesis of $LaMnO_3$ from La_2O_3 and Mn_2O_3 powders.* Journal of Alloys and Compounds, 2000. **297**(1–2): p. 99-103.

254. Muroi, M., R. Street, and P.G. McCormick, *Enhancement of critical temperature in fine $La_{0.7}Ca_{0.3}MnO_3$ particles prepared by mechanochemical processing.* Journal of Applied Physics, 2000. **87**(7): p. 3424-3431.

255. Rougier, A., S. Soiron, I. Haihal, L. Aymard, B. Taouk, and J.M. Tarascon, *Influence of grinding on the catalytic properties of oxides.* Powder Technology, 2002. **128**(2–3): p. 139-147.

256. Poinsignon, C., H. Klein, P. Strobel, C. Roux, and C. Surcin, *Electrochemical response of nanocrystalline tetragonal manganese dioxides prepared by spray vapor pyrolysis and ball milling.* The Journal of Physical Chemistry C, 2007. **111**(27): p. 9644-9651.

257. Shin, J.-H., K.-W. Kim, and H.-J. Ahn, *Preparation of leady oxide for lead–acid battery by cementation reaction.* Journal of Power Sources, 2000. **89**(1): p. 46-51.

258. Varin, R.A., T. Czujko, C. Chiu, and Z. Wronski, *Particle size effects on the desorption properties of nanostructured magnesium dihydride (MgH_2) synthesized by controlled reactive mechanical milling (CRMM).* Journal of Alloys and Compounds, 2006. **424**(1–2): p. 356-364.

259. Padella, F., C. Alvani, A.L. Barbera, G. Ennas, R. Liberatore, and F. Varsano, *Mechanosynthesis and process characterization of nanostructured manganese ferrite.* Materials Chemistry and Physics, 2005. **90**(1): p. 172-177.

260. Wang, D. and Y. Li, *Bimetallic nanocrystals: Liquid-phase synthesis and catalytic applications.* Advanced Materials, 2011. **23**(9): p. 1044-1060.

261. Courty, P. and C. Marcilly, *A scientific approach to the preparation of bulk mixed oxide catalysts*, in *Studies in Surface Science and Catalysis*, P.G. G. Poncelet and P.A. Jacobs, Editors. 1983, Elsevier. p. 485-519.

262. Portehault, D., S. Cassaignon, E. Baudrin, and J.-P. Jolivet, *Morphology control of cryptomelane type MnO_2 nanowires by soft chemistry. Growth mechanisms in aqueous medium.* Chemistry of Materials, 2007. **19**(22): p. 5410-5417.

263. Keyser, M.J., R.C. Everson, and R.L. Espinoza, *Fischer–Tropsch studies with cobalt–manganese oxide catalysts: Synthesis performance in a fixed bed reactor.* Applied Catalysis A: General, 1998. **171**(1): p. 99-107.

264. Arulmurugan, R., Jeyadevan, B., Vaidyanathan, G., Sendhilnathan, S., *Effect of zinc substitution on Co–Zn and Mn–Zn ferrite nanoparticles prepared by co-precipitation.* Journal of Magnetism and Magnetic Materials, 2005. **288**(0): p. 470-477.

265. Rabiei, S., D. Miser, J. Lipscomb, K. Saoud, S. Gedevanishvili, and F. Rasouli, *Conversion of hausmanite (Mn_3O_4) particles to nano-fibrous manganite (MnOOH) at ambient conditions.* Journal of Materials Science, 2005. **40**(18): p. 4995-4998.

266. Hutchings, G.J., A.A. Mirzaei, R.W. Joyner, M.R.H. Siddiqui, and S.H. Taylor, *Ambient temperature CO oxidation using copper manganese oxide catalysts prepared by coprecipitation: Effect of ageing on catalyst performance.* Catalysis Letters, 1996. **42**(1): p. 21-24.

267. Mirzaei, A.A., M. Faizi, and R. Habibpour, *Effect of preparation conditions on the catalytic performance of cobalt manganese oxide catalysts for conversion of synthesis gas to light olefins.* Applied Catalysis A: General, 2006. **306**(0): p. 98-107.

268. Liu, M., G.-J. Zhang, Z.-R. Shen, P.-C. Sun, D.-T. Ding, and T.-H. Chen, *Synthesis and characterization of hierarchically structured mesoporous MnO_2 and Mn_2O_3.* Solid State Sciences, 2009. **11**(1): p. 118-128.

269. Kang, M., E.D. Park, J.M. Kim, and J.E. Yie, *Manganese oxide catalysts for NO_x reduction with NH_3 at low temperatures.* Applied Catalysis A: General, 2007. **327**(2): p. 261-269.

270. Perego, C. and P. Villa, *Catalyst preparation methods.* Catalysis Today, 1997. **34**(3–4): p. 281-305.

271. Chen, H., A. Sayari, A. Adnot, and F.ç. Larachi, *Composition-activity effects of Mn-Ce-O composites on phenol catalytic wet oxidation.* Applied Catalysis B: Environmental, 2001. **32**(3): p. 195-204.

272. Vaja, F., C. Comanescu, O. Oprea, D. Ficai, and G. Guran, *Effects of ZnO nanoparticles on the wet scrub resistance and photocatalytic properties of acrylic coatings.* REV. CHIM., 2012. **7**(63): p. 722-726.

273. Chen, P.-L. and I.W. Chen, *Reactive cerium(IV) oxide powders by the homogeneous precipitation method.* Journal of the American Ceramic Society, 1993. **76**(6): p. 1577-1583.

274. Xu, B., T. Xiao, Z. Yan, X. Sun, J. Sloan, S.L. González-Cortés, F. Alshahrani, and M.L.H. Green, *Synthesis of mesoporous alumina with highly thermal stability using glucose template in aqueous system.* Microporous and Mesoporous Materials, 2006. **91**(1–3): p. 293-295.

275. Heinrichs, B., S. Lambert, N. Job, and J. and Pirard, *Sol-gel synthesis of supported metals.* CATALYST PREPARATION Science and Engineering, 2006. **CRC Press 2006**: p. 163-208.

276. Mehrotra, R.C., *Synthesis and reactions of metal alkoxides.* Journal of Non-Crystalline Solids, 1988. **100**(1–3): p. 1-15.

277. Ward, D.A. and E.I. Ko, *Preparing catalytic materials by the sol-gel method.* Industrial & Engineering Chemistry Research, 1995. **34**(2): p. 421-433.

278. Gonzalez, R.D., T. Lopez, and R. Gomez, *Sol-Gel preparation of supported metal catalysts.* Catalysis Today, 1997. **35**(3): p. 293-317.

279. Li, B. and R.D. Gonzalez, *Sol−gel synthesis and catalytic properties of sulfated zirconia catalysts.* Industrial & Engineering Chemistry Research, 1996. **35**(9): p. 3141-3148.

280. Lu, Z.-l., E. Lindner, and H.A. Mayer, *Applications of sol-gel processed interphase catalysts.* ChemInform, 2003. **34**(3): p. no-no.

281. Gao, X., Y. Jiang, Y. Zhong, Z. Luo, and K. Cen, *The activity and characterization of CeO_2-TiO_2 catalysts prepared by the sol–gel method for selective catalytic reduction of NO with NH_3.* Journal of Hazardous Materials, 2010. **174**(1–3): p. 734-739.

282. Miller, J.B. and E.I. Ko, *Control of mixed oxide textural and acidic properties by the sol-gel method.* Catalysis Today, 1997. **35**(3): p. 269-292.

283. Antonelli, D.M. and J.Y. Ying, *Synthesis of hexagonally packed mesoporous TiO_2 by a modified sol-gel method.* Angewandte Chemie International Edition in English, 1995. **34**(18): p. 2014-2017.

284. Lu, Y., Y. Yin, B.T. Mayers, and Y. Xia, *Modifying the surface properties of superparamagnetic iron oxide nanoparticles through a sol−gel approach.* Nano Letters, 2002. **2**(3): p. 183-186.

285. Wu, N.-L., S.-Y. Wang, and I.A. Rusakova, *Inhibition of crystallite growth in the sol-gel synthesis of nanocrystalline metal oxides.* Science, 1999. **285**(5432): p. 1375-1377.

286. Thammachart, M., V. Meeyoo, T. Risksomboon, and S. Osuwan, *Catalytic activity of CeO_2–ZrO_2 mixed oxide catalysts prepared via sol–gel technique: CO oxidation.* Catalysis Today, 2001. **68**(1–3): p. 53-61.

287. Veith, M., S. Mathur, N. Lecerf, V. Huch, T. Decker, H.P. Beck, W. Eiser, and R. Haberkorn, *Sol-Gel synthesis of nano-scaled $BaTiO_3$, $BaZrO_3$ and $BaTi_{0.5}Zr_{0.5}O_3$ oxides via single-source alkoxide precursors and semi-alkoxide routes.* Journal of Sol-Gel Science and Technology, 2000. **17**(2): p. 145-158.

288. Veith, M., S. Mathur, A. Kareiva, M. Jilavi, M. Zimmer, and V. Huch, *Low temperature synthesis of nanocrystalline $Y_3Al_5O_{12}$ (YAG) and Ce-doped $Y_3Al_5O_{12}$ via different sol-gel methods.* Journal of Materials Chemistry, 1999. **9**(12): p. 3069-3079.

289. Wang, X., X. Wang, W. Huang, P.J. Sebastian, and S. Gamboa, *Sol–gel template synthesis of highly ordered MnO_2 nanowire arrays.* Journal of Power Sources, 2005. **140**(1): p. 211-215.

290. Hashemzadeh, F., M. Mehdi Kashani Motlagh, and A. Maghsoudipour, *A comparative study of hydrothermal and sol–gel methods in the synthesis of MnO_2 nanostructures.* Journal of Sol-Gel Science and Technology, 2009. **51**(2): p. 169-174.

291. Shen, L., L. Gong, and J. Zhang, *Research on β-MnO_2 nanorods synthesized with sawdust template* Chinese Battery Industry, 2009(6): p. 404-408.

292. Lakshmi, B.B., C.J. Patrissi, and C.R. Martin, *Sol−gel template synthesis of semiconductor oxide micro- and nanostructures.* Chemistry of Materials, 1997. **9**(11): p. 2544-2550.

293. Somiya, S. and R. Roy, *Hydrothermal synthesis of fine oxide powders.* Bull. Mater. Sci, 2000. **23**(6): p. 453-460.

294. Byrappa, K. and M. Yoshimura, *Handbook of hydrothermal technology - A technology for crystal growth and materials processing*. 2001, William Andrew Publishing/Noyes.

295. Subramanian, V., H. Zhu, R. Vajtai, P.M. Ajayan, and B. Wei, *Hydrothermal synthesis and pseudocapacitance properties of MnO_2 nanostructures.* The Journal of Physical Chemistry B, 2005. **109**(43): p. 20207-20214.

296. Wang, X. and Y. Li, *Selected-Control Hydrothermal Synthesis of α- and β-MnO_2 Single Crystal Nanowires.* Journal of the American Chemical Society, 2002. **124**(12): p. 2880-2881.

297. Ma, R., Y. Bando, L. Zhang, and T. Sasaki, *Layered MnO_2 nanobelts: Hydrothermal synthesis and electrochemical measurements.* Advanced Materials, 2004. **16**(11): p. 918-922.

298. Ni, J., W. Lu, L. Zhang, B. Yue, X. Shang, and Y. Lv, *Low-temperature synthesis of monodisperse 3D manganese oxide nanoflowers and their pseudocapacitance properties.* The Journal of Physical Chemistry C, 2008. **113**(1): p. 54-60.

299. Hayashi, H. and K. Torii, *Hydrothermal synthesis of titania photocatalyst under subcritical and supercritical water conditions.* Journal of Materials Chemistry, 2002. **12**(12): p. 3671-3676.

300. Adschiri, T., Y. Hakuta, and K. Arai, *Hydrothermal synthesis of metal oxide fine particles at supercritical conditions.* Industrial & Engineering Chemistry Research, 2000. **39**(12): p. 4901-4907.

301. Oliveira, M.M., D.C. Schnitzler, and A.J.G. Zarbin, *$(Ti,Sn)O_2$ mixed oxides nanoparticles obtained by the sol−gel route.* Chemistry of Materials, 2003. **15**(9): p. 1903-1909.

302. Andersson, M., L. Österlund, S. Ljungström, and A. Palmqvist, *Preparation of nanosize anatase and rutile TiO_2 by hydrothermal treatment of microemulsions and their activity for photocatalytic wet oxidation of phenol.* The Journal of Physical Chemistry B, 2002. **106**(41): p. 10674-10679.

303. Desilets, D., M. Zreda, P.F. Almasi, and D. Elmore, *Determination of cosmogenic 36Cl in rocks by isotope dilution: innovations, validation and error propagation.* Chemical Geology, 2006. **233**(3–4): p. 185-195.

304. Lalena, J.N., D.A. Cleary, E.E. Carpenter, and N.F. Dean, *Solid–liquid reactions*, in *Inorganic Materials Synthesis and Fabrication*. 2007, John Wiley & Sons, Inc. p. 141-181.

305. Sheets, W.C., E. Mugnier, A. Barnabe, T.J. Marks, and K.R. Poeppelmeier, *Hydrothermal Synthesis of Delafossite-Type Oxides.* Chem Mater, 2006. **18**(1): p. 7-20.

306. Cheng, F., J. Zhao, W. Song, C. Li, H. Ma, J. Chen, and P. Shen, *Facile controlled synthesis of MnO_2 nanostructures of novel shapes and their application in batteries.* Inorganic Chemistry, 2006. **45**(5): p. 2038-2044.

307. Wang, X. and Y. Li, *Synthesis and formation mechanism of manganese dioxide nanowires/nanorods.* Chemistry – A European Journal, 2003. **9**(1): p. 300-306.

308. Song, X.C., Y. Zhao, and Y.F. Zheng, *Synthesis of MnO_2 nanostructures with sea urchin shapes by a sodium dodecyl sulfate-assisted hydrothermal process.* Crystal Growth & Design, 2006. **7**(1): p. 159-162.

309. Li, W.N., J. Yuan, X.F. Shen, S. Gomez-Mower, L.P. Xu, S. Sithambaram, M. Aindow, and S.L. Suib, *Hydrothermal synthesis of structure- and shape-controlled manganese oxide octahedral molecular sieve nanomaterials.* Advanced Functional Materials, 2006. **16**(9): p. 1247-1253.

310. Yuan, J., W.-N. Li, S. Gomez, and S.L. Suib, *Shape-controlled synthesis of manganese oxide octahedral molecular sieve three-dimensional nanostructures.* Journal of the American Chemical Society, 2005. **127**(41): p. 14184-14185.

311. Qiu, G., H. Huang, S. Dharmarathna, E. Benbow, L. Stafford, and S.L. Suib, *Hydrothermal synthesis of manganese oxide nanomaterials and their catalytic and electrochemical properties.* Chemistry of Materials, 2011. **23**(17): p. 3892-3901.

312. Rozman, M. and M. Drofenik, *Hydrothermal synthesis of manganese zinc ferrites.* Journal of the American Ceramic Society, 1995. **78**(9): p. 2449-2455.

313. Zhang, Y., H. Wang, B. Wang, H. Yan, and M. Yoshimura, *Low-temperature hydrothermal synthesis of pure metastable γ-manganese sulfide (MnS) crystallites.* Journal of Crystal Growth, 2002. **243**(1): p. 214-217.

314. Gui, Y., L. Qian, and X. Qian, *Hydrothermal synthesis of uniform rock salt (α-) MnS transformation from wurtzite (γ-) MnS.* Materials Chemistry and Physics, 2011. **125**(3): p. 698-703.

315. Chen, Y., H. Yuan, G. Li, G. Tian, and S. Feng, *Crystal growth and magnetic property of orthorhombic $RMnO_3$ (R=Sm–Ho) perovskites by mild hydrothermal synthesis.* Journal of Crystal Growth, 2007. **305**(1): p. 242-248.

316. Khaydarov, R., R. Khaydarov, O. Gapurova, Y. Estrin, and T. Scheper, *Electrochemical method for the synthesis of silver nanoparticles.* Journal of Nanoparticle Research, 2009. **11**(5): p. 1193-1200.

317. Zhou, Y., R.J. Phillips, and J.A. Switzer, *Electrochemical synthesis and sintering of nanocrystalline Cerium(IV) oxide powders.* Journal of the American Ceramic Society, 1995. **78**(4): p. 981-985.

318. Löwe, H. and W. Ehrfeld, *State-of-the-art in microreaction technology: concepts, manufacturing and applications.* Electrochimica Acta, 1999. **44**(21–22): p. 3679-3689.

319. Yousefi, T., A.N. Golikand, M.H. Mashhadizadeh, and M. Aghazadeh, *Template-free synthesis of MnO_2 nanowires with secondary flower like structure: Characterization and supercapacitor behavior studies.* Current Applied Physics, 2012. **12**(1): p. 193-198.

320. Therese, G.H.A. and P.V. Kamath, *Electrochemical synthesis of metal oxides and hydroxides.* Chemistry of Materials, 2000. **12**(5): p. 1195-1204.

321. Bengisu, M., *Engineering ceramics* 2001, Berlin: Springer.

322. van Dillen, A.J., R.J.A.M. Terörde, D.J. Lensveld, J.W. Geus, and K.P. de Jong, *Synthesis of supported catalysts by impregnation and drying using aqueous chelated metal complexes.* Journal of Catalysis, 2003. **216**(1–2): p. 257-264.

323. Ahmadpour, A. and D.D. Do, *The preparation of active carbons from coal by chemical and physical activation.* Carbon, 1996. **34**(4): p. 471-479.

324. Parasad, S. and G. Rattan, *Preparation methods and applications of CuO-CeO_2 catalysts: A short review.* Bulletin of Chemical Reaction Engineering & Catalysis, 2010. **5**(1): p. 7-30.

325. Pulido Melián, E., O. González Díaz, J.M. Doña Rodríguez, G. Colón, J.A. Navío, M. Macías, and J. Pérez Peña, *Effect of deposition of silver on structural characteristics and photoactivity of TiO_2-based photocatalysts.* Applied Catalysis B: Environmental, 2012. **127**(0): p. 112-120.

326. Yori, J.C. and J.M. Parera, *Preparation of $Pt/SO_{42}{-}ZrO_2$ by incipient wetness impregnation: Influence of the sulfur concentration in the isomerization of n-butane.* Applied Catalysis A: General, 1995. **129**(2): p. L151-L156.

327. Chang, F.-W., W.-Y. Kuo, and K.-C. Lee, *Dehydrogenation of ethanol over copper catalysts on rice husk ash prepared by incipient wetness impregnation.* Applied Catalysis A: General, 2003. **246**(2): p. 253-264.

328. Chin, Y.-H., Y. Wang, R.A. Dagle, and X. Shari Li, *Methanol steam reforming over Pd/ZnO: Catalyst preparation and pretreatment studies.* Fuel Processing Technology, 2003. **83**(1–3): p. 193-201.

329. Banerjee, R. and P.A. Crozier, *In situ synthesis and nanoscale evolution of model supported metal catalysts: Ni on Silica.* The Journal of Physical Chemistry C, 2012. **116**(21): p. 11486-11495.

330. Liang, H., H. Sun, A. Patel, P. Shukla, Z.H. Zhu, and S. Wang, *Excellent performance of mesoporous Co_3O_4/MnO_2 nanoparticles in heterogeneous activation of peroxymonosulfate for phenol degradation in aqueous solutions.* Applied Catalysis B: Environmental, 2012. **127**(0): p. 330-335.

331. Campanati, M., G. Fornasari, and A. Vaccari, *Fundamentals in the preparation of heterogeneous catalysts.* Catalysis Today, 2003. **77**(4): p. 299-314.

332. Al-Sabti, M., D., *New technological root for regenerating demineralized water plants for safe environment.* International Journal of Water Resources and Environmental Engineering, 2011. **3**(2): p. 52-56.

333. *Deposition of active component*, in *Preparation of Solid Catalysts*. 2008, Wiley-VCH Verlag GmbH. p. 315-371.

334. De Lucas, A., J.L. Valverde, F. Dorado, A. Romero, and I. Asencio, *Influence of the ion exchanged metal (Cu, Co, Ni and Mn) on the selective catalytic reduction of NO_X over mordenite and ZSM-5.* Journal of Molecular Catalysis A: Chemical, 2005. **225**(1): p. 47-58.

335. Choudary, B.M., M.L. Kantam, B. Bharathi, P. Sreekanth, and F. Figueras, *Epoxidations of olefins catalysed by new Mn(II) salen immobilized mesoporous materials.* Journal of Molecular Catalysis A: Chemical, 2000. **159**(2): p. 417-421.

336. Ogawa, M. and K. Kuroda, *Preparation of inorganic-organic nanocomposites through intercalation of organoammonium ions into layered silicates.* Bulletin of the Chemical Society of Japan, 1997. **70**(11): p. 2593-2618.

337. Schwarz, J.A., C. Contescu, and A. Contescu, *Methods for preparation of catalytic materials.* Chemical Reviews, 1995. **95**(3): p. 477-510.

338. Geoffrey, P., *Solid-state ion-exchange of zeolites*, in *Catalyst Preparation*. 2006, CRC Press. p. 283-295.

339. Stanciulescu, M., G. Caravaggio, A. Dobri, J. Moir, R. Burich, J.P. Charland, and P. Bulsink, *Low-temperature selective catalytic reduction of NO_x with NH_3 over Mn-containing catalysts.* Applied Catalysis B: Environmental, 2012. **123–124**(0): p. 229-240.

340. Slavcheva, E., P., *Magnetron sputtered iridium oxide as anode catalyst for pem hydrogen generation.* Macedonian Journal of Chemistry and Chemical Engineering, 2011. **30**(1): p. 45-54.

341. Cassell, A.M., J.A. Raymakers, J. Kong, and H. Dai, *Large scale CVD synthesis of single-walled carbon nanotubes.* The Journal of Physical Chemistry B, 1999. **103**(31): p. 6484-6492.

342. Öncel, Ç. and Y. Yürüm, *Carbon nanotube synthesis via the catalytic CVD method: A review on the effect of reaction parameters.* Fullerenes, Nanotubes and Carbon Nanostructures, 2006. **14**(1): p. 17-37.

343. Gurav, A., T. Kodas, T. Pluym, and Y. Xiong, *Aerosol processing of materials.* Aerosol Science and Technology, 1993. **19**(4): p. 411-452.

344. Koch, C.C., *Nanostructured Materials - Processing, Properties, and Applications (2nd Edition)*, William Andrew Publishing. p. 47-90.

345. Gleiter, H., *Nanocrystalline materials.* Progress in Materials Science, 1989. **33**(4): p. 223-315.

346. Suryanarayana, C. and C.C. Koch, *Nanocrystalline materials – Current research and future directions.* Hyperfine Interactions, 2000. **130**(1): p. 5-44.

347. Tjong, S.C. and H. Chen, *Nanocrystalline materials and coatings.* Materials Science and Engineering: R: Reports, 2004. **45**(1–2): p. 1-88.

348. Hahn, H., *Gas phase synthesis of nanocrystalline materials.* Nanostructured Materials, 1997. **9**(1–8): p. 3-12.

349. Simchi, A., R. Ahmadi, S.M.S. Reihani, and A. Mahdavi, *Kinetics and mechanisms of nanoparticle formation and growth in vapor phase condensation process.* Materials & Design, 2007. **28**(3): p. 850-856.

350. Hai, N.H., R. Lemoine, S. Remboldt, M. Strand, J.E. Shield, D. Schmitter, R.H. Kraus, Michelle Espy, Jr., and D.L. Leslie-Pelecky, *Iron and cobalt-based magnetic fluids produced by inert gas condensation.* Journal of Magnetism and Magnetic Materials, 2005. **293**(1): p. 75-79.

351. Tiwari, J.N., R.N. Tiwari, and K.S. Kim, *Zero-dimensional, one-dimensional, two-dimensional and three-dimensional nanostructured materials for advanced electrochemical energy devices.* Progress in Materials Science, 2012. **57**(4): p. 724-803.

352. Dimesso, L., L. Heider, and H. Hahn, *Synthesis of nanocrystalline Mn-oxides by gas condensation.* Solid State Ionics, 1999. **123**(1–4): p. 39-46.

353. Chen, C.-Y., C.-K. Lin, M.-H. Tsai, C.-Y. Tsay, P.-Y. Lee, and G.-S. Chen, *Characterization of nanocrystalline manganese oxide powder prepared by inert gas condensation.* Ceramics International, 2008. **34**(7): p. 1661-1666.

354. Jensen Klavs, F., *Chemical vapor deposition*, in *Microelectronics Processing*. 1989, American Chemical Society. p. 199-263.

355. Ohring, M., *Materials science of thin films*. 2002, San Diego: Academic Press.

356. Choy, K.L., *Chemical vapour deposition of coatings.* Progress in Materials Science, 2003. **48**(2): p. 57-170.

357. Jensen, J.A., J.E. Gozum, D.M. Pollina, and G.S. Girolami, *Titanium, zirconium, and hafnium tetrahydroborates as "tailored" CVD precursors for metal diboride thin films.* Journal of the American Chemical Society, 1988. **110**(5): p. 1643-1644.

358. Cao, G.-z., H.W. Brinkman, J. Meijerink, K.J. de Vries, and A.J. Burggraaf, *Pore narrowing and formation of ultrathin yttria-stabilized zirconia layers in ceramic membranes by chemical vapor deposition/electrochemical vapor deposition.* Journal of the American Ceramic Society, 1993. **76**(9): p. 2201-2208.

359. Kuykendall, T., P. Pauzauskie, S. Lee, Y. Zhang, J. Goldberger, and P. Yang, *Metalorganic chemical vapor deposition route to GaN nanowires with triangular cross sections.* Nano Letters, 2003. **3**(8): p. 1063-1066.

360. Yang, J.L., S.J. An, W.I. Park, G.C. Yi, and W. Choi, *Photocatalysis using ZnO thin films and nanoneedles grown by metal-organic chemical vapor deposition.* Advanced Materials, 2004. **16**(18): p. 1661-1664.

361. Leila F. Deravi , J.D.S.a.D.W.W., *The biomimetic synthesis of metal oxide nanomaterials.* WILEY-VCH Verlag GmbH & Co. KGaA, Weinheim, 2009. **2**: p. 3-54.

362. Lee, C.J., J. Park, S.Y. Kang, and J.H. Lee, *Growth of well-aligned carbon nanotubes on a large area of Co-Ni co-deposited silicon oxide substrate by thermal chemical vapor deposition.* Chemical Physics Letters, 2000. **323**(5-6): p. 554-559.

363. Lee, C.J., J. Park, Y. Huh, and J. Yong Lee, *Temperature effect on the growth of carbon nanotubes using thermal chemical vapor deposition.* Chemical Physics Letters, 2001. **343**(1–2): p. 33-38.

364. Lee, C.W., H.S. Jang, C.K. Oh, and K.S. Kwon, *A case of the pterygium due to lichen planus limited to the nails.* Korean J Dermatol, 2000. **38**: p. 560-562.

365. Le, H.A., S. Chin, E. Park, L.T. Linh, G.-N. Bae, and J. Jurng, *Chemical vapor synthesis and characterization of manganese oxides.* Chemical Vapor Deposition, 2011. **17**(7-9): p. 228-234.

Chapter 3

Catalytic Oxidation of Toxic Organics in Aqueous Solution Using MnO_2 and Peroxymonosulfate

Abstract

Several α-MnO_2 catalysts in the forms of nanosphere, nanorod and nanowire were synthesized, characterized and tested in heterogeneous activation of peroxymonosulfate for phenol degradation in aqueous solutions. The α-MnO_2 materials exhibited varying activities in activation of peroxymonosulfate to produce sulfate radicals for phenol degradation depending on structure and morphology. Crystalline structure of MnO_2 is more important than porous structure in influencing the activity because crystalline α-MnO_2 exhibited higher phenol degradation. Nanowired α-MnO_2 presented the highest activity with stable performance while the mesoporous α-MnO_2 nanosphere with amorphous structure presented the lowest activity and stability. In addition, Three one-dimensional MnO_2 nanoparticles with different crystallographic phases, α-, β- and γ-MnO_2, were also synthesized, characterized, and tested in heterogeneous activation of oxone for phenol degradation in aqueous solution. The α-, β- and γ-MnO_2 nanostructured materials presented in morphologies of nanowires, nanorods, and nanotubes, respectively. They showed varying activities in activation of oxone to generate sulfate radicals for phenol degradation depending on surface area and crystalline structure. α-MnO_2 nanowires exhibited the highest activity and could degrade phenol in 60 min at phenol concentrations ranging in 25-100 ppm. It was found that phenol degradation on α-MnO_2 followed first order kinetics with activation energy of 21.9 kJ/mol.

Part A: α-MnO_2 Activation of Peroxymonosulfate for Catalytic Phenol Degradation in Aqueous Solutions

3.1. Introduction

Wastewater from various households and industrial processes contains many organic compounds. Most organic compounds are toxic to the environment and human beings. Complete degradation of organic pollutants in wastewater is one of the focuses in water treatment. In the last decades, advanced oxidation processes (AOPs) have emerged as effective processes to completely degrade organic compounds in aqueous media. Currently, most AOPs are based on the generation of very reactive species, such as hydroxyl radicals (OH•) that oxidize a broad range of pollutants quickly and non-selectively [1-4].

Recently, MnO_2 nanomaterials have attracted much attention because of their physical and chemical properties and possess a great potential as heterogeneous catalysts[5-8], adsorbents[9-11], and battery materials[12, 13]. However, few studies have been conducted on the catalytic properties of MnO_2 materials in water treatment. Watts et al. [7] investigated amorphous and crystalline MnO_2 as catalysts for the Fenton-like decomposition of hydrogen peroxide and found the amorphous and crystalline β-MnO_2 at near-neutral pH resulted in significant carbon tetrachloride degradation. Zhang et al. [6] reported the synthesis of β-MnO_2 nanorods and the use in the oxidation of methylene blue in the presence of H_2O_2. Xu et al. [14] investigated the oxidative removal of steroid estrogens from water by MnO_2 and the factors influencing the reactions. They found MnO_2 exhibited a promising chemical agent under optimized conditions for estrogen removal from water. Ai et al. [5] used microwave irradiation to synthesize MnO_2 and tested catalytic degradation of Rhodamine B in aqueous solution. Dong et al. [15] also evaluated the catalytic properties of β-MnO_2 nanowires for the degradation of phenol and revealed good separability and remarkable catalysis for the degradation of phenol on β-MnO_2 nanowires. Sui et al. [16] prepared α/β-MnO_2 by a molten salt route and found that they showed excellent catalytic performance in the Fenton-like reaction.

In most previous investigations in water treatment, MnO_2 was usually used for the Fenton-like reaction for production of hydroxyl radicals from H_2O_2 and oxidation of organic compounds. Recently, sulfate radicals produced by Co^{2+}/Oxone have attracted intense attention in degradation of organic compounds for water treatment [17-19]. However, Co^{2+} is highly toxic and will cause secondary pollution. Therefore, alternative metals, like Fe^{2+}, have been proposed, but Fe exhibited much lower activity. Anipsitakis and Dionysiou [20] studied nine transition metal ions for the activation of three oxidants and the generation of sulfate, peroxymonosulfate, and hydroxyl radicals. They suggested that the conjunction of Ce^{3+}, Mn^{2+}, and Ni^{2+} ions with peroxymonosulfate (PMS, HSO_5^-) also showed the generation of sulfate radicals. However, no further work has been reported for solid MnO_2 for activation of peroxymonosulfate to generate sulfate radicals.

MnO_2 has several different phases such as α-, β-, γ-, δ-, η-, and ε-MnO_2 with varying structures. Using MnO_2 instead of Co oxides for heterogeneous activation of peroxymonosulfate will be an alternative technique for advanced oxidation process. In this chapter, we first report the synthesis of several α-MnO_2 with different porous structures and morphologies and evaluate their performance in activation of peroxymonosulfate for sulfate radical generation to decompose phenol in aqueous solution.

3.2. Experimental section

3.2.1. Material synthesis

A mesoporous MnO_2 sample was first prepared by reduction of $KMnO_4$ with maleic acid reported earlier by Hong et al. [21]. In this synthesis, potassium permanganate was dissolved in distilled water and mixed with a maleic acid solution. The molar ratio of the mixture was $KMnO_4$: Maleic acid =1:3. The resulting solution was mixed thoroughly and aged for 24 h at room temperature. After that, brown precipitates were filtered and washed with water several times. The precipitates were dried at room temperature for 24 h and calcined at 300 °C for 4 h at the rate of 3 °C/min. This

sample was referred as MnO_2-300. The second sample was obtained by calcination of the precipitates at 500 °C for 4 h, which was referred as MnO_2-500.

Another MnO_2 was obtained by a hydrothermal method reported by Wang and Li [22]. Typically, $MnSO_4 \bullet H_2O$ (0.008 mol) and an equal amount of ammonium persulfate ($(NH_4)_2S_2O_8$) were put into distilled water at room temperature to form a homogeneous solution, which was then transferred into a 40 mL Teflon-lined stainless steel autoclave, sealed and maintained at 140 ºC for 12 h. The resulting solid product was filtered, washed with distilled water, and finally dried in air at 100 ºC overnight. This sample was referred as MnO_2-140.

3.2.2. Characterization

Surface area and pore size measurements of various MnO_2 samples were carried out by N_2 adsorption analysis at -196 ºC using a Micromeretics Tristar 3000. The MnO_2 samples were degassed at 200 ºC for 24 h prior to adsorption analysis. The surface area and pore size distribution were obtained by the BET and BJH methods, respectively. The crystal structure of the synthesized MnO_2 powders was characterized by an X-ray diffractometer (XRD, Bruker D8 Advance) equipped with Cu Kα radiation (λ = 1.54178 Å) operated at 40 kV and 30 mA. The particle morphology was examined from transmission electron microscopy (TEM) using a JEOL JEM1010 electron microscope.

3.2.3. Catalytic activity test

Phenol degradation tests were carried out at 25 °C in 1 L glass vessel with 500 mL of phenol solutions at 30 ppm with a constant stirring of 400 rpm. Firstly, peroxymonosulfate (PMS using Oxone, $2KHSO_5 \cdot KHSO_4 \cdot K_2SO_4$, obtained from Sigma-Aldrich) was added into the phenol solutions at 2.0 g/L and then 0.20 g MnO_2 catalysts were added in. At certain time intervals, a water samples (1 mL) was withdrawn into a HPLC vial, 0.5 mL of pure methanol was injected into the vial to quench the reaction. The concentration of phenol was analyzed using a Varian HPLC with a UV detector set at λ = 270 nm (Detection limit < 50 ppb). A C–18 column was used to separate the organics while the mobile phase made of 30% CH_3CN and 70%

water was passed at a flow rate of 1.5 mL/min. For a comparison, some control tests using either MnO_2 or PMS were also conducted. For some samples, total organic carbon (TOC) was obtained using a Shimadzu TOC-5000 CE analyzer. For the measurement of TOC, 5 mL sample was extracted at a fixed interval and quenched with 5 mL of 3M sodium nitrite solution and then analyzed on the TOC analyzer.

For multiple uses of MnO_2 catalysts, the reacted MnO_2 after each run was collected by filtration followed by thoroughly washing with distilled water several times, and then it was dried at 80 °C for 2 h for reuse again.

3.3. Result and discussion

Figure 3.1 shows XRD patterns of three synthesized MnO_2 samples. The three MnO_2 samples present similar crystalline peaks at 2θ = 12.8, 18.1, 28.6 and 37.5º, which was identified as α-MnO_2. The as-synthesized MnO_2-300 did not show strong crystalline peaks while the other two MnO_2 presented strong XRD diffraction. This means that MnO_2-300 is not fully crystallized with large extent as an amorphous phase. The other two MnO_2 catalysts are in well-developed crystalline phase.

Figure 3.2 shows TEM images of three MnO_2 samples. As seen, the synthesized α-MnO_2-300 particles presented in an aggregated amorphous phase with spherical shape and porous structure. The particle size is about 5-10 nm. After calcination at 500 ºC, most amorphous α-MnO_2 nanoparticles were transformed into nanorods with a diameter of 10-40 nm and particle size differs in the range of 50-200 nm. MnO_2-140 showed as well-defined nanowires with a diameter of 10-20 nm.

Figure 3.3 shows N_2 adsorption isotherms and pore size distributions of three MnO_2 samples. As can be seen, three samples showed quite different N_2 adsorption isotherms. MnO_2-300 showed a hysteresis loop at p/p_0=0.4, indicating a typical mesoporous structure. MnO_2-140 also showed a hysteresis loop but at lower pressure of p/p_0=0.2-0.4, suggesting the presence of smaller mesopore size. Meanwhile the pore size distributions indicate that MnO_2-300 and MnO_2-140 have a typical mesoporous structure profile with a peak centred at 3.5 and 3.0 nm, respectively.

However, MnO_2-500 seems to be a nonporous material based on adsorption isotherm and pore size distribution.

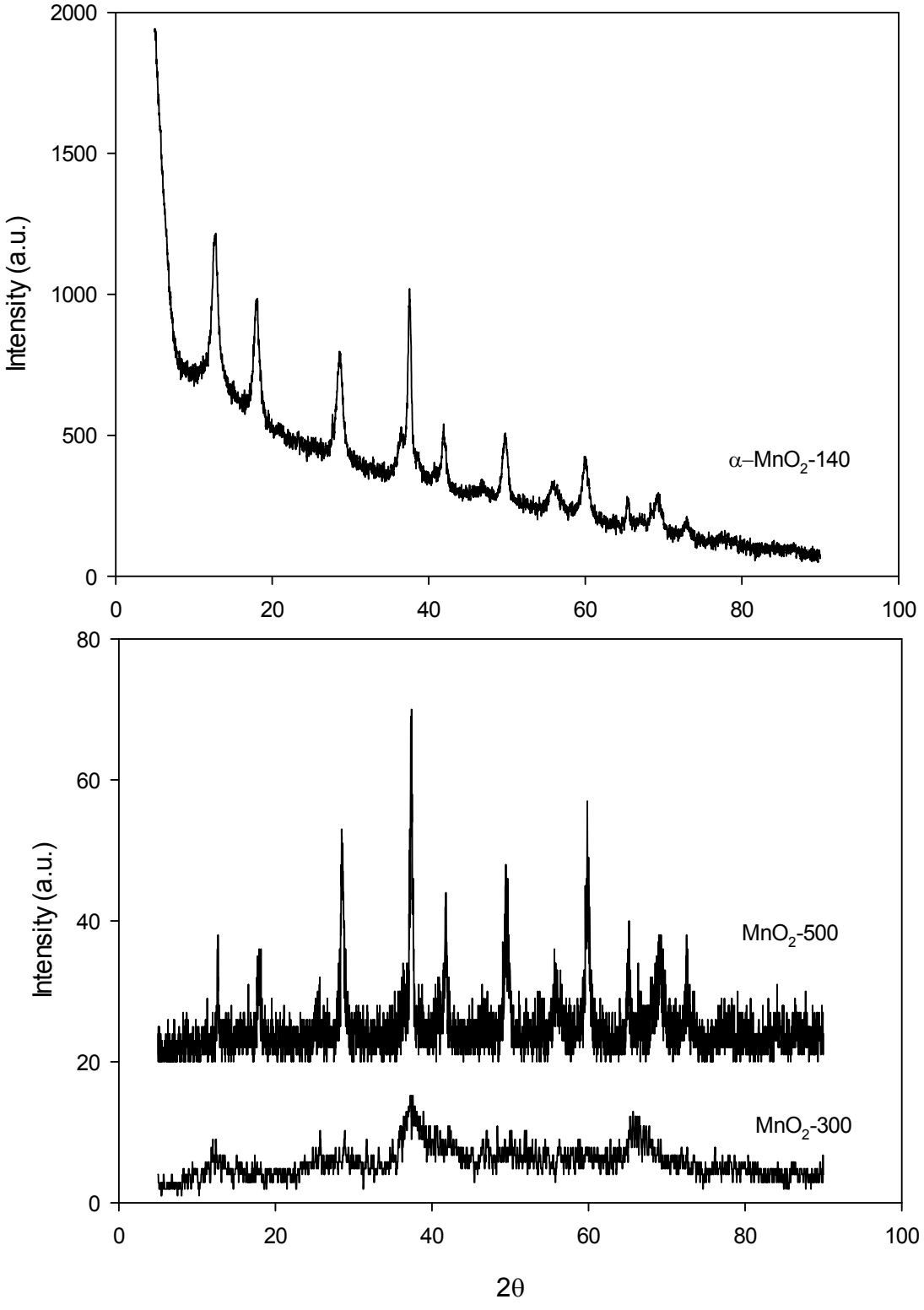

Figure 3.1. XRD patterns of MnO_2 catalysts.

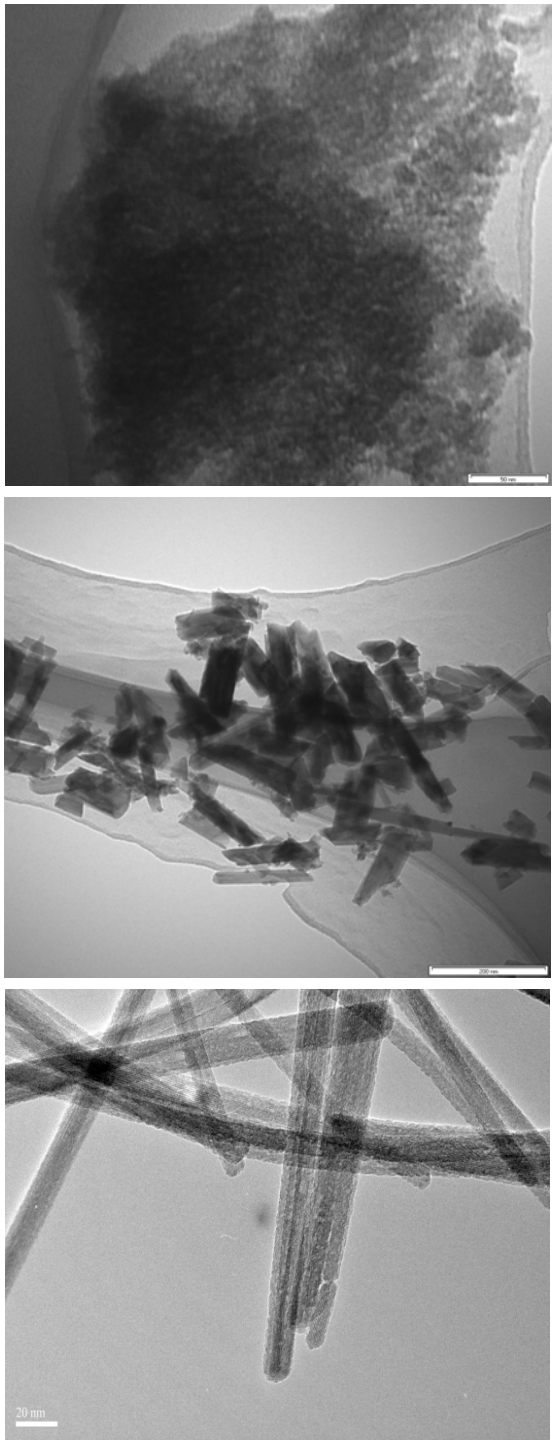

Figure 3.2. TEM photos of MnO_2 catalysts. (a) MnO_2-300 (b) MnO_2-500 (c) MnO_2-140

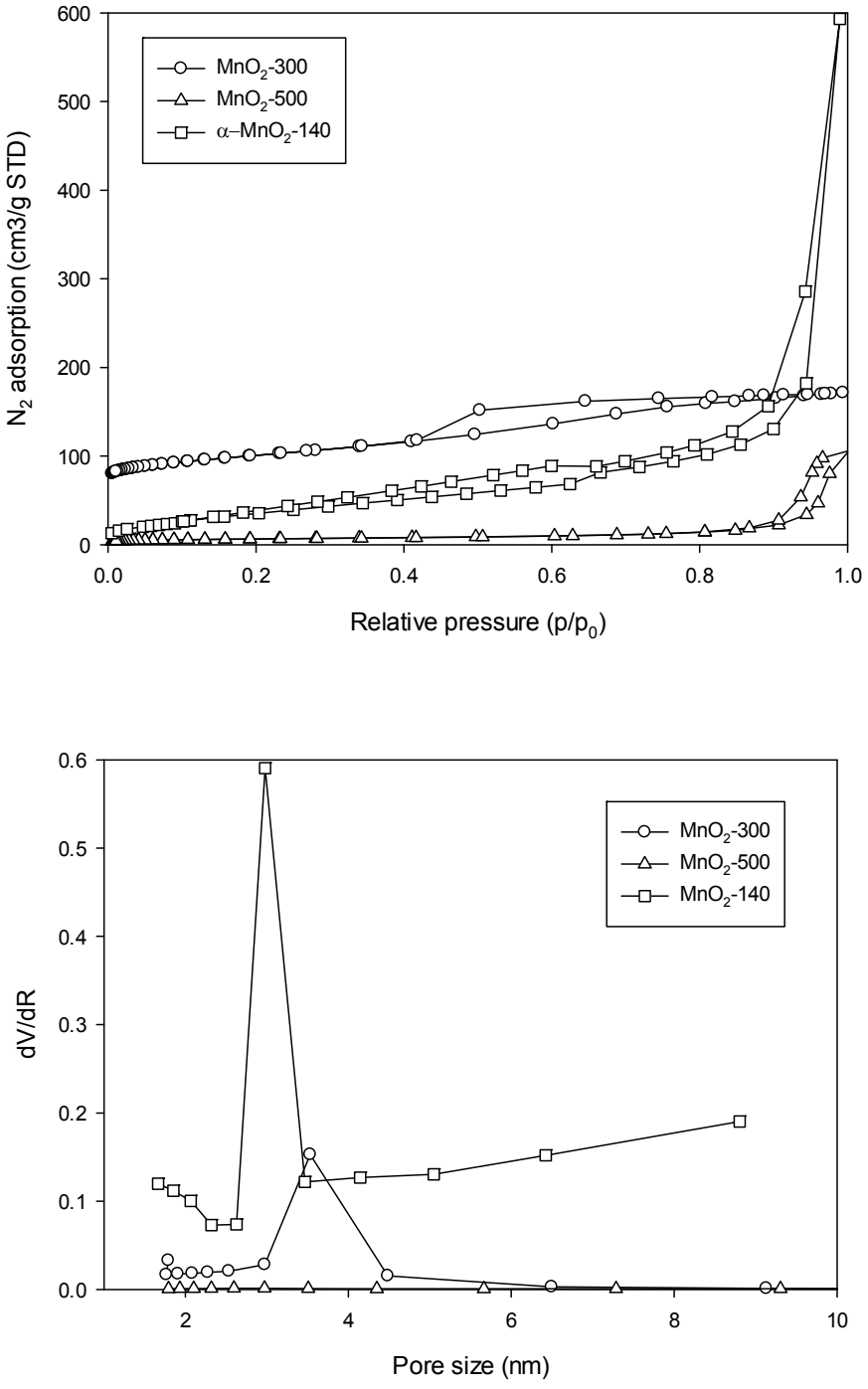

Figure 3.3. N_2 adsorption isotherms and pore size distribution of MnO_2 catalysts. (a) Adsorption isotherm (b) pore size distribution.

The BET surface area and pore volume are given in **Table 3.1**. MnO_2-300 has the highest BET surface area while MnO_2-500 has the lowest BET surface area. MnO_2-140 has the medium value of BET surface area. From XRD results, it is seen that MnO_2-300 presents in amorphous phase with low crystalline structure. TEM also showed that MnO_2-300 has many pores, which contributes to higher surface area. Meanwhile, MnO_2-500 presented in crystalline phase with nanorod morphology, thus it has the lowest surface area. MnO_2-140 is also in crystalline phase, however, the nanowires have micropores and the interwoven could produce pores among the wires.

Table 3.1. Porous structure and reaction rate constants of three α-MnO_2 catalysts.

Catalyst	S_{BET}(m^2/g)	V (cm^3/g)	Rate constant (min^{-1})	TOC reduction (%)	R^2
MnO_2-300	179	0.187	0.0457	90.5	0.938
MnO_2-500	23	0.151	0.0873	98.9	0.999
MnO_2-140	146	0.918	0.359	99.8	0.999

Figure 3.4 displays phenol degradation profiles with time on three α-MnO_2 samples. Some control tests were also conducted with either peroxymonosulfate (PMS) or MnO_2. As seen, no phenol degradation occurred with the presence of only PMS, indicating no activation of PMS for sulfate radical generation. However, there was a slow reduction in phenol concentration to 18% at 40 min on MnO_2-140, which could be attributed to minor adsorption of phenol on MnO_2-140. With the presence of PMS and MnO_2, phenol degradation occurred. MnO_2-300 presented a low rate of phenol degradation with 100% phenol decomposition occurring at 150 min. MnO_2-500 showed a faster phenol degradation rate than MnO_2-300 with 100% phenol decomposition at 60 min. MnO_2-140 exhibited the highest reaction rate with 100% phenol decomposition at 20 min. For the three MnO_2 catalysts, measurements of TOC reduction showed that the TOC reductions at 90 min are 90.5, 98.9 and 99.8% for MnO_2-300, MnO_2-500 and MnO_2-140, respectively, suggesting much higher degradation of the organics in this reaction.

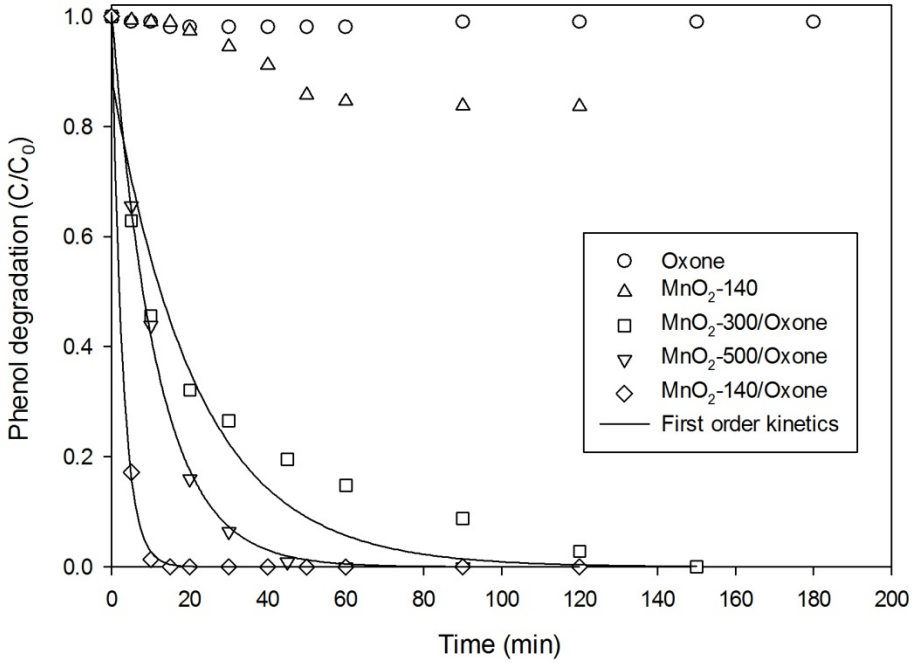

Figure 3.4. Phenol degradation profiles versus time on various MnO_2 catalysts. Reaction conditions: $[phenol]_0$ = 30 ppm, catalyst loading = 0.4 g/L, oxone loading = 2.0 g/L.

BET surface area (**Table 3.1**) of three α-MnO_2 followed the order of MnO_2-300 > MnO_2-140 > MnO_2-500, which is different from the order of their activity in phenol degradation. This suggests that porous structure is not the dominating factor influencing MnO_2 catalytic activity. XRD and TEM showed that MnO_2-140 and MnO_2-500 were fully crystalline materials in nanowires and nanorods, respectively. MnO_2-140 presented high crystallinity and low crystal diameter. Thus, it is deduced that crystallinity of MnO_2 is more important in their catalytic activity.

For phenol decomposition, a first-order kinetic model was employed to fit the variation of phenol concentration against time. The rate constant and regression coefficients are given in **Table 3.1**. It was found that the model fit well to the experiments with high regression coefficients. Previously, MnO_2 has been investigated for activation of H_2O_2 to produce hydroxyl radicals for several organics oxidation and it showed effective activity. Watts et al. [7] investigated oxidative and reductive pathways in manganese-catalyzed Fenton's reactions and found that

reductants were generated by crystalline and amorphous manganese oxide-catalyzed decomposition of H_2O_2. In this investigation, MnO_2 can catalyze the decomposition of peroxymonosulfate and produce sulfate radicals as shown in the following equations.

$$HSO_5^- + 2MnO_2 \rightarrow SO_5^{2-\bullet} + OH^- + Mn_2O_3 \quad (3.1)$$

$$HSO_5^- + Mn_2O_3 \rightarrow SO_4^{2-\bullet} + H^+ + 2MnO_2 \quad (3.2)$$

$$SO_4^{2-\bullet} + H_2O \rightarrow OH^\bullet + H^+ + SO_4^{2-} \quad (3.3)$$

$$C_6H_5OH + SO_4^{2-\bullet} \rightarrow \text{several steps} \rightarrow CO_2 + H_2O + SO_4^{2-} \quad (3.4)$$

Anipsitakis and Dionysiou [20] studied homogeneous activation of peroxymonosulfate with Mn^{2+} for 2,4-dichlorophenol (2,4-DCP) oxidation and found that transformation of 2,4-DCP in 4 h of reaction time was 24% at 50 ppm 2,4-DCP and 1.244 mM HSO_5^-. Several heterogeneous cobalt systems have also been tested in activation of peroxymonosulfate for oxidation of organics in water. Anipsitakis et al. [23] used CoO and Co_3O_4 with peroxymonosulfate for 2,4-DCP degradation at 20 ppm. Complete destruction of 2, 4-DCP on CoO took place within 30 min while 74% transformation was obtained using Co_3O_4. Chen et al. [24] used nano-Co_3O_4 with an average size of 20 nm to activate peroxymonosulfate for degradation of Acid Orange 7 (AO7). They found that 98% decomposition of AO7 could be achieved in 30 min at the conditions of 0.2 mM AO7, 0.5 g/L nano-Co_3O_4 and 2 mM HSO_5^-. Yang et al. [25] used Fe-Co mixed oxide ($CoFe_2O_4$) nanocatalysts for the heterogeneous activation of peroxymonosulfate to generate sulphate radicals targeting the decomposition of 2,4-DCP. About 50-80% 2, 4-DCP decomposition in 50 ppm could be obtained in 2 h on various Fe-Co mixed oxides. Therefore, it is seen that MnO_2 presented higher activity in phenol degradation than Mn^{2+} and heterogeneous Co systems.

Figure 3.5 shows the catalytic performance of MnO_2-300 and MnO_2-140 in multiple uses. For MnO_2-300, significant reduction of phenol degradation was observed in three runs, suggesting a deactivation of the catalyst. In the third run, phenol degradation was 70% at 100 min compared with 100% in the first run. For MnO_2-140, phenol degradation was still much high with 100% degradation at 20 min, same

as that in the first run. This suggests that MnO_2-140 is much stable and can be recycled for multiple uses.

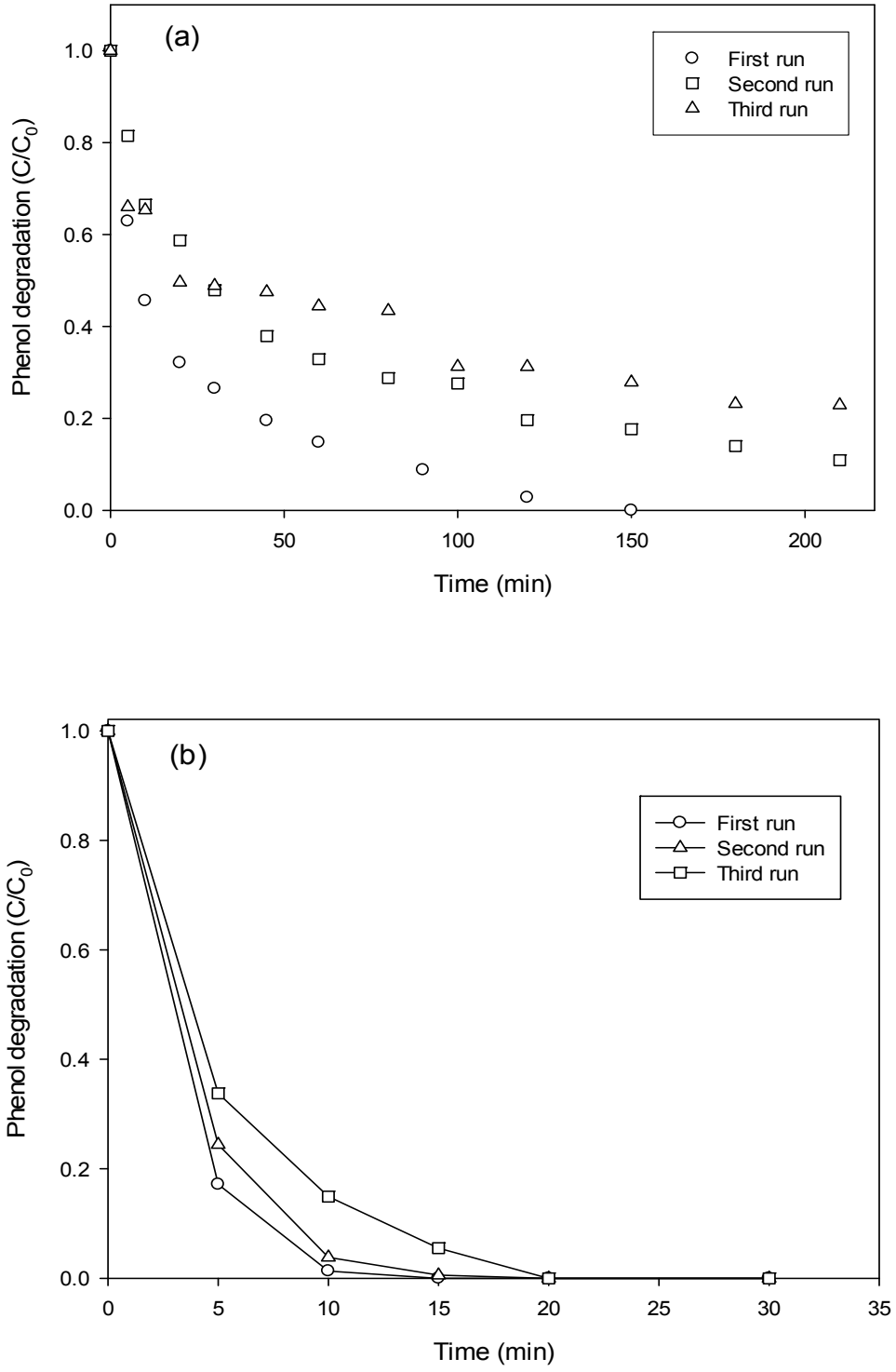

Figure 3.5. A comparison of phenol degradation at different runs on MnO_2. Reaction conditions: $[phenol]_0$ = 30 ppm, catalyst loading = 0.4 g/L, oxone loading = 2.0 g/L. (a) MnO_2-300 (b) MnO_2-140

Several heterogeneous Co systems have been tested for the stability in activation of peroxymonosulfate for organic decomposition. Chen et al. [24] have found that nano-Co_3O_4 presented a long-term stability in the degradation of AO7. Shukla et al. [26] tested cobalt exchanged zeolites for heterogeneous catalytic oxidation of phenol in the presence of peroxymonosulfate and found that Co-ZSM-5 presented stable performance for phenol degradation. They further tested activated carbon (AC) supported cobalt catalysts for advanced oxidation of phenol in aqueous solution. Co/AC exhibited stable performance after several rounds of regeneration[27]. Compared with Co/AC, MnO_2-140 in this work showed higher activity and stable performance. Therefore, it can be a promising catalyst replacing toxic Co^{2+} for activation of peroxymonosulfate to produce sulphate radicals for organic oxidation.

3.4. Conclusions

Three α-MnO_2 catalysts with different morphologies were synthesized and they showed high activity in heterogeneous activation of peroxymonosulfate for sulfate radical generation to decompose phenol in aqueous solution. Crystalline MnO_2 demonstrated high activity. Nanowired MnO_2-140 produced the highest phenol degradation with 100% phenol degradation and 99% TOC reduction in 90 min and it also exhibited high stability. However, amorphous MnO_2-300 with mesoporous structure gave the lowest activity and less stability. Phenol degradation on MnO_2 could be described by the first-order kinetics.

Part B: Different Crystallographic One-dimensional MnO_2 Nanomaterials and Their Superior Performance in Catalytic Phenol Degradation

3.5. Introduction

Organic compounds are important pollutants in water and they come from various sources including natural processes, households and industrial waste discharge. These organic compounds are usually toxic to the environment and humans, and should be removed from water. Several techniques have been developed for removal of organic contaminants from water. The oxidative degradation of organic pollutants in wastewater is one of the focuses in water treatment. In the last decades, advanced oxidation processes (AOPs) have emerged as a viable strategy to degrade a wide range of organic compounds in aqueous media. Currently, most of AOPs are based on the generation of very reactive species, such as superoxide radicals (O_2^{-}•) and hydroxyl radicals (OH•) that oxidize a broad range of pollutants quickly and non-selectively [1-4]. Apart from those oxygen radicals, sulfate radicals are also important and have been recently explored [17, 28, 29].

Mn oxides are widely used in catalysis. However, few studies have been conducted on the catalytic properties of manganese dioxide materials in water treatment and most of the investigations focused on Fenton-like reaction using H_2O_2. Zhang et al. [6] synthesized β-MnO_2 nanorods for methylene blue oxidation with H_2O_2. Watts et al. [7] investigated Fenton-like decomposition of H_2O_2 into oxidants and reductants on amorphous and crystalline MnO_2 and found that significant carbon tetrachloride degradation at near-neutral pH. Xu et al. [14] studied the oxidative removal of steroid estrogens from water by MnO_2 and reported that MnO_2 exhibited as a promising chemical agent under optimized conditions for estrogen removal from water. Dong et al. [15] also evaluated the catalytic properties of β-MnO_2 nanowires for the degradation of phenol and revealed good separability and remarkable catalysis for the degradation of phenol on β-MnO_2 nanowires. Sui et al. [16] prepared α- and β-MnO_2 single-crystalline nanostructured particles by the molten salt route. The prepared α- and β-MnO_2 nanoparticles exhibited excellent catalytic performance in the Fenton-

like reaction of dye degradation. Cao et al.[8] also reported excellent catalytic performance of α-MnO_2 and β-MnO_2 nanorods in the Fenton-like reaction of removal of methylene blue.

Previously, Fenton reagents (Fe^{2+}/H_2O_2) are commonly used in AOPs[3]. For sulfate radical production, Co^{2+}/oxone has been found to show high activity [17, 20]. Anipsitakis and Dionysiou [20] tested nine transition metal ions for the homogeneous activation of oxone and found that Co(II), Ru(III), and Fe(II) interact with oxone to form freely diffusible sulfate radicals while Ce(III), Mn(II), and Ni(II) with oxone generate caged or bound to the metal sulfate radicals. However, Co^{2+} in water is toxic and can induce various health problems. Thus, several heterogeneous Co oxide catalysts have been investigated for sulfate radical production [26, 27, 30-34]. In addition, Ru-based catalysts were also found to be highly effective [35]. However, few other heterogeneous metal oxide systems including MnO_2 have been investigated [36, 37].

It is believed that MnO_2 is much abundant in the nature and it has been widely used for many applications in catalysis and energy storage as electrode and supercapacitors. In nature, MnO_2 can be found in different crystalline structures such as α-, β-, γ-, δ-, η-, and ε-MnO_2 and they may show different behaviour in catalysis[22]. Compared with Co ions, Mn ions have low toxicity. Thus, MnO_2 can be a promising alternative to Co_3O_4 in oxone activation; however, no such a work has been reported. In this section, we report an investigation of the synthesis of different MnO_2 phases in 1D structure and evaluation of their performance in activation of oxone to generate sulfate radicals for phenol degradation.

3.6. Experimental section

3.6.1. Synthesis of α-, β-, γ-MnO_2

All chemicals were obtained from Sigma-Aldrich. Synthesis of α-, β- and γ-MnO_2 followed the hydrothermal method with some modifications based on the redox reactions of Mn^{2+} ions with persulphate [22]. Typically, $MnSO_4 \bullet H_2O$ (0.008 mol) and

an equal amount of ammonium persulfate ($(NH_4)_2S_2O_8$) were put into distilled water at room temperature to form a homogeneous solution, which was then transferred into a 40 mL Teflon-lined stainless steel autoclave, sealed and maintained at different temperatures for 12 h. For α- and β-MnO_2, the temperature was set at 140 ºC while for γ-MnO_2, the temperature was set 90 ºC. After the reaction was completed, the resulting solid product was filtered, washed with distilled water to remove ions possibly remnant in the final products, and finally dried in air.

3.6.2. Characterization of α-, β-, γ-MnO_2

The crystal structure of the synthesized materials was characterized by an X-ray diffractormeter (XRD, Bruker D8 Advance) equipped with Cu Kα radiation at accelerating voltage and current of 40 kV and 40 mA, respectively. The particle morphology was examined from scanning electron microscopy (SEM) obtained using a JEOL JEM1010 electron microscope. The optical absorption of the samples was determined by UV-Vis absorbance spectroscopy using the diffuse reflectance method (JASCO V-670 Spectrometer). The particle surface area and pore size measurement were carried out by N_2 adsorption analysis at -196 ºC using a Micromeretics AS-1. Samples were degassed at 200 ºC for 24 h prior to adsorption analysis. The surface area and pore size distribution were obtained by the BET and BJH methods. Thermogravimetric analysis (TGA) was conducted on a TGA/DSC1 STAR^e system (METTLER TOLEDO). MnO_2 samples were loaded into a pan and heated to 900 ºC at a rate of 15 ºC/min. The N_2 gas flow rate was maintained at 20 mL/min.

3.6.3. Catalytic activity test

Phenol degradation tests were carried out at 30 °C in 1 L glass vessel with 500 mL of phenol solution at 25-100 ppm with a constant stirring of 400 rpm. Firstly, a catalyst at varying amounts (0.05-0.20 g) was added into the phenol solution for a while, then oxone ($2KHSO_5 \cdot KHSO_4 \cdot K_2SO_4$, PMS) was added into the solution at 0.04-2.0 g/L. At certain time, water sample (1 mL) was withdrawn into a HPLC vial, 0.5 mL of pure methanol was then injected into the vial to quench the reaction. The concentration of phenol was analyzed using a Varian HPLC with a UV detector set at λ = 270 nm. A C–18 column was used to separate the organics while the mobile

phase with a flow rate of 1.5 mL/min was made of 30% CH_3CN and 70% water. For the recycle tests of the catalyst, after each run, the catalyst was obtained by filtration and thoroughly washed with distilled water several times, then dried at 80 °C for 2 h.

3.7. Result and discussion

3.7.1. Characterization of MnO_2 materials

Figure 3.6 shows XRD patterns of various MnO_2 nanostructured materials synthesized. XRD patterns of the three MnO_2 particles are different, but they are corresponding to the structures of α-, β- and γ-MnO_2, respectively [22], and no other phases were found. **Figure 3.7** shows SEM images of the three MnO_2 samples. As can be seen, three materials presented different morphologies. α-MnO_2 showed to be ribbon-like nanowires with diameters of 5-20 nm and lengths ranging between 0.4 and 5 μm. β-MnO_2 was observed to be as nanorods with diameters 5-100 nm and lengths ranging between 0.4 and 1.2 μm. γ-MnO_2, however, presented in quite uniformed as nanotube with diameters of 30 nm. This is different from the previous report, in which γ-MnO_2 nanorods were produced [22].

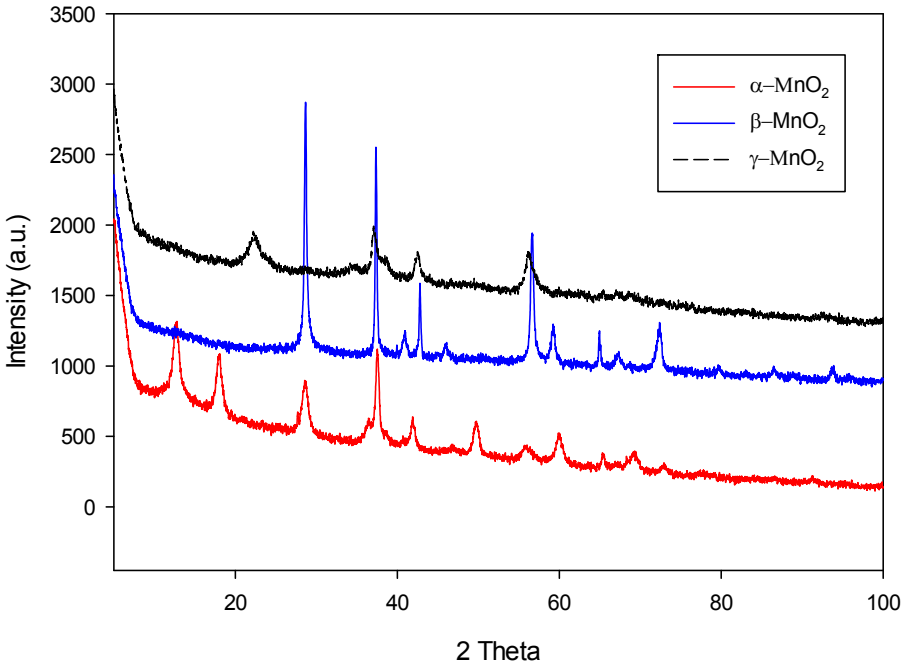

Figure 3.6. XRD patterns of various MnO_2 catalysts.

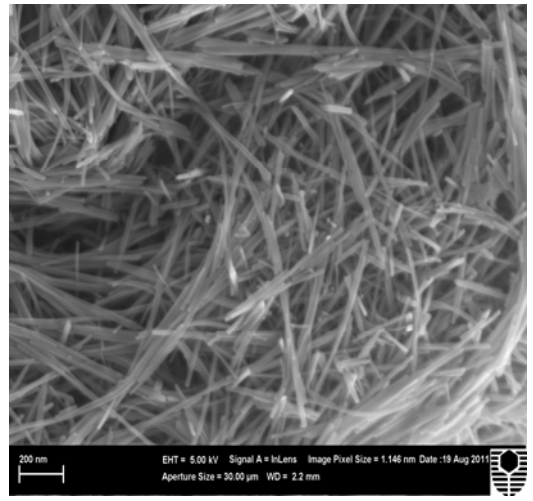

α-MnO_2

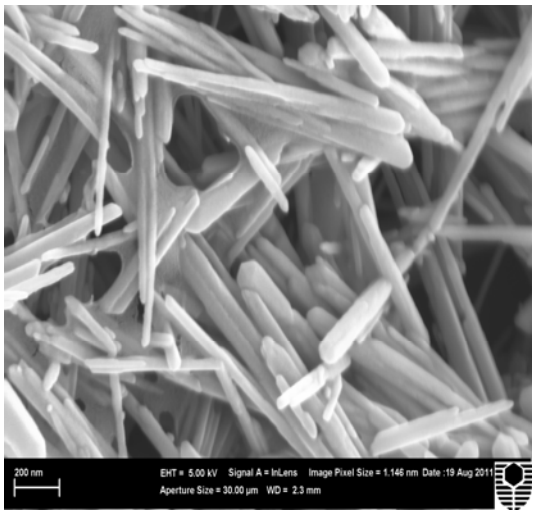

β-MnO_2

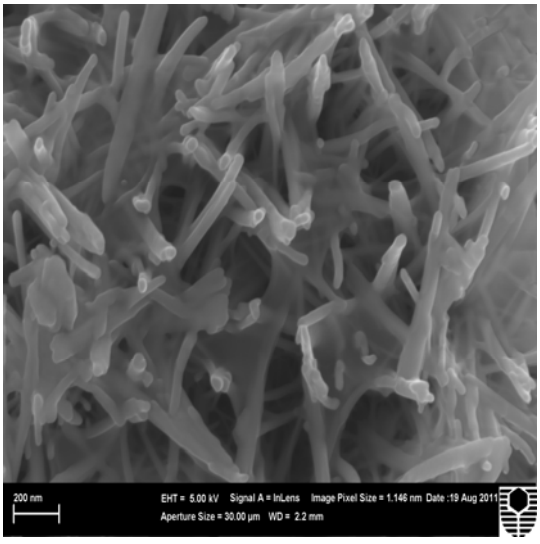

γ-MnO_2

Figure 3.7. SEM images of various MnO_2 catalysts.

Figure 3.8 shows UV-vis diffuse reflectance spectra of three MnO_2 samples. They show similar profiles with a broad and strong absorption at 400-700 nm, however, α- and γ-MnO_2 presented a stronger absorption intensity than β-MnO_2. Normally, the absorption in the visible light range can be attributed to the d-d transitions of Mn ions in the MnO_2 nanostructures [38].

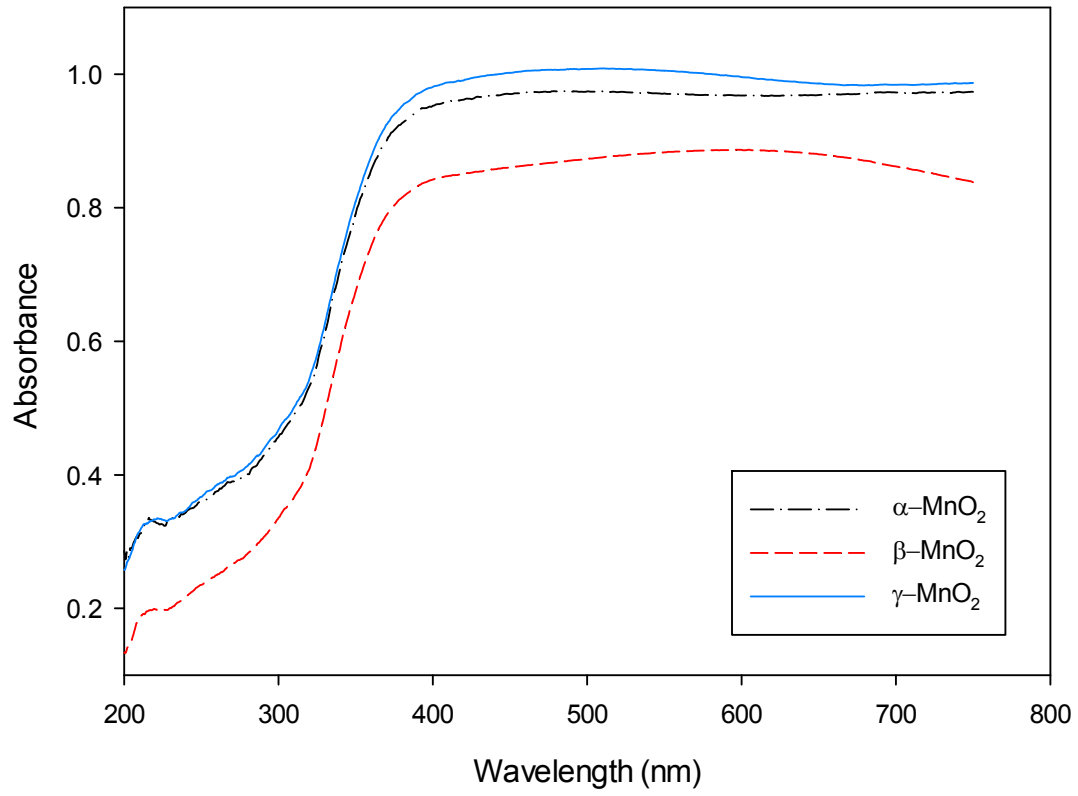

Figure 3.8. UV-vis profiles of various MnO_2 catalysts.

Figure 3.9 shows N_2 adsorption/desorption isotherms and pore size distributions of three MnO_2 materials. The BET surface area and pore volume are given in **Table 3.2**. It seems that β-MnO_2 has the highest BET surface area and γ-MnO_2 shows the lowest surface area. Three materials presented a mesoporous characteristic. The pore size distributions also showed that three materials have different pore sizes. α-MnO_2 has two larger pore ranges centered at 5.3 nm and 15 nm, respectively. β-MnO_2 has a single lower pore size peak centered at 2.6 nm while γ-MnO_2 showed two pore sizes centered at 2.4 and 6.2 nm, respectively.

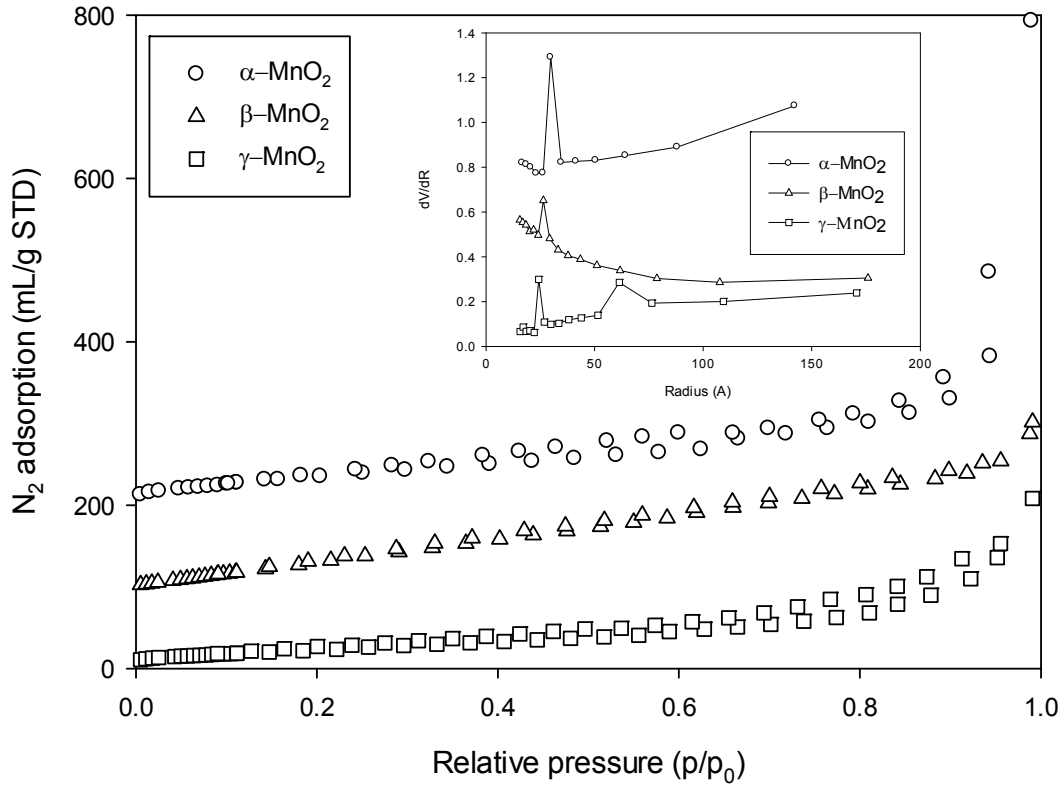

Figure 3.9. N_2 adsorption/desorption isotherms and pore size distributions of MnO_2.

Figure 3.10 shows weight loss profiles of three MnO_2 samples. Three MnO_2 samples presented quite different thermal stability profiles. β-MnO_2 showed a much strong thermal stability with only one sharp weight loss occurring at 600 ºC, which refers to the transformation of MnO_2 to Mn_2O_3 [39]. α-MnO_2 presented three stages in weight loss. The first weight loss occurred before 300 ºC, which is attributed to loss of surface adsorbed water. The second weight loss occurred between 400-570 ºC, which is due to the loss of lattice oxygen and reduction of MnO_2 to Mn_2O_3. The third weight loss occurred at 700-800 ºC, which is referred to further lattice oxygen and reduction of Mn_2O_3 to Mn_3O_4. γ-MnO_2 presented two weight losses. The first weight loss appeared before 300 ºC and the second weight loss occurred at 400-560 ºC, representing surface water loss and reduction of MnO_2 to Mn_2O_3, respectively.

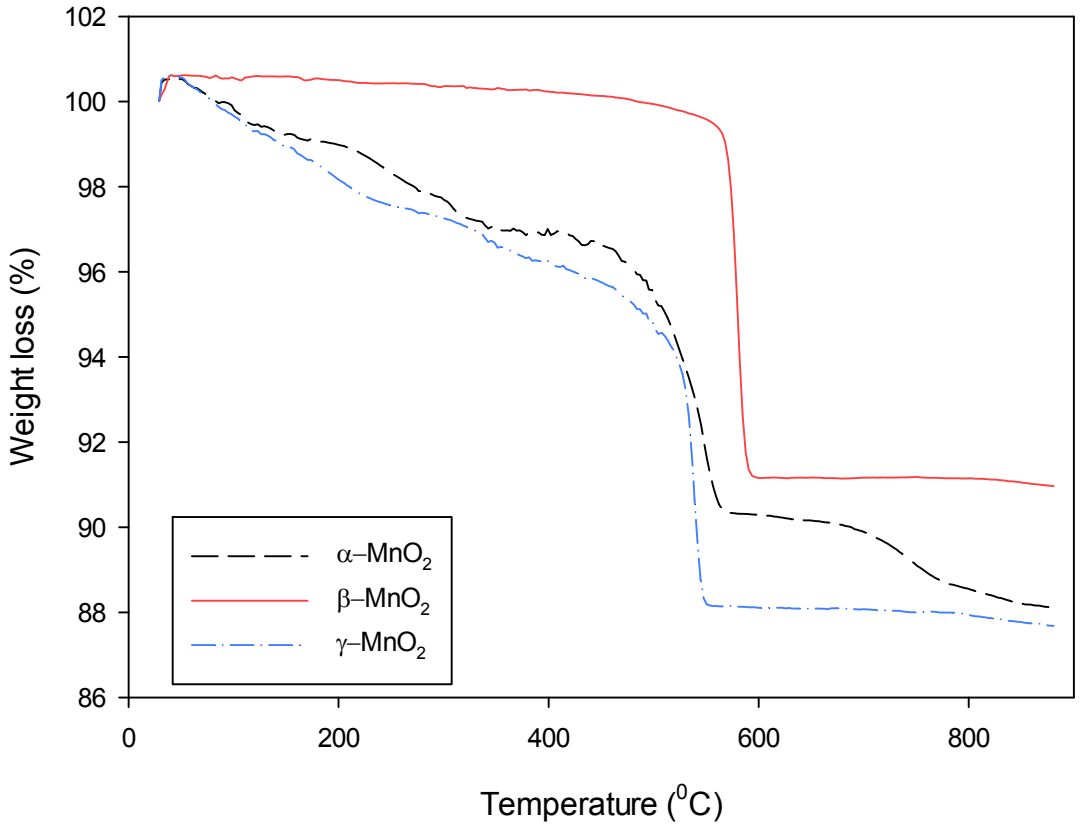

Figure 3.10. TGA profiles of various MnO_2 catalysts.

Table 3.2. Physicochemical properties of MnO_2 and their activities in phenol degradation.

Catalyst	Tunnel [39]	Size [39] (Å)	S_{BET} (m^2/g)	V (cm^3/g)	First-order rate constant (min^{-1})	R^2
α-MnO_2	(1× 1), (2× 2)	1.89, 4.6	148	0.282	0.359	0.999
β-MnO_2	(1× 1)	1.89	194	0.238	0.0723	0.993
γ-MnO_2	(1× 1), (1 × 2)	1.89, 2.3	83	0.210	0.224	0.999

3.7.2. Phenol degradation on MnO_2

The adsorption and degradation profiles of phenol against time on various MnO_2 materials are shown in **Figure 3.11**. Without MnO_2, oxone could not induce strong phenol degradation, suggesting no thermal activation of oxone for production of

sulfate radicals. Without the presence of oxone, three MnO_2 materials showed little adsorption of phenol at less than 10% after 120 min. α-MnO_2 presented higher adsorption than β-MnO_2 and γ-MnO_2, which is due to higher BET surface and pore volume. With the presence of both MnO_2 and oxone, phenol degradation was much fast and the activities of three MnO_2 were significantly different. For β-MnO_2, phenol degradation achieved 100% at about 50 min. For γ-MnO_2, phenol degradation was faster and could reach 100% at 30 min. Meanwhile, α-MnO_2 exhibited the highest reaction rate with 100% phenol degradation at 20 min. Based on the profiles, first order kinetics was used for data simulation and it was found that phenol degradation followed the first order kinetics with much high values of regression coefficients (>0.99) as presented in Table 3.2.

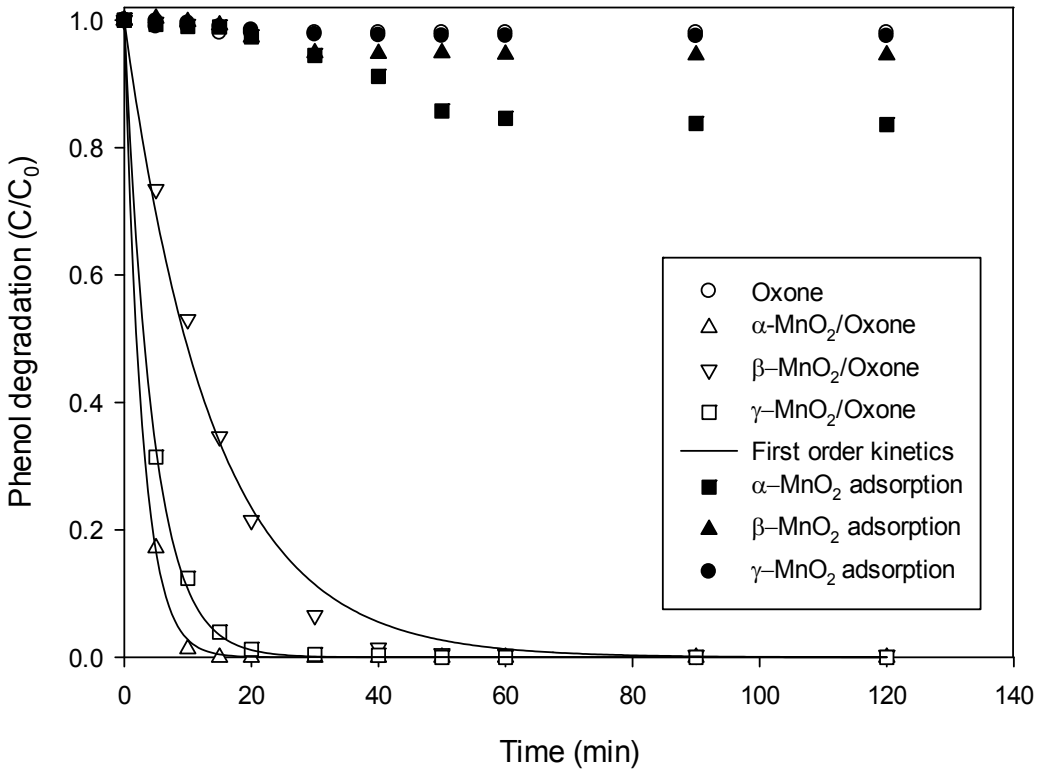

Figure 3.11. Phenol degradation on different MnO_2 samples. Reaction conditions: $[phenol]_0$ = 25 ppm, catalyst loading = 0.4 g/L, oxone loading = 2.0 g/L, T=25 ºC.

Previously, Anipsitakis and Dionysiou [23] tested various commercial Co_3O_4 for heterogeneous activation of oxone for 2,4-dichlorophenol degradation. At the conditions of 20 mg/L 2,4-DCP, 0.19 g/L Co_3O_4, 72-99% conversion of 2,4-dichlorophenol could be achieved in 30 min. Shukla et al. prepared several supported Co_3O_4 catalysts for phenol degradation and found Co_3O_4/carbon exhibited higher activity. At the similar conditions to this investigation, 100% decomposition and 80% TOC removal could be achieved in 60 min, higher than homogeneous Co^{2+}/oxone [27]. Very recently, Liang et al. [37] reported that Co_3O_4/MnO_2 could also demonstrated higher activity for phenol degradation. At the conditions of 25 ppm phenol, 0.5 g_{cat}/L and 2.0 g_{oxone}/L, phenol conversion could reach 100% at 20 min on 1 wt%Co/MnO_2. Therefore, α-MnO_2 nanowires in this report presented much better activity than Co_3O_4-based systems.

In general, MnO_2 forms the framework of "octahedral molecular sieve" (OMS) structures. The building blocks of these structures are columns of edge-sharing MnO_6 octahedra. Because these structures differ in the way MnO_6 octahedra are interlinked, they possess tunnels or interlayers with gaps of different magnitudes [22, 39]. α-MnO_2 consists of double chains of edge-sharing MnO_6 octahedra with (2 x 2) and (1 x 1) tunnels. β-MnO_2 is composed of single strands of edge-sharing MnO_6 octahedra with (1 x 1) tunnel. γ-MnO_2 forms in random intergrowth of ramsdellite (1 x 2) and pyrolusite (1 x 1) structure [39]. Table 3.2 presents the crystallographic parameters of different MnO_2 forms.

It has been proposed that activation of peroxymonosulfate (PMS) was induced by redox reactions. Transition of Mn^{4+}/Mn^{3+} involving a single electron transfer is responsible for catalytic reaction. For MnO_2/oxone, MnO_2 can induce the decomposition of peroxymonosulfate and produce sulfate radicals as shown in the following equations.

$$HSO_5^- + 2MnO_2 \rightarrow SO_5^{-\bullet} + OH^- + Mn_2O_3 \quad (3.5)$$

$$HSO_5^- + Mn_2O_3 \rightarrow SO_4^{-\bullet} + H^+ + 2MnO_2 \quad (3.6)$$

$$SO_4^{-\bullet} + H_2O \rightarrow OH^{\bullet} + H^+ + SO_4^{2-} \quad (3.7)$$

$$C_6H_5OH + SO_4^{-\bullet} \rightarrow \text{several steps} \rightarrow CO_2 + H_2O + SO_4^{2-} \quad (3.8)$$

Devaraj and Munichandraiah [39] investigated electrochemical capacitance properties of different MnO_2 crystallographic structures, namely, α, β, γ, δ, and λ structures. The specific capacitance (SC) measured for α-, β-, γ-MnO_2 was found to decrease in the following order: α > γ > β. A wide (~4.6 Å) tunnel size and large surface area of α-MnO_2 are ascribed as favorable factors for its high SC.

Cao et al. [8] studied decomposition of methylene blue (MB) with H_2O_2 on α-MnO_2 and β-MnO_2 nanorods and found that, after 90 min of reaction, the decoloration efficiencies of MB dye for α-MnO_2 and β-MnO_2 nanorod catalysts were about 50% and 95%, respectively. The differences in their catalytic activities between the α-MnO_2 and β-MnO_2 nanorod catalysts may be resulted from the difference of their surface areas and active sites. Liang et al. [40] synthesized α-, β-, γ-, and δ-MnO_2 nanorods for CO oxidation. The activity for CO oxidation was mainly predominated by the crystal phase and channel structure of the MnO_2 nanorods in the order of α- ≈ δ- > γ- > β-MnO_2. Wang et al. [41] prepared nanosized rod-like, wire-like, and tubular α-MnO_2 for toluene oxidation. They found the presence of surface Mn ions in multiple oxidation states (e.g., Mn^{3+}, Mn^{4+}, or even Mn^{2+}) and the formation of surface oxygen vacancies. The activity decreased in the order of rod-like α-MnO_2 > tube-like α-MnO_2 > wire-like α-MnO_2.

In this investigation, three crystallographic MnO_2 nanostructures also showed different activities in activation of oxone for phenol degradation, which can be related to the variation in structure and other physicochemical properties. Anipsitakis and Dionysiou [20] reported that Mn(II) activation of oxone would generate caged or bound to the metal sulfate radicals. For heterogeneous activation of oxone by MnO_2, sulfate radicals would be bounded to MnO_2 surface and phenol oxidation would occur on the solid surface. Adsorption tests showed that α-MnO_2 exhibited higher phenol adsorption, which promoted the reaction between sulfate radical and phenol. TGA analysis showed that α-, β-, and γ-MnO_2 presented different oxygen loss potentials. α-MnO_2 could have oxidation transformation processes of $Mn^{4+}\rightarrow Mn^{3+}\rightarrow Mn^{2+}$, while β-, and γ-$MnO_2$ could only have one process of $Mn^{4+}\rightarrow Mn^{3+}$, but this reduction process occurs easily on γ-MnO_2. Compared with structure of α-, β-, and γ-MnO_2,

two-tunnel structured α-, and γ-MnO_2 will show higher activity than the single-tunnel structured β-MnO_2.

Further investigations were conducted to understand the effect of reaction conditions on phenol degradation using the most effective α-MnO_2. **Figure 3.12** presents phenol degradation efficiencies at varying initial phenol concentrations. With increased phenol concentration, phenol degradation efficiency would decrease. At 75 or 100 ppm phenol, phenol degradation at 100% would take 90 min.

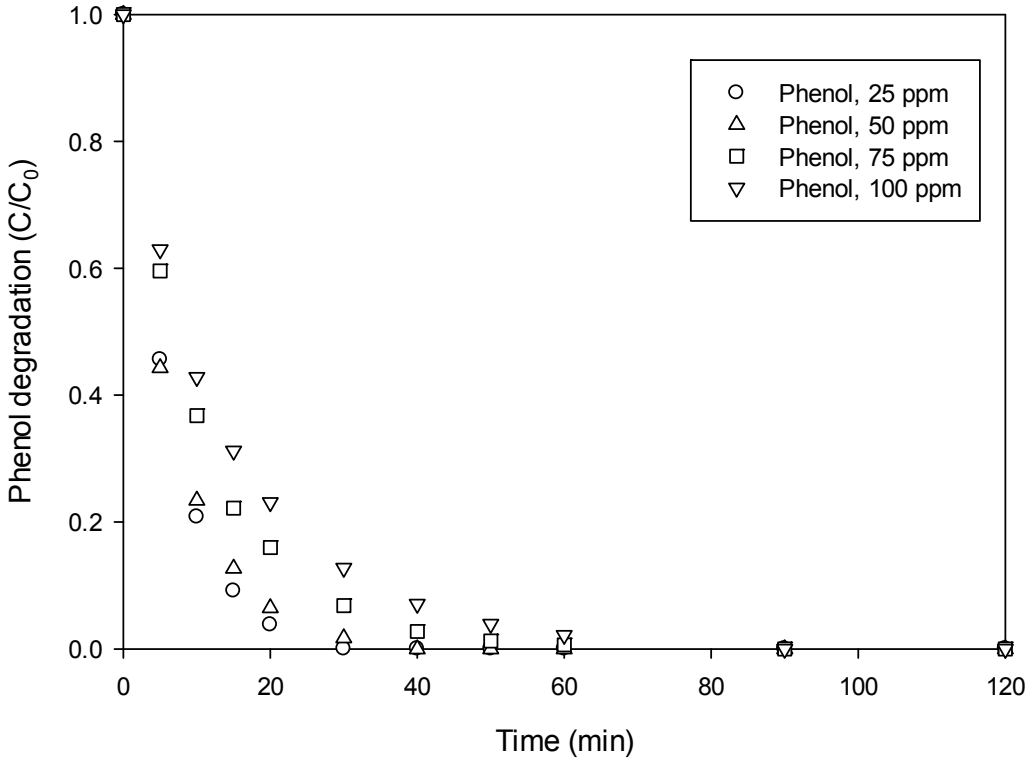

Figure 3.12. Effect of phenol concentration on phenol degradation on α-MnO_2. Reaction conditions: catalyst loading = 0.4 g/L, oxone loading = 2.0 g/L, T=25 ºC.

Figure 3.13 shows the effect of α-MnO_2 loading on phenol degradation. It is seen that high α-MnO_2 loading in solution would significantly increase phenol degradation. At 0.05 g α-MnO_2, phenol degradation at 100% would require 60 min. However, when α-MnO_2 loading was increased to 0.1 g, 100% phenol degradation would be reached at 30 min. Further enhancement of α-MnO_2 loading resulted in much less time to reach 100% phenol degradation. At 0.2 g, 100% phenol degradation would be

reached at 15 min. The higher of α-MnO_2 loading in solution would increase the reaction between α-MnO_2 and oxone for production of more amounts of sulfate radicals, resulting in high phenol degradation efficiency.

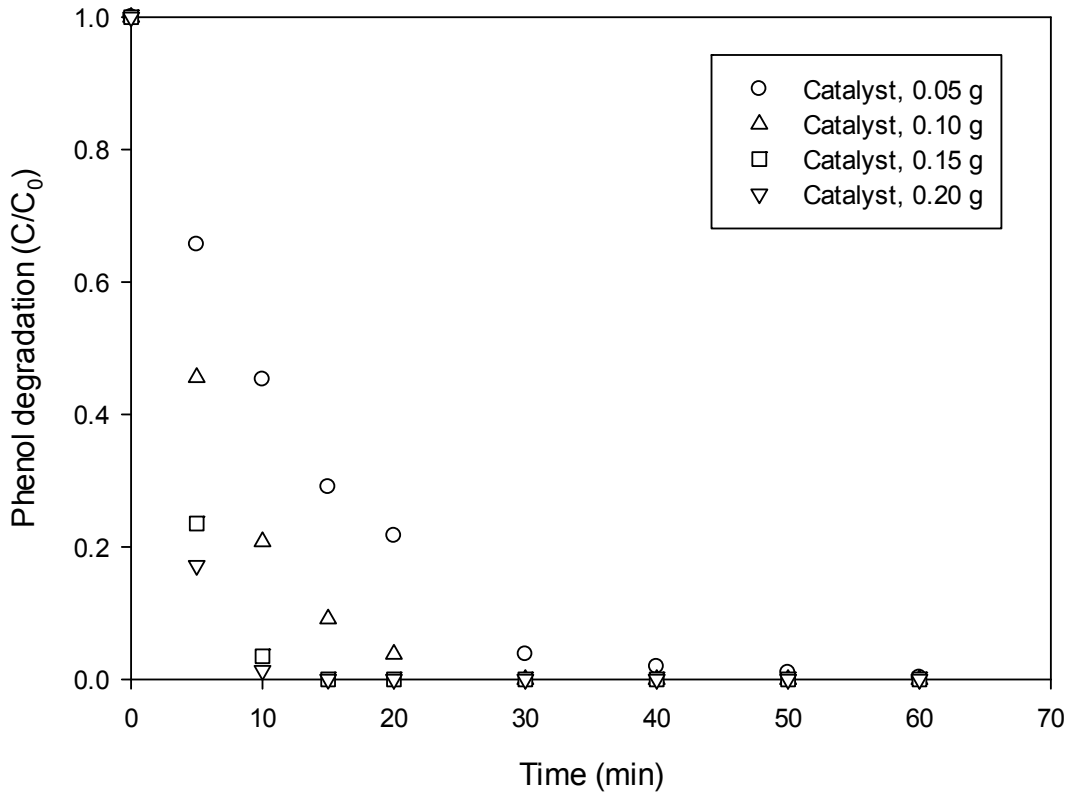

Figure 3.13. Effect of catalyst loading on phenol degradation on α-MnO_2 at varying time. Reaction conditions: $[phenol]_0$ = 25 ppm, oxone loading = 2.0 g/L, T=25 ºC.

Figure 3.14 shows the effect of oxone loading on phenol degradation. As can be seen, higher amount of oxone in solution will also result in higher phenol degradation rate and efficiency. At 0.2 g oxone, phenol degradation can reach 100% at 90 min, but it will reach 100% at 30 min at 1.0 g oxone.

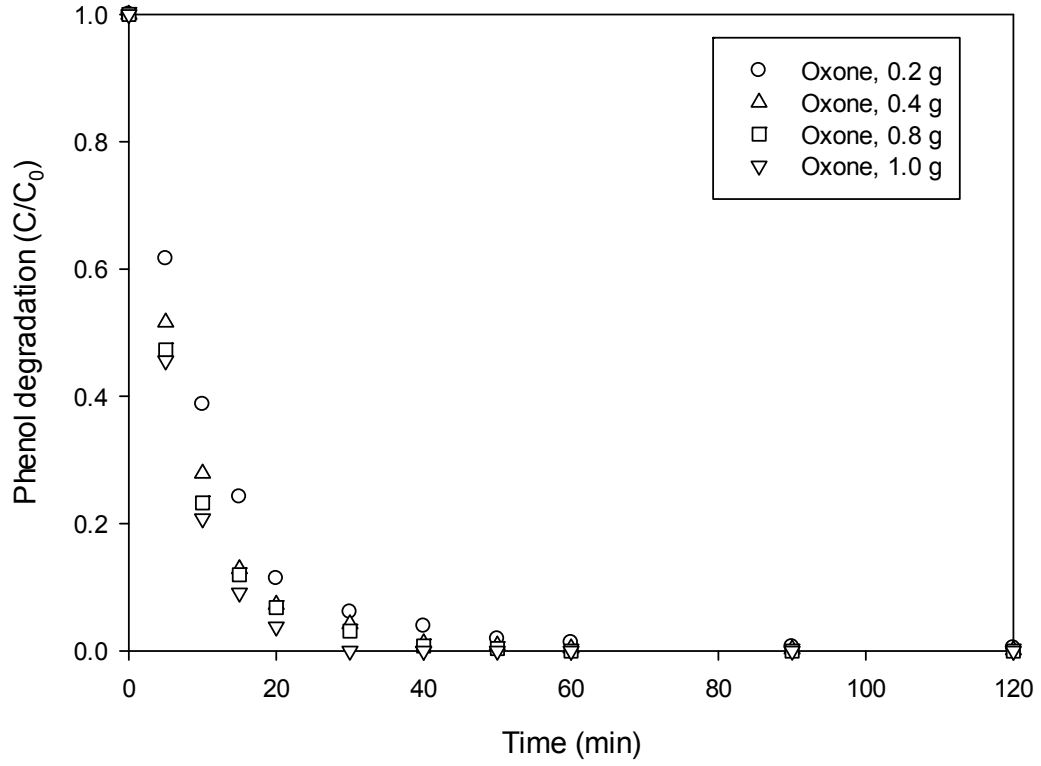

Figure 3.14. Effect of oxone loading on phenol degradation on α-MnO_2 at varying time. Reaction conditions: $[phenol]_0$ = 25 ppm, catalyst loading = 0.4 g/L, T=25 ºC.

Table 3.3. Activation energies of heterogeneous Co-based catalysts and α-MnO_2 with oxone for phenol degradation.

Catalysts	Ea (kJ/mol)	References
Co_3O_4/ZSM5	69.7	[26]
Co_3O_4/SBA-15	67.4	[33]
Co_3O_4/SiO_2	61.7-75.5	[34]
Co_3O_4/Fly-ash	47.0-56.5	[42]
Co_3O_4/Red-mud	46.2-47.0	[43]
Co_3O_4/Activated-carbon	59.7	[27]
Co_3O_4/Carbon-aerogel	62.9	[44]
Co_3O_4−rGO	26.5	[45]
$CoFe_2O_4$−rGO	15.8	[46]
α-MnO_2	21.9	This work

Figure 3.15 shows the effect of temperature on phenol degradation. In general, higher temperature will enhance the reaction rate and it is seen that phenol degradation can reach 100% at 15 min at 45 ºC. Based on the first order kinetics, reaction rate

constants were determined and the correlation between the constant and temperature was fitted by the Arrhenius relationship as shown in an inset of **Figure 3.15**. The activation energy was thus calculated to be 21.9 kJ/mol.

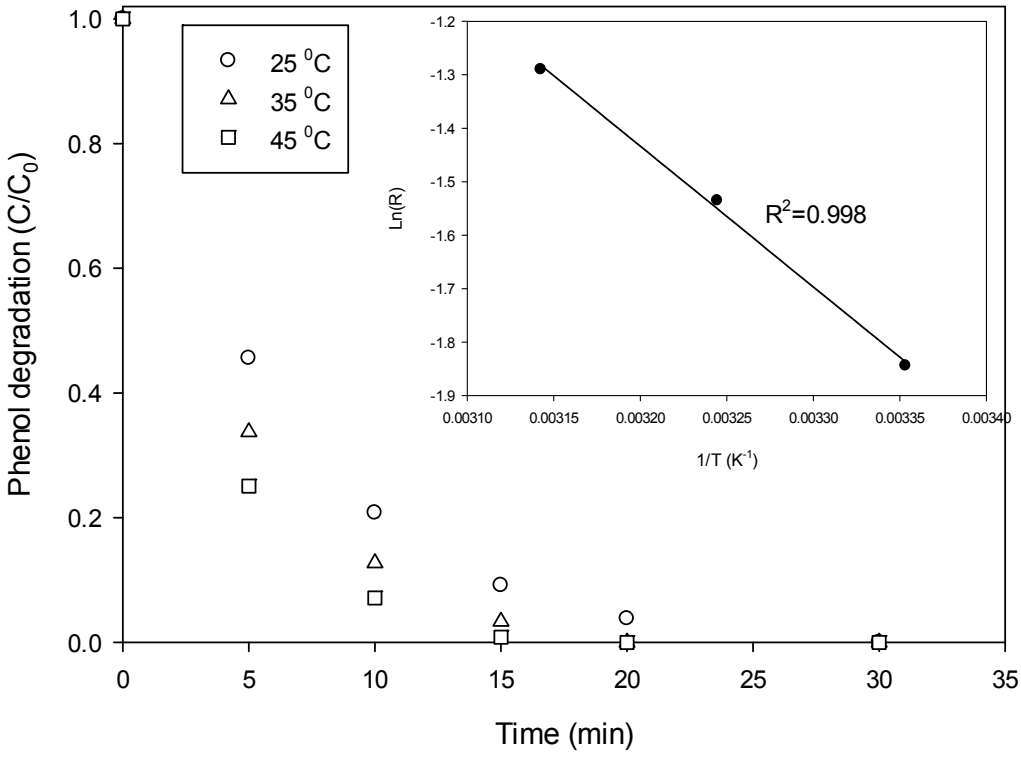

Figure 3.15. Phenol degradation on α-MnO_2 at varying temperatures. Reaction conditions: $[phenol]_0$ = 25 ppm, catalyst loading = 0.4 g/L, oxone loading = 2.0 g/L.

Previously, no investigation has been reported in MnO_2 activation of oxone for phenol degradation. However, some investigations have been reported in heterogeneous activation of oxone by Co catalysts for phenol degradation. The activation energies of phenol degradation in Co catalysts with oxone are presented in Table 2. As can be seen that the activation energies of supported Co catalysts are about 40-70 kJ/mol. The lower activation energy of reduced graphene oxide (rGO) supported Co catalysts is due to the active support, graphene, which can also activate oxone for sulfate radical generation [36]. Thus, α-MnO_2 presented much lower activation energy than those of supported Co catalysts.

Figure 3.16 shows the activity of regenerated α-MnO_2 by simple water washing in phenol degradation. One can see that α-MnO_2 presented similar activity in second and third runs. Phenol degradation efficiency could also be at 100% in 20 min, suggesting high stability of α-MnO_2 and its usability.

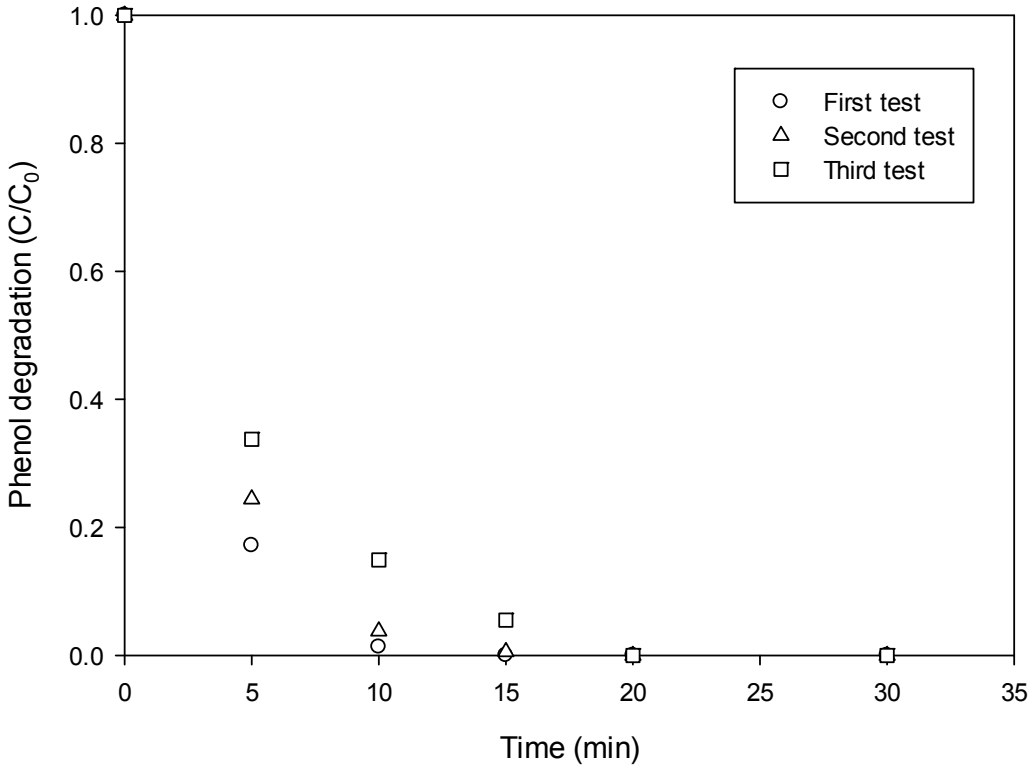

Figure 3.16. Phenol degradation on α-MnO_2 at different runs after recycling. Reaction conditions: $[phenol]_0$ = 25 ppm, catalyst loading = 0.4 g/L, oxone loading = 2.0 g/L, T=25 ºC.

3.8. Conclusions

In summary, different crystallographic phases of MnO_2 materials were synthesized and they presented varying structures and morphologies. α-MnO_2 presented as nanowires and showed the highest activity in activation of oxone for phenol degradation due to high surface area and double tunneled structure. β-MnO_2 had a nanorod form but showed the lowest activity attributed to single tunnel and stable

oxygen reduction. γ-MnO_2 presented in nanotube and showed intermediate activity. Further investigations indicated that phenol degradation rate was affected by MnO_2 and oxone loadings, phenol concentration and temperature and that the degradation followed the first order kinetics with the activation energy of 21.9 kJ/mol. The high activity, low activation energy and stable performance of α-MnO_2 make it as a promising alternative to the toxic Co_3O_4.

References

1. Bautista, P., A.F. Mohedano, J.A. Casas, J.A. Zazo, and J.J. Rodriguez, *An overview of the application of Fenton oxidation to industrial wastewaters treatment.* Journal of Chemical Technology and Biotechnology, 2008. **83**(10): p. 1323-1338.

2. Neyens, E. and J. Baeyens, *A review of classic Fenton's peroxidation as an advanced oxidation technique.* Journal of Hazardous Materials, 2003. **98**(1-3): p. 33-50.

3. Pignatello, J.J., E. Oliveros, and A. MacKay, *Advanced oxidation processes for organic contaminant destruction based on the Fenton reaction and related chemistry.* Critical Reviews in Environmental Science and Technology, 2006. **36**(1): p. 1-84.

4. Wang, S., *A comparative study of Fenton and Fenton-like reaction kinetics in decolourisation of wastewater.* Dyes and Pigments, 2008. **76**(3): p. 714-720.

5. Ai, Z.H., L.Z. Zhang, F.H. Kong, H. Liu, W.T. Xing, and J.R. Qiu, *Microwave-assisted green synthesis of MnO_2 nanoplates with environmental catalytic activity.* Materials Chemistry and Physics, 2008. **111**(1): p. 162-167.

6. Zhang, W., Z. Yang, X. Wang, Y. Zhang, X. Wen, and S. Yang, *Large-scale synthesis of β-MnO_2 nanorods and their rapid and efficient catalytic oxidation of methylene blue dye.* Catalysis Communications, 2006. **7**(6): p. 408-412.

7. Watts, R.J., J. Sarasa, F.J. Loge, and A.L. Teel, *Oxidative and reductive pathways in manganese-catalyzed Fenton's reactions.* Journal of Environmental Engineering-Asce, 2005. **131**(1): p. 158-164.

8. Cao, G., L. Su, X. Zhang, and H. Li, *Hydrothermal synthesis and catalytic properties of α- and β-MnO_2 nanorods.* Materials Research Bulletin, 2010. **45**(4): p. 425-428.

9. Zhao, D., X. Yang, H. Zhang, C. Chen, and X. Wang, *Effect of environmental conditions on Pb(II) adsorption on β-MnO_2.* Chemical Engineering Journal, 2010. **164**(1): p. 49-55.

10. Singh, M., D.N. Thanh, P. Ulbrich, N. Strnadová, and F. Štěpánek, *Synthesis, characterization and study of arsenate adsorption from aqueous solution by α- and δ-phase manganese dioxide nanoadsorbents.* Journal of Solid State Chemistry, 2010. **183**(12): p. 2979-2986.

11. Saleh, T.A., S. Agarwal, and V.K. Gupta, *Synthesis of MWCNT/MnO_2 and their application for simultaneous oxidation of arsenite and sorption of arsenate.* Applied Catalysis B: Environmental, 2011. **106**(1-2): p. 46-53.

12. Lee, S., B. Choi, N. Hamasuna, C. Fushimi, and A. Tsutsumi, *Characterization of MnO_2 positive electrode for Fuel Cell/Battery (FCB).* Journal of Power Sources, 2008. **181**(1): p. 177-181.

13. Choi, B., S. Lee, C. Fushimi, and A. Tsutsumi, *Fibrous MnO_2 electrode electrodeposited on carbon fiber for a fuel cell/battery system.* Electrochimica Acta, 2011. **56**(19): p. 6696-6701.

14. Xu, L., C. Xu, M.R. Zhao, Y.P. Qiu, and G.D. Sheng, *Oxidative removal of aqueous steroid estrogens by manganese oxides.* Water Research, 2008. **42**(20): p. 5038-5044.

15. Dong, Y.M., H.X. Yang, K. He, S.Q. Song, and A.M. Zhang, *β-MnO_2 nanowires: A novel ozonation catalyst for water treatment.* Applied Catalysis B-Environmental, 2009. **85**(3-4): p. 155-161.

16. Sui, N., Y. Duan, X. Jiao, and D. Chen, *Large-Scale Preparation and Catalytic Properties of One-Dimensional α/β-MnO_2 Nanostructures.* The Journal of Physical Chemistry C, 2009. **113**(20): p. 8560-8565.

17. Anipsitakis, G.P. and D.D. Dionysiou, *Degradation of organic contaminants in water with sulfate radicals generated by the conjunction of peroxymonosulfate with cobalt.* Environmental Science & Technology, 2003. **37**(20): p. 4790-4797.

18. Sun, J., X. Li, J. Feng, and X. Tian, *Oxone/Co^{2+} oxidation as an advanced oxidation process: Comparison with traditional Fenton oxidation for treatment of landfill leachate.* Water Research, 2009. **43**(17): p. 4363-4369.

19. Ling, S.K., S. Wang, and Y. Peng, *Oxidative degradation of dyes in water using Co^{2+}/H_2O_2 and Co^{2+}/peroxymonosulfate.* Journal of Hazardous Materials, 2010. **178**(1-3): p. 385-389.

20. Anipsitakis, G.P. and D.D. Dionysiou, *Radical generation by the interaction of transition metals with common oxidants.* Environmental Science & Technology, 2004. **38**(13): p. 3705-3712.

21. Hong, X.L., G.Y. Zhang, H.Q. Yang, and Y.Y. Zhu, *Synthesis and characterization of mesoporous manganese oxides.* Journal of Materials Synthesis and Processing, 2002. **10**(6): p. 297-302.

22. Wang, X. and Y.D. Li, *Synthesis and formation mechanism of manganese dioxide nanowires/nanorods.* Chemistry-a European Journal, 2003. **9**(1): p. 300-306.

23. Anipsitakis, G.P., E. Stathatos, and D.D. Dionysiou, *Heterogeneous activation of oxone using Co_3O_4.* Journal of Physical Chemistry B, 2005. **109**(27): p. 13052-13055.

24. Chen, X., J. Chen, X. Qiao, D. Wang, and X. Cai, *Performance of nano-Co_3O_4/peroxymonosulfate system: Kinetics and mechanism study using Acid Orange 7 as a model compound.* Applied Catalysis B-Environmental, 2008. **80**(1-2): p. 116-121.

25. Yang, Q., H. Choi, S.R. Al-Abed, and D.D. Dionysiou, *Iron-cobalt mixed oxide nanocatalysts: Heterogeneous peroxymonosulfate activation, cobalt leaching, and ferromagnetic properties for environmental applications.* Applied Catalysis B-Environmental, 2009. **88**(3-4): p. 462-469.

26. Shukla, P., S.B. Wang, K. Singh, H.M. Ang, and M.O. Tade, *Cobalt exchanged zeolites for heterogeneous catalytic oxidation of phenol in the presence of peroxymonosulphate.* Applied Catalysis B-Environmental, 2010. **99**(1-2): p. 163-169.

27. Shukla, P.R., S.B. Wang, H.Q. Sun, H.M. Ang, and M. Tade, *Activated carbon supported cobalt catalysts for advanced oxidation of organic contaminants in aqueous solution.* Applied Catalysis B-Environmental, 2010. **100**(3-4): p. 529-534.

28. Shukla, P., I. Fatimah, S.B. Wang, H.M. Ang, and M.O. Tade, *Photocatalytic generation of sulphate and hydroxyl radicals using zinc oxide under low-power UV to oxidise phenolic contaminants in wastewater.* Catalysis Today, 2010. **157**(1-4): p. 410-414.

29. Zhou, G., H. Sun, S. Wang, H. Ming Ang, and M.O. Tadé, *Titanate supported cobalt catalysts for photochemical oxidation of phenol under visible light irradiations.* Separation and Purification Technology, 2011. **80**(3): p. 626-634.

30. Yang, Q., H. Choi, Y. Chen, and D.D. Dionysiou, *Heterogeneous activation of peroxymonosulfate by supported cobalt catalysts for the degradation of 2,4-dichlorophenol in water: The effect of support, cobalt precursor, and UV radiation.* Applied Catalysis B-Environmental, 2008. **77**(3-4): p. 300-307.

31. Yang, Q., H. Choi, and D.D. Dionysiou, *Nanocrystalline cobalt oxide immobilized on titanium dioxide nanoparticles for the heterogeneous activation of peroxymonosulfate.* Applied Catalysis B-Environmental, 2007. **74**(1-2): p. 170-178.

32. Hu, L., X. Yang, and S. Dang, *An easily recyclable Co/SBA-15 catalyst: Heterogeneous activation of peroxymonosulfate for the degradation of phenol in water.* Applied Catalysis B-Environmental, 2011. **102**(1-2): p. 19-26.

33. Shukla, P., H. Sun, S. Wang, H.M. Ang, and M.O. Tadé, *Co-SBA-15 for heterogeneous oxidation of phenol with sulfate radical for wastewater treatment.* Catalysis Today, 2011. **175**: p. 380-385.

34. Shukla, P., H.Q. Sun, S.B. Wang, H.M. Ang, and M.O. Tade, *Nanosized Co_3O_4/SiO_2 for heterogeneous oxidation of phenolic contaminants in waste water.* Separation and Purification Technology, 2011. **77**(2): p. 230-236.

35. Muhammad, S., P.R. Shukla, M.O. Tadé, and S. Wang, *Heterogeneous activation of peroxymonosulphate by supported ruthenium catalysts for phenol degradation in water.* Journal of Hazardous Materials, 2012. **215–216**(0): p. 183-190.

36. Saputra, E., S. Muhammad, H. Sun, A. Patel, P. Shukla, Z.H. Zhu, and S. Wang, *α-MnO_2 activation of peroxymonosulfate for catalytic phenol degradation in aqueous solutions.* Catalysis Communications, 2012. **26**(0): p. 144-148.

37. Liang, H., H. Sun, A. Patel, P. Shukla, Z.H. Zhu, and S. Wang, *Excellent performance of mesoporous Co_3O_4/MnO_2 nanoparticles in heterogeneous activation of peroxymonosulfate for phenol degradation in aqueous solutions.* Applied Catalysis B: Environmental, 2012. **127**(0): p. 330-335.

38. Gao, T., M. Glerup, F. Krumeich, R. Nesper, H. Fjellvåg, and P. Norby, *Microstructures and spectroscopic roperties of cryptomelane-type manganese dioxide nanofibers.* The Journal of Physical Chemistry C, 2008. **112**(34): p. 13134-13140.

39. Devaraj, S. and N. Munichandraiah, *Effect of crystallographic structure of MnO_2 on its electrochemical capacitance properties.* The Journal of Physical Chemistry C, 2008. **112**(11): p. 4406-4417.

40. Liang, S., F. Teng, G. Bulgan, R. Zong, and Y. Zhu, *Effect of Phase Structure of MnO_2 Nanorod Catalyst on the Activity for CO Oxidation.* The Journal of Physical Chemistry C, 2008. **112**(14): p. 5307-5315.

41. Wang, F., H. Dai, J. Deng, G. Bai, K. Ji, and Y. Liu, *Manganese Oxides with Rod-, Wire-, Tube-, and Flower-Like Morphologies: Highly Effective Catalysts for the Removal of Toluene.* Environmental Science & Technology, 2012. **46**(7): p. 4034-4041.

42. Muhammad, S., E. Saputra, H. Sun, J.d.C. Izidoro, D.A. Fungaro, H.M. Ang, M.O. Tade, and S. Wang, *Coal fly ash supported Co_3O_4 catalysts for phenol degradation using peroxymonosulfate.* RSC Advances, 2012. **2**(13): p. 5645-5650.

43. Muhammad, S., E. Saputra, H. Sun, H.-M. Ang, M.O. Tadé, and S. Wang, *Heterogeneous Catalytic Oxidation of Aqueous Phenol on Red Mud-Supported Cobalt Catalysts.* Industrial & Engineering Chemistry Research, 2012. **51**(47): p. 15351-15359.

44. Hardjono, Y., H. Sun, H. Tian, C.E. Buckley, and S. Wang, *Synthesis of Co oxide doped carbon aerogel catalyst and catalytic performance in heterogeneous oxidation of phenol in water.* Chemical Engineering Journal, 2011. **174**(1): p. 376-382.

45. Yao, Y., Z. Yang, H. Sun, and S. Wang, *Hydrothermal Synthesis of Co_3O_4–Graphene for Heterogeneous Activation of Peroxymonosulfate for Decomposition of Phenol.* Industrial & Engineering Chemistry Research, 2012. **51**(46): p. 14958-14965.

46. Yao, Y., Z. Yang, D. Zhang, W. Peng, H. Sun, and S. Wang, *Magnetic $CoFe_2O_4$–Graphene Hybrids: Facile Synthesis, Characterization, and Catalytic Properties.* Industrial & Engineering Chemistry Research, 2012. **51**(17): p. 6044-6051.

Chapter 4

Manganese Oxides at Different Oxidation States for Heterogeneous Activation of Peroxymonosulfate for Phenol Degradation in Aqueous Solution

Abstract

A series of manganese oxides (MnO, MnO_2, Mn_2O_3 and Mn_3O_4) were synthesized and tested in heterogeneous activation of peroxymonosulfate (PMS) for phenol degradation in aqueous solutions. Their properties were characterized by several techniques such as X-ray diffraction (XRD), thermogravimetric analysis (TGA), scanning electron microscopy (SEM), and N_2 adsorption/desorption isotherms. Catalytic activities of Mn oxides were found to be closely related to the chemical states of Mn. Mn_2O_3 is highly effective in heterogeneous activation of PMS to produce sulfate radicals for phenol degradation compared with other catalysts (MnO, MnO_2, and Mn_3O_4). The activity shows an order of Mn_2O_3 > MnO > Mn_3O_4 > MnO_2. Mn_2O_3 could completely remove phenol in 60 min at the conditions of 25 ppm phenol, 0.4 g/L catalyst, 2 g/L PMS, and 25 ^oC. After heat regeneration, the activity could be fully recovered. A pseudo first order model would fit to phenol degradation kinetics and activation energy was obtained as 11.4 kJ/mol.

4.1. Introduction

Over the last decades, water treatment plays an important role in our lives, because of fresh water crisis and the increasing awareness of human health and ecological systems as a result of industrial waste pollution. Industrial activities generate large amounts of organic hazardous substances discharged into the environment. The organic wastes can be found in many industries as by-products such as petroleum refining, petrochemical, pharmaceutical, plastic, pesticides, chemical industries, agrochemicals, and pulp and paper industries [1, 2]. The organic pollutants e.g. phenol, are toxic and cause considerable damage and threat to the ecosystem in water bodies and to the human health even at low concentrations [3]. It is important to dispose of wastewater in a proper way in order to comply with environmental regulations. However, the organics in wastewaters from chemical and related industries cannot be well treated by conventional processes due to degradation of these pollutants being very slow or ineffective and not environmentally compatible [4, 5]. The most promising method for degradation of organic pollutants in wastewater is advanced oxidation processes (AOPs). AOPs are based on generation and utilization of reactive species, such as hydroxyl radicals (OH•) that have a high standard oxidation potential and react none selectively [6, 7]. Heterogeneous catalytic oxidation systems have recently attracted much interest due to easily recovery and reuse of the catalysts [8].

Lately, manganese oxides, such as MnO, MnO_2, Mn_2O_3 and Mn_3O_4, have attracted much attention due to their physical and chemical properties for being used as catalysts, adsorbents, supercapacitors, and battery materials [9-15]. Kim and Shim [16] have conducted a study on the catalytic combustion of aromatic hydrocarbons (benzene and toluene) on manganese oxides. The results indicated that the catalysts showed high activity in the oxidation of hydrocarbons at temperatures below 300 ^{o}C. Furthermore, the reactivity of catalysts exhibited an order of Mn_3O_4 > Mn_2O_3 > MnO_2, which was correlated with oxygen mobility on the catalysts. Rames et al. [17] have studied CO oxidation over a series of manganese oxide catalysts and found that Mn_2O_3 is the best catalyst, with the sequence of catalytic activity as MnO ≤ MnO_2 < Mn_2O_3. Santos et al. [18] reported the synthesis of manganese oxide nanoparticles for

ethyl acetate oxidation. Complete oxidation of ethyl acetate was achieved at temperature below 300 ^{o}C. However, few investigations have been conducted in the activity of a series of manganese oxides at different valence states in water treatment.

In the most of previous investigations in water treatment, MnO_x was usually used for Fenton-like reaction for production of hydroxyl radicals from H_2O_2 and oxidation of organic compounds. Recently, sulfate radicals produced by Co^{2+}/oxone or Ru^{3+}/oxone have attracted intense attention in degradation of organic compounds for water treatment. However, Co^{2+} or Ru^{3+} may generate a secondary pollutant [19, 20]. Therefore, alternative metal such as Fe^{2+}, has been proposed by Zazo et al. [21]. They found that Fe^{2+}/H_2O_2 have a high catalytic activity for degradation of phenol. In contrary, a recent study by Watts et al. [22] revealed that Mn^{2+}/H_2O_2 was significantly more reactive than Fe^{2+}/H_2O_2. Moreover, they found that catalytic activity was influenced significantly by pH. Saputra et al. [19] reported the oxidative removal of phenol from water by MnO_2 and studied the factors influencing the reactions. They found that MnO_2 exhibited as a promising chemical agent under certain conditions for phenol removal from waste water. However, no further investigation has been reported for solid MnO_x for the activation of peroxymonosulfate to generate sulfate radicals.

In this research, we investigate the performance of a series of manganese oxides at varying valence states for heterogeneous generation of sulfate radicals for chemical mineralization of phenol in the solution. These catalysts will be an alternative for advanced oxidation process. Several key parameters in the kinetic study such as phenol concentration, catalyst loading, oxone concentration and temperature were investigated. Regeneration of used catalysts was also investigated.

4.2. Experimental methods

4.2.1 Preparation of Mn catalysts

A manganese dioxide (MnO_2) was purchased from Sigma-Aldrich Company and used without further treatment. Mn_2O_3 was obtained by treating the MnO_2 at 550 ^{o}C in air for 5 h. In addition, MnO_2 was calcined at 950 ^{o}C in air for 2 h to get Mn_3O_4. Another

catalyst (MnO) was obtained by a two-step method. First, $MnCO_3$ was synthesized by a hydrothermal method [23] and then calcination was made. Typically, $KMnO_4$ (3 mmol) and an equal amount of glucose were put into distilled water at room temperature to form a homogeneous solution, which was transferred into a 45 mL Teflon-lined autoclave. The autoclave was sealed and maintained at 150 ^oC for 10 h, and was then cooled down to room temperature naturally. The resulted solid product ($MnCO_3$) was filtered, washed with distilled water and dried in air at 100 ^oC overnight. Finally, MnO catalyst was obtained by calcination of $MnCO_3$ at 500 ^oC under argon flow at the rate 60 mL/min for 2 h.

4.2.2 Characterization of catalysts

Catalysts were characterized by X-ray diffraction (XRD), N_2 adsorption/desorption isotherm, scanning electron microscopy (SEM) and thermogravimetric analysis (TGA). XRD patterns were obtained on a Bruker D8 (Bruker-AXS, Karlsruhe, Germany) diffractometer using a filtered Cu Kα radiation source (λ = 1.54178 Å), with accelerating voltage 40 kV, current 30 mA and scanned at 2θ from 5 to 70^o. N_2 adsorption/desorption was measured using a Micromeritics Tristar 3000 to obtain pore volume and the Brunauer-Emmett-Teller (BET) specific surface area. Prior to measurement the samples were degased at 120 ^oC for 5 h under vacuum condition. The external morphology and chemical compositions of the samples were observed on a ZEISS NEON 40EsB scanning electron microscope (SEM) equipped with an energy dispersive spectrometer (SEM-EDS).

4.2.3 Kinetic study of phenol oxidation

The catalytic oxidation of phenol was carried out in a 500 mL glass beaker containing 25-100 ppm of phenol solutions, which was attached to a stand and dipped in a water bath with a temperature controller. The reaction mixture was stirred constantly at 400 rpm to maintain a homogenous solution. A fixed amount of peroxymonosulfate (Oxone, Dupont's triple salt, $2KHSO_5 \bullet KHSO_4 \bullet K_2SO_4$ (PMS), Sigma-Aldrich) was added into the solution and allowed to dissolve completely before reaction. Further, a fixed amount of catalyst was added into the reactor to start the oxidation reaction of

phenol. The reaction was carried on for 120 min and at a fixed time interval, 0.5 mL of solution sample was taken from the mixture using a syringe with a filter of 0.45 μm and then mixed with 0.5 mL methanol to quench the reaction. Concentration of phenol was analyzed using a HPLC with a UV detector at wavelength of 270 nm. The column used was C-18 with a mobile phase of 30% acetonitrile and 70% ultrapure water. For selected samples, total organic carbon (TOC) was obtained using a Shimadzu TOC-5000 CE analyzer.

For recycled catalyst tests, two regeneration methods were used. One is simple washing treatment and the other is high-temperature calcination. In general, Mn oxides were collected by filtration after reaction, washing with water and drying at 80 ºC overnight for reuse test. Some dried samples were further calcined at 500 ºC in air for 1 h and then reused for test again.

4.3. Result and discussion

4.3.1 Characterization of manganese oxide catalysts

MnO_2 and $MnCO_3$ were studied by TGA under air and argon atmosphere, respectively (**Figure 4.1**). The TGA pattern of MnO_2 (**Figure 4.1A**) shows 5% weight loss below 300 ^oC, which corresponds to a loss of surface adsorbed water, organic and trace amount of oxygen. At around 550 ^oC, weight loss of about 8% corresponds to the loss of oxygen from MnO_2 lattice resulting in the phase transformation to Mn_2O_3. Another 5% weight loss at around 950 ^oC corresponds to continuous loss of oxygen resulting in further phase transformation from Mn_2O_3 to Mn_3O_4. For $MnCO_3$, TGA pattern in **Figure 4.1B** shows 10% weight loss below 350 ^oC, which corresponds to a loss of water, organic and trace amount of carbon dioxide, and another 29% weight loss at around 450 ^oC corresponds to loss of carbon dioxide from $MnCO_3$ lattice resulting in the phase transformation to MnO. The nature of TGA and different phase transitions are agreement with the previous reports for MnO_2 and $MnCO_3$ [24, 25].

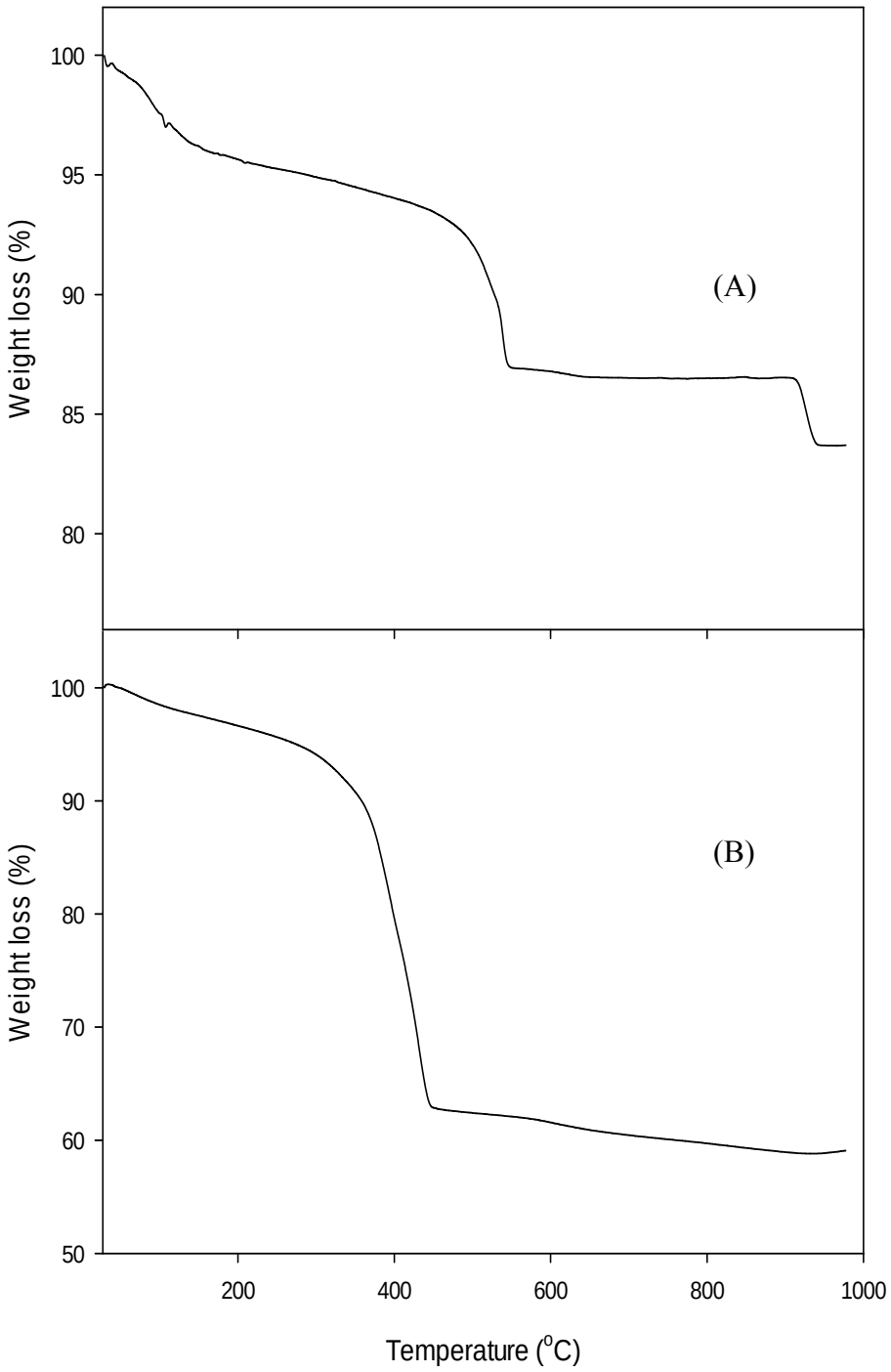

Figure 4.1. TGA curves of (A) MnO_2, (B) $MnCO_3$ recorded in air and argon, respectively, at a heating rate of 10 $^{o}C\ min^{-1}$.

Figure 4.2 shows XRD patterns of four manganese oxides. The four samples present different crystalline peaks. In **Figure 4.2A**, the diffraction peaks occurred at 22.43°, 34.46°, 37.12°, 38.78°, and 57.36°, corresponding to the diffractions of γ-MnO_2 (JCPDS No. 14-0664, *a* = 6.360Å). The diffraction peaks in **Figure 4.2B** occurred at 34.94°, 40.57°, 58.72°, 70.19°, and 73.81°, confirming the structure of MnO (JCPDS No. 75-0626, *a* = 4.444Å). In **Figure 4.2C**, the diffraction peaks occurred at 28.91°, 30.99°, 32.38°, 36.08°, 38.09°, 44.40°, 50.83°, 53.86° and 59.90°, corresponding to γ-Mn_3O_4 (JCPDS No. 80-0382, *a* = 5.749Å) while in **Figure 4.2D** the diffraction peaks occurred at 23.08°, 32.84°, 38.14°, 45.05°, 49.22°, 55.04°, and 65.16°, confirming the crystalline structure of α-Mn_2O_3 (JCPDS No. 89-4836, *a* = 9.406Å). Those XRD results show the successful synthesis of MnO, Mn_2O_3 and Mn_3O_4 compounds from thermal decomposition of $MnCO_3$ and MnO_2.

SEM images show that MnO_2, Mn_2O_3 and Mn_3O_4 present as spherical particles with a small particle size of 50 nm while MnO presents in cubic form with a large particle size of 1 μm.

Table 4.1. Surface area, pore volume and pore radius of a series of manganese oxides.

Catalyst	Structure	Coordination	Surface area (S_{BET}, $m^2.g^{-1}$)	Pore volume ($cm^3.g^{-1}$)	Average pore radius (Å)
Mn_3O_4	Spinel	4,6	157.0	0.237	30.1
Mn_2O_3	"C" bixbyite	6(Octahedral)	95.4	0.336	70.4
MnO_2	Rutile	6(Octahedral)	104.1	0.191	36.6
MnO	Rock salt	6(Octahedral)	57.7	0.169	22.5

Figure 4.3 shows N_2 adsorption/desorption isotherms and pore size distributions of manganese oxides. The BET surface area, pore volume and average pore size are given in **Table 4.1** Mn_3O_4 has higher surface area (157 m^2g^{-1}) than others while Mn_2O_3 has higher pore volume and pore radius. MnO shows the lowest surface area, pore volume and pore radius. Furthermore, all catalysts have pore radius between 20 Å and 80 Å, which means they are mesoporous materials. The pore size distribution profiles show that MnO, Mn_3O_4, and MnO_2 present a single mode of pore size, which is centred at 37.2, 26.3, and 29.1 Å, respectively. Mn_2O_3 shows two modes, centred at

18.2 and 32.7Å, respectively, indicating that Mn_2O_3 is a typical micro and mesoporous material

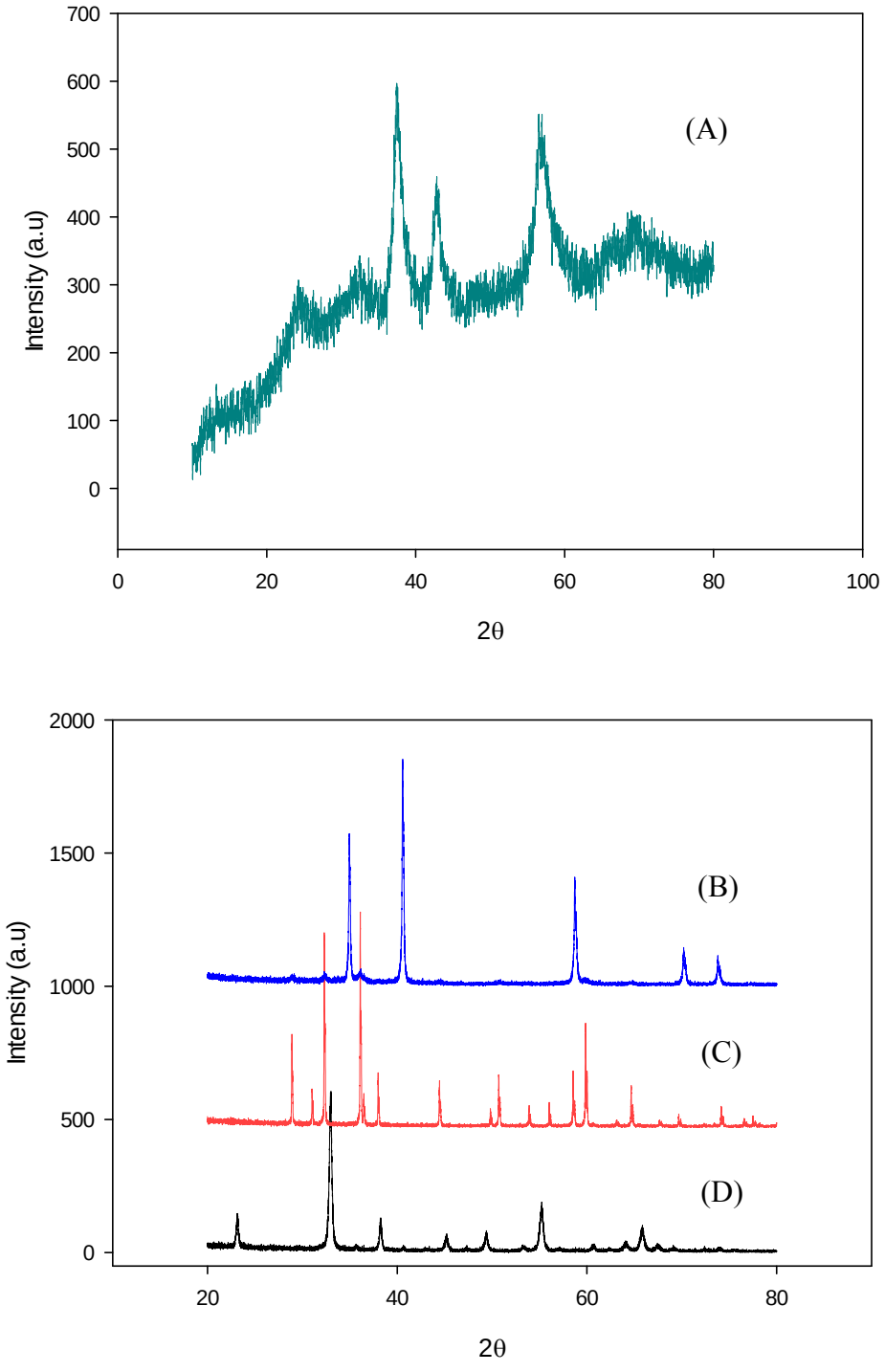

Figure 4.2. XRD patterns of manganese oxide catalysts. (A) MnO_2, (B) MnO, (C) Mn_3O_4, and (D) Mn_2O_3

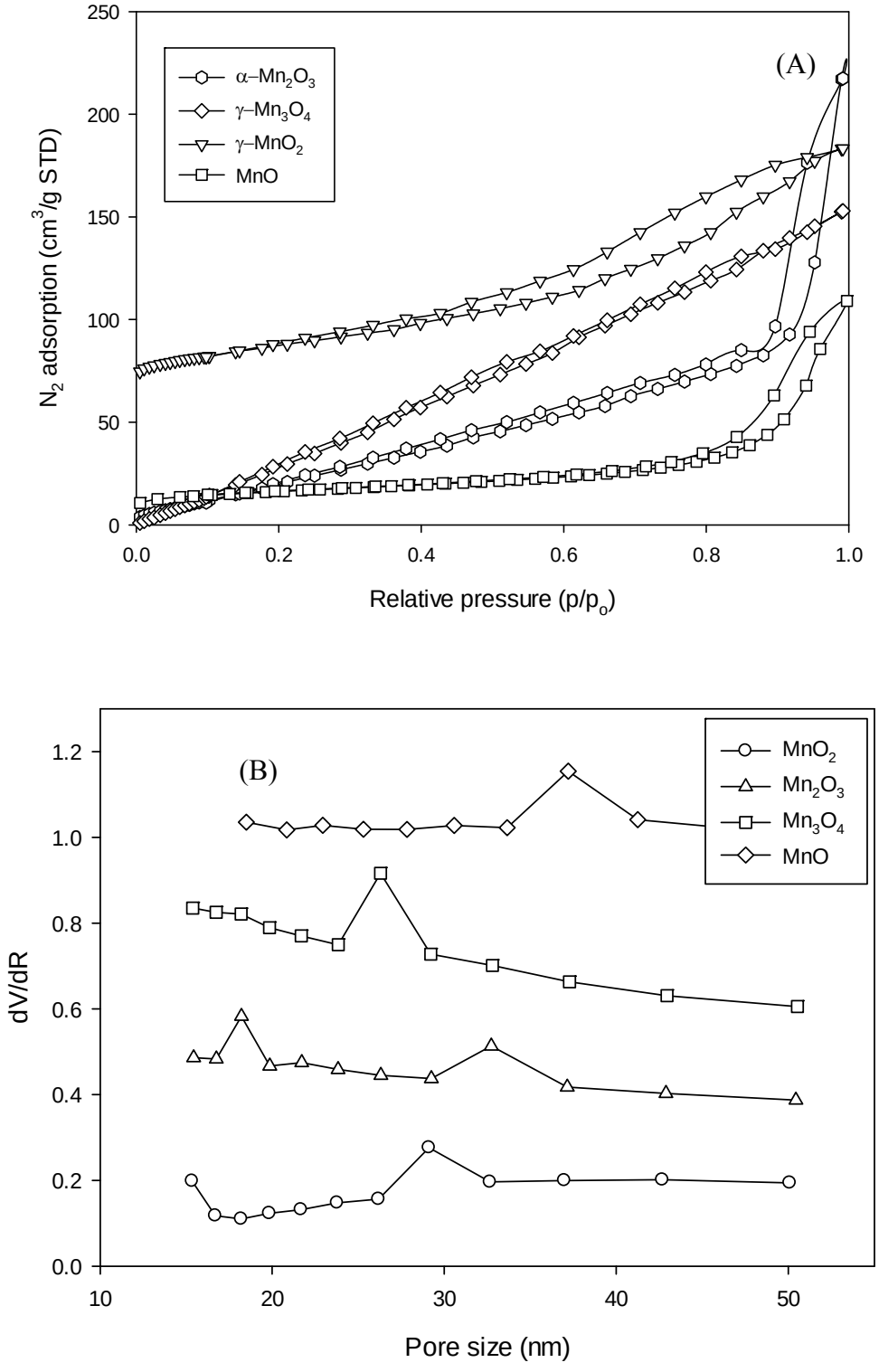

Figure 4.3. N_2 adsorption isotherm and pore size distributions of manganese oxide catalysts. (A) N_2 isotherm and (B) pore size distributions.

4.3.2 Preliminary study of phenol oxidation using catalysts

Figure 4.4 shows phenol degradation efficiency on a series of Mn oxides at varying oxidation states. Adsorption tests showed that Mn oxides presented minor adsorption of phenol, giving less than 10% in 120 min, which is due to low surface area[19]. In catalytic oxidation tests, addition of PMS without the presence of a catalyst did not induce phenol oxidation reaction. Phenol degradation would only occur when Mn oxide catalyst and oxidant (PMS) were simultaneously present in the solution. In a comparison of all catalyst performances, Mn_2O_3 is most effective in activating PMS to generate sulfate radicals. Mn_2O_3-PMS exhibited much better performance, producing complete removal of phenol in 60 min while the other three showed low phenol degradation. The results also showed that about 90%, 66.4%, and 61.5% of phenol concentration reduction were obtained for MnO-PMS, Mn_3O_4-PMS and MnO_2-PMS, respectively, within 120 min. Thus, the order of the catalytic activity of the series of catalysts is as follows: Mn_2O_3 > MnO > Mn_3O_4 > MnO_2, according to the conversion profiles. This reveals that the catalytic activity is apparently dependent on the oxidation state of manganese. In addition, TOC removal in Mn_2O_3-PMS system was also examined and about 86.39% of TOC removal was obtained within 120 min.

Previously, Mn^{2+} has been investigated for the activation of ozone or H_2O_2 to produce hydroxyl radicals for several organics oxidation and it showed effective activity. Lie at al. [26] investigated homogeneous activation of ozone with Mn^{2+} for 2-chloro-2'6'-diethyl-N-methoxymethyl acetanilide oxidation and found that Mn^{2+} is an effective metal ion for the activation of ozone. Anipsitakis and Dionysiou [27] studied Mn^{2+} for activation of H_2O_2 and PMS to found that Mn^{2+} could activate H_2O_2 and PMS to produce hydroxyl radicals and sulfate radicals, respectively, although the rate of reaction was still low.

Several heterogeneous cobalt systems have also been tested in activation of peroxymonosulfate for oxidation of toxic organics in water. Shukla et al. used Co_3O_4-SiO_2 [28] and Co-SBA-15 [29] with peroxymonosulfate for phenol degradation at 30 ppm. Co_3O_4-SiO_2 could achieve complete degradation of phenol in 190 min while

Co-SBA-15 could achieve 100% phenol degradation within 180 min. Yang et al. used Co-Fe mixed oxide ($CoFeO_4$) nanocatalyst for heterogeneous activation of peroxymonosulfate to generate sulfate radicals targeting the decomposition of 2,4-DCP. Co-Fe oxide could achieve 80% 2,4-DCP degradation in 120 min. Anipsitakis and Dionysiou [27] studied homogeneous activation of peroxymonosulfate with Mn^{2+} for 2,4-DCP oxidation. It was reported that 24% of 2,4-DCP removal could be achieved at 2,4-DCP concentration of 50 ppm in 240 min of reaction time. Therefore, it is seen that Mn_2O_3 presented a higher activity in phenol degradation than Mn^{2+} and most of reported heterogeneous Co systems.

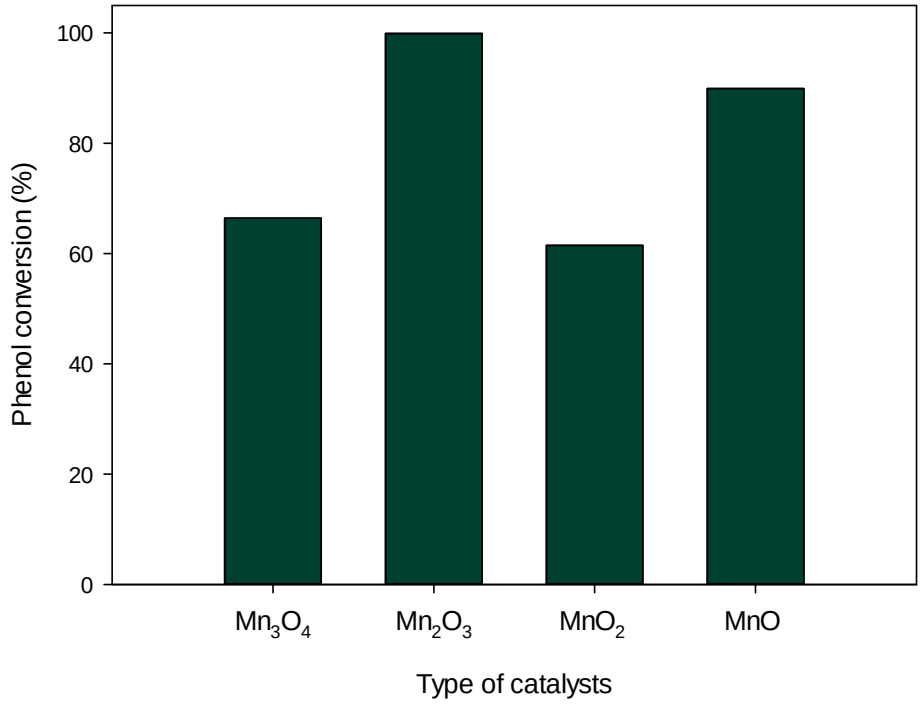

Figure 4.4. Phenol removal in catalytic oxidation using a series of manganese oxides. Reaction conditions: [Phenol] = 25ppm, catalyst = 0.4 g/L, PMS = 2g/L, and T = 25 ^{o}C.

In this investigation, Mn oxides at different oxidation states can activate peroxymonosulfate to produce sulfate radicals ($SO_4^{-\bullet}$ and $SO_5^{-\bullet}$) for phenol degradation as shown in the following equations.

$$HSO_5^- + 2\ MnO_2 \longrightarrow Mn_2O_3 + SO_5^{-\bullet} + OH^- \quad (4.1)$$

$$HSO_5^- + Mn_3O_4 \longrightarrow Mn_2O_3 + SO_4^{-\bullet} + H^+ \quad (4.2)$$

$$HSO_5^- + Mn_2O_3 \longrightarrow 2\ MnO_2 + SO_4^{-\bullet} + H^+ \quad (4.3)$$

$$HSO_5^- + 2\ MnO \longrightarrow Mn_2O_3 + SO_4^{-\bullet} + H^+ \quad (4.4)$$

$$HSO_5^- + 3\ Mn_2O_3 \longrightarrow 2\ Mn_3O_4 + SO_5^{-\bullet} + OH^- \quad (4.5)$$

$$SO_4^{-\bullet} + H_2O \longrightarrow OH^{\bullet} + H^+ + SO_4^{2-} \quad (4.6)$$

$$C_6H_5OH + SO_4^{-\bullet} \longrightarrow \text{several steps} \longrightarrow CO_2 + H_2O + SO_4^{2-} \quad (4.7)$$

$$C_6H_5OH + SO_5^{-\bullet} \longrightarrow \text{several steps} \longrightarrow CO_2 + H_2O + SO_4^{2-} \quad (4.8)$$

The reactivity of MnO, Mn_2O_3, Mn_3O_4 and MnO_4 is likely associated with the capacity of manganese to form various oxidation states, e.g., redox reaction of Mn^{2+}/Mn^{3+} or Mn^{3+}/Mn^{4+}, and ‘‘oxygen mobility’’ in the oxide lattice. In general, Mn^{3+} tends to undergo disproportionation reaction under the influence of H^+ and OH^-, thus, Mn_2O_3 can activate PMS via reactions (4.3) and (4.5) to produce $SO_4^{-\bullet}$ and $SO_5^{-\bullet}$, respectively. MnO_2 and MnO, however, will activate PMS via reactions (4.1) or (4.4) to generate $SO_5^{-\bullet}$ and $SO_4^{-\bullet}$, respectively. Due to the higher activity of $SO_4^{-\bullet}$ than $SO_5^{-\bullet}$, MnO presents a higher phenol degradation rate. Mn_3O_4 will produce $SO_4^{-\bullet}$ via reaction (4.2). But due to lower redox potential, Mn_3O_4 is less active than MnO. Therefore, the activities of MnO, Mn_2O_3, Mn_3O_4 and MnO_4 present in the order of $Mn_2O_3 > MnO > Mn_3O_4 > MnO_2$.

4.3.3 Effect of reaction parameters on phenol degradation on Mn_2O_3

Due to high activity of Mn_2O_3, further investigations on Mn_2O_3 were carried out to understand the effects of operating conditions. The effect of initial phenol concentration at 25, 50, 75 and 100 mg/L on phenol degradation is presented in

Figure 4.5 Phenol degradation efficiency decreased with increasing phenol concentration. The complete phenol removal could be achieved at phenol concentration of 25 mg/L in 60 min while at phenol concentration of 50, 75 and 100 mg/L, removal efficiency obtained in 120 min are 98, 91 and 75%, respectively. Due to the same concentration of Mn_2O_3 and PMS, sulfate radical concentrations produced in solution will be the same. Thus, high amount of phenol in solution will require more time to achieve the same removal rate, thus lowering phenol degradation efficiency.

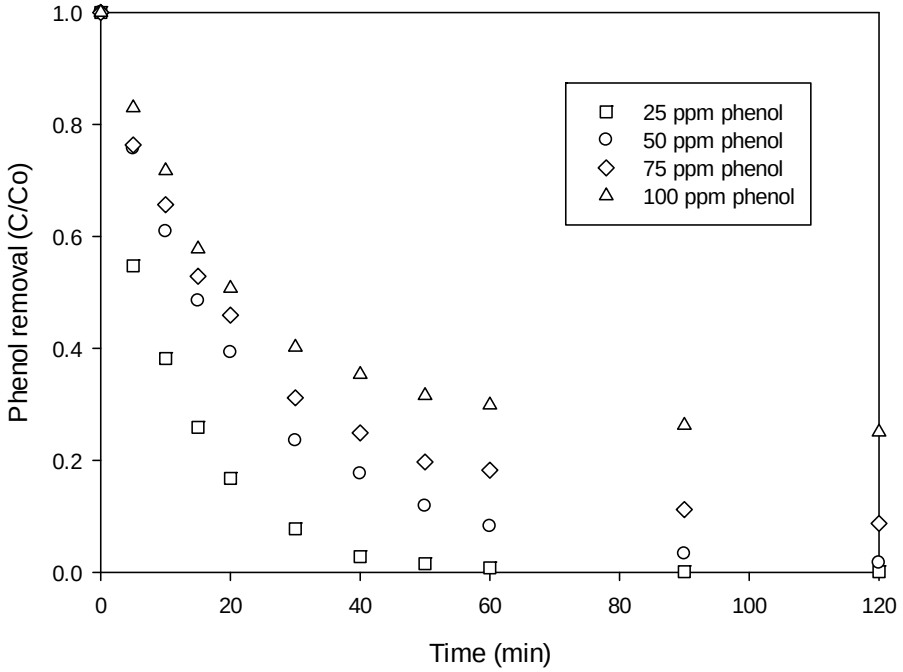

Figure 4.5. Effect of phenol concentration on phenol removal. Reaction conditions: catalyst (Mn_2O_3) = 0.4 g/L, PMS = 2g/L, and T = 25 ^oC.

Phenol removal efficiency is also affected by Mn_2O_3 loading in the system as shown in **Figure 4.6**. A complete removal of phenol could be reached within 60 min at 0.4 g/L Mn_2O_3 loading. While 97.7, 93.3, and 68% removals could be reached in 120 min at Mn_2O_3 loading of 0.30, 0.20, and 0.10 g/L, respectively. For phenol degradation, increased catalyst loading would enhance the rate of activation of PMS to generate the active sulfate radicals, resulting in an increase in the rate of phenol removal.

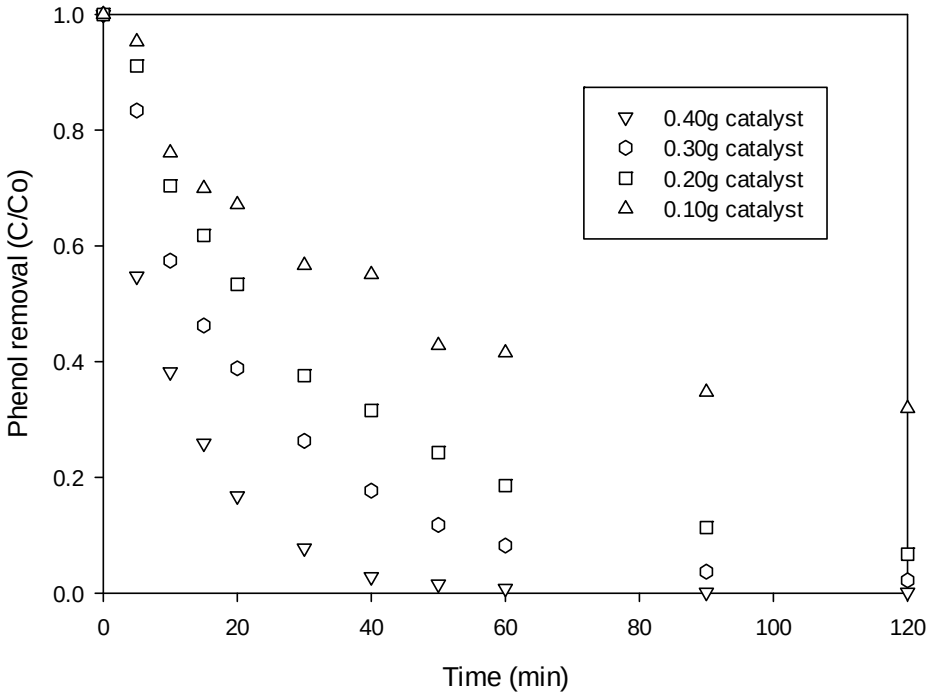

Figure 4.6. Effect of catalyst loading (Mn_2O_3) on phenol removal. Reaction conditions: [Phenol] = 25 ppm, PMS = 2 g/L, and T = 25 ^{o}C.

Figure 4.7 illustrates the effect of oxone concentration on phenol oxidation. As expected, phenol degradation rate was increased when PMS concentration was increased from 0.8 to 2 g/L. However, further increase in PMS concentration would decrease phenol degradation efficiency, suggesting the optimal loading at 2 g/L.

In addition, the temperature is also a key factor influencing catalyst activity on phenol degradation. **Figure 4.8** shows the effect of temperature on phenol degradation. Higher phenol removal was obtained at increased temperature. For instance, at temperature of 25 ^{o}C, the complete removal of phenol was achieved in 60 min while at 35 and 45 ^{o}C, complete removal of phenol could be achieved in 40 and 30 min, respectively.

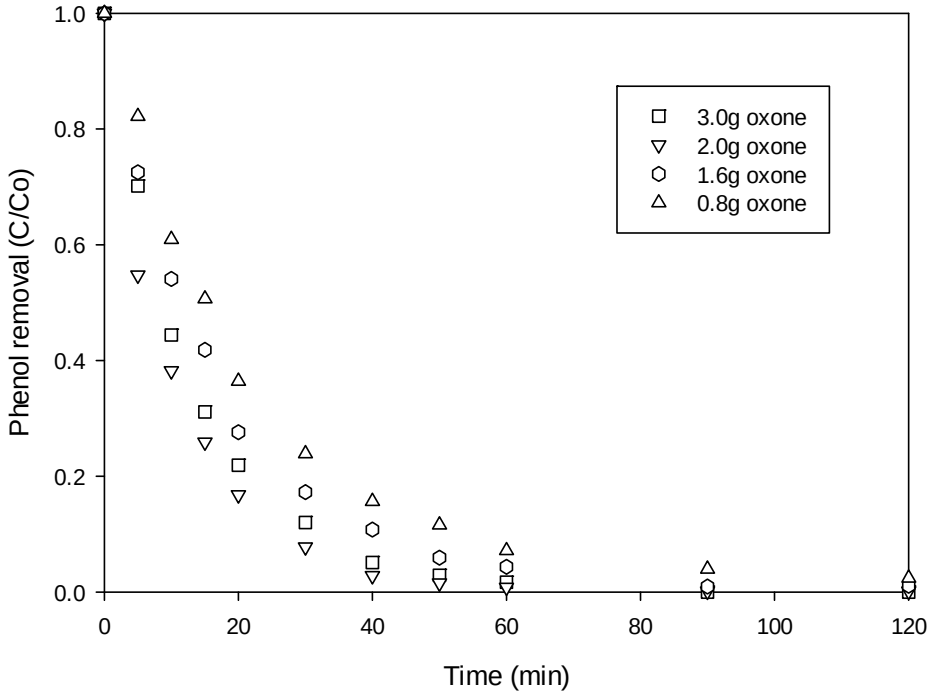

Figure 4.7 Effect of oxone concentration on phenol removal. Reaction conditions: [Phenol] = 25 ppm, catalyst (Mn_2O_3) = 0.4 g/L, and T = 25 ^oC.

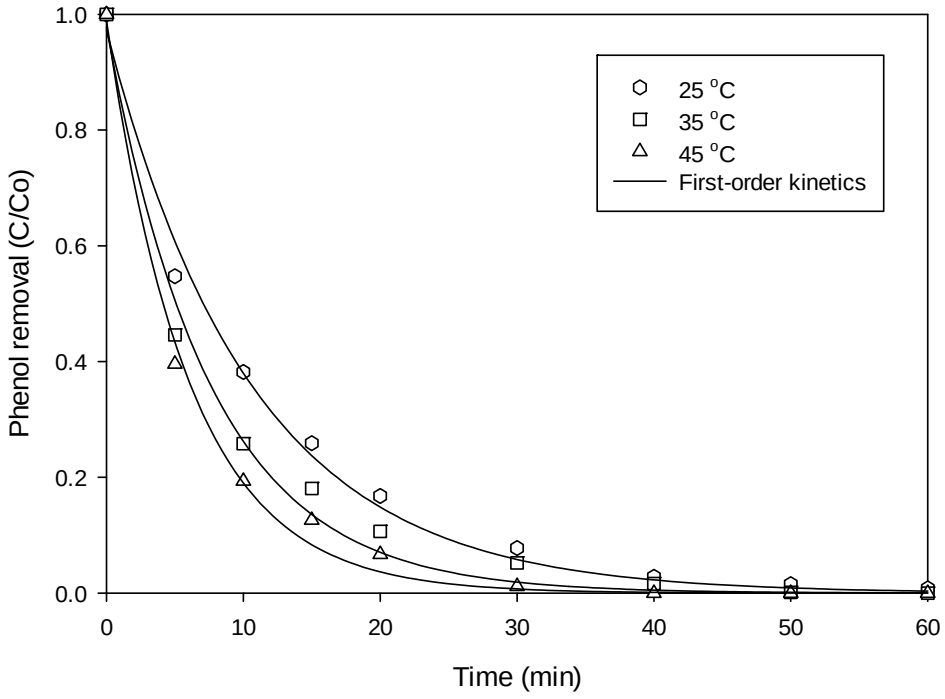

Figure 4.8 Effect of temperature on phenol removal. Reaction conditions: [Phenol] = 25 ppm, catalyst (Mn_2O_3) = 0.4 g/L, and PMS = 2 g/L.

In order to estimate the kinetic rates, a general pseudo first order kinetics for phenol degradation was employed, as shown in equation below.

$$\ln\left(\frac{C}{Co}\right) = -k \bullet t \qquad (4.9)$$

Where k is the apparent first order rate constant of phenol removal, C is the concentration of phenol at various time (t). C_o is the initial phenol concentration. Data fitting (**Figure 4.8**) showed that phenol degradation could be described by the first order kinetics. Kinetic constants are presented in **Table 4.2**. As can be seen that kinetic rate of reaction would be increased with increasing temperature. Furthermore, the Arrhenius plot of rate constants with temperature for Mn_2O_3 presented a good linear correlation and the activation energy for Mn_2O_3 was derived as 11.4 kJ/mol. Yao et al. [30] very recently reported a Mn_3O_4/Graphene system in activation of PMS for Orange II degradation and found the activation energy at 49.5 kJ/mol. Our previous investigations on Co_3O_4-based systems for phenol degradation showed that activation energies of supported Co_3O_4 catalysts are in the range of 47 – 70 kJ/mol [28, 31-33]. Therefore, Mn_2O_3 presents much lower activation energy than other catalysts and would be a promising material.

Table 4.2. Kinetic constants of phenol degradation at different temperatures on Mn_2O_3 catalyst.

Catalyst	Temperature, ^oC	k (min^{-1})	R^2
Mn_2O_3	25	0.087	0.97
	35	0.122	0.96
	45	0.154	0.99

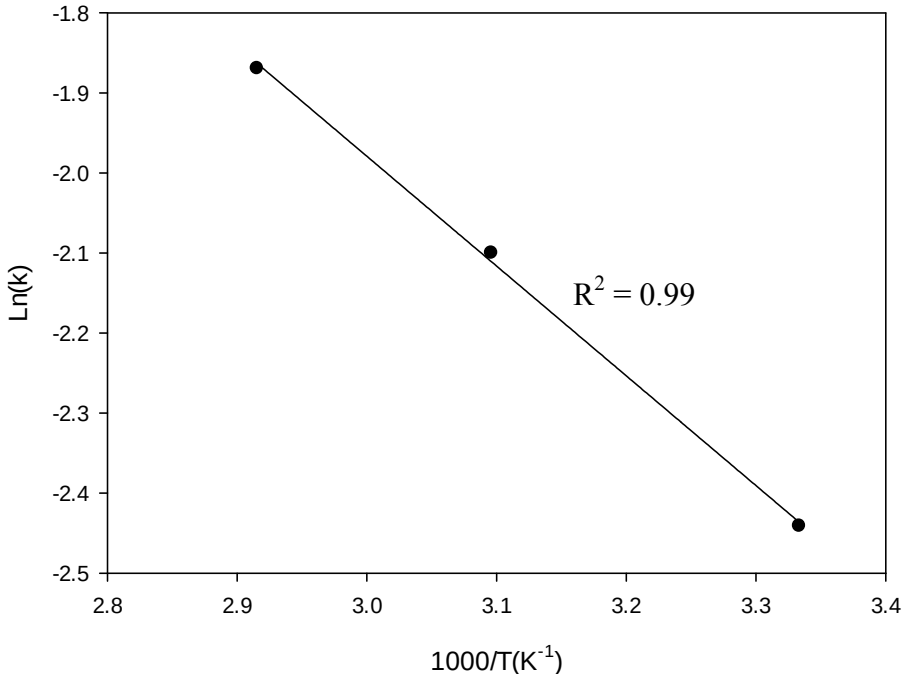

Figure 4.9. Arrhenius plot of phenol degradations on Mn_2O_3 catalyst.

4.3.4 Reactivity of spent Mn_2O_3 catalyst and reusability

Figure 4.10 shows the catalytic activity of recycled α-Mn_2O_3 for phenol degradation. As can be seen, the catalytic activity was significantly reduced in the second use if the catalyst was recovered by simple water washing, suggesting a deactivation of the catalyst. In the second use, phenol degradation was 27% at 120 min compared with 100% in the first use. However, after heat treatment at 500 ^oC for 1 hour, the activity of α-Mn_2O_3 was fully recovered and complete degradation of phenol can be achieved at 120 min as the same as the first use.

Deactivation of α-Mn_2O_3 could be attributed to intermediate deposition on the surface and chemical phase change [34]. XRD analysis showed that no phase change occurred after reaction. This suggests that the intermediate deposits on the catalyst surface plays important role for catalyst deactivation and they can be removed by heat treatment.

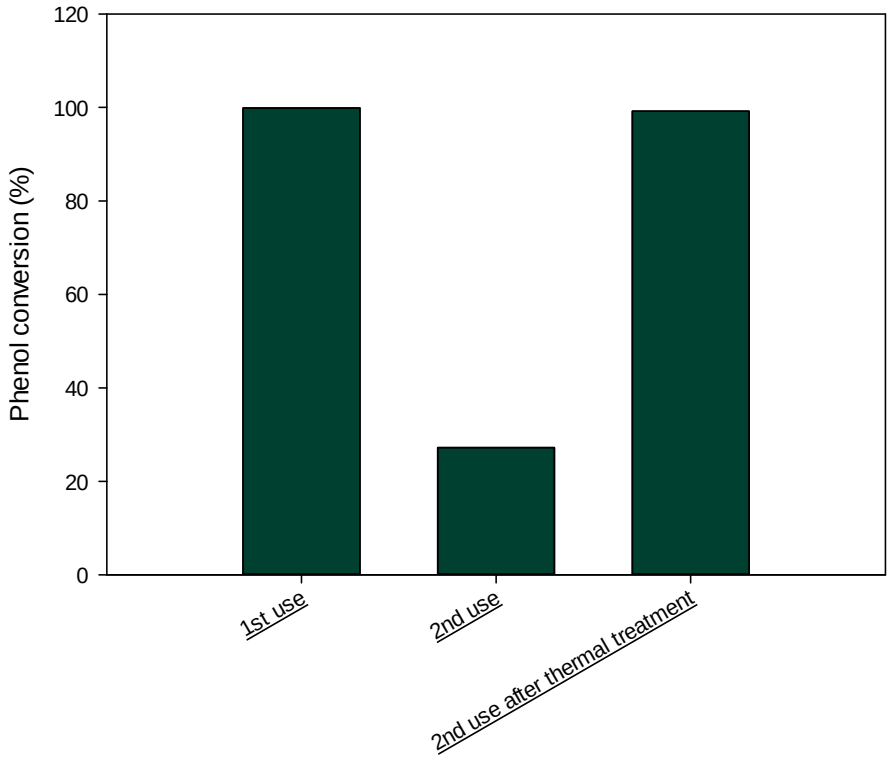

Figure 4.10. Phenol degradation in tests of recycled Mn_2O_3 catalyst. Reaction conditions: [Phenol] = 25 ppm, catalyst = 0.4 g/L, PMS = 2 g/L, and T = 25^{o}C.

4.4. Conclusions

Different oxidation states of manganese oxide were synthesized and tested for catalytic oxidation of phenolic contaminants with PMS. Among them, Mn_2O_3 is the most effective catalyst for generating sulfate radicals to degrade phenol. The catalytic activity followed the trend of Mn_2O_3 > MnO > Mn_3O_4 > MnO_2, which is related to redox potential. Several reaction factors influenced the removal efficiency of phenol such as PMS concentration, phenol concentration, catalyst loading and temperature. Kinetic studies showed that the phenol degradation followed first order reaction and activation energy of Mn_2O_3 were obtained to be 11.4 kJ/mol. Although deactivation occurred on Mn_2O_3, the activity could be fully recovered by high temperature calcination.

References

1. Christoskova, S.G., M. Stoyanova, and M. Georgieva, *Low-temperature iron-modified cobalt oxide system: Part 2. Catalytic oxidation of phenol in aqueous phase.* Applied Catalysis A: General, 2001. **208**(1-2): p. 243-249.

2. Fortuny, A., C. Bengoa, J. Font, and A. Fabregat, *Bimetallic catalysts for continuous catalytic wet air oxidation of phenol.* Journal of Hazardous Materials, 1999. **64**(2): p. 181-193.

3. Dohnal, V. and D. Fenclova, *Air-Water Partitioning and Aqueous Solubility of Phenols.* Journal of Chemical & Engineering Data, 1995. **40**(2): p. 478-483.

4. Marco, A., S. Esplugas, and G. Saum, *How and why combine chemical and biological processes for wastewater treatment.* Water Science and Technology, 1997. **35**(4): p. 321-327.

5. Andreozzi, R., V. Caprio, A. Insola, and R. Marotta, *Advanced oxidation processes (AOP) for water purification and recovery.* Catalysis Today, 1999. **53**(1): p. 51-59.

6. Huang, C.-P. and Y.-H. Huang, *Application of an active immobilized iron oxide with catalytic H_2O_2 for the mineralization of phenol in a batch photo-fluidized bed reactor.* Applied Catalysis A: General, 2009. **357**(2): p. 135-141.

7. Calleja, G., J.A. Melero, F. Martínez, and R. Molina, *Activity and resistance of iron-containing amorphous, zeolitic and mesostructured materials for wet peroxide oxidation of phenol.* Water Research, 2005. **39**(9): p. 1741-1750.

8. Fajerwerg, K. and H. Debellefontaine, *Wet oxidation of phenol by hydrogen peroxide using heterogeneous catalysis Fe-ZSM-5: a promising catalyst.* Applied Catalysis B: Environmental, 1996. **10**(4): p. L229-L235.

9. Liang, S., F. Teng, G. Bulgan, R. Zong, and Y. Zhu, *Effect of Phase Structure of MnO_2 Nanorod Catalyst on the Activity for CO Oxidation.* The Journal of Physical Chemistry C, 2008. **112**(14): p. 5307-5315.

10. Zaki, M.I., M.A. Hasan, and L. Pasupulety, *Influence of CuOx additives on CO oxidation activity and related surface and bulk behaviours of Mn_2O_3, Cr_2O_3 and WO_3 catalysts.* Applied Catalysis A: General, 2000. **198**(1–2): p. 247-259.

11. Baldi, M., E. Finocchio, F. Milella, and G. Busca, *Catalytic combustion of C3 hydrocarbons and oxygenates over Mn_3O_4.* Applied Catalysis B: Environmental, 1998. **16**(1): p. 43-51.

12. Fang, M., X. Tan, M. Liu, S. Kang, X. Hu, and L. Zhang, *Low-temperature synthesis of Mn_3O_4 hollow-tetrakaidecahedrons and their application in electrochemical capacitors.* CrystEngComm, 2011. **13**(15): p. 4915-4920.

13. Yang, M., D. Li, T. Zhao, and J. Ma, *Synthesis of Monodispersed Nanospheres of Mn_3O_4 and Its Adsorption Behavior for Alizarin Red.* Journal of Dispersion Science and Technology, 2010. **31**(4): p. 563-566.

14. Zhou, F., X. Zhao, C. Yuan, and H. Xu, *Synthesis of γ-MnOOH nanorods and their isomorphous transformation into β-MnO_2 and α-Mn_2O_3 nanorods.* Journal of Materials Science, 2007. **42**(24): p. 9978-9982.

15. Wu, R., J. Qu, and Y. Chen, *Magnetic powder MnO–Fe_2O_3 composite—a novel material for the removal of azo-dye from water.* Water Research, 2005. **39**(4): p. 630-638.

16. Kim, S.C. and W.G. Shim, *Catalytic combustion of VOCs over a series of manganese oxide catalysts.* Applied Catalysis B: Environmental, 2010. **98**(3–4): p. 180-185.

17. Ramesh, K., L. Chen, F. Chen, Y. Liu, Z. Wang, and Y.-F. Han, *Re-investigating the CO oxidation mechanism over unsupported MnO, Mn_2O_3 and MnO_2 catalysts.* Catalysis Today, 2008. **131**(1–4): p. 477-482.

18. Santos, V., M. Pereira, J. Órfão, and J. Figueiredo, *Synthesis and Characterization of Manganese Oxide Catalysts for the Total Oxidation of Ethyl Acetate.* Topics in Catalysis, 2009. **52**(5): p. 470-481.

19. Saputra, E., S. Muhammad, H. Sun, A. Patel, P. Shukla, Z.H. Zhu, and S. Wang, *α-MnO_2 activation of peroxymonosulfate for catalytic phenol degradation in aqueous solutions.* Catalysis Communications, 2012. **26**(0): p. 144-148.

20. Muhammad, S., P.R. Shukla, M.O. Tadé, and S. Wang, *Heterogeneous activation of peroxymonosulphate by supported ruthenium catalysts for phenol degradation in water.* Journal of Hazardous Materials, 2012. **215–216**(0): p. 183-190.

21. Zazo, J.A., J.A. Casas, A.F. Mohedano, M.A. Gilarranz, and J.J. Rodríguez, *Chemical Pathway and Kinetics of Phenol Oxidation by Fenton's Reagent.* Environmental Science & Technology, 2005. **39**(23): p. 9295-9302.

22. Watts, R., J. Sarasa, F. Loge, and A. Teel, *Oxidative and Reductive Pathways in Manganese-Catalyzed Fenton's Reactions.* Journal of Environmental Engineering, 2005. **131**(1): p. 158-164.

23. Lei, S., K. Tang, Z. Fang, Q. Liu, and H. Zheng, *Preparation of α-Mn_2O_3 and MnO from thermal decomposition of $MnCO_3$ and control of morphology.* Materials Letters, 2006. **60**(1): p. 53-56.

24. Zhu, H.T., J. Luo, H.X. Yang, J.K. Liang, G.H. Rao, J.B. Li, and Z.M. Du, *Birnessite-type MnO_2 Nanowalls and Their Magnetic Properties.* The Journal of Physical Chemistry C, 2008. **112**(44): p. 17089-17094.

25. Aragón, M.J., B. León, C. Pérez Vicente, and J.L. Tirado, *A new form of manganese carbonate for the negative electrode of lithium-ion batteries.* Journal of Power Sources, 2011. **196**(5): p. 2863-2866.

26. Li, H.-Y., J.-H. Qu, X. Zhao, and H.-J. Liu, *Removal of Alachlor from Water by Catalyzed Ozonation in the Presence of Fe^{2+}, Mn^{2+}, and Humic Substances.* Journal of Environmental Science and Health, Part B, 2004. **39**(5-6): p. 791-803.

27. Anipsitakis, G.P. and D.D. Dionysiou, *Radical Generation by the Interaction of Transition Metals with Common Oxidants.* Environmental Science & Technology, 2004. **38**(13): p. 3705-3712.

28. Shukla, P., H. Sun, S. Wang, H.M. Ang, and M.O. Tadé, *Nanosized Co_3O_4/SiO_2 for heterogeneous oxidation of phenolic contaminants in waste water.* Separation and Purification Technology, 2011. **77**(2): p. 230-236.

29. Shukla, P., H. Sun, S. Wang, H.M. Ang, and M.O. Tadé, *Co-SBA-15 for heterogeneous oxidation of phenol with sulfate radical for wastewater treatment.* Catalysis Today, 2011. **175**(1): p. 380-385.

30. Yao, Y., C. Xu, S. Yu, D. Zhang, and S. Wang, *Facile Synthesis of Mn3O4–Reduced Graphene Oxide Hybrids for Catalytic Decomposition of Aqueous Organics.* Industrial & Engineering Chemistry Research, 2013.

31. Saputra, E., S. Muhammad, H. Sun, H.M. Ang, M.O. Tadé, and S. Wang, *Red mud and fly ash supported Co catalysts for phenol oxidation.* Catalysis Today, 2012. **190**(1): p. 68-72.

32. Shukla, P.R., S. Wang, H. Sun, H.M. Ang, and M. Tadé, *Activated carbon supported cobalt catalysts for advanced oxidation of organic contaminants in aqueous solution.* Applied Catalysis B: Environmental, 2010. **100**(3–4): p. 529-534.

33. Shukla, P., S. Wang, K. Singh, H.M. Ang, and M.O. Tadé, *Cobalt exchanged zeolites for heterogeneous catalytic oxidation of phenol in the presence of peroxymonosulphate.* Applied Catalysis B: Environmental, 2010. **99**(1–2): p. 163-169.

34. Sun, H., H. Liang, G. Zhou, and S. Wang, *Supported cobalt catalysts by one-pot aqueous combustion synthesis for catalytic phenol degradation.* Journal of Colloid and Interface Science, 2013. **394**(0): p. 394-400.

Chapter 5

Synthesis of Mn_3O_4, Co_3O_4 and Fe_3O_4 Nanoparticles and Their Catalytic Performances In Oxidation of Phenolic Contaminants in Aqueous Solutions

Abstract

Nanosized Mn_3O_4, Co_3O_4 and Fe_3O_4 particles were prepared, characterised, and tested in degradation of aqueous phenol in the presence of peroxymonosulphate. It was found that Mn_3O_4 and Co_3O_4 nanoparticles are highly effective in heterogeneous activation of peroxymonosulphate to produce sulphate radicals for phenol degradation. The activity shows an order of Mn_3O_4 > Co_3O_4 > Fe_3O_4. Mn_3O_4 and Co_3O_4 could completely remove phenol in about 20 min, at the conditions of 25 ppm phenol, 0.4 g/L catalyst, 2 g/L oxone®, and 25 ^oC. A pseudo first order model would fit to phenol degradation kinetics and activation energies on Mn_3O_4 and Co_3O_4 were obtained as 38.5 and 66.2 kJ/mol, respectively. In addition, Mn_3O_4 exhibited high catalytic stability.

5.1. Introduction

Phenol and its derivatives are important water pollutants due to their strong toxicity to many living organisms even at low concentrations [1]. These chemicals can be discharged from many industries as by-products such as petroleum refining, petrochemical, pharmaceutical, plastic and pesticide industries [2, 3]. In many countries, the maximum threshold allowed for phenol in water streams is less than 1 mg/L, for instance 0.5 mg/L for Australia wastewaters [4, 5]. Therefore, the phenol containing wastewaters have to be treated before discharged into the environment.

Currently, conventional wastewater treatment technology has been proven to be limited in treating toxic organic compounds because degradation of various pollutants is often very slow or ineffective and not environmentally compatible [6, 7]. One promising technology that can be used as an effective process to completely degrade organic compounds in aqueous media is advanced oxidation processes (AOPs). AOPs are based on the generation of reactive species, such as hydroxyl radicals, that have a strong oxidizing potential for mineralizing organic pollutants into simple compounds, CO_2 and H_2O [8, 9]. Apart from hydroxyl radicals, sulphate radicals have also been recently suggested as an alternative due to their higher oxidation potential.

Homogeneous catalysts are commonly more efficient compared to solid or heterogeneous catalysts because every single catalytic entity can act as a single active site. This characteristic makes homogeneous catalysts intrinsically more active and selective [10]. However, recovery of the catalysts needs further processes for separation of the homogeneous catalysts. Moreover, most of the dissolved metal catalysts are harmful to the environment. This disadvantage can be overcome by using heterogeneous catalysts, in which the catalysts will be recoverable and reusable [11].

In most previous investigations, homogeneous Co^{2+}/peroxymonosulphate (PMS, HSO_5^-) has been found to be an effective route of AOP for sulphate radical production and oxidation of various organics [12-17]. However, a major issue in using Co^{2+} metal ions is the toxicity and health problems to humans such as asthma

and pneumonia [18]. Therefore, metal oxide catalysts for activation of PMS, such as Co_3O_4 [19, 20], Co exchanged zeolites [21], supported Co_3O_4 [22-30], and $CoFe_2O_4$ [31, 32] have been proposed to overcome this drawback. Recently, α-MnO_2 has also been reported to be effective for phenol degradation [33].

Co_3O_4, Fe_3O_4, and Mn_3O_4 are important oxides with spinel structure consisting of M^{2+} and M^{3+} ions. They are active in generating hydroxyl radicals via Fenton reaction for advanced oxidation processes. However, no comprehensive investigation has been reported in their application for PMS activation. In this research, three metal oxides, Mn_3O_4, Co_3O_4, Fe_3O_4, were synthesized in two ways, hydrothermal and solvothermal methods. Their physicochemical properties were characterized. The prepared metal oxide materials were then employed as catalysts for heterogeneous generation of sulphate radicals for phenol mineralization in solution. Several key parameters in the kinetic study such as phenol concentration, catalyst loading, PMS concentration and temperature were investigated.

5.2. Experimental methods

5.2.1 Material synthesis

A nano-sized Mn_3O_4 sample was prepared by a solvothermal method reported by Zhang et al. [34]. In this synthesis, 1.0 g potassium permanganate was dissolved in 60 mL aqueous ethanol (60%) at room temperature to form a homogeneous solution. The solution was transferred into a 125 mL Teflon-lined stainless steel autoclave, sealed and maintained at 120 ^oC for 8 h. The resulting precipitates were filtered and washed with distilled water and dried in air at 80 ^oC overnight. The second sample, nanostructured Co_3O_4, was prepared by a hydrothermal method [35]. Typically, $Co(NO_3)_2$•$6H_2O$ (5 mmol) and $CO(NH_2)_2$ (25 mmol) were dissolved in 50 mL of distillate water under stirring. The d solution was transferred into a 125 mL Teflon-lined stainless steel autoclave, sealed and maintained at 120 ^oC for 5 h. The resulted precipitates were filtered and washed with water and dried in air at 80 ^oC overnight. Then, the dried solid was calcined at 400 ^oC under air for 4 h. Fe_3O_4 nanoparticles were obtained by a solvothermal method [36]. Typically, ferric sulfate (0.45 g),

sodium acetate anhydrous (1.2 g), and poly(vinylpyrrolidone) (average Mw = 40,000) (0.3 g) were dissolved in ethylene glycol (25 mL) under stirring. The mixture was then transferred into a 45 mL Teflon-lined stainless steel autoclave, sealed and maintained at 200 ^{o}C for 8 h. The resulting precipitates were filtered and washed with water and dried in air at 80 ^{o}C for 24 h.

5.2.2 Characterization catalysts

Catalysts were characterized by XRD, N_2 adsorption/desorption, and SEM. XRD patterns were obtained on a Bruker D8 (Bruker-AXS, Karlsruhe, Germany) diffractometer using filtered Cu Kα radiation source (λ = 1.54178 Å), with accelerating voltage 40 kV, current 30 mA and scanned at 2θ from 5 to 100^{o}. N_2 adsorption/desorption was measured using a Micromeritics Tristar 3000 to obtain pore volume and Brunauer-Emmett-Teller (BET) specific surface area. Prior to measurement the samples were degassed at 120 ^{o}C for 5 h under vacuum condition. The external morphology and chemical compositions of the samples were observed on a ZEISS NEON 40EsB scanning electron microscope (SEM) equipped with an energy dispersive spectrometer (SEM-EDS).

5.2.3 Catalytic activity test

Phenol degradation tests were carried out in a 1-L glass beaker with 500 mL containing 25, 50, 75 and 100 mg/L of phenolic solutions. The reaction mixture was stirred constantly at 400 rpm. Firstly, a fixed amount of peroxymonosulphate (oxone®, DuPont's triple salt: $2KHSO_5 \bullet KHSO_4 \bullet K_2SO_4$, Sigma-Aldrich) was added into the solution for a while, then a catalyst was added into the solution to start the oxidation reaction of phenol. At certain time, 0.5 mL of water sample was withdrawn from the mixture using a syringe filter of 0.45 μm and then mixed with 0.5 mL of pure methanol to quench the reaction. The concentration of phenol was analysed using a Varian HPLC with a UV detector at λ = 270 nm. The column used was C-18 with mobile phase of 30 % CH_3CN and 70% ultrapure water. For selected samples, total organic carbon (TOC) was obtained using a Shimadzu TOC-5000 CE analyser.

5.3. Result and discussion

5.3.1 Characterization of oxide catalysts

Figure 5.1 shows the XRD patterns of Mn_3O_4, Co_3O_4 and Fe_3O_4 catalysts. The three samples present different crystalline peaks. The peaks in **Figure 5.1a** match well with those from the JCPDS card (19-0629) for magnetite Fe_3O_4. The diffraction peaks in **Figure 5.1b** match well with those from the JCPDS card (24-0734) for Mn_3O_4. Meanwhile, the diffractions in **Figure 5.1c** match with those from the JCPDS card (43-1003) for Co_3O_4.

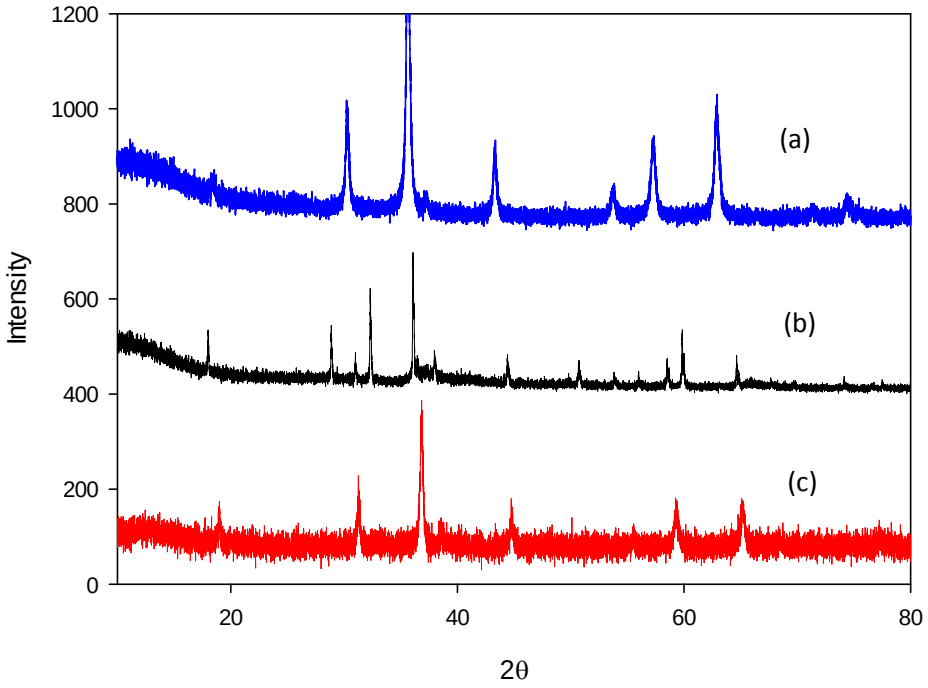

Figure 5.1. XRD patterns of metal oxide catalysts. (a) Fe_3O_4, (b) Mn_3O_4, and (c) Co_3O_4

Figure 5.2 shows N_2 adsorption/desorption isotherms of oxide catalysts. As seen from Table 5.1, Mn_3O_4 has higher surface area (184.6 $m^2.g^{-1}$) and pore volume (0.772 $cm^3.g^{-1}$) than others. Co_3O_4 and Fe_3O_4 have the similar surface area. In addition, Mn_3O_4 has the smaller pore radius at 8 Å, less than 20 Å while others catalysts have the radius more than 20 Å, which means Mn_3O_4 is mainly microporous and Fe_3O_4 and Co_3O_4 are mesoporous materials.

Table 5.1 Surface area, pore volume and pore radius of oxide catalysts.

Catalyst	S_{BET}, $m^2.g^{-1}$	Pore volume ($cm^3.g^{-1}$)	Average Pore radius (Å)
Fe_3O_4	21.4	0.096	180
Mn_3O_4	184.6	0.772	8
Co_3O_4	20.0	0.120	240

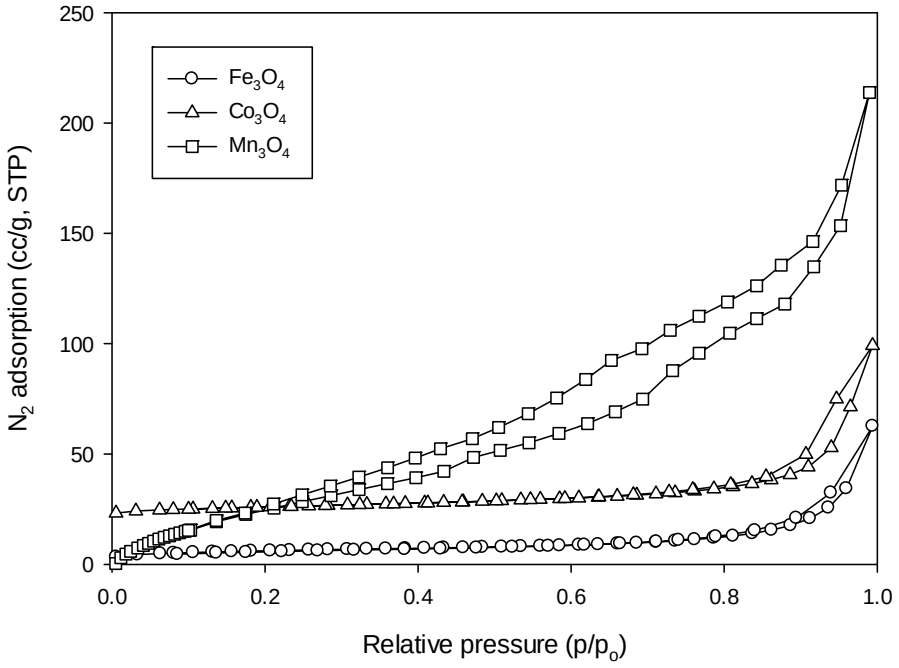

Figure 5.2. N_2 adsorption isotherms of Fe_3O_4, Mn_3O_4, and Co_3O_4.

Figure 5.3 presents SEM images of three oxide catalyst samples. As seen, the morphology of Fe_3O_4 particles in the uniform size with spherical shape. The particle size is about 0.05-0.2 μm. Mn_3O_4 shows a larger particle size varying in a range of 0.15-2.5 μm. Another oxide (Co_3O_4) shows the particle size at about 0.02-0.25 μm.

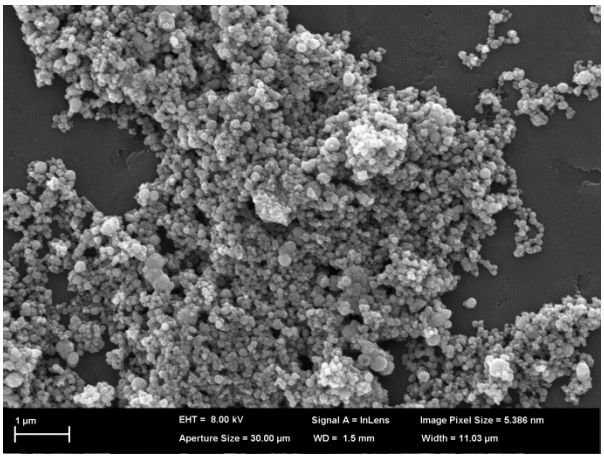

(a)

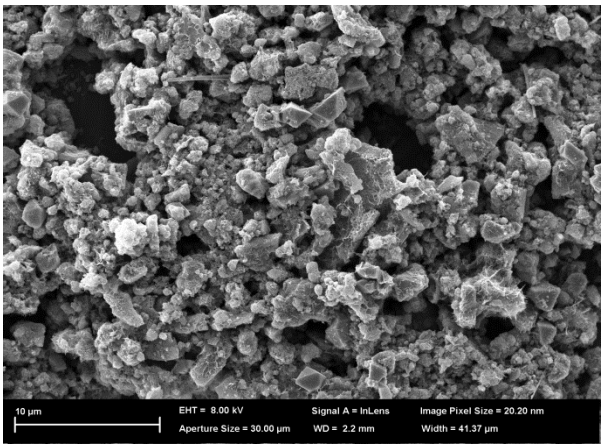

(b)

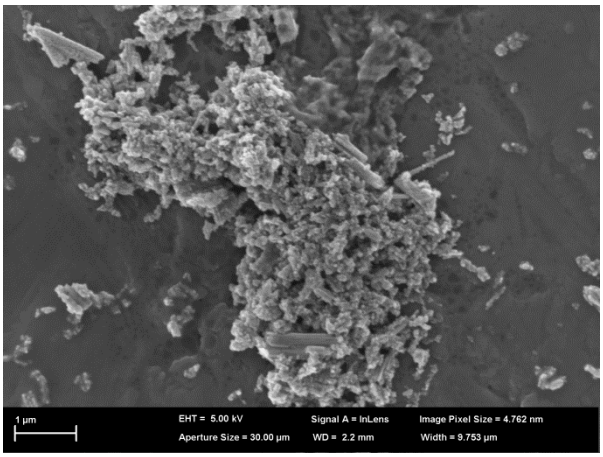

(c)

Figure 5.3. SEM photos of oxide catalysts. (a) Fe_3O_4, (b) Mn_3O_4, and (c) Co_3O_4.

5.3.2 Preliminary study of phenol oxidation using catalysts

The degradation of phenol and adsorption on Fe_3O_4, Mn_3O_4, and Co_3O_4 are presented in **Figure 5.4**. In adsorption tests, all catalysts can adsorb phenol compound at low efficiency. Among the catalysts, Mn_3O_4 has the highest efficiency in phenol adsorption with 15% removal in 90 min prior to reaching equilibrium. Meanwhile, Co_3O_4 has lower adsorption efficiency with 10% removal in 90 min. Mn_3O_4 has much higher surface area and pore volume than others, resulting in higher phenol adsorption. In the presence of oxone® without a catalyst, no phenol degradation occurred, indicating that oxone® itself could not produce sulfate radicals to induce phenol oxidation.

In catalytic oxidation tests, phenol degradation would only occur when catalyst and oxidant were simultaneously present in the solution. In a comparison of three catalyst performances, Co_3O_4 and Mn_3O_4 are effective in activating oxone® to generate sulfate radicals. Co_3O_4-oxone® system exhibited similar efficiency to Mn_3O_4-oxone® presenting complete phenol removal in 20 min. In contrary, Fe_3O_4-oxone® system presented much low degradation of phenol at less than 15% in 90 min. Thus, the order of catalytic activity of the catalysts is as follows, $Co_3O_4 \sim Mn_3O_4 > Fe_3O_4$. In addition, TOC removal in Co_3O_4-oxone® and Mn_3O_4-oxone® systems were also examined and about 68% and 50% of TOC reduction were obtained within 60 min, respectively.

The heterogeneous activation of PMS by Co_3O_4 has been proposed in Eqs.(5.1–5.2) [19]. Due to the similar chemical structure of Fe_3O_4 and Mn_3O_4 to Co_3O_4, activation of PMS by Mn_3O_4 and Fe_3O_4 will follow the same routes as shown in Eqs.(5.3–5.6). As shown in the reactions, redox reactions are involved in sulfate radical generation and the redox potential of M^{2+}/M^{3+} will be important. The standard reduction potentials (E^0) of Co^{3+}/Co^{2+}, Mn^{3+}/Mn^{2+}, and Fe^{3+}/Fe^{2+} are 1.92, 1.54, and 0.77 V, respectively [37]. Due to higher value of E^0, Mn_3O_4 and Co_3O_4 exhibit high activity. In addition, Mn_3O_4 has high surface area and phenol adsorption, which makes it more active in phenol degradation.

$$HSO_5^- + Co_2O_3 \longrightarrow SO_5^{-\bullet} + OH^- + 2CoO \quad (5.1)$$

$$HSO_5^- + 2CoO \longrightarrow SO_4^{-\bullet} + H^+ + Co_2O_3 \quad (5.2)$$

$$HSO_5^- + Mn_2O_3 \longrightarrow SO_5^{-\bullet} + OH^- + 2MnO \quad (5.3)$$

$$HSO_5^- + 2MnO \longrightarrow SO_4^{-\bullet} + H^+ + Mn_2O_3 \quad (5.4)$$

$$HSO_5^- + Fe_2O_3 \longrightarrow SO_5^{-\bullet} + OH^- + 2FeO \quad (5.5)$$

$$HSO_5^- + 2FeO \longrightarrow SO_4^{-\bullet} + H^+ + Fe_2O_3 \quad (5.6)$$

Anipsitakis and Dionysiou [37] investigated homogeneous activation of PMS by several metal ions, Fe^{2+}, Fe^{3+}, Co^{2+}, Mn^{2+}, Ni^{2+}, Ru^{3+}, Ce^{3+}, and Ag^{+}, for 2,4-dichlorophenol degradation. They found that Co^{2+} and Ru^{3+} are the best metal catalysts for the activation of peroxymonosulfate. Co^{2+}, Ru^{3+}, and Fe^{2+} interact with PMS to produce freely diffusible sulfate radicals while Mn^{2+}, Ni^{2+}, and Ce^{3+} with PMS generate caged or bound to the metal sulfate radicals. They also tested various commercial Co_3O_4 for heterogeneous activation of PMS for 2,4-dichlorophenol degradation and proposed that both CoO and Co_2O_3 contained in Co_3O_4 are responsible for PMS activation [19]. At the conditions of 20 mg/L 2,4-DCP, 0.19 g/L Co_3O_4, 72-99% conversion of 2,4-dichlorophenol could be achieved in 30 min.

Some other investigations using unsupported Co oxide heterogeneous catalysts have been carried out in activation of PMS for oxidation of organic toxics in water. Liang et al. [38] studied a nanostructured Co_3O_4 which was synthesized by solution combustion for heterogeneous activation of oxone® to generate sulphate radical ($SO_5^{-\bullet}$, and $SO_4^{-\bullet}$) for phenol degradation. They found that Co_3O_4 could achieve 50% phenol removal at phenol concentration of 25 ppm within 240 min. Ding et al. [39] used nano-Co_3O_4 with oxone® for a dye (methylene blue, MB) degradation at 20 μmol/L. The nano-Co_3O_4 could achieve 40% MB removal in 30 min. Chen et al. [40] studied Mn_3O_4 nanoparticles with ozone for phenol degradation at 100 mg/L. It was reported that 80% phenol removal could be achieved in 60 min. Previously, we tested a mesoporous MnO_2 for activation of oxone® to degrade phenol and 100% phenol decomposition occurred in 150 min under the similar conditions in this investigation

[33]. Therefore, it is seen that synthesised Co_3O_4 and Mn_3O_4 with oxone® in this investigation presented higher activity in phenol degradation. Due to their high activity, further investigations on Co_3O_4 and Mn_3O_4 were carried out to understand the effects of operating conditions.

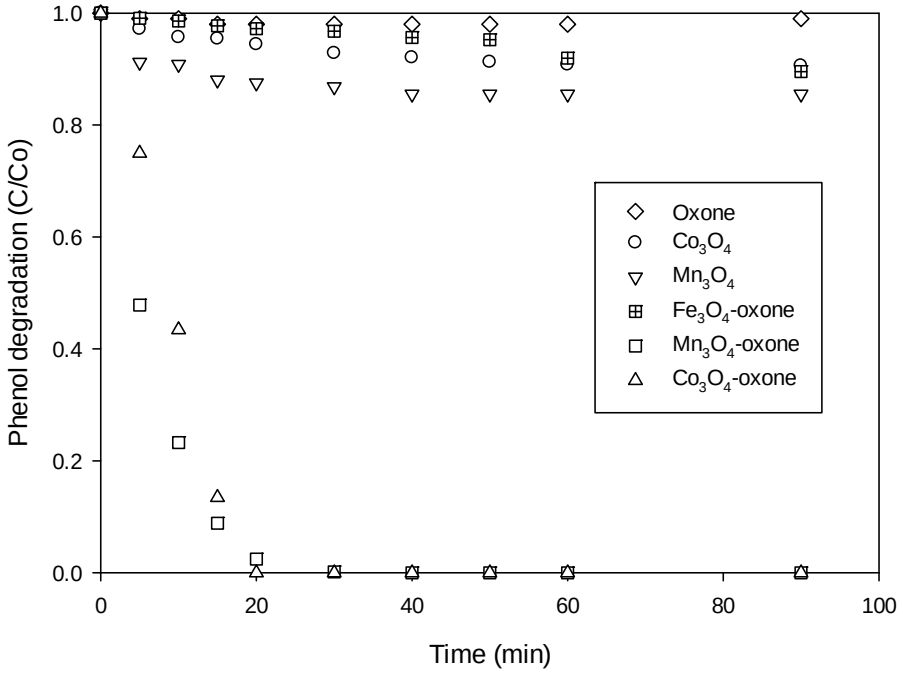

Figure 5.4. Phenol reduction with time in adsorption and catalytic oxidation. Reaction conditions: [Phenol] = 25 mg/L, catalyst = 0.4 g/L, oxone = 2 g/L, and T = 25 ^oC.

5.3.3 Effect of reaction parameters on phenol degradation

The first parameter investigated in this study was phenol concentration, which was maintained at 25, 50, 75 or 100 mg/L. The effect of initial phenol concentration on phenol degradation is shown in **Figure 5.5**. Overall, removal efficiency of phenol decreased with increasing phenol concentration. For Mn_3O_4, 100% degradation efficiency of phenol was achieved within 30 min at phenol concentration 25 mg/L, while in the same duration at phenol concentration of 50, 75 and 100 mg/L, degradation efficiency would only achieved at 96, 93 and 89%, respectively. A

similar variation could also be seen in **Figure 5.5b** using Co_3O_4. At 25 mg/L phenol concentration, complete degradation of phenol was achieved within 20 min, while in the same duration at phenol concentration of 50, 75 and 100 mg/L, removal efficiencies obtained are 82, 58 and 51%, respectively. For phenol degradation in Mn_3O_4-oxone® and Co_3O_4-oxone®, phenol degradation is dependent on sulfate radicals. Due to the same concentrations of catalyst and oxidant, sulfate radical concentration produced in solution will be the same. Thus, high concentration of phenol in mixture will require more time to obtain the same removal rate, thus lowering phenol degradation efficiency.

In order to estimate the kinetic rates, a general pseudo first order kinetics for phenol degradation was employed, as shown in equation below.

$$\ln\left(\frac{C}{Co}\right) = -k \bullet t \qquad (5.7)$$

Where k is the apparent first order rate constant of phenol removal, C is the concentration of phenol at various time (t). C_o is the initial phenol concentration. Using this model to draw plots of ln(C/Co) versus time produced a straight line for three different phenol concentrations as shown in **Figure 5.5** (inset). Based on regression coefficients, it is clear that phenol degradation followed the first order kinetics. The rate constants at varying phenol concentrations for the two systems are shown in **Table 5.2**. As seen, rate constants will decrease as the concentration of phenol increases and Mn_3O_4 presented higher rate values.

Table 5.2. Rate constants at different feed concentration of phenol

Catalyst	Initial phenol concentration (mg/L)	Rate constant (min^{-1})	R^2
Mn_3O_4	25	0.171	0.98
	50	0.102	0.99
	75	0.073	0.99
	100	0.068	0.96
Co_3O_4	25	0.092	0.91
	50	0.080	0.99
	75	0.053	0.98
	100	0.038	0.99

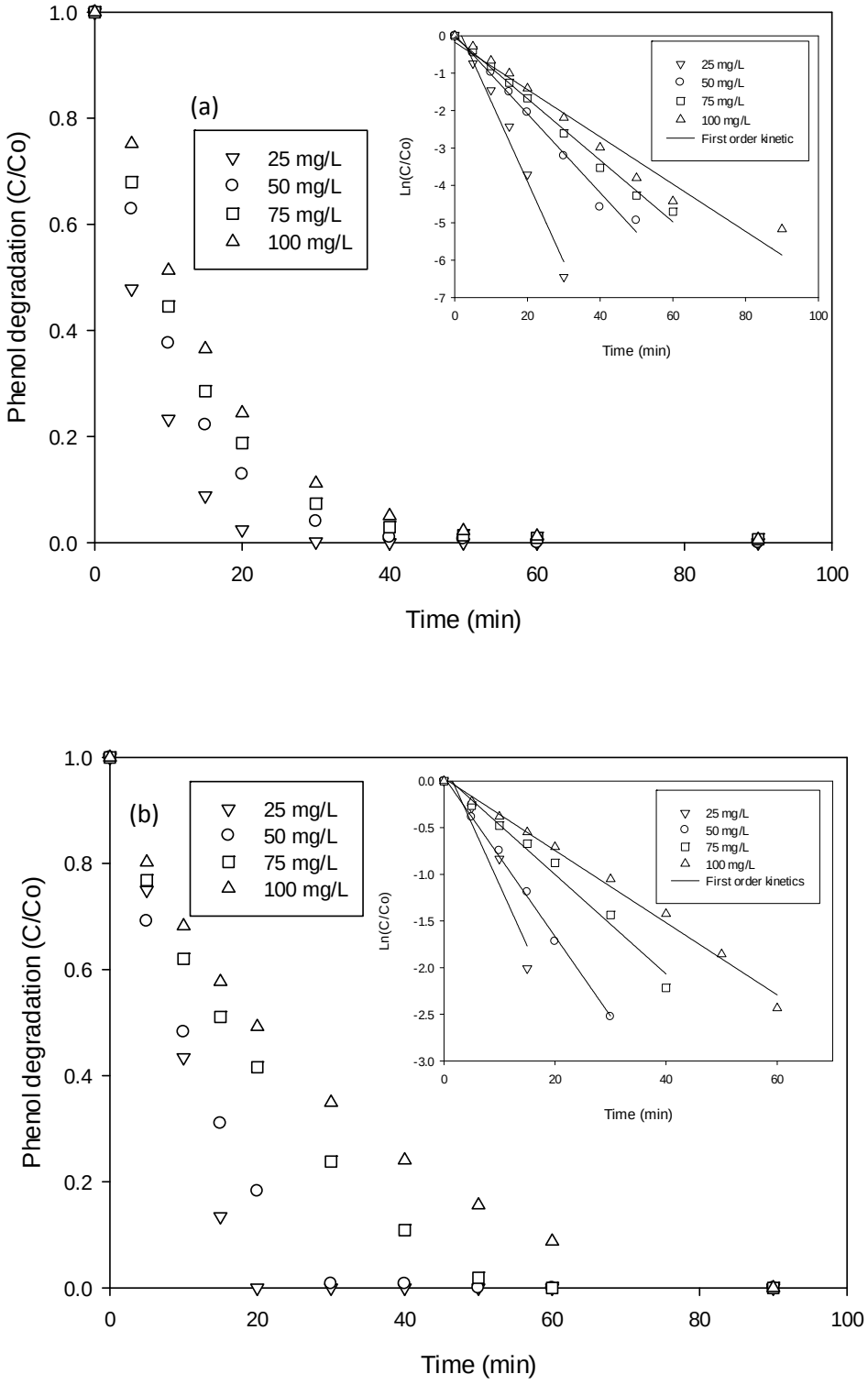

Figure 5.5. Effect of phenol concentration on phenol removal. (a) Mn_3O_4 and (b) Co_3O_4. Reaction conditions: catalyst = 0.4 g/L, oxone = 2 g/L, and T = 25 ^oC.

Figure 5.6 presents phenol degradation efficiency at varying initial concentrations of oxone® in the solution. As can be seen, for both Mn_3O_4 and Co_3O_4 catalysts, the degradation of phenol depended on concentration of oxone®. Higher concentration of oxone® resulted in more removal of phenol. For Mn_3O_4, at 1.6 g oxone® loading, complete removal would be achieved in 50 min, while at 2.0 g oxone® loading, 100% removal efficiency would be achieved in 30 min. However, a further increase of oxone® loading in solution up to 2.4 g would not enhance the rate of reaction. In contrary, For Co_3O_4, the phenol degradation rate was increased when oxone® loading was decreased from 2.4 to 1.6 g/L. At 2.4 g oxone® loading, 84 % removal efficiency would be achieved in 15 min, while in the same duration at 1.6 g oxone® loading, removal efficiency obtained is 99 %. For both Mn_3O_4 and Co_3O_4, an optimal oxone® loadings were achieved at 2.0 and 1.6 g, respectively. Based on stoichiometric reaction between phenol and oxone® (Eq. 5.8), the amount of oxone® needed for total mineralization of phenol is 2.2 g/L at 25 mg/L phenol. However, due to incomplete oxidation of phenol, optimal oxone® in this study seems to be lower than that in complete phenol mineralization.

$$C_6H_6O + 28\ HSO_5^- \longrightarrow 6\ CO_2 + 17\ H_2O + 28\ SO_4^{2-} \quad (5.8)$$

The effect of Mn_3O_4 and Co_3O_4 loading in solution on phenol degradation is shown in **Figure 5.7**. Similar to the effect of oxone loading, an increased amount of catalysts in the solutions enhanced phenol degradation efficiency. For Mn_3O_4, a complete removal of phenol could be reached within 30 min at 0.4 g/L catalyst loading. While in the same duration, 74, 63, and 50% removal could be reached at Mn_3O_4 loading of 0.3, 0.2, and 0.1 g/L, respectively. For Co_3O_4, phenol degradation rate was increased when catalyst loading was increased from 0.1 to 0.3 g/L. For instance, at 0.1 g/L catalyst loading, 48% degradation efficiency of phenol was achieved within 20 min while in the same duration, 70 and 100% removal efficiency could be reached at Co_3O_4 loading of 0.2, and 0.3 g/L, respectively. However, a further increase in Co_3O_4 loading in solution up to 0.4 g/L would not enhance the rate of reaction.

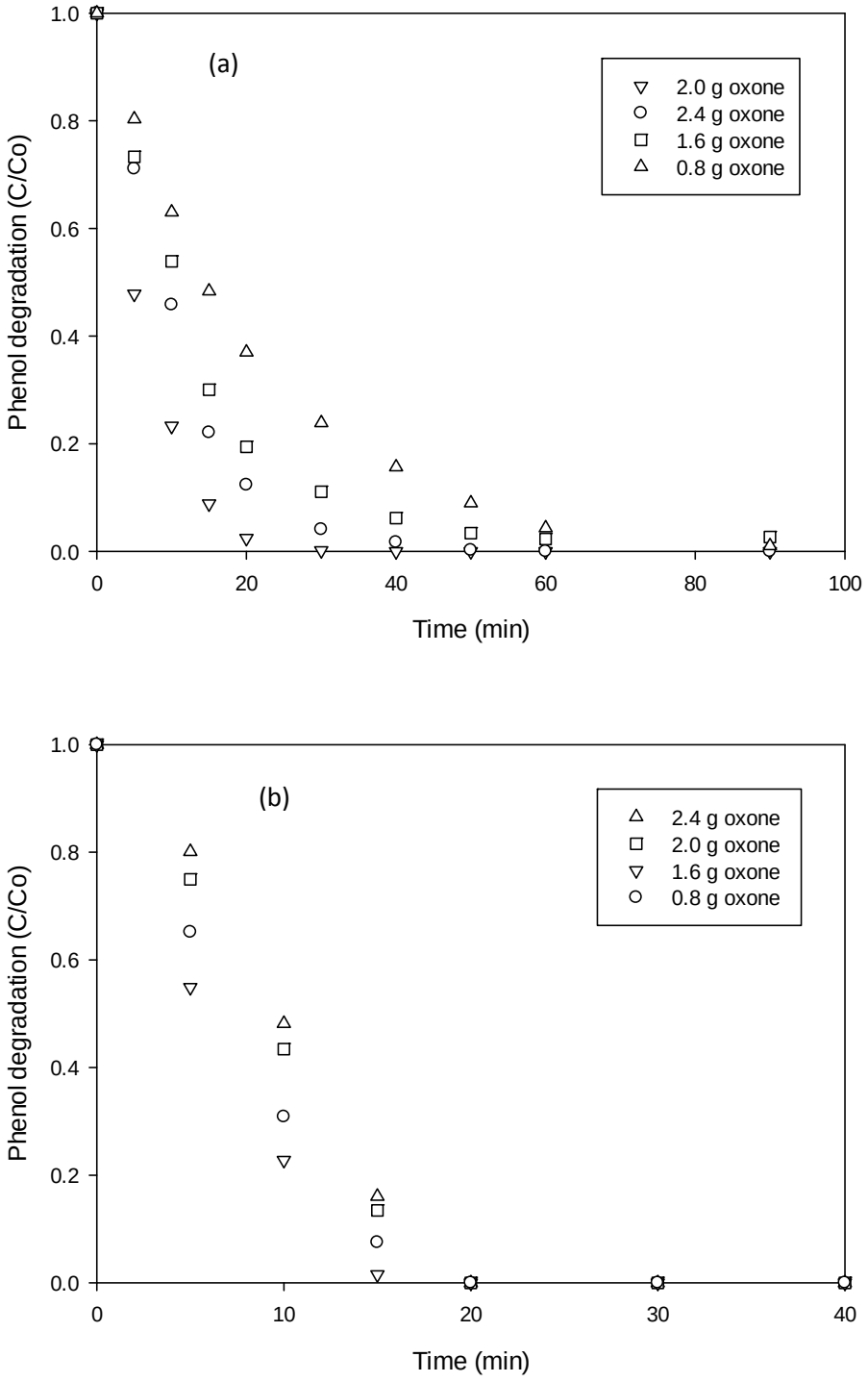

Figure 5.6. Effect of oxone concentration on phenol removal. (a) Mn_3O_4 and (b) Co_3O_4. Reaction conditions: [phenol] = 25 mg/L, catalyst = 0.4 g/L, and T = 25 ^oC.

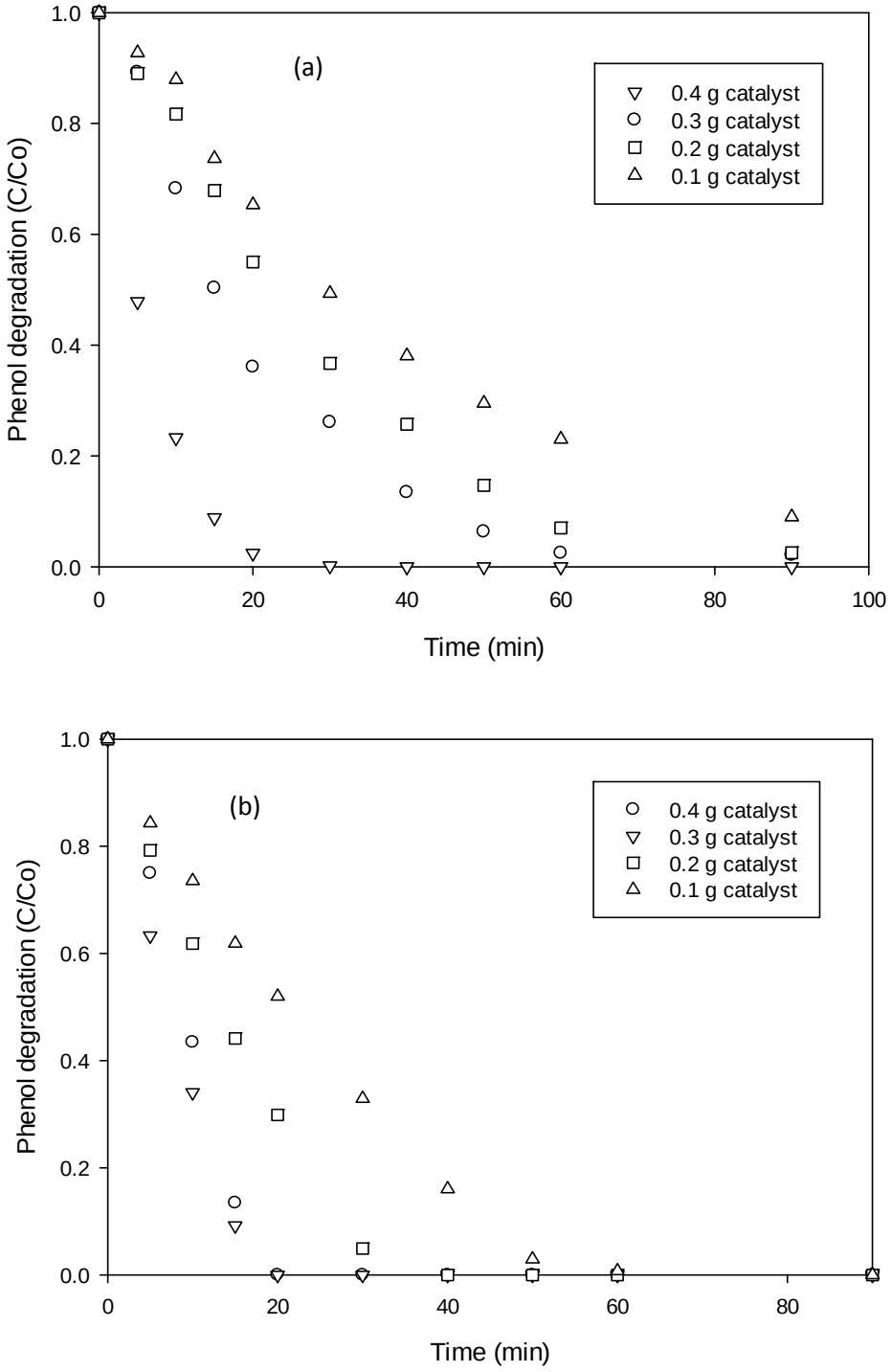

Figure 5.7 Effect of catalyst loading on phenol removal. (a) Mn_3O_4 and (b) Co_3O_4. Reaction conditions: [phenol] = 25 mg/L, oxone = 2 g/L, and T = 25 ^{o}C.

In addition, the temperature is also a key factor influencing catalyst activity and phenol degradation. **Figure 5.8** shows the effect of temperature on phenol degradation. As can be seen, the rate of reaction would increase with temperature. For Mn_3O_4, complete phenol degradation at 25 ^oC would be achieved in 30 min. Further increase of 10 ^oC, 100% degradation efficiency of phenol was achieved within 20 min. At 45 ^oC, phenol removal would reach 100% at 10 min. A same profile was also obtained on Co_3O_4. Complete degradation efficiency of phenol at 15, 25, and 35 ^oC would be achieved in 40, 20 and 10 min, respectively. Using the first order kinetic rate constants and the Arrhenius equation, the activation energies of Mn_3O_4 and Co_3O_4 were derived as 38.5 and 66.2 kJ/mol, respectively. Compared with the activation energies of supported Co_3O_4 catalysts, Co/SiO_2 (61.7- 75.5 kJ/mol) [27], Co/AC (59.7 kJ/mol) [41], Co/Fly-ash (66.3 kJ/mol) [23] and Co/Red-mud (47.0 kJ/mol) [23], Co_3O_4 has the similar value while Mn_3O_4 has a much lower value.

5.3.4 Reactivity of spent Mn_3O_4 and Co_3O_4 catalysts and reusability

Figure 5.9 presents the performance of Mn_3O_4 and Co_3O_4 in phenol degradation after catalyst recycling with filtration and water washing. As can be seen, both catalysts, showed slight deactivation in the second and third runs. However, the deactivation was not significant. In the second run, phenol degradation was still much high with 100% degradation at 40 min for Mn_3O_4 and 30 min for Co_3O_4. This suggests that Mn_3O_4 and Co_3O_4 are much stable and can be recycled for multiple uses.

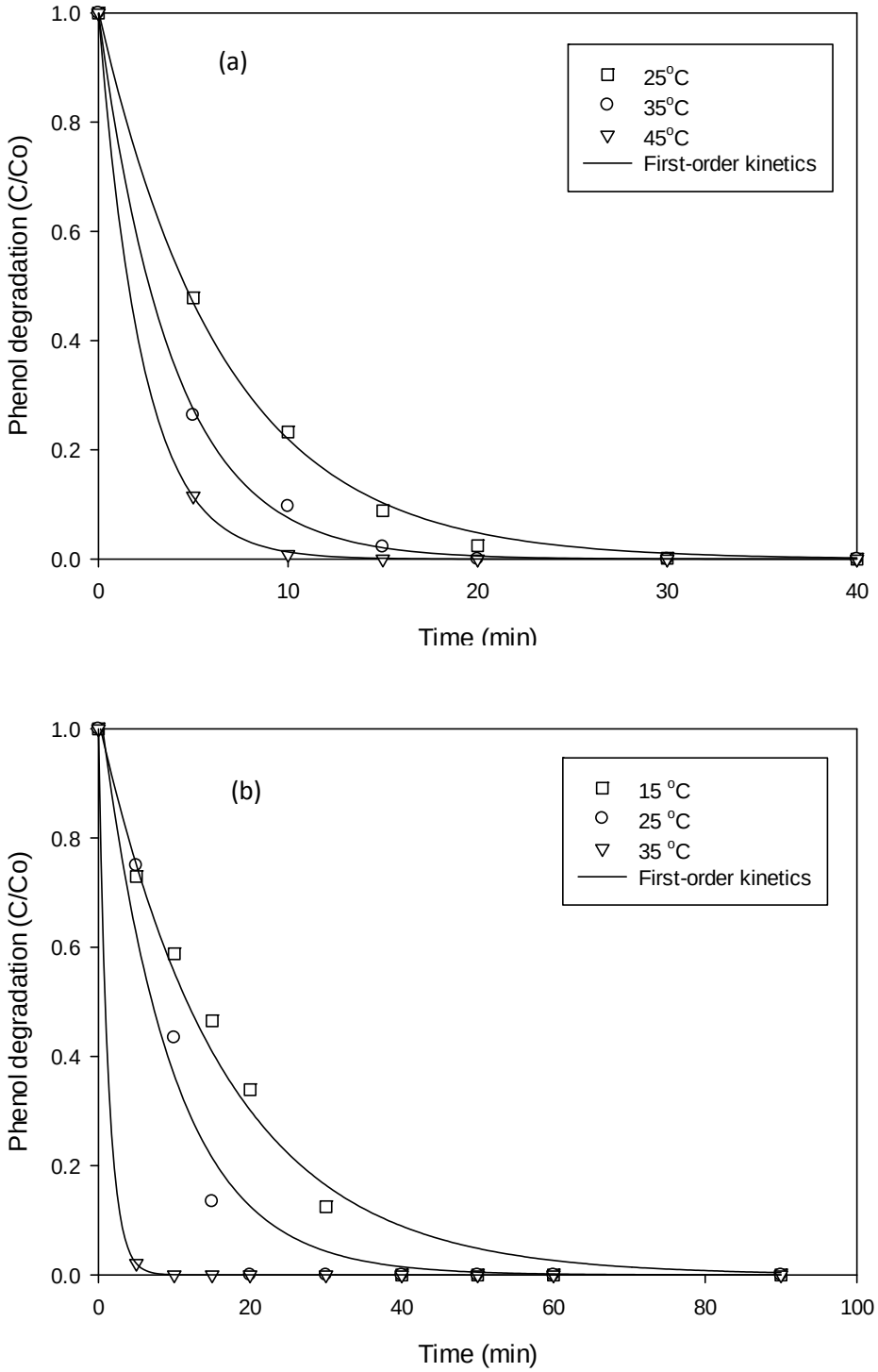

Figure 5.8. Effect of temperature on phenol removal. (a) Mn_3O_4 and (b) Co_3O_4. Reaction conditions: [phenol] = 25 mg/L, catalyst = 0.4 g/L, and oxone = 2 g/L.

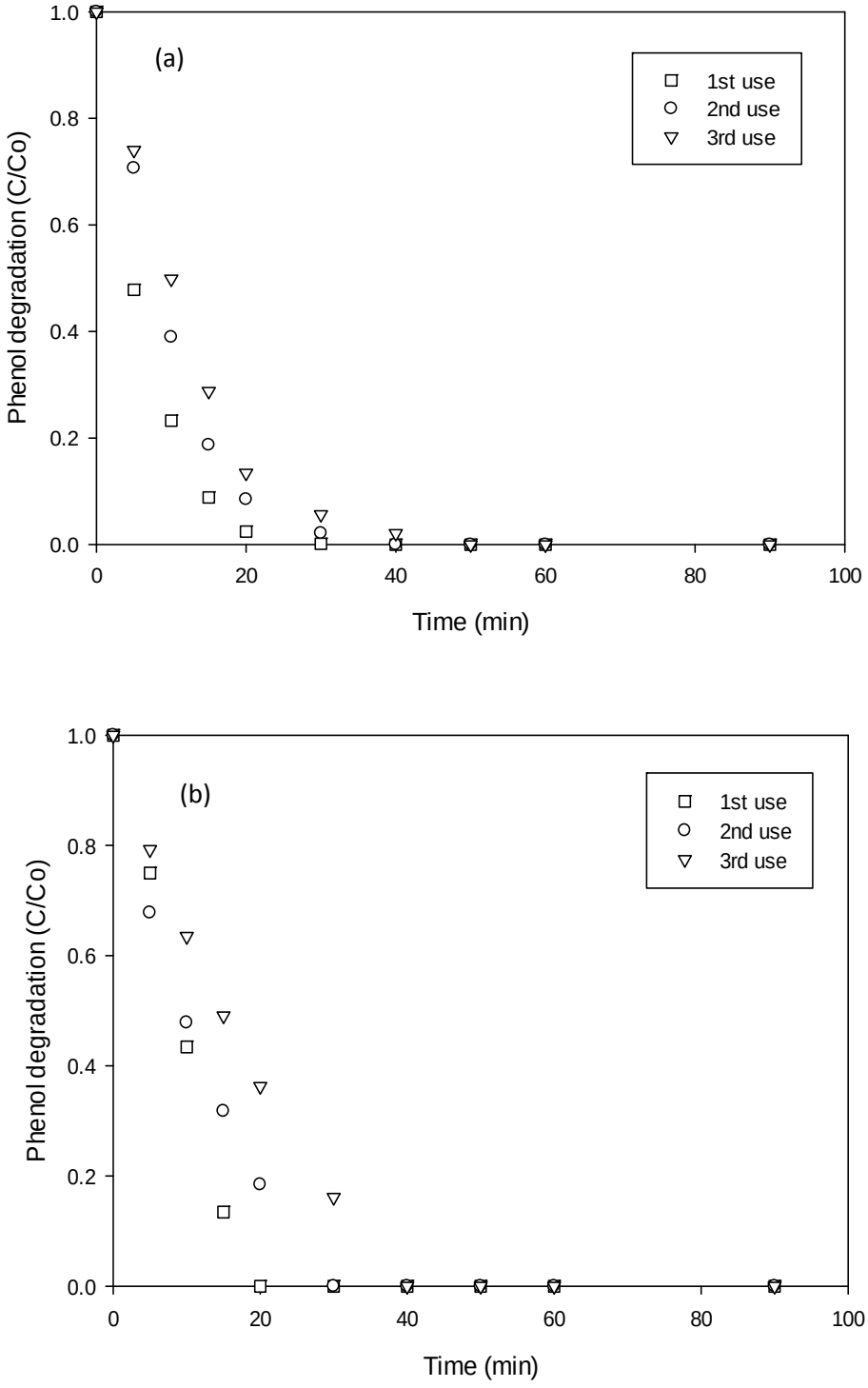

Figure 5.9. Degradation of phenol in multiple use of catalyst. (a) Mn_3O_4 and (b) Co_3O_4. Reaction conditions: [phenol] = 25 mg/L, catalyst = 0.4 g/L, and oxone = 2 g/L.

5.4. Conclusions

Different metal oxide catalysts, Mn_3O_4, Co_3O_4 and Fe_3O_4, were synthesized and tested for catalytic oxidation of phenol contaminant in water. Among them, Mn_3O_4 and Co_3O_4 are effective catalysts for generating sulfate radicals in the presence of oxone® to degrade phenol. The catalytic activity follows the trend of Mn_3O_4 > Co_3O_4 > Fe_3O_4. For the reaction, higher catalyst and oxone® loading would increase phenol degradation. Kinetic studies showed that phenol degradation followed first order reaction and activation energies on Mn_3O_4 and Co_3O_4 were obtained to be 38.5 and 66.2 kJ/mol, respectively. Mn_3O_4 also presented strong stability in catalytic performance in three runs, suggesting it can be used as a promising catalyst.

References

1. Dohnal, V. and D. Fenclova, *Air-Water Partitioning and Aqueous Solubility of Phenols.* Journal of Chemical & Engineering Data, 1995. **40**(2): p. 478-483.

2. Christoskova, S.G., M. Stoyanova, and M. Georgieva, *Low-temperature iron-modified cobalt oxide system: Part 2. Catalytic oxidation of phenol in aqueous phase.* Applied Catalysis A: General, 2001. **208**(1-2): p. 243-249.

3. Fortuny, A., et al., *Bimetallic catalysts for continuous catalytic wet air oxidation of phenol.* Journal of Hazardous Materials, 1999. **64**(2): p. 181-193.

4. Matheswaran, M. and I.S. Moon, *Influence parameters in the ozonation of phenol wastewater treatment using bubble column reactor under continuous circulation.* Journal of Industrial and Engineering Chemistry, 2009. **15**(3): p. 287-292.

5. M. Bosnic, J.B. and, and R.P. Daniels, *Pollutants in tannery effluents.* United Nations Industrial Development Organization, 2000: p. 1-26.

6. Marco, A., S. Esplugas, and G. Saum, *How and why combine chemical and biological processes for wastewater treatment.* Water Science and Technology, 1997. **35**(4): p. 321-327.

7. Andreozzi, R., et al., *Advanced oxidation processes (AOP) for water purification and recovery.* Catalysis Today, 1999. **53**(1): p. 51-59.

8. Bautista, P., et al., *An overview of the application of Fenton oxidation to industrial wastewaters treatment.* Journal of Chemical Technology and Biotechnology, 2008. **83**(10): p. 1323-1338.

9. Wang, S., *A Comparative study of Fenton and Fenton-like reaction kinetics in decolourisation of wastewater.* Dyes and Pigments, 2008. **76**(3): p. 714-720.

10. Miyamura, H., et al., *Aerobic Oxidation of Alcohols at Room Temperature and Atmospheric Conditions Catalyzed by Reusable Gold Nanoclusters Stabilized by the Benzene Rings of Polystyrene Derivatives.* Angewandte Chemie, 2007. **119**(22): p. 4229-4232.

11. Cole-Hamilton, D.J., *Homogeneous Catalysis--New Approaches to Catalyst Separation, Recovery, and Recycling.* Science, 2003. **299**(5613): p. 1702-1706.

12. Anipsitakis, G.P. and D.D. Dionysiou, *Degradation of Organic Contaminants in Water with Sulfate Radicals Generated by the Conjunction of Peroxymonosulfate with Cobalt.* Environmental Science & Technology, 2003. **37**(20): p. 4790-4797.

13. Chan, K.H. and W. Chu, *Degradation of atrazine by cobalt-mediated activation of peroxymonosulfate: Different cobalt counteranions in homogenous process and cobalt oxide catalysts in photolytic heterogeneous process.* Water Research, 2009. **43**(9): p. 2513-2521.

14. Chen, X., et al., *Kinetics of oxidative decolorization and mineralization of Acid Orange 7 by dark and photoassisted Co^{2+}-catalyzed peroxymono sulfate system.* Chemosphere, 2007. **67**(4): p. 802-808.

15. Fernandez, J., et al., *Bleaching and photobleaching of Orange II within seconds by the oxone/Co^{2+} reagent in Fenton-like processes.* Applied Catalysis B-Environmental, 2004. **49**(3): p. 207-215.

16. Ling, S.K., S. Wang, and Y. Peng, *Oxidative degradation of dyes in water using Co^{2+}/H_2O_2 and Co^{2+}/peroxymonosulfate.* Journal of Hazardous Materials, 2010. **178**(1-3): p. 385-389.

17. Madhavan, J., et al., *Kinetics of degradation of acid red 88 in the presence of Co^{2+}-ion/peroxomonosulphate reagent.* Applied Catalysis a-General, 2009. **368**(1-2): p. 35-39.

18. Başoğlu, A., et al., *Selective Recognition of Cobalt (II) Ion by a New Cryptand Compound with $N_2O_2S_2$ Donor Atom Possessing 2-Hydroxy-1-Naphthylidene Schiff Base Moiety.* Journal of Fluorescence, 2009. **19**(4): p. 655-662.

19. Anipsitakis, G.P., E. Stathatos, and D.D. Dionysiou, *Heterogeneous activation of oxone using Co_3O_4.* Journal of Physical Chemistry B, 2005. **109**(27): p. 13052-13055.

20. Chen, X., et al., *Performance of nano-Co_3O_4/peroxymonosulfate system: Kinetics and mechanism study using Acid Orange 7 as a model compound.* Applied Catalysis B-Environmental, 2008. **80**(1-2): p. 116-121.

21. Shukla, P., et al., *Cobalt exchanged zeolites for heterogeneous catalytic oxidation of phenol in the presence of peroxymonosulphate.* Applied Catalysis B: Environmental, 2010. **99**(1–2): p. 163-169.

22. Muhammad, S., et al., *Heterogeneous Catalytic Oxidation of Aqueous Phenol on Red Mud-Supported Cobalt Catalysts.* Industrial & Engineering Chemistry Research, 2012.

23. Saputra, E., et al., *Red mud and fly ash supported Co catalysts for phenol oxidation.* Catalysis Today, 2012. **190**(1): p. 68-72.

24. Liang, H., et al., *Excellent performance of mesoporous Co_3O_4/MnO_2 nanoparticles in heterogeneous activation of peroxymonosulfate for phenol degradation in aqueous solutions.* Applied Catalysis B: Environmental, 2012. **127**(0): p. 330-335.

25. Zhang, W., et al., *Supported cobalt oxide on MgO: Highly efficient catalysts for degradation of organic dyes in dilute solutions.* Applied Catalysis B-Environmental, 2010. **95**(1-2): p. 93-99.

26. Yang, Q., et al., *Heterogeneous activation of peroxymonosulfate by supported cobalt catalysts for the degradation of 2,4-dichlorophenol in water: The effect of support, cobalt precursor, and UV radiation.* Applied Catalysis B-Environmental, 2008. **77**(3-4): p. 300-307.

27. Shukla, P., et al., *Nanosized Co_3O_4/SiO_2 for heterogeneous oxidation of phenolic contaminants in waste water.* Separation and Purification Technology, 2011. **77**(2): p. 230-236.

28. Zhou, G., et al., *Titanate supported cobalt catalysts for photochemical oxidation of phenol under visible light irradiations.* Separation and Purification Technology, 2011. **80**(3): p. 626-634.

29. Yao, Y., et al., *Hydrothermal Synthesis of Co_3O_4–Graphene for Heterogeneous Activation of Peroxymonosulfate for Decomposition of Phenol.* Industrial & Engineering Chemistry Research, 2012. **51**(46): p. 14958-14965.

30. Hu, L., X. Yang, and S. Dang, *An easily recyclable Co/SBA-15 catalyst: Heterogeneous activation of peroxymonosulfate for the degradation of phenol in water.* Applied Catalysis B: Environmental, 2011. **102**(1–2): p. 19-26.

31. Yang, Q., et al., *Iron-cobalt mixed oxide nanocatalysts: Heterogeneous peroxymonosulfate activation, cobalt leaching, and ferromagnetic properties for environmental applications.* Applied Catalysis B-Environmental, 2009. **88**(3-4): p. 462-469.

32. Yao, Y., et al., *Magnetic $CoFe_2O_4$–Graphene Hybrids: Facile Synthesis, Characterization, and Catalytic Properties.* Industrial & Engineering Chemistry Research, 2012. **51**(17): p. 6044-6051.

33. Saputra, E., et al., *α-MnO_2 activation of peroxymonosulfate for catalytic phenol degradation in aqueous solutions.* Catalysis Communications, 2012. **26**(0): p. 144-148.

34. Zhang, W., et al., *Controlled synthesis of Mn_3O_4 nanocrystallites and MnOOH nanorods by a solvothermal method.* Journal of Crystal Growth, 2004. **263**(1–4): p. 394-399.

35. Jiang, J., et al., *General Synthesis of Large-Scale Arrays of One-Dimensional Nanostructured Co_3O_4 Directly on Heterogeneous Substrates.* Crystal Growth & Design, 2009. **10**(1): p. 70-75.

36. Zhai, Y., et al., *Ordered magnetic core-manganese oxide shell nanostructures and their application in water treatment.* Journal of Materials Chemistry, 2009. **19**(38): p. 7030-7035.

37. Anipsitakis, G.P. and D.D. Dionysiou, *Radical generation by the interaction of transition metals with common oxidants.* Environmental Science & Technology, 2004. **38**(13): p. 3705-3712.

38. Liang, H., et al., *Solution combustion synthesis of Co oxide-based catalysts for phenol degradation in aqueous solution.* Journal of Colloid and Interface Science, 2012. **372**(1): p. 58-62.

39. Ding, Y., et al., *A heterogeneous Co_3O_4-Bi_2O_3 composite catalyst for oxidative degradation of organic pollutants in the presence of peroxymonosulfate.* Catalysis Science & Technology, 2012. **2**(9): p. 1977-1984.

40. Chen, C., et al., *Microstructure evolution and advanced performance of Mn_3O_4 nanomorphologies.* Nanoscale, 2012. **4**(8): p. 2590-2596.

41. Shukla, P.R., et al., *Activated carbon supported cobalt catalysts for advanced oxidation of organic contaminants in aqueous solution.* Applied Catalysis B: Environmental, 2010. **100**(3-4): p. 529-534.

Chapter 6

Synthesis of α-Mn_2O_3@α-MnO_2 Core/Shell Nanocomposite and Catalytic Oxidation of Phenolic Contaminants in Aqueous Solutions

Abstract

A α-Mn_2O_3@α-MnO_2 core/shell nanocomposite was prepared in a hydrothermal process and tested in catalytic advanced oxidation of phenol in aqueous solution using oxone®. The properties of the composite were characterized by several techniques such as X-ray diffraction (XRD), N_2 adsorption, and scanning electron microscopy (SEM). The core/shell material is highly effective in heterogeneous activation of oxone® to produce sulfate radicals for phenol degradation. The catalytic activity depends on catalyst loading, oxone® concentration, phenol concentration, and temperature. α-Mn_2O_3@α-MnO_2 core/shell demonstrated much better activity than homogeneous Mn^{2+} in phenol degradation, achieving 100% phenol degradation efficiency and 78% TOC removal in 50 min at the condition of 25 ppm phenol, 0.4 g/L catalyst, 2 g/L oxone®, and 25 ^oC. The catalyst also shows stable activity in several cycles. Kinetic study showed that phenol degradation followed first order reaction and activation energy of α-Mn_2O_3@ α-MnO_2 core/shell was obtained as 39.9 kJ/mol.

6.1. Introduction

In the 21st century, wastewater treatment for its recycling is an important issue in social, economic and politic areas. It causes the research of wastewater treatment rapidly growing. One of the promising methods for degradation of organic pollutants in wastewater is advanced oxidation process (AOP), being able to completely degrade organic compounds into simple compounds, CO_2 and H_2O. Currently, most AOPs are based on generation of very reactive species, such as hydroxyl radicals ($OH^{\bullet}$) that have a high standard oxidation potential for reaction non-selectively [1-3].

In the past decade, core-shell-structured nano-materials have attracted much attention because of their physical and chemical properties and wide potential applications as heterogeneous catalysts [4-6], adsorbents [7-9], enhanced luminescence [10, 11], battery materials [12-14], biolabeling [15, 16] and supercapacitor [17, 18]. Recently, some core-shell-structured manganese oxides have been synthesized, such as γ-MnO_2@α-MnO_2, Co_3O_4@MnO_2, and Fe_3O_4@MnO_2 [19-22]. However, few studies have been conducted on the catalytic properties of manganese oxides with different oxidation states in water treatment. Xing et al. [23] investigated Fe_3O_4@$FeMnO_x$ nanoparticle as a catalyst for heterogeneous activation of H_2O_2 to generate hydroxyl radical targeting the decolourisation of methylene blue. They found Fe_3O_4@$FeMnO_x$ nanoparticles exhibited a promising performance as a chemical agent under optimized conditions for methylene blue (MB) removal from water. They [24] also prepared Fe_3O_4@MnO_x by redox reaction between metal cations (Mn^{2+}) and MnO_4^- and found that they showed excellent catalytic performance in MB and 2,4-dichlorophenoxyacetic acid degradation with H_2O_2. Park et al. [25] used a facile route to synthesize stable core-shell structured silica-Mn nanocomposites and tested catalytic degradation of MB in aqueous solution in the presence of H_2O_2. Cao et al. [20] reported the synthesis of a new type of core/shell structure, γ-MnO_2@α-MnO_2 and used it as an adsorbent to remove organic pollutants and heavy metal ions in water.

Recently, many investigations have reported that sulphate radicals are superior to hydroxyl radicals in oxidation for water treatment. In most previous investigations, Co^{2+}/peroxymonosulphate (oxone®, HSO_5^-) has been found to be an effective route

for sulphate radical generation [26]. However, a major issue in using Co metal ions is the toxicity and secondary pollution. Therefore, alternative catalysts with less toxicity and environmental benign for peroxymonosulfate activation are highly required. We have recently reported the excellent performance of α-MnO_2 [27] and α-Mn_2O_3 [28] in activation of oxone® for phenol degradation. Using α-Mn_2O_3@α-MnO_2 oxide core-shell structured will be a promising alternative material for advance oxidation process. Manganese oxide has several different phases and oxidation states, such as MnO, MnO_2, Mn_2O_3 and Mn_3O_4, with varying structures. In this study, α-Mn_2O_3@α-MnO_2 core/shell structure was synthesized for the first time by using a hydrothermal method. Their physicochemical properties were characterized. The prepared metal oxide core/shell materials were then employed as catalysts for heterogeneous production of sulphate radicals for chemical mineralizing of phenol in the solution. Several key parameters in the kinetic study such as phenol concentration, catalyst loading, oxone® concentration and temperature were also investigated.

6.2. Experimental section

6.2.1 Material synthesis

A α-Mn_2O_3@α-MnO_2 was obtained with two-step preparation. First, $MnCO_3$ was synthesized by a hydrothermal method reported by Li et al. [29]. Typically, potassium permanganate (3 mmol) and an equal amount of glucose were put into 60 mL distilled water at room temperature, and then 0.1 M tartaric acid was added to the above mixture and continually stirred to form a homogeneous solution, which was then transferred into a 125 mL Teflon-lined autoclave. The autoclave was sealed and maintained at 150 ^oC for 10 h, and then cooled down to room temperature naturally. The resulted solid product ($MnCO_3$) was filtered, washed with distilled and dried in air at 100 ^oC overnight. Later on, α-Mn_2O_3@α-MnO_2 was prepared using a modified method from Cao et al. [20]. The as-synthesized $MnCO_3$ (0.1 g) were put into distilled water (50 mL) at room temperature, and then $KMnO_4$ (0.05 g) was added to the mixture and sealed. The mixture was stirred vigorously for 15 min and then allowed to stand for 17 h at room temperature. The resulted solid product ($MnCO_3$@MnO_x) was filtered, washed with distilled and dried in air at 100 ^oC

overnight. After that, the product was calcined at 400 ^{o}C in air for 2 h to form α-Mn_2O_3@α-MnO_2.

6.2.2 Characterization catalysts

Catalysts were characterized by XRD, N_2 adsorption/desorption, and SEM, . XRD patterns were obtained on a Bruker D8 (Bruker-AXS, Karlsruhe, Germany) diffractometer using filtered Cu Kα radiation source (λ = 1.54178 Å), with accelerating voltage 40 kV, current 30 mA and scanned at 2θ from 10 to 80^{o}. N_2 adsorption/desorption was measured using a Micromeritics Tristar 3000 to obtain pore volume and Brunauer-Emmett-Teller (BET) specific surface area. Prior to measurement the samples were degased at 120 ^{o}C for 5 h under vacuum condition. The external morphology and chemical compositions of the samples were observed on a ZEISS NEON 40EsB scanning electron microscope (SEM) equipped with an energy dispersive spectrometer (SEM-EDS).

6.2.3 Kinetic study of phenol oxidation

Phenol degradation tests were carried out in a 1-L glass beaker with 500 mL containing 25, 50, 75 and 100 mg/L of phenolic solutions. The reaction mixture was stirred constantly at 400 rpm. Firstly, a fixed amount of peroxymonosulfate (oxone®, DuPont's triple salt: $2KHSO_5 \bullet KHSO_4 \bullet K_2SO_4$, Sigma-Aldrich) was added into the solution for a while, then a catalyst was added into the solution to start the oxidation reaction of phenol. At certain time, 0.5 mL of water sample was withdrawn from the mixture using a syringe filter of 0.45 μm and then mixed with 0.5 mL of pure methanol to quench the reaction. The concentration of phenol was analysed using a Varian HPLC with a UV detector at λ = 270 nm. The column used was C-18 with mobile phase of 30 % CH_3CN and 70% ultrapure water. For comparison, a homogeneous oxidation with manganese ions and oxone was also conducted by addition $Mn(NO_3)_2.4H_2O$ of the chemicals into the phenol solution simultaneously. The Mn^{2+} concentration was kept as the same as the catalyst loaded in solution. For selected samples, total organic carbon (TOC) was obtained using a Shimadzu TOC-5000 CE analyzer.

6.3. Result and discussion

6.3.1 Characterization of manganese oxide core/shell catalysts

Figure 6.1 show XRD pattern of α-Mn_2O_3@α-MnO_2, including thermal treatment of $MnCO_3$ precursor at 400 ^oC in air for 2 h. The two samples present different crystalline peaks. In **Figure 6.1A**, the diffraction peaks occurred at 23.13^o, 32.95^o, 35.68^o, 38.23^o, 45.17^o, 49.34^o, 53.27^o, 55.18^o 64.07^o, and 65.08^o, confirming the formation of α-Mn_2O_3 (JCPDS No. 41-1442). A small amount of α-MnO_2 could also be detected. The diffraction peaks in **Figure 6.1B** occurred at 12.78^o, 18.10^o, 25.71^o, 28.84^o, 36.69^o, 37.52^o, 41.25^o, 41.96^o, 49.86^o, and 60.27^o, confirms the formation of α-MnO_2 (JCPDS No. 44-0141). **Figure 6.1B** also shows the diffraction peaks of α-Mn_2O_3, suggesting the presence of mixed two phases of α-MnO_2 and α-Mn_2O_3. This is different from the report of Cao et al, who obtained a γ-MnO_2@α-MnO_2 composite [20]. The difference in material structure is due to the varying preparation conditions.

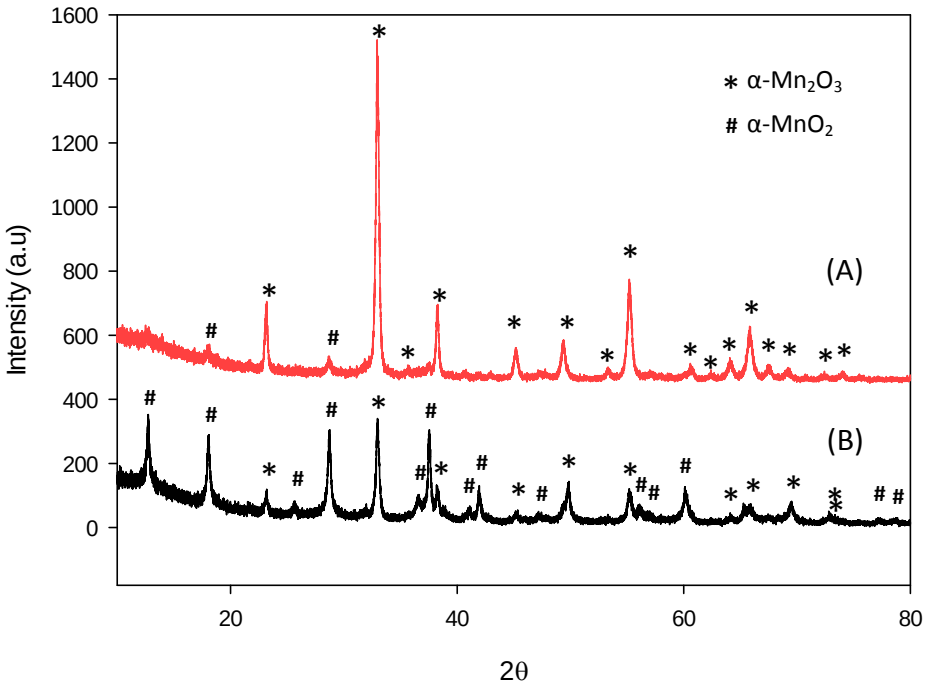

Figure 6.1. XRD patterns of manganese oxide catalysts. (A) α-Mn_2O_3 (direct calcination of $MnCO_3$ precursor), (B) α-Mn_2O_3@α-MnO_2.

Figure 6.2 shows N_2 adsorption/desorption isotherm and pore size distribution of α-Mn_2O_3@α-MnO_2 core/shell composite. It was found that BET surface area and pore volume of the catalyst were 37.2 m^2/g and 0.266 cm^3/g, respectively. The sample has an average pore radius of 28 nm, which means α-Mn_2O_3@α-MnO_2 is a mesoporous material. The pore size distribution of the composite presented multiple peaks, majorly centred at 1.3, and 3 nm.

Figure 6.3 presents SEM images of α-Mn_2O_3@α-MnO_2 core/shell catalyst. The morphology of the composite presents in the uniform ellipsoid structure (**Figure 6.3A**). The particle size varies in a range of 1-2 μm. As can be seen from the high magnification SEM image of α-Mn_2O_3@α-MnO_2, the ellipsoid is actually composed of an inside core (α-Mn_2O_3) and an outside shell (α-MnO_2) (**Figure 6.3B**), similar to the core/shell γ-MnO_2@α-MnO_2 structure [20]. The image also shows that some hollow interior space is present between the core and the shell, probably attributing to core shrinkage during the transformation from $MnCO_3$ to α-Mn_2O_3 [20].

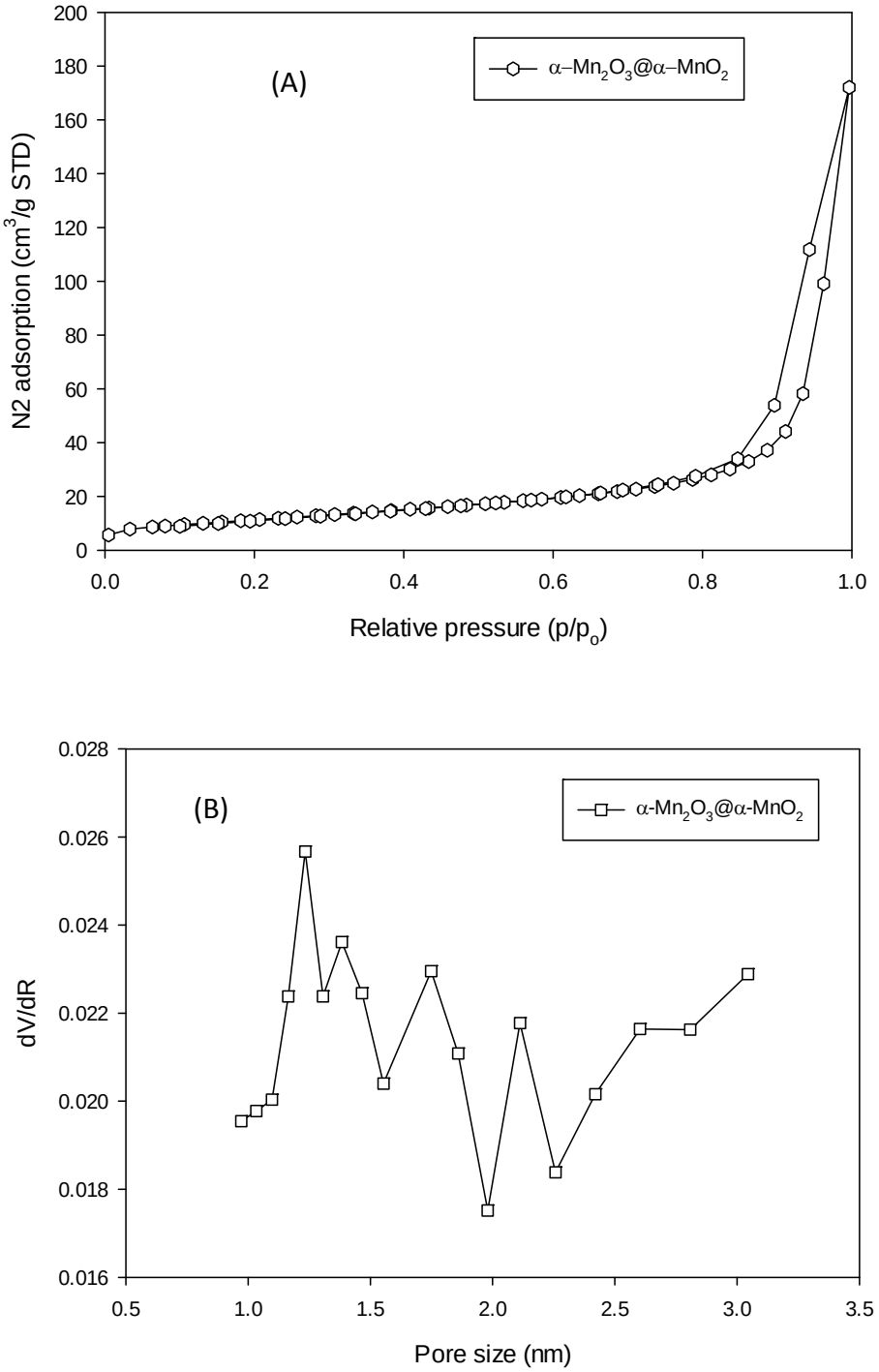

Figure 6.2. N_2 adsorption isotherm and pore size distribution of α-Mn_2O_3@α-MnO_2 catalyst.

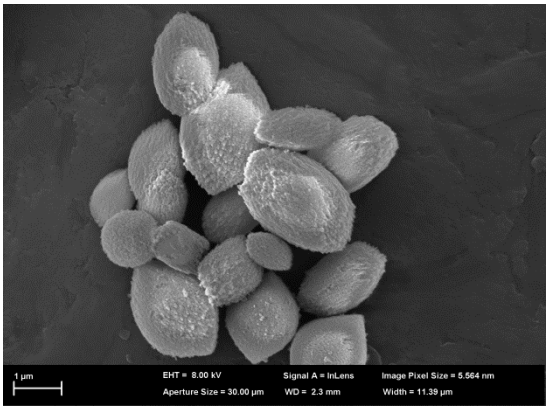

(A)

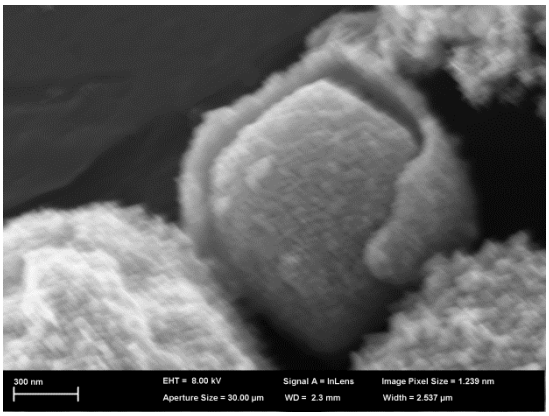

(B)

Figure 6.3. SEM images of α-Mn_2O_3@α-MnO_2 catalyst.

6.3.2 Preliminary study of phenol oxidation using manganese oxide core/shell catalysts

Figure 6.4 shows the preliminary tests of adsorption and catalytic oxidation of phenol using α-Mn_2O_3@α-MnO_2 core/shell catalyst. The α-Mn_2O_3@α-MnO_2 showed little adsorption of phenol at less than 5% removal efficiency. From the figure, it is also seen that phenol removal would not change significantly in the presence of oxone® without a catalyst, indicating that oxone® itself could not produce sulfate radicals to induce phenol oxidation. Phenol degradation would occur when catalyst and oxidant were simultaneously present in the solution. α-Mn_2O_3@α-MnO_2 core/shell catalyst could degrade phenol at 100% in 30 min in the presence of oxone®. The high degradation rate was due to the activation of oxone® by α-Mn_2O_3@α-MnO_2 core/shell catalyst to produce sulfate radicals. Compared with the efficiency of homogeneous oxidation, Mn^{2+}/oxone® system, the heterogeneous system exhibited

much higher activity. The homogeneous system could result in removal of phenol at 97% in 120 min. In addition, TOC measurements indicated that TOC removal in α-Mn_2O_3@α-MnO_2/oxone® system was about 78% within 60 min. The reaction mechanism for heterogeneous phenol oxidation can be proposed as below.

$$HSO_5^- + 2MnO_2 \longrightarrow SO_5^{-\bullet} + OH^- + 2Mn_2O_3 \quad (6.1)$$

$$HSO_5^- + 2Mn_2O_3 \longrightarrow SO_4^{-\bullet} + H^+ + 2MnO_2 \quad (6.2)$$

$$SO_4^{-\bullet} + H_2O \longrightarrow OH^\bullet + H^+ + SO_4^{2-} \quad (6.3)$$

$$C_6H_5OH + SO_4^{-\bullet} \longrightarrow \text{several steps} \longrightarrow CO_2 + H_2O + SO_4^{2-} \quad (6.4)$$

Several investigations have been reported for heterogeneous core/shell catalysts for organic decomposition using different oxidants. Xing et al. [23] studied Fe_3O_4/$FeMnO_x$ core/shell nanoparticles for methylene blue discoloration with H_2O_2. The Fe_3O_4/$FeMnO_x$ core/shell nanoparticles could achieve 90% colour removal at dye (methylene blue) concentration of 25 mg/L within 240 min. Park et al. [25] used silica-Mn core-shell structured nano-composites with H_2O_2 for methylene blue degradation at 5 mg/L. The silica-Mn core-shell composite could achieved 82% methylene blue degradation within 120 min. Xing et al. [24] studied the magnetic core-shell nano-composite (Fe_3O_4@MnOx) for heterogeneous activation of H_2O_2 to generate hydroxyl radicals (OH•), targeting the decomposition of 2,4-dichlorophenoxyacetic acid. They found that Fe_3O_4@MnOx could activate H_2O_2 to achieve 86% removal at 2,4-dichlorophenoxyacetic acid concentration of 20 mg/L in 150 min. Thus, it appears that α-MnO_2@Mn_2O_3 core/shell catalyst presented higher activity in the degradation of phenol in the presence of oxone®.

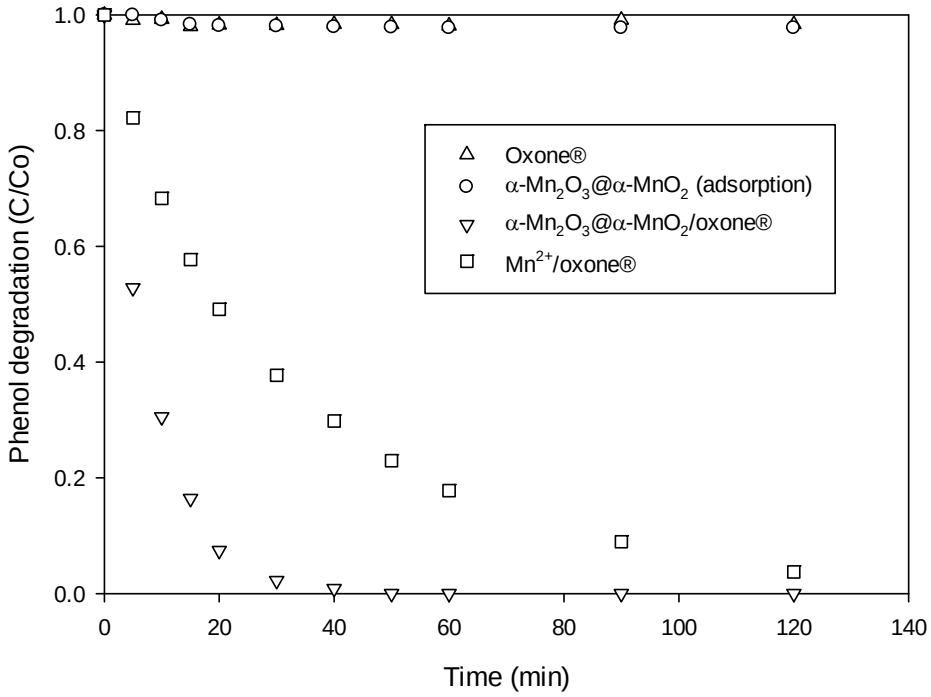

Figure 6.4. Phenol reduction with time in adsorption and catalytic oxidation. Reaction conditions: = 25 ppm, catalyst = 0.4 g/L, oxone = 2 g/L, and T = 25 ^{o}C.

6.3.3 Phenol degradation kinetics at varying reaction conditions

Further investigations on the performance of α-MnO_2@Mn_2O_3 core/shell catalyst at different reaction conditions were carried out. Effect of phenol concentration at 25-100 ppm on phenol degradation is presented in **Figure 6.5**. As can be seen, phenol degradation efficiency decreased with increasing initial phenol concentration. At 25 ppm, 100% phenol removal could be achieved in 30 min while at phenol concentrations of 50, 75 and 100 ppm, complete phenol removal could be obtained in 50, 90 and 120 min, respectively. Due to the same amounts of catalyst and oxone® in solution at varying phenol concentration, higher phenol concentration would requires a longer time to achieve 100% degradation efficiency.

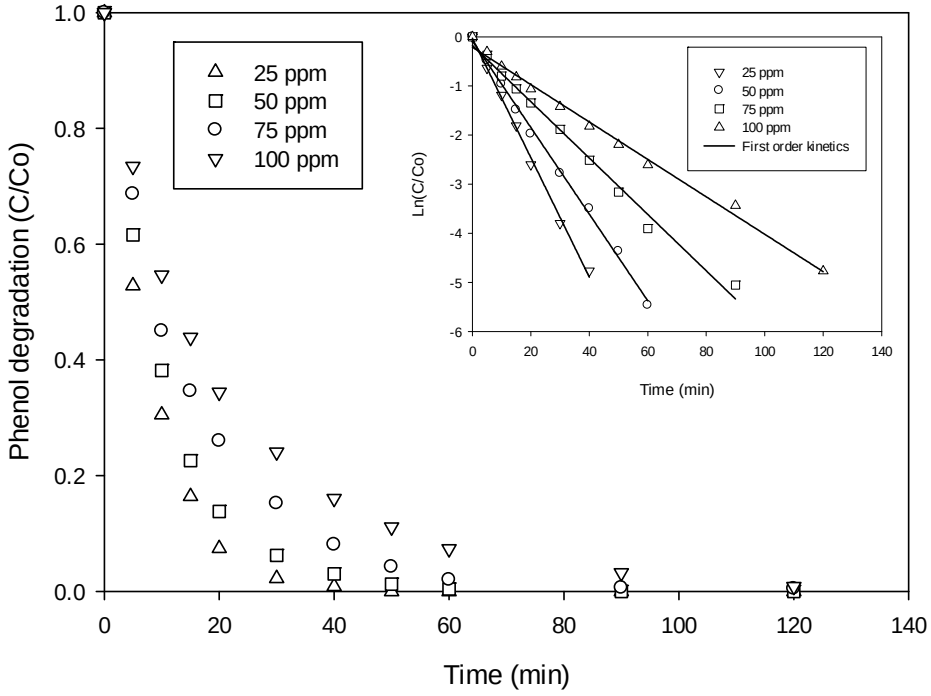

Figure 6.5. Effect of phenol concentration on phenol removal. Reaction conditions: catalyst = 0.4 g/L, oxone = 2 g/L, and T = 25 ^{o}C.

In order to estimate the kinetic rates, a general pseudo first order kinetics for phenol degradation was employed, as shown in equation below.

$$\ln\left(\frac{C}{Co}\right) = -k \bullet t \qquad (6.5)$$

Where k is the apparent first order rate constant of phenol removal, C is the concentration of phenol at various time (t). C_o is the initial phenol concentration. Using this model by plotting ln(C/Co) versus time, straight line should be produce as shown in **Figure 6.5** (inset). Based on regression coefficients, it is clearly demonstrated that phenol degradation followed the first order kinetics. The rate constants at varying phenol concentrations are shown in **Table 6.1**. As can be seen, the rate constant will decrease as the concentration of phenol increases.

Table 6.1. Rate constant at different feed concentration of phenol.

Initial phenol concentration	Rate constant min^{-1}	R^2
25 ppm	0.1237	0.99
50 ppm	0.0937	0.99
75 ppm	0.0670	0.99
100 ppm	0.0489	0.99

Several researchers have investigated the kinetic rate of toxic organic degradation in the presence of oxone®. Hu et al. [30] reported a pseudo first order degradation of dye (Rhodamine B) in aqueous solution induced by CoMg/SBA-15-oxone®. Su et al. [31] studied heterogeneous activation of oxone® with $Co_xFe_{3-x}O_4$ for decolourisation of Rhodamine B. They found that the degradation of Rhodamine B followed the first order kinetics. Saputra et al. [27] used α-MnO_2 nanocatalyst-oxone® system for phenol removal, α-MnO_2 nanocatalyst-oxone® also presents the first order kinetics. Therefore, α-Mn_2O_3@α-MnO_2 core/shell catalyst with oxone® shows the similar result to the previous investigations.

Phenol removal efficiency is also affected by α-Mn_2O_3@α-MnO_2 core/shell loading in the system as shown in **Figure 6.6**. Higher α-Mn_2O_3@α-MnO_2 loading in solution resulted in higher phenol degradation efficiency. At 0.1 g/L of α-Mn_2O_3@α-MnO_2, phenol degradation efficiency would achieve at 88% in 120 min while at 0.2, 0.3, and 0.4 g/L of catalyst loading, phenol degradation could be reached 100% within 120, 60, and 50 min, respectively. The increased catalyst loading would enhance the active sites in solution for reaction with oxone® thus generating more amounts of active sulfate radicals ($SO_4^{-\bullet}$ and $SO_5^{-\bullet}$), resulting in an increase in the rate of phenol removal.

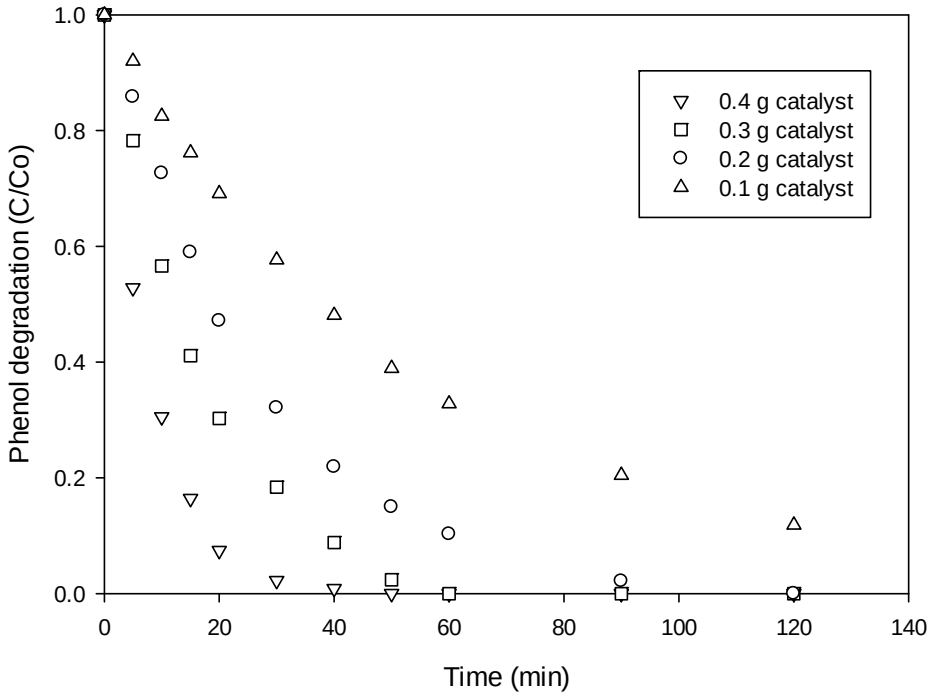

Figure 6.6. Effect of catalyst loading on phenol removal. Reaction conditions: [phenol] = 25 ppm, oxone = 2 g/L, and T = 25 ^{o}C.

Figure 6.7 shows oxidation of phenol on α-Mn_2O_3@α-MnO_2 at different oxidant loadings. In general, increased concentrations of oxone® in solution will increase phenol degradation. However the influence was not as significant as catalyst loading. At 0.4 g/L oxone®, complete phenol removal could be achieved in about 60 min while at 0.8 and 1.6 g/L of oxone® loading, phenol degradation could reach 100% within 50 and 30 min, respectively. However, further increase in oxone® concentration at 2.0 g/L would slightly decrease phenol degradation efficiency. Shukla et al. [32] studied the effect of concentration of oxone® with Co-SBA-15 catalyst for removing phenol from aqueous solutions. They found that high oxone® concentration can reduce the rate of oxidation of phenol when oxone® loading was increased from 2 to 4 g/L. A higher concentration of oxone® would consume the active $SO_4^{-\bullet}$, resulting in a lower degradation rate, according to the mechanism as follows.

$$HSO_5^- + SO_4^{-\bullet} \longrightarrow SO_5^{-\bullet} + SO_4^{2-} + H^+ \quad (7.6)$$

$$HSO_5^- + OH^\bullet \longrightarrow SO_5^{-\bullet} + H_2O \quad (7.7)$$

$SO_5^{-\bullet}$ has a low oxidation rate than $SO_4^{-\bullet}$. Therefore, the current study using α-Mn_2O_3@α-MnO_2 heterogeneous catalyst for activation of oxone to generate sulfate radicals shows the same observation and optimum loading of oxone® should be determined.

.

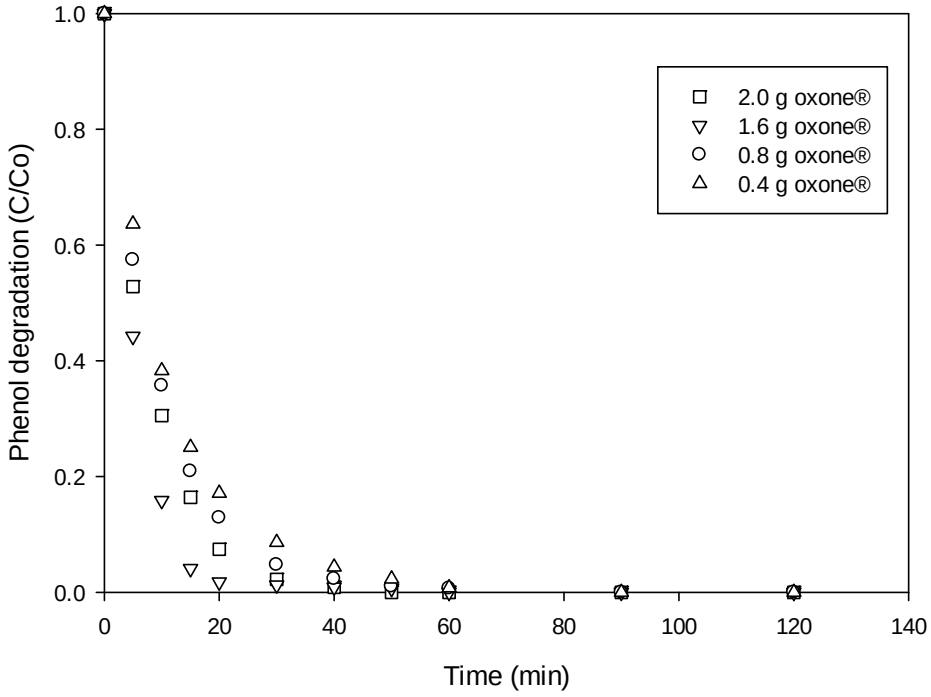

Figure 6.7. Effect of oxone concentration on phenol removal. Reaction conditions: [phenol] = 25 ppm, catalyst = 0.4 g/L, and T = 25 ^oC.

Figure 6.8 shows the reduction of phenol concentration against time at various temperatures of 25 - 45 ^oC. As can be seen, the reaction temperature plays a significant role in phenol degradation. The rate of reaction would increase significantly with increasing temperature. At 25 ^oC, degradation efficiency of phenol would reach 100% at 30 min. Further increase by 10 ^oC, complete phenol removal was achieved within 20 min while complete phenol degradation at 45 ^oC would be achieved in 15 min. Based on first-order kinetic model of the reaction, the rate constant with temperature variation was obtained and the relationship followed the

Arrhenius equation (Inset **Figure 6.8**). The Arrhenius plot presented a good linear correlation and the activation energy of phenol degradation on α-Mn_2O_3@α-MnO_2 core/shell was derived as 39.9 kJ/mol. This value is much great than that of the effective α-MnO_2 [27] and α-Mn_2O_3 [28] catalysts.

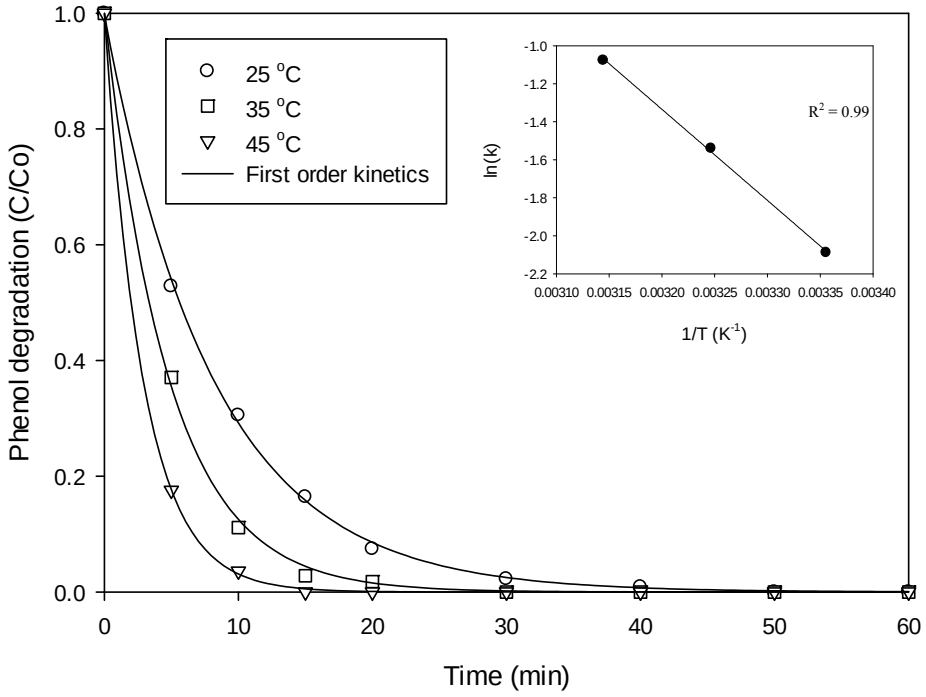

Figure 6.8. Effect of temperature on phenol removal. Reaction conditions: [phenol] = 25 ppm, catalyst = 0.4 g/L, and oxone = 2 g/L.

More importantly, **Figure 6.9** presents the performance of α-Mn_2O_3@α-MnO_2 core/shell composite in phenol degradation after the catalyst recycling with filtration and water washing for reuse. In the second and third runs, phenol degradation profile is much similar to the first test. This suggests that α-Mn_2O_3@α-MnO_2 core/shell catalyst has high stability in heterogeneous catalytic oxidation and is a promising material for other applications.

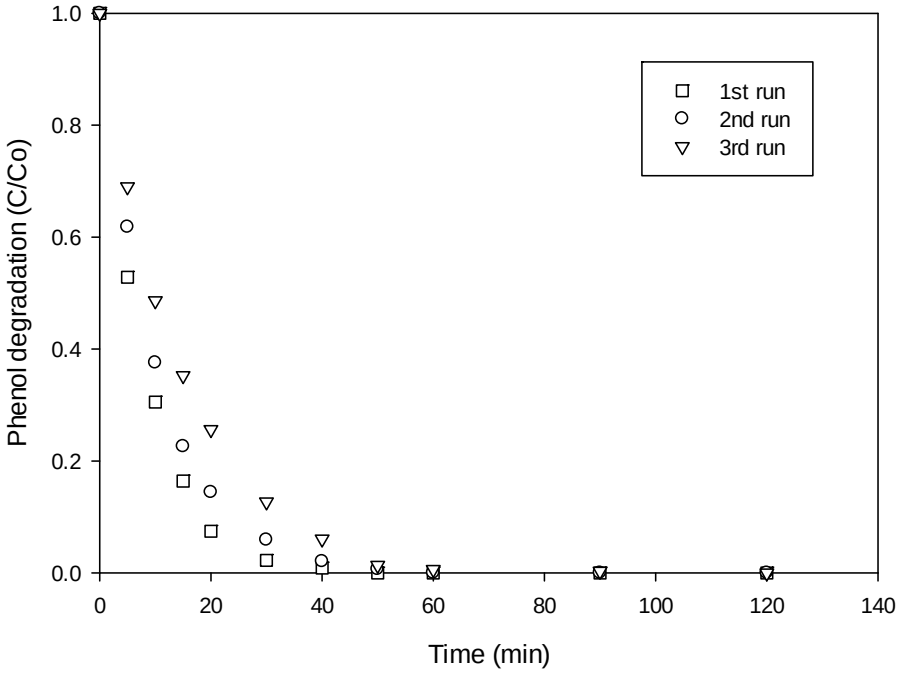

Figure 6.9. Degradation of phenol in multiple use of α-Mn_2O_3@α-MnO_2 composite catalyst. Reaction condition: [phenol] = 25 ppm, catalyst = 0.4 g/L, and oxone = 2 g/L.

6.4. Conclusions

A α-Mn_2O_3@α-MnO_2 core/shell composite was successfully synthesized by a shape-controlled method. The particle shows as uniformed ellipsoid and it exhibits high and stable activity in heterogeneous activation of oxone® for oxidation of phenol in water. The kinetic studies showed that phenol degradation followed first order reaction and activation energy of α-Mn_2O_3@α-MnO_2 core/shell was obtained to be 39.9 kJ/mol. This value is much great than that of the effective α-MnO_2 [27] and α-Mn_2O_3 [28] catalysts.

References

1. Bautista, P., et al., *An overview of the application of Fenton oxidation to industrial wastewaters treatment.* Journal of Chemical Technology and Biotechnology, 2008. **83**(10): p. 1323-1338.

2. Wang, S., *A comparative study of Fenton and Fenton-like reaction kinetics in decolourisation of wastewater.* Dyes and Pigments, 2008. **76**(3): p. 714-720.

3. Pignatello, J.J., E. Oliveros, and A. MacKay, *Advanced Oxidation Processes for Organic Contaminant Destruction Based on the Fenton Reaction and Related Chemistry.* Critical Reviews in Environmental Science and Technology, 2006. **36**(1): p. 1-84.

4. Yang, X., et al., *Hydrolytic dehydrogenation of ammonia borane catalyzed by carbon supported Co core–Pt shell nanoparticles.* Journal of Power Sources, 2011. **196**(5): p. 2785-2789.

5. Zhang, M., et al., *Synthetic core-shell Ni@Pd nanoparticles supported on graphene and used as an advanced nanoelectrocatalyst for methanol oxidation.* New Journal of Chemistry, 2012. **36**(12): p. 2533-2540.

6. Li, P., et al., *Core-shell structured mesoporous silica as acid-base bifunctional catalyst with designated diffusion path for cascade reaction sequences.* Chemical Communications, 2012. **48**(85): p. 10541-10543.

7. Yao, Y., et al., *Fabrication of Fe_3O_4/SiO_2 core/shell nanoparticles attached to graphene oxide and its use as an adsorbent.* Journal of Colloid and Interface Science, 2012. **379**(1): p. 20-26.

8. Park, M., et al., *Functionalized $Ni@SiO_2$ core/shell magnetic nanoparticles as a chemosensor and adsorbent for Cu^{2+} ion in drinking water and human blood.* Analyst, 2010. **135**(11): p. 2802-2805.

9. Emadi, M., E. Shams, and M.K. Amini, *Removal of Zinc from Aqueous Solutions by Magnetite Silica Core-Shell Nanoparticles.* Journal of Chemistry, 2013. **2013**: p. 10.

10. Zhang, H.-J., et al., *ZnO@silica core-shell nanoparticles with remarkable luminescence and stability in cell imaging.* Journal of Materials Chemistry, 2012. **22**(26): p. 13159-13165.

11. Ansari, A.A., et al., *Luminescent mesoporous $LaVO_4:Eu^{3+}$ core-shell nanoparticles: synthesis, characterization, biocompatibility and their cytotoxicity.* Journal of Materials Chemistry, 2011. **21**(48): p. 19310-19316.

12. Luo, Y., et al., *Seed-assisted synthesis of highly ordered $TiO_2@\alpha$-Fe_2O_3 core/shell arrays on carbon textiles for lithium-ion battery applications.* Energy & Environmental Science, 2012. **5**(4): p. 6559-6566.

13. Zhang, H.P., et al., *Core-shell structured electrode materials for lithium ion batteries.* Journal of Solid State Electrochemistry, 2009. **13**(10): p. 1521-1527.

14. Lee, H. and J. Cho, *$Sn_{78}Ge_{22}$@Carbon Core−Shell Nanowires as Fast and High-Capacity Lithium Storage Media.* Nano Letters, 2007. **7**(9): p. 2638-2641.

15. Liu, F., et al., *Synthesis of stable carboxy-terminated $NaYF_4$: Yb^{3+}, Er^{3+}@SiO2 nanoparticles with ultrathin shell for biolabeling applications.* Nanoscale, 2013.

16. Aldeek, F., et al., *Enhanced Photostability from CdSe(S)/ZnO Core/Shell Quantum Dots and Their Use in Biolabeling.* European Journal of Inorganic Chemistry, 2011. **2011**(6): p. 794-801.

17. Wang, Y., et al., *Core-shell TiN@$SrTiO_3$ structure for grain boundary barrier layer capacitor.* Materials Letters, 2012. **74**(0): p. 191-193.

18. Wen, H., et al., *Modeling of the core-shell microstructure of temperature-stable $BaTiO_3$ based dielectrics for multilayer ceramic capacitors.* Journal of Electroceramics, 2008. **21**(1-4): p. 545-548.

19. Lee, K.S., et al., *Seed Size-Dependent Formation of Fe_3O_4/MnO Hybrid Nanocrystals: Selective, Magnetically Recyclable Catalyst Systems.* Chemistry of Materials, 2012. **24**(4): p. 682-687.

20. Cao, J., et al., *Fabrication of γ-MnO_2/α-MnO_2 hollow core/shell structures and their application to water treatment.* Journal of Materials Chemistry, 2011. **21**(40): p. 16210-16215.

21. Liu, J., et al., *Co_3O_4 Nanowire@MnO_2 Ultrathin Nanosheet Core/Shell Arrays: A New Class of High-Performance Pseudocapacitive Materials.* Advanced Materials, 2011. **23**(18): p. 2076-2081.

22. Zhao, Z., et al., *One pot synthesis of tunable Fe_3O_4-MnO_2 core-shell nanoplates and their applications for water purification.* Journal of Materials Chemistry, 2012. **22**(18): p. 9052-9057.

23. Xing, S., et al., *Characterization and reactivity of Fe_3O_4/$FeMnO_x$ core/shell nanoparticles for methylene blue discoloration with H_2O_2.* Applied Catalysis B: Environmental, 2011. **107**(3–4): p. 386-392.

24. Xing, S., et al., *Fabrication of magnetic core-shell nanocomposites with superior performance for water treatment.* Journal of Materials Chemistry A, 2013. **1**(5): p. 1694-1700.

25. Park, J.-H., et al., *Formation of manganese oxide shells on silica spheres with various crystal structures using surfactants for the degradation of methylene blue dye.* Materials Research Bulletin, 2013. **48**(2): p. 469-475.

26. Anipsitakis, G.P. and D.D. Dionysiou, *Degradation of Organic Contaminants in Water with Sulfate Radicals Generated by the Conjunction of Peroxymonosulfate with Cobalt.* Environmental Science & Technology, 2003. **37**(20): p. 4790-4797.

27. Saputra, E., et al., *α-MnO_2 activation of peroxymonosulfate for catalytic phenol degradation in aqueous solutions.* Catalysis Communications, 2012. **26**(0): p. 144-148.

28. Saputra, E., et al., *Manganese oxides at different oxidation states for heterogeneous activation of peroxymonosulfate for phenol degradation in aqueous solutions.* Applied Catalysis B: Environmental, 2013. **142–143**(0): p. 729-735.

29. Lei, S., et al., *Preparation of α-Mn_2O_3 and MnO from thermal decomposition of $MnCO_3$ and control of morphology.* Materials Letters, 2006. **60**(1): p. 53-56.

30. Hu, L., et al., *Heterogeneous activation of oxone with CoMg/SBA-15 for the degradation of dye Rhodamine B in aqueous solution.* Applied Catalysis B: Environmental, 2013. **134–135**(0): p. 7-18.

31. Su, S., et al., *Heterogeneous activation of Oxone by $Co_xFe_{3-x}O_4$ nanocatalysts for degradation of rhodamine B.* Journal of Hazardous Materials, 2013. **244–245**(0): p. 736-742.

32. Shukla, P., et al., *Co-SBA-15 for heterogeneous oxidation of phenol with sulfate radical for wastewater treatment.* Catalysis Today, 2011. **175**(1): p. 380-385.

Chapter 7

Carbon Supported Manganese Catalysts For Phenol Degradation in Water

Abstract

Manganese oxide supported on activated carbons (2.5% Mn/AC-P and 2.5% Mn/AC-N) and graphene oxide (2.5% Mn/GO) were prepared and tested to degrade aqueous phenol in the presence of peroxymonosulphate. The physico-chemical properties of manganese oxide based catalysts were characterized by several techniques such as N_2 adsorption, X-ray diffraction (XRD), scanning electron microscopy (SEM), and energy dispersive X-ray spectroscopy (EDS). It was found that 2.5% Mn/AC-P was highly effective in heterogeneous activation of peroxymonosulphate to produce sulphate radicals in higher rate compared with other catalysts. Degradation efficiency of phenol could be achieved at 100% of phenol decomposition and 90% of total organic carbon (TOC) removal in 90 min at the condition of 75 ppm phenol, 0.2 g catalyst, and 1 g peroxymonosulphate in 500 mL solution at 25^{o}C. Phenol degradation followed first-order kinetics and activation energy on 2.5% Mn/AC-P is 15.0 kJ/mol.

7.1 Introduction

Since the beginning of the 21st century, wastewater treatment is becoming a more and more important issue in social and politic areas and the research in water purification is rapidly growing. The effluents from industry or domestics have to be treated in a proper way to achieve a certain minimum level to comply with environmental regulations. There are many types of organics in wastewater; however, one of the most important class of water pollutants is phenol and its derivatives due to their strong toxicity to many living organisms even at low concentrations [1]. These pollutants have been considered on the EPAs priority list since 1976 [2]. In many countries, the maximum threshold allowed for phenol in water streams is less than 1 mg/L; for instance 0.01 mg/L for Indonesian wastewater [3, 4]. Therefore, due to the strict regulations, complete degradation of organic pollutants in wastewater is one of the focuses in water treatment.

In the last decades, advanced oxidation processes (AOPs) have emerged as effective processes to completely degrade organic compounds in aqueous media. AOPs are based on generation and utilization of reactive species, such as hydroxyl radicals (OH•) in Fenton reaction with a high standard oxidation potential and reacting non-selectively [5, 6]. However, Fenton oxidation suffers from the requirements of acidic pH, large quantity of chemical reagents, very slow catalysis of the ferrous ion generation and large production of ferric hydroxide sludge [7].

Currently, sulphate radicals ($SO_4^{-\bullet}$) produced by peroxymonosulfate have been proposed as an alternative to hydroxyl radicals for organic degradation due to the higher oxidizing potential (1.82 V) than that of H_2O_2 (1.76 V). In most previous investigations in water treatment, Co ions and peroxymonosulphate (PMS, HSO_5^-) has been found to be an effective route [8-10]. However, Co^{2+} is highly toxic and will cause secondary pollution. Thereby, alternative ion metals, such as Mn^{2+}, have been proposed. Anipsitakis and Dionysiou [11] investigated some transition metal ions and three oxidants. They found that Mn^{2+} ions can activate peroxymonosulfate to generate sulphate radicals. However, no further investigation has been reported for manganese oxide for the activation of peroxymonosulfate to generate sulphate radicals. In this

research, we investigate the supported manganese catalysts for heterogeneous activation of sulphate radicals for chemical mineralizing of phenol in the solution. These catalysts will be an alternative technique for advanced oxidation process. Several key parameters in the kinetic study such as phenol concentration, catalyst loading, PMS concentration and temperature were investigated.

7.2 Experimental section

7.2.1 Carbon support materials

Two commercial activated carbons in powder were purchased from Pancasari Puspa Company, Indonesia (AC-P) and Sigma-Aldrich, Australia (AC-N), respectively. AC-P and AC-N were used as received. Another carbon support, graphite oxide (GO) was prepared using a modification of Hummers and Offeman's method from graphite powders (Bay carbon, SP-1), and a detailed procedure can be found in the literature [12]. In a typical reaction, 0.5 g of graphite, 0.5 g of $NaNO_3$, and 23 mL of H_2SO_4 were stirred together in an ice bath. Further, 3 g of $KMnO_4$ was slowly added. All chemicals were purchased from Sigma-Aldrich and were used as received. Once mixed, the solution is transferred to a 35 ± 5C water bath and stirred for about 1 h, forming a thick paste. Moreover, 40 mL of water was added, and the solution was stirred for 30 min while the temperature was raised to 90 ± 5 ^{o}C. Finally, 100 mL of water was added, followed by the slow addition of 3 mL of H_2O_2 (30%), turning the colour of the solution from dark brown to yellow. The warm solution was then filtered and washed with 100 mL of water, and the solids were collected by filtration and dried at 50 ^{o}C.

7.2.2 Synthesis of manganese based catalysts

Catalyst synthesis was carried out following a general impregnation method. For manganese (MnO_x)/AC-P, a fix amount of manganese nitrate (Sigma-Aldrich) was added into 100 mL ultrapure water. AC-P was then added into the solution and kept stirring at 60 ^{o}C until total evaporation of H_2O. After that the solids were dried at 120 ^{o}C overnight and calcined at 450 ^{o}C for 3 h in nitrogen. For other two supports (AC-N

and GO), the same method was also implemented. The loading of Mn on the three supports was maintained at 2.5 wt%.

7.2.3 Characterisation of catalysts

The synthesised catalysts were characterised by X-ray diffraction (XRD), scanning electron microscopy (SEM) with energy dispersive X-ray spectroscopy (EDS), and N_2 adsorption. XRD pattern was obtained on a Siemen, D501 diffractometer using filtered Cu Kα radiation with accelerating voltage of 40 kV and current of 30 mA. The samples was scanned at 2θ from 10-80^o. N_2 adsorption-desorption was measured on a TriStar II 3020 (Micromeritics) to obtain specific surface area using the Brunauer-Emmett-Teller (BET) method. Prior to measurement the samples were degased at 120 ^{o}C for 12 h under vacuum condition. The external morphology and chemical compositions of the samples were observed on a ZEISS NEON 40EsB scanning electron microscope (SEM) equipped with an energy dispersive spectrometer (SEM-EDS).

7.2.4 Catalytic activity test

Phenol degradation tests were carried out at 30 °C in 1 L glass vessel with 500 mL of phenol solution at 25-100 ppm with a constant stirring of 400 rpm. Firstly, a catalyst at varying amounts (0.05-0.20 g) was added into the phenol solution for a while, then oxone ($2KHSO_5•KHSO_4•K_2SO_4$, PMS) was added into the solution at 0.04-2.0 g/L. At certain time, water sample (1 mL) was withdrawn into a HPLC vial, 0.5 mL of pure methanol was then injected into the vial to quench the reaction. The concentration of phenol was analyzed using a Varian HPLC with a UV detector set at λ = 270 nm. A C–18 column was used to separate the organics while the mobile phase with a flow rate of 1.5 mL/min was made of 30% CH_3CN and 70% water. For the recycle tests of the catalyst, after each run, the catalyst was obtained by filtration and thoroughly washed with distilled water several times, then dried at 80 °C for 2 h.

7.3 Result and discussion

7.3.1 Characterization of supported Mn catalysts

Figure 7.1 shows XRD spectra of supported Mn catalysts prepared from three different carbon supports. In general, a large broad peak at 2θ=20-30° was observed, indicating an amorphous structure of the supports. For 2.5% Mn/AC-N catalyst, the peaks of manganese oxide were observed. The profile showed the presence of MnO_2 crystallites with the major peaks at 20.84, 26.61, 50.14, 68.06, and 77.09°.Minor Mn_3O_4 was also found at 32.38, 36.10, and 59.91°. For 2.5% Mn/AC-P catalyst, the presence of Mn_3O_4 crystallite was found with the peaks at 28.92 °, and 36.10 °. However, manganese species in crystalline form were not identified on 2.5% Mn/GO catalyst, possibly due to high dispersion.

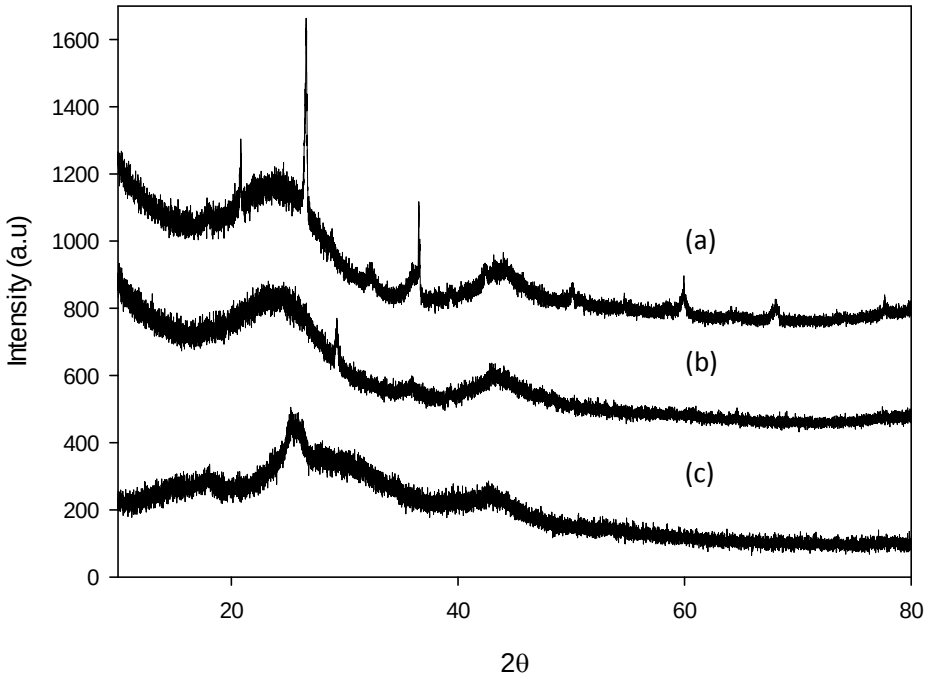

Figure 7.1. XRD pattern of supported manganese catalysts. (a) 2.5% Mn/AC-N, (b) 2.5% Mn/AC-P, and (c) 2.5% Mn/GO

Figure 7.2 shows N_2 adsorption/desorption isotherms and pore size distribution of Mn/AC-P, Mn/AC-N and Mn/GO catalysts. As seen in **Table 7.1**, Mn/AC-P has a higher surface area (870.2 m^2/g) than others. In addition, Mn/AC-P also has the a lowest pore radius (22.0 Å). The pore size distribution of Mn/AC-P presented three peaks, centred at 24.5, 30, and 35 Å, respectively while Mn/GO presented two peaks, centred at 20.5 and 30 Å, respectively. However, Mn/AC-N showed a different profile with one peak, which is centred at 30 Å.

Table 7.1. Surface area, pore volume and pore radius of catalysts

Catalyst	S_{BET}, $m^2.g^{-1}$	Pore volume ($cm^3.g^{-1}$)	Average pore radius (Å)
2.5% Mn/AC-P	870.2	0.478	22.0
2.5% Mn/AC-N	495.6	0.331	26.7
2.5% Mn/GO	154.4	0.612	158.6

7.3.2 Preliminary study of phenol oxidation using catalysts

Figure 7.3 shows the preliminary tests of adsorption and catalytic oxidation of phenol using 2.5% Mn/AC-P, 2.5% Mn/AC-N and 2.5% Mn/GO catalysts in aqueous solution under various experimental conditions. As can be seen, AC-P presented low adsorption of phenol at 53% in 90 min prior to reaching equilibrium while 2.5% Mn/AC-P has the highest efficiency in phenol adsorption with 67.5 % removal in 90 min, which can be ascribed to manganese oxides on the support. Zhang et al. [13] investigated Mn_3O_4 with nano size for adsorption of pentachlorophenol from aqueous solution and found that Mn_3O_4 has a good ability to adsorb pentachlorophenol. The complete pentachlorophenol removal could be achieved at pentachlorophenol concentration of 20 mg/L in 50 min. Therefore, 2.5% Mn/AC-P catalyst has the highest phenol adsorption efficiency than AC-P catalyst. In the presence of only oxone® in phenol solution, no phenol degradation occurred, suggesting that oxone® itself could not produce sulphate radicals to induce phenol oxidation. In oxidation test, AC-P, AC-N and GO supported Mn catalysts could produce significant phenol degradation. 2.5% Mn/AC-P in the presence of oxone® could degrade phenol at 100% in 30 min while in the same duration, 2.5% Mn/AC-N and 2.5% Mn/GO could reach around 97% and 28% phenol removal, respectively.

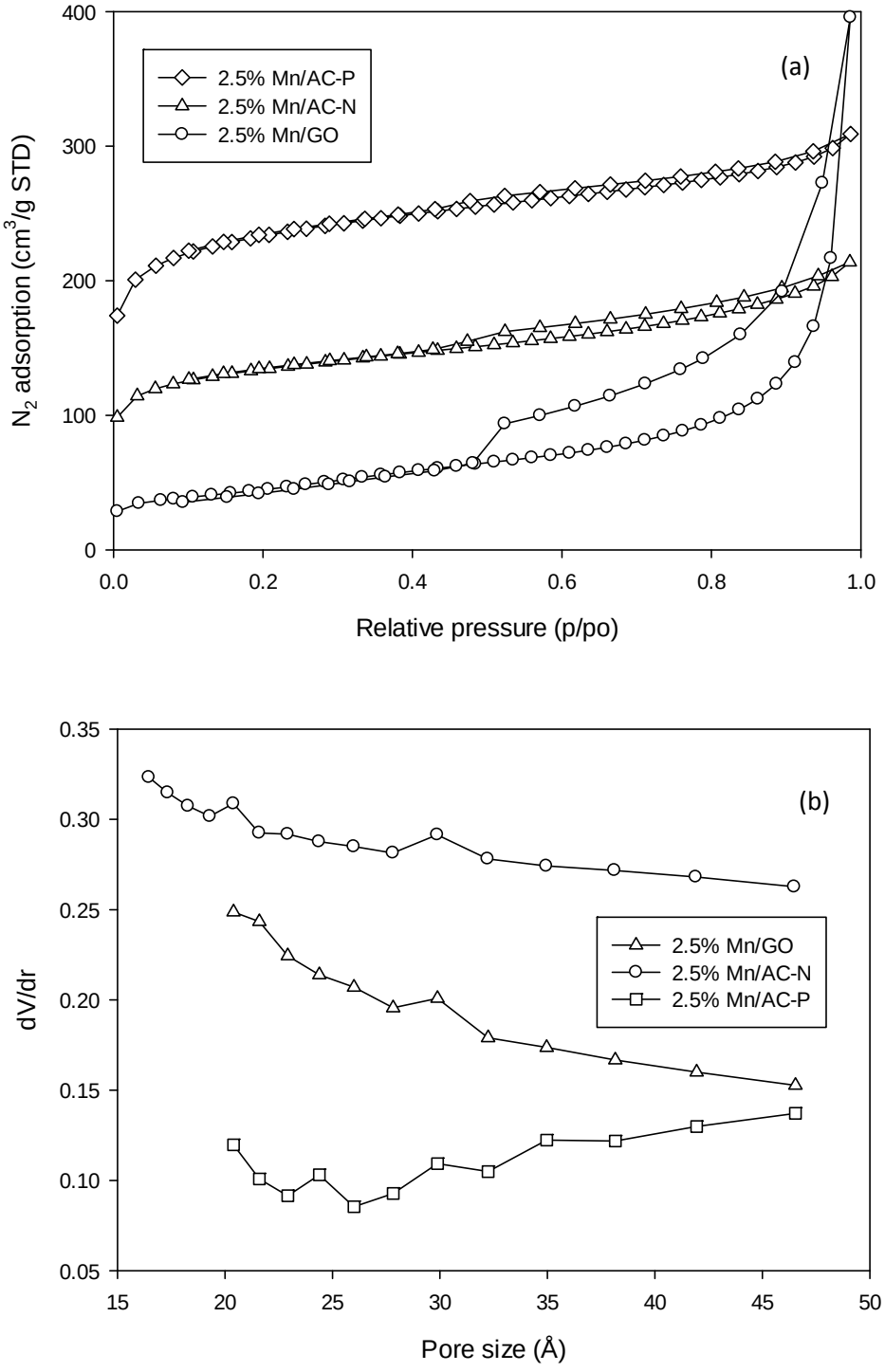

Figure 7.2. N_2 adsorption isotherms and pore size distribution of Mn/AC-P, Mn/AC-N and Mn/GO catalysts. (a) N_2 Isotherms and (b) pore size distributions.

In addition, AC-P with oxone® could degrade phenol at 91% in 30 min. Saputra et al. [14] studied the powder active carbon for heterogeneous activation of oxone® to generate sulphate radical ($SO_5^{-\bullet}$, and $SO_4^{-\bullet}$) targeting the decomposition of phenol. They found that the powder activated carbon could activate oxone®, which previously could only be achieved by metal ions, heat and light toxicity [15-17]. However, Mn/AC-P catalyst presented higher phenol degradation than AC-P, suggesting a synergistic effect of AC-P support and Mn oxides.

In addition, TOC removal in 2.5% Mn/AC-P- oxone® system also examined and the result showed that about 90% of TOC were obtained within 30 min. Significant degradation of phenol in the systems confirms that manganese oxide and activated carbon could activate oxone® to generate sulphate radicals for phenol decomposition in solution. The activation reaction could be expressed as below.

$$AC + HSO_5^- \longrightarrow AC^+ + SO_4^{-\bullet} + OH^- \quad (7.1)$$

$$AC^+ + HSO_5^- \longrightarrow AC + SO_5^{-\bullet} + H^+ \quad (7.2)$$

$$S - Mn(III) + HSO_5{}^- \longrightarrow S - Mn(IV) + SO_5{}^{\bullet -} + H^+ \ (S - support) \quad (7.3)$$

$$S - Mn(IV) + HSO_5{}^- \longrightarrow S - Mn(III) + SO_4{}^{\bullet -} + OH^- \ (S - support) \quad (7.4)$$

Previously, several heterogeneous cobalt systems have been tested in activation of oxone® for oxidation of organic toxics in water. Saputra et al. [17] used Co/Red mud and Co/Fly ash with oxone® for phenol degradation at 30 ppm. The both catalysts could achieve 100% and 40% degradation of phenol in 90 min, respectively. Shukla et al. used Co_3O_4/SiO_2 [18] and Co/SBA-15 [19] for heterogeneous activation of oxone® to generate sulphate radicals targeting the decomposition phenol. Co_3O_4/SiO_2 could achieve 100% phenol degradation at 30 ppm in 190 min while Co/SBA-15 could achieve complete degradation of phenol in 190 min. Anipsitakis and Dionysiou [11] studied homogeneous activation of oxone® with Mn^{2+} for 2,4-DCP oxidation. They found that Mn^{2+} could achieve 24% degradation of phenol at 2,4-DCP concentration of 50 ppm in 240 min of reaction time. Therefore, 2.5% Mn/AC-P presented higher activity in phenol degradation than some heterogeneous Co systems and Mn^{2+}.

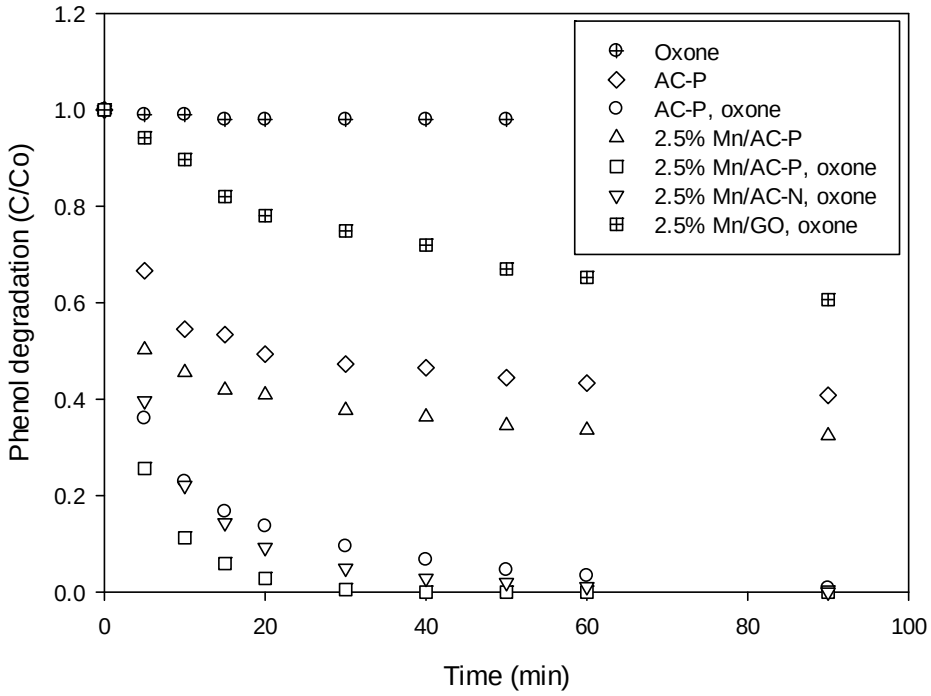

Figure 7.3. Phenol reduction with time in adsorption and catalytic oxidation. Reaction conditions: [Phenol] = 75 ppm, catalyst = 0.4 g/L, oxone = 2 g/L, and T = 25 ^{o}C.

7.3.3 Effects of reaction parameters on phenol degradation

The first parameter measured in this study was phenol concentration which was maintained between 50 to 100 ppm. The effect of initial phenol concentration on phenol degradation is shown in **Figure 7.4**. Removal efficiency of phenol decreased with increasing phenol concentration. Phenol removal at 100% could be achieved at phenol concentration of 50 ppm within 10 min. Meanwhile, at phenol concentration of 75 and 100 ppm, completed phenol removal could be achieved in 30 and 90 min, respectively. In phenol degradation, production of sulphate is the key reaction, which depends on 2.5% Mn/AC-P catalyst and oxone®. Under the same concentration of catalyst and oxone®, high concentration of phenol will require more time to achieve the same removal rate, resulting in lower phenol removal efficiency.

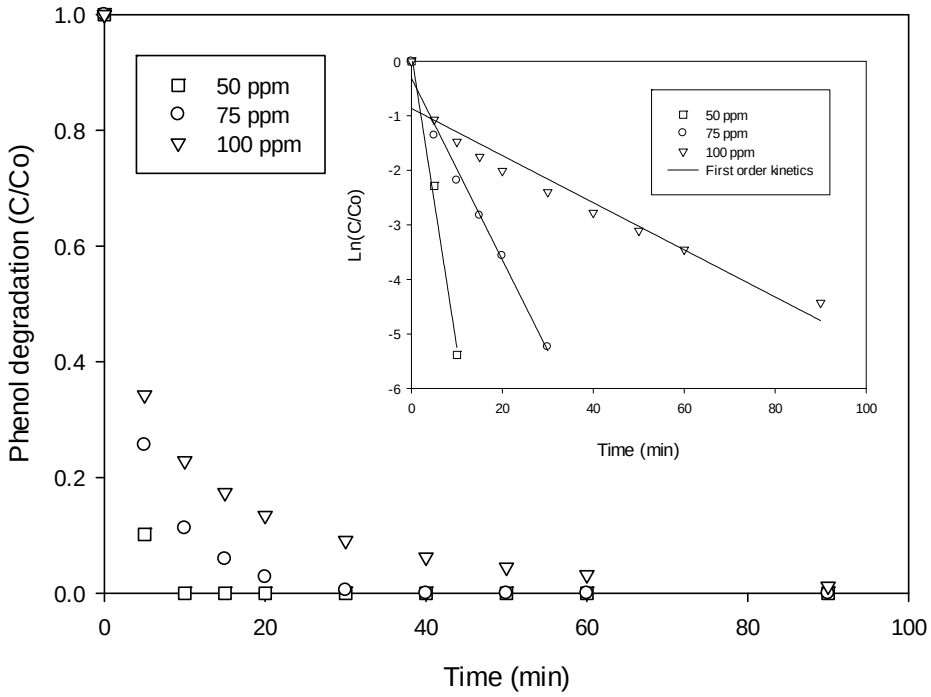

Figure 7.4. Effect of phenol concentration on phenol removal. Reaction conditions: catalyst = 0.4 g/L, oxone = 2 g/L, and T = 25 ^{o}C.

In order to estimate the kinetic rate constants, a general pseudo first order kinetics for phenol degradation was employed, as shown in the equation below.

$$\ln\left(\frac{C}{Co}\right) = -k \bullet t \qquad (7.5)$$

Where k is the apparent first order rate constant of phenol removal, C is the concentration of phenol at various time (t). C_o is the initial phenol concentration. Using this model showed that ln(C/Co) versus time produced a straight line for three different concentrations as shown inset of **Figure. 7.4**. Based on regression coefficient, it is clear that phenol degradation followed the first order kinetics. The rate constants at varying phenol concentrations are shown in **Table 7.2**. As seen, rate constant will decrease as the concentration of phenol increases.

Table 7.2. Rate constant at different feed concentration of phenol

Initial phenol concentration	Rate constant min^{-1}	R^2
50 ppm	0.4570	0.99
75 ppm	0.2065	0.99
100 ppm	0.0603	0.96

Figure 7.5 shows the effect of catalyst loading on phenol degradation. An increase in amount of catalyst in solution would result in higher phenol degradation efficiency. This occurs because increased amount of catalyst will increase the adsorption as well as the availability of catalyst active sites for generation of active sulphate radical ($SO_4^{-\bullet}$ and $SO_5^{-\bullet}$), resulting in high phenol degradation. At 0.1 g/L 2.5% Mn/AC-P, phenol removal would be 28% at 90 min, while in same duration at 0.2, and 0.3 g/L, removal efficiency were 68, and 98%, respectively. The complete phenol degradation could be achieved at 0.4 g/L loading of 2.5% Mn/AC-P in 30 min.

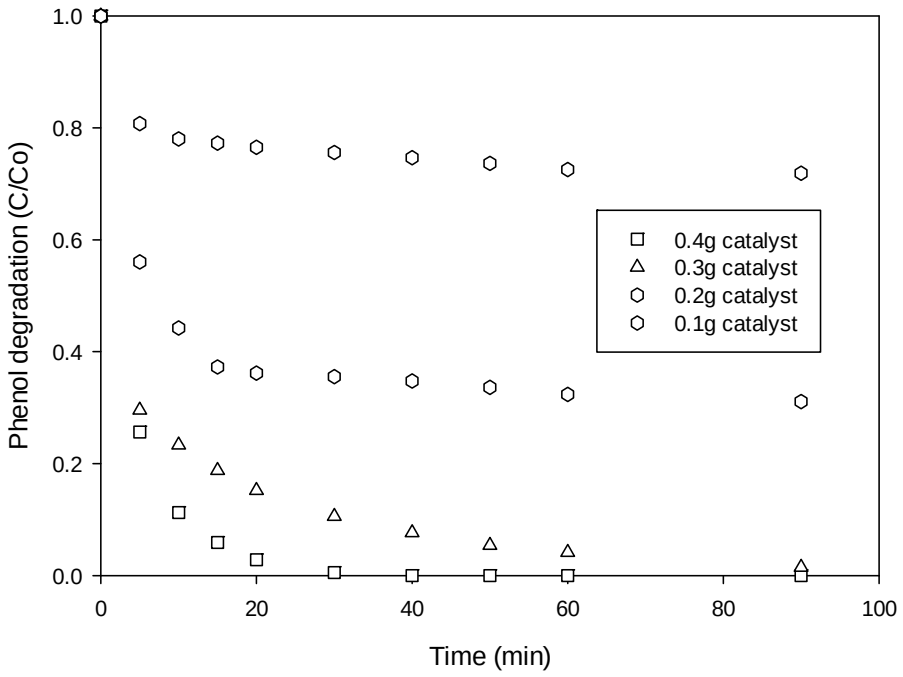

Figure 7.5. Effect of catalyst loading on phenol removal. Reaction conditions: [phenol] = 75 ppm, oxone = 2 g/L, and T = 25 ^oC.

Figure 7.6 presents phenol degradation efficiency at varying initial concentrations of oxone® in solution. As can be seen, degradation of phenol depended on initial concentration of oxone®. Higher concentration of oxone® in solution resulted in higher phenol degradation rate. However, the influence was not as significant as the case of catalyst loading. The change in oxone® loading from 0.2 to 2 g/L would only result in 20% increase in phenol degradation efficiency.

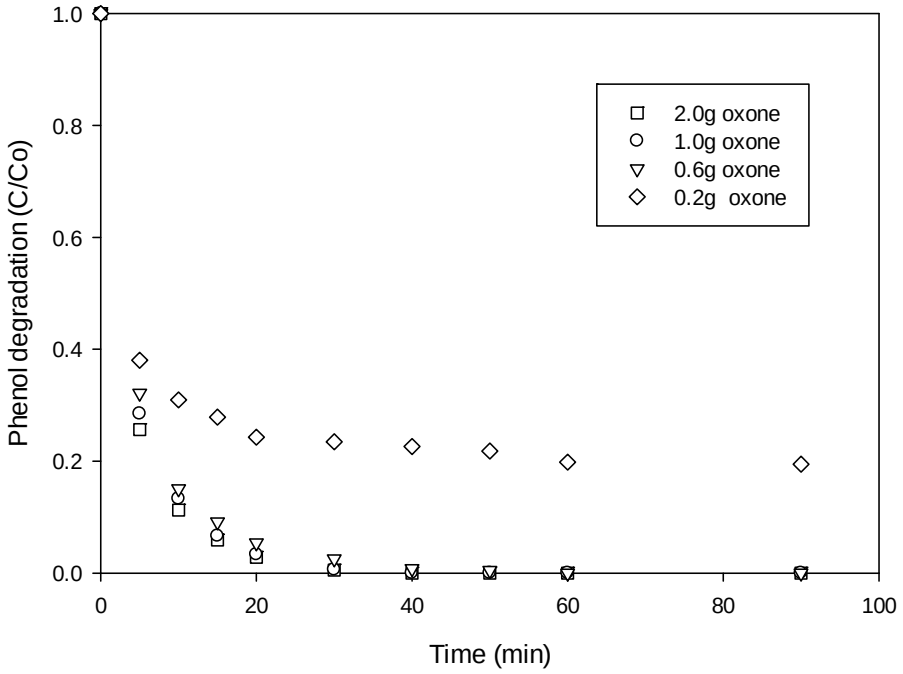

Figure 7.6. Effect of oxone concentration on phenol removal. Reaction conditions: [phenol] = 75 ppm, catalyst = 0.4 g/L, and T = 25 ^{o}C.

Figure 7.7 shows the effect of manganese loading on AC-P on phenol degradation. As can be seen, manganese loading on AC-P showed a quite significant impact on phenol degradation. The increase in manganese loading from 1.5 to 2.5 wt% would increase degradation of phenol. However, a further increase of manganese loading on AC-P up to 10% would not enhance the rate of reaction, suggesting the optimal manganese loading on AC-P at 2.5%. Higher amount of manganese loading provides additional sites for generation of active sulphate radicals, thus enhancing the rate of reaction.

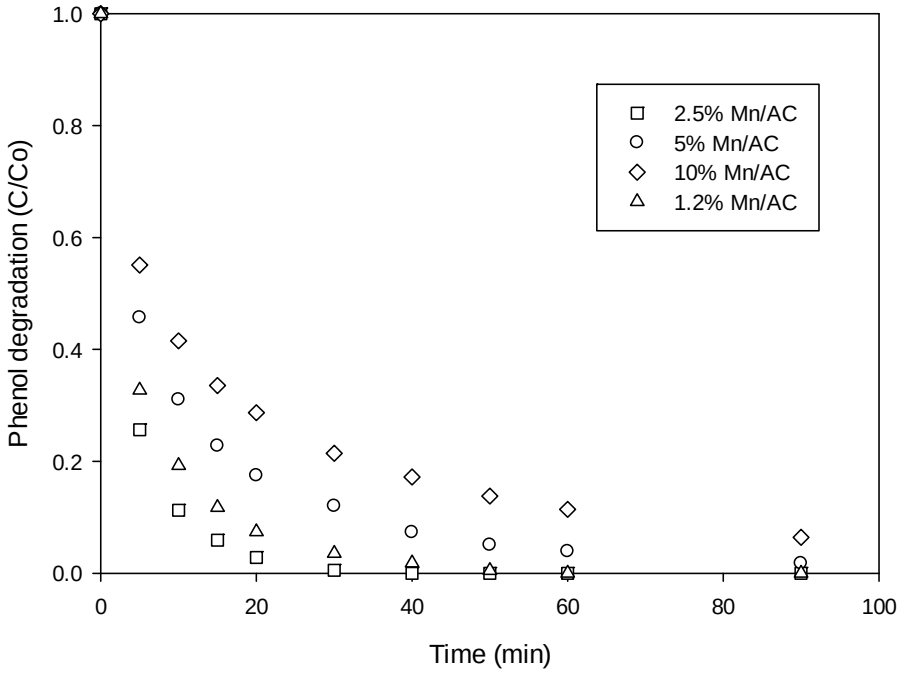

Figure 7.7. Effect of metal loading on catalyst on phenol removal. Reaction conditions: [phenol] = 75 ppm, oxone = 2 g/L, and T = 25 ^{o}C.

Figure 7.8 shows that phenol degradation also depended on reaction temperature. The rate of reaction would increase with increased temperature. Complete phenol degradation at 25 ^{o}C would be achieved in 30 min. Further increase of 10 ^{o}C, 100% degradation efficiency of phenol was achieved within 20 min while at 45 ^{o}C, phenol degradation would be achieved at 100% in 15 min. **Figure 7.8** (inset) shows the Arrhenius plots of rate constants with temperature. As shown, the plot presented a good linear correlation and the activation energy of 2.5% Mn/AC-P was derived as 15.0 kJ/mol. In the past few years, several heterogeneous carbon supported Co and Ru catalysts synthesised by impregnation method have been reported for oxone® activation and the activation energies obtained are presented in **Table 7.3**. As can be seen, that 2.5% Mn/AC-P presented lower activation energy than oxide supported Co and Ru catalysts.

Table 7.3. Activation energies of various catalysts with oxone® for degradation of phenol.

Catalyst	Activation energy (kJ/mol)	Reference
Co/AC	59.7	[20]
Co/CX-1	48.3	[21]
Co/CX-G	62.9	[21]
RuO_2/AC	61.4	[22]
2.5% Mn/AC-P	15.0	This work

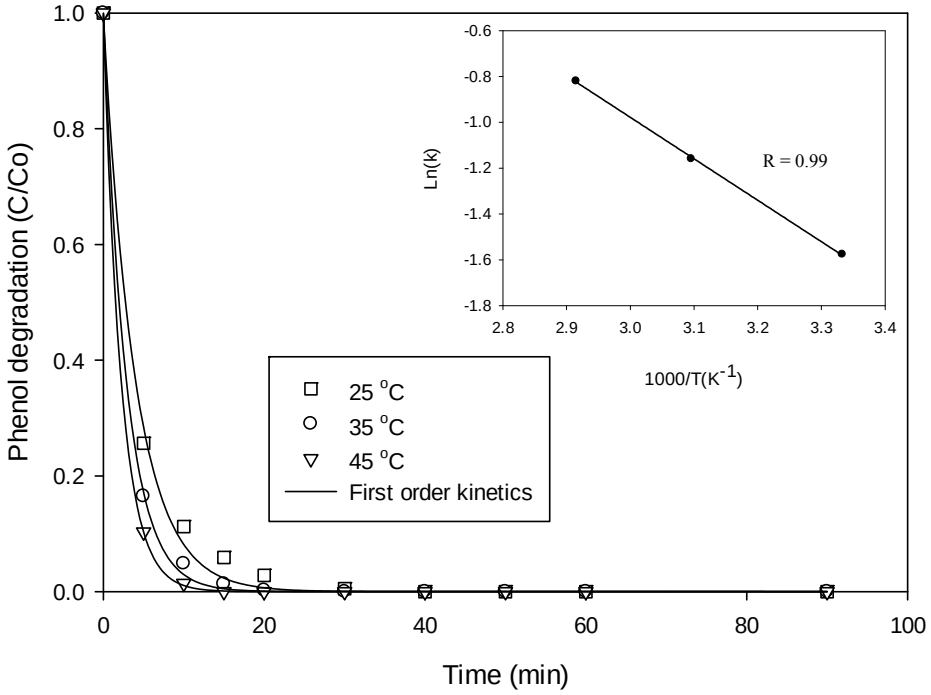

Figure 7.8. Effect of temperature on phenol removal. Reaction conditions: [phenol] = 75 ppm, catalyst = 0.4 g/L, and oxone = 2 g/L.

7.3.4 Reactivity of spent 2.5% Mn/AC-P catalyst and reusability

Figure 7.9 shows the catalytic activity of recycled 2.5% Mn/AC-P for phenol degradation. As can be seen, the catalytic activity significant reduced in the second use, suggesting a deactivation of the catalyst. In the second use, phenol degradation was 38% at 90 min compared with 100% in the first use. Furthermore, for 2.5% Mn/AC-P second use after heat treatment at 500 ^{o}C for 1 hour, it appears that the catalyst activity increased again and 80% degradation of phenol could be achieved at 90 min. This suggests that the carbon deposits on the catalyst during the reaction process can be removed by heat treatment.

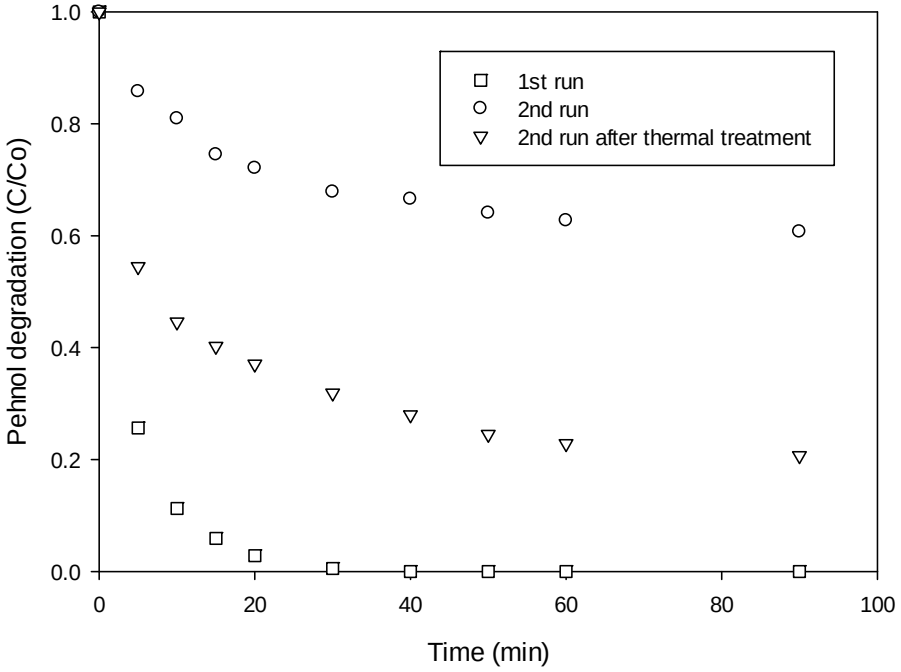

Figure 7.9. Degradation of phenol in multiple use of Mn/AC catalyst. Reaction conditions: [phenol] = 75 ppm, catalyst = 0.4 g/L, and oxone = 2 g/L.

7.4 Conclusions

Several types of carbon supported manganese catalysts, 2.5% Mn/AC-P, 2.5% Mn/AC-N and 2.5% Mn/GO, were tested for catalytic oxidation of phenolic contaminants 2. Among them, 2.5% Mn/AC-P is an effective catalyst for generating

sulphate radicals in the presence of PMS to degrade phenol. Several factors influenced the removal efficiency of phenol such as PMS concentration, Mn loading in catalyst, phenol concentration, catalyst loading and temperature. Kinetic studies showed that phenol degradation followed first order reaction and activation energy of 2.5% Mn/AC-P was obtained to be 15.0 kJ/mol.

References

1. Dohnal, V. and D. Fenclova, *Air-Water Partitioning and Aqueous Solubility of Phenols.* Journal of Chemical & Engineering Data, 1995. **40**(2): p. 478-483.

2. Keith, L. and W. Telliard, *ES&T Special Report: Priority pollutants: I-a perspective view.* Environmental Science & Technology, 1979. **13**(4): p. 416-423.

3. Matheswaran, M. and I.S. Moon, *Influence parameters in the ozonation of phenol wastewater treatment using bubble column reactor under continuous circulation.* Journal of Industrial and Engineering Chemistry, 2009. **15**(3): p. 287-292.

4. Rachmat Priatna, a.B. Edi Syahbandi, and Sudewo, *Phenol compound in produced water.* Second International Conference on Health, Safety &Environment in Oil &Gas Exploration &Production, 1994: p. 365-371.

5. Huang, C.-P. and Y.-H. Huang, *Application of an active immobilized iron oxide with catalytic H_2O_2 for the mineralization of phenol in a batch photo-fluidized bed reactor.* Applied Catalysis A: General, 2009. **357**(2): p. 135-141.

6. Calleja, G., J.A. Melero, F. Martínez, and R. Molina, *Activity and resistance of iron-containing amorphous, zeolitic and mesostructured materials for wet peroxide oxidation of phenol.* Water Research, 2005. **39**(9): p. 1741-1750.

7. Liang, H., Y.Y. Ting, H. Sun, H.M. Ang, M.O. Tadé, and S. Wang, *Solution combustion synthesis of Co oxide-based catalysts for phenol degradation in aqueous solution.* Journal of Colloid and Interface Science, 2012. **372**(1): p. 58-62.

8. Anipsitakis, G.P. and D.D. Dionysiou, *Transition metal/UV-based advanced oxidation technologies for water decontamination.* Applied Catalysis B: Environmental, 2004. **54**(3): p. 155-163.

9. Shukla, P., I. Fatimah, S. Wang, H.M. Ang, and M.O. Tadé, *Photocatalytic generation of sulphate and hydroxyl radicals using zinc oxide under low-power UV to oxidise phenolic contaminants in wastewater.* Catalysis Today, 2010. **157**(1-4): p. 410-414.

10. Sun, J., M. Song, J. Feng, and Y. Pi, *Highly efficient degradation of ofloxacin by UV/Oxone/Co^{2+} oxidation process.* Environmental Science and Pollution Research, 2012. **19**(5): p. 1536-1543.

11. Anipsitakis, G.P. and D.D. Dionysiou, *Degradation of organic contaminants in water with sulfate radicals generated by the conjunction of peroxymonosulfate with cobalt.* Environmental Science and Technology, 2003. **37**(20): p. 4790-4797.

12. Titelman, G.I., V. Gelman, S. Bron, R.L. Khalfin, Y. Cohen, and H. Bianco-Peled, *Characteristics and microstructure of aqueous colloidal dispersions of graphite oxide.* Carbon, 2005. **43**(3): p. 641-649.

13. Zhang, H., C. Liang, Z. Tian, G. Wang, and W. Cai, *Single phase Mn_3O_4 nanoparticles obtained by pulsed laser ablation in liquid and their application in rapid removal of trace pentachlorophenol.* The Journal of Physical Chemistry C, 2010. **114**(29): p. 12524-12528.

14. Saputra, E., S. Muhammad, Hongqi Sun, Ha-Ming Ang, a. Moses O. Tadé, and S. Wang, *Green catalytic degradation of aqueous contaminants by activated carbon.* 5th International Symphosium on Carbon for Catalysis, CARBOCAT-V, Brixten-Italy, June, 2012.

15. Huang, K.-C., R.A. Couttenye, and G.E. Hoag, *Kinetics of heat-assisted persulfate oxidation of methyl tert-butyl ether (MTBE).* Chemosphere, 2002. **49**(4): p. 413-420.

16. Shukla, P.R., S. Wang, H.M. Ang, and M.O. Tadé, *Photocatalytic oxidation of phenolic compounds using zinc oxide and sulphate radicals under artificial solar light.* Separation and Purification Technology, 2010. **70**(3): p. 338-344.

17. Saputra, E., S. Muhammad, H. Sun, H.M. Ang, M.O. Tadé, and S. Wang, *Red mud and fly ash supported Co catalysts for phenol oxidation.* Catalysis Today, 2012. **190**(1): p. 68-72.

18. Shukla, P., H. Sun, S. Wang, H.M. Ang, and M.O. Tadé, *Nanosized Co_3O_4/SiO_2 for heterogeneous oxidation of phenolic contaminants in waste water.* Separation and Purification Technology, 2011. **77**(2): p. 230-236.

19. Shukla, P., H. Sun, S. Wang, H.M. Ang, and M.O. Tadé, *Co-SBA-15 for heterogeneous oxidation of phenol with sulfate radical for wastewater treatment.* Catalysis Today, 2011. **175**(1): p. 380-385.

20. Shukla, P.R., S. Wang, H. Sun, H.M. Ang, and M. Tadé, *Activated carbon supported cobalt catalysts for advanced oxidation of organic contaminants in aqueous solution.* Applied Catalysis B: Environmental, 2010. **100**(3-4): p. 529-534.

21. Sun, H., H. Tian, Y. Hardjono, C.E. Buckley, and S. Wang, *Preparation of cobalt/carbon-xerogel for heterogeneous oxidation of phenol.* Catalysis Today, 2012. **186**(1): p. 63-68.

22. Muhammad, S., P.R. Shukla, M.O. Tadé, and S. Wang, *Heterogeneous activation of peroxymonosulphate by supported ruthenium catalysts for phenol degradation in water.* Journal of Hazardous Materials, 2012. **215–216**(0): p. 183-190.

Chapter 8

Metal Free Catalytic Degradation of Aqueous Contaminants by Activated Carbon

Abstract

In this study, activated carbon (AC) was used as a catalyst for degradation of a toxic organic compound, phenol, in the presence of different oxidants, H_2O_2, peroxydisulphate (PDS) and peroxymonosulphate (PMS). It was found that AC is effective in heterogeneous activation of PMS to produce sulphate radicals for degradation of phenol. The complete phenol removal could be achieved at 0.4 g AC/L in 15 min. It was also found that phenol degradation is significantly influenced by amount of PMS loading and particle size of AC.

8.1 Introduction

Nowadays, conventional wastewater treatments have been proved to be limited in treating toxic organic compounds. One of the promising methods for degradation of organic pollutants in wastewater is advanced oxidation process (AOP) which can completely degrade organic compounds into carbon dioxide and water. AOPs are based on generation and utilization of reactive species, such as hydroxyl radicals (OH•) that have a high standard oxidation potential and react non-selectively [1, 2]. Among the AOP methods, heterogeneous catalytic oxidation systems have attracted much attention because of economics and easy recovery of catalysts [3]. In the heterogeneous systems, the solid catalysts play an important role in achieving a highly efficient oxidation process, not harmful to the environment. Therefore, many studies have concentrated on developing new and effective catalysts but most of them are metal-based systems [4-6].

Activated carbons (AC) have been widely used in heterogeneous catalysis either as supports or catalysts due to their porous structure, high specific surface area and pore volume, inexpensiveness and environmentally friendliness [7-10]. A number of studies have shown that activated carbons are active in the degradation of some dissolved organic pollutants such as 4-chlorophenol, trichlorophenol, trichloroethane, methyl tert-butyl ether, methylamines and dimethylamines in the presence of H_2O_2 [11-13]. It was shown that AC can promote hydrogen peroxide decomposition through the formation of hydroxyl radicals as shown in the following equations.

$$AC + H_2O_2 \longrightarrow AC^+ + OH^- + OH^\bullet \quad (8.1)$$

$$AC^+ + H_2O_2 \longrightarrow AC + H^+ + HO_2^\bullet \quad (8.2)$$

Reactions (Equation (8.1) and (8.2)) are commonly known as electron-transfer catalysis similar to the Haber-Weiss mechanism, following the Fenton reaction mechanism involving the oxidized (AC^+) and reduced (AC) catalyst states [14]. However, AC exhibits much low activity in such a reaction. Recently, sulphate radicals ($SO_4^{-\bullet}$) have been proposed as an alternative to hydroxyl radicals for organic degradation due to the higher oxidizing potential (1.82 V) than that of H_2O_2 (1.76 V).

Sulphate radicals can be produced from persulphate (PS) or peroxymonosulphate (PMS). Up to now, activation of PS or PMS was only achieved by metal ions, heat and light, which either requires high energy input or produces metal toxicity [15-17]. However, no investigation has been reported using carbonaceous materials for production of sulphate radicals. We recently found that graphene could be a good catalyst for PMS activation. In this paper, we report that AC powder can be a green catalyst in effective activation of PMS, showing an excellent capability of degrading phenol. Several factors influencing the phenol degradation with PMS oxidation were studied at varying phenol concentration, AC and PMS loading and also temperature.

8.2 Experimental section

Two activated carbons were obtained in powder and granule from Pancasari Puspa Company, Indonesia. Powder activated carbon (PAC) was used without further treatment. Granular activated carbon (GAC) was crushed into small particles and seperated according to their sizes into two sections: 60-90 μm (GAC-1) and 90-120 μm (GAC-2). The oxidant peroxymonosulphate ($KHSO_5^-$, PMS) derived from the triple salt Oxone ($2KHSO_5 \cdot KHSO_4 \cdot K_2SO_4$) was supplied by Sigma-Aldrich, Australia. Phenol solution of the required concentrations (i.e. 25, 50, 75 and 100 ppm) were prepared from phenic acid (C_6H_5OH, 99% purity, Sigma-Aldrich) by mixing with ultrapure water. Methanol as a quenching reagent (CH_3OH, 100% purity) for HPLC analysis was purchased from Perth Scientific, Australia. Sodium nitrite for quenching the reaction for the total organic carbon (TOC) analysis was purchased from Sigma-Aldrich. H_2O_2 (30 wt%) and peroxydisulphate (PDS) were also obtained from Sigma-Aldrich.

The AC surface area and pore size measurements were carried out by N_2 adsorption using Autosorb-1, Quantachrome (USA). The AC samples were degassed at 100 ^oC for 24 h prior to adsorption analysis. The surface area and pore size distribution were obtained by the Brunauer-Emmett-Teller (BET).

The catalytic oxidation of phenol was carried out in a 500 mL glass beaker containing 25, 50, 75 and 100 ppm of phenolic solutions, which was attached to a stand and

dipped in a water bath with a temperature controller. The reaction mixture was stirred constantly at 400 rpm to maintain a homogenous solution. A fixed amount of PMS was added into the solution and allowed to dissolve completely before reaction. Further, a fixed amount of catalysts was added into the reactor to start the oxidation reaction of phenol. The reaction was carried on for 90 minutes and at a fixed interval time, 0.5 ml of solution sample was taken out from the mixture using a syringe filter of 0.45 μm and then mixed with 0.5 mL methanol to quench the reaction. A few other tests were carried out with different oxidants, hydrogen peroxide and peroxydisulphate (PDS). Concentration of phenol was analysed using a HPLC with a UV detector set at λ = 270 nm. The column used was C-18 with mobile phase of 30% CH_3CN and 70% water.

8.3 Result and discussion

8.3.1 Characterization of activated carbons catalysts

The BET surface area, pore volume and pore radius for the carbons are shown in **Table 8.1**. It can be observed that there is a significant difference in the surface area and pore volume. PAC has the higher surface area (824.7 m^2g^{-1}), pore volume (0.470 cm^3/g) and pore radius (22.8 Å) than others. For both granule AC particles (GAC-1 and GAC-2), GAC-1 has slightly higher surface area, pore volume and pore radius due to smaller particle size.

Table 8.1. Surface area, pore volume and pore radius

Catalyst	S_{BET} (m^2/g)	V (cm^3/g)	Pore radius (Å)
PAC	824.7	0.470	22.8
AC-1	586.9	0.250	17.0
AC-2	560.9	0.236	16.9

8.3.2 Preliminary study of phenol oxidation using catalysts

Figure 8.1 shows the preliminary tests of adsorption and catalytic oxidation of phenol using different AC samples. It is generally accepted that AC has a good adsorption capacity. As can be seen, all ACs are able to adsorb phenol though at low efficiency. Both GAC-1 and GAC-2 showed low adsorption of phenol at less than 20% in 90 min. While PAC presented phenol adsorption efficiency doubled in 90 min, which can be ascribed to higher surface area of PAC. Inset of **Figure 8.1** displayed oxidation of phenol by PMS and negligible change in phenol concentration was observed. Less than 3% in phenol concentration reduction was found after 90 min, suggesting that PMS itself could not produce sulfate radical to induce significant oxidation of phenol. In oxidation tests, PAC with PMS in the heterogeneous system could degrade phenol up to 85% in 90 min. Meanwhile, GAC-1 and GAC-2 could only reach around 30 and 25% phenol removal, respectively. The experimental results show that surface area of heterogeneous catalysts influencing significantly of phenol degradation. Phenol degradation is dependent on sulfate radicals ($SO_4^{-\bullet}$ and $SO_5^{-\bullet}$) due to the same concentrations of PMS, sulfate radical concentration produced will depend on active sites on surface area of catalyst. Thus, the catalysts with a high surface area can provide more active sites to produce more sulfate radical, resulting in high phenol degradation. In addition, TOC removal in PAC/PMS system was also examined and the result showed that about 75% TOC removal was obtained within 90 min. The reaction mechanism for heterogeneous phenol oxidation can be proposed as follows.

$$AC + HSO_5^- \longrightarrow AC^+ + SO_4^{-\bullet} + OH^- \quad (8.3)$$

$$AC^+ + HSO_5^- \longrightarrow AC + SO_5^{-\bullet} + H^+ \quad (8.4)$$

$$SO_4^{-\bullet} + H_2O \rightarrow SO_4^{2-} + OH^\bullet + H^+ \quad (8.5)$$

$$SO_4^{-\bullet} + C_6H_5OH \longrightarrow \text{several steps} \longrightarrow CO_2 + H_2O + SO_4^{2-} \quad (8.6)$$

Several investigations have been reported for heterogeneous activated carbon catalysts for organic decomposition using different oxidants. Santos et al. [18] studied the modified activated carbon (100-300 μm) for heteregoneous activation of H_2O_2 to

generate hydroxyl radical targeting the decolorourisation of reactive red 241. Modified activated carbon could achieve 65% colour removal at reactive red 241 concentration of 50 ppm within 150 min. They also found that the catalytic activity influenced significantly by pH. Yao et al. [19] used reduced graphene oxide (rGO) nanoparticle with peroxymonosulfate for phenol degradation at 20 mg/L. rGO could achieve 20% phenol degradation within 60 min. Shukla et al. [8] studied activated carbon with peroxymonosulfate for phenol degradation at 25 mg/L. The activated carbon could achieve 48% phenol degradation within 60 min. Therefore, it is seen that PAC with peroxymonosulfate presented higher activity in phenol degradation than other activated carbon and rGO.

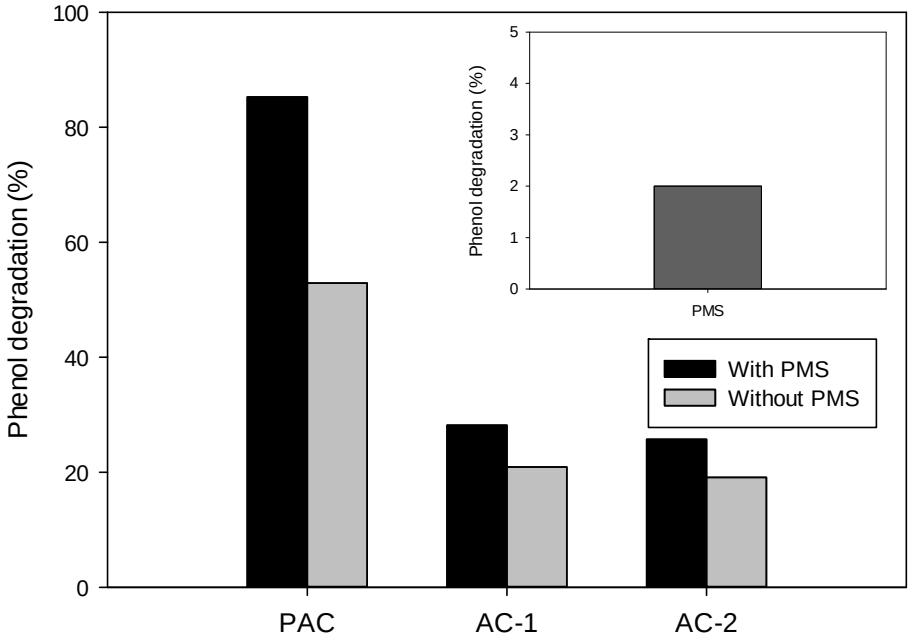

Figure 8.1. Prelimenary study of phenol at different size of catalyst. Reaction conditions: [Phenol] = 50 ppm, catalyst = 0.2 g/L, PMS = 6.5 mmol/L, and T = 25 ^{o}C.

8.3.3 Effect of reaction parameters on phenol degradation

Figure 8.2 shows a comparison in oxidation of phenol on PAC with different oxidants (PMS, PDS, and H_2O_2). As can be seen, PAC could activate all three oxidants although the removal efficiency of phenol is different. PAC with

peroxymonosulphate resulted in complete degradation of phenol in less than 20 min. PAC with PDS could achieve 100% removal of phenol in 90 min while PAC with H_2O_2 could achieve only 50% phenol removal in 90 min. In addition, this experimental results indicating that the catalytic activity is apparently dependent on the oxidation potential of oxidants. The catalytic activity shows an order of PAC/H_2O_2 < PAC/PDS < PAC/PMS in phenol degradation. Anipsitakis and Dionysiou [20] studied homogeneous activation of PMS, PDS and H_2O_2 with Mn^{2+} for 2,4-DCP oxidation. It was reported that Mn^{2+}/PMS is the highest of 2,4-DCP removal, followed by Mn^{2+}/PDS and Mn^{2+}/H_2O_2. Thus, it would be expected a similar reaction rate for heterogeneous systems in this investigation.

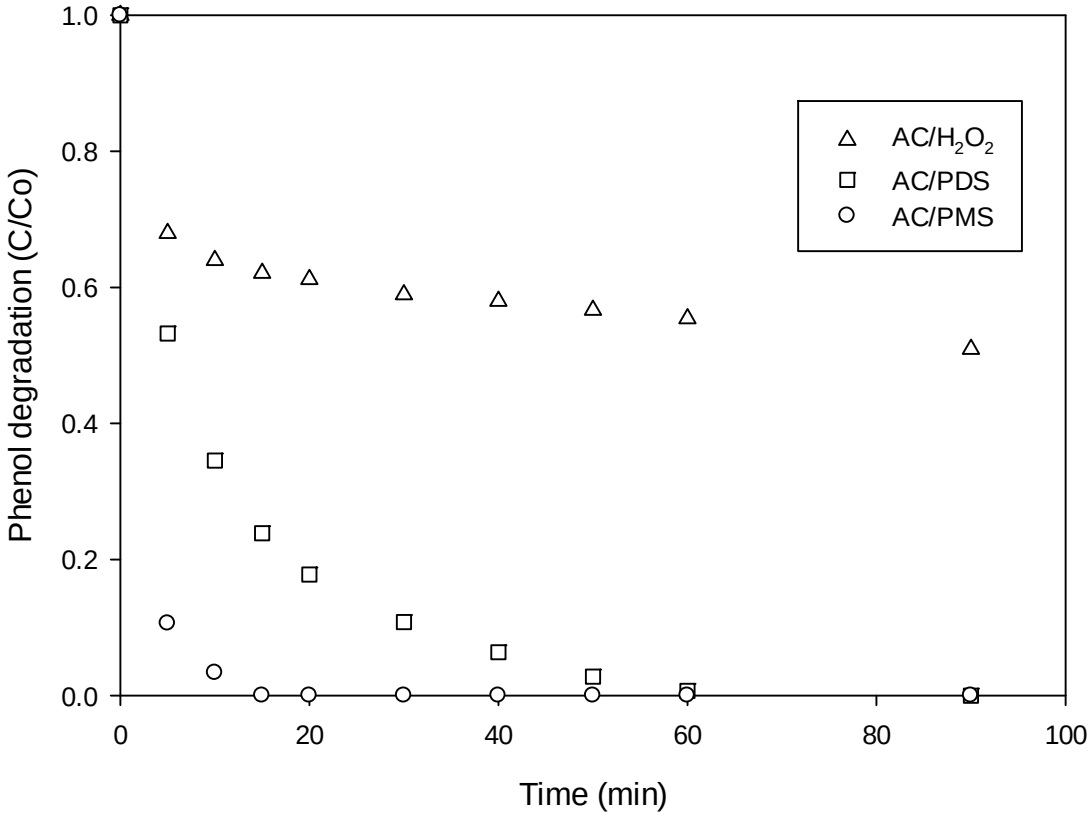

Figure 8.2. Phenol trasfomation by the interaction of PAC and three different oxidants. Reaction conditions: [Phenol] = 25 ppm, catalyst = 0.2 g/L, oxidant = 6.5 mmol/L, and T = 25 ^{o}C.

Figure 8.3 presents the variation of normalised phenol concentration as function of PMS concentration in the solution. As can be seen, the degradation of phenol by PAC/PMS depended on initial concentration of PMS. Higher concentration of PMS resulted in more removal efficiency of phenol. The complete phenol degradation could be achieved at 6.5 mmol PMS loading in 15 min, while in the same duration at PMS concentrations of 5.5, 2.6, and 1.3 mmol, removal efficiency were obtained at 98, 94, and 87%, respectively.

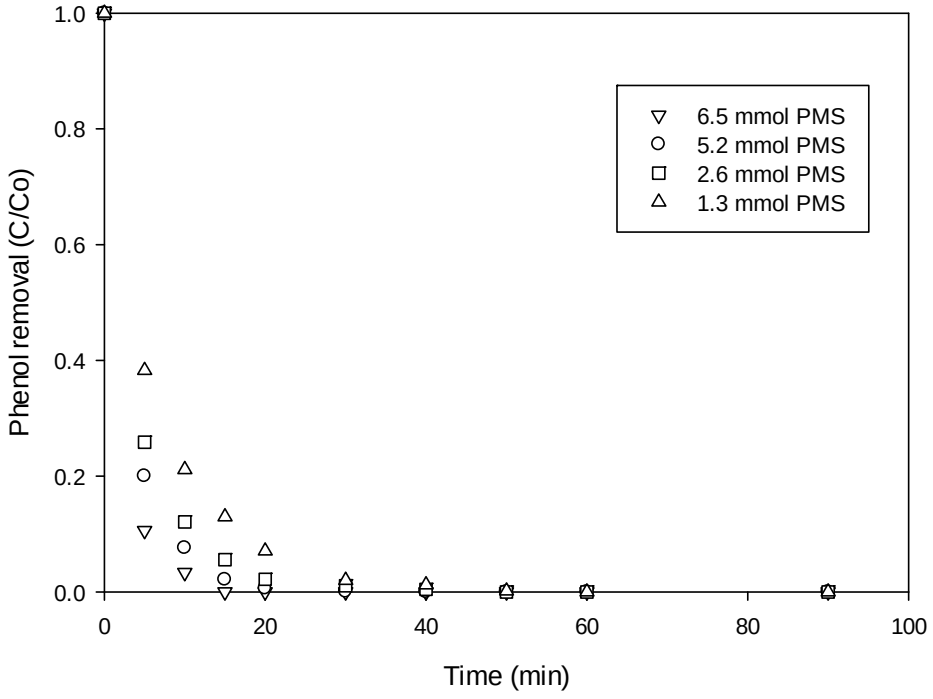

Figure 8.3. Effect of PMS concentration on phenol removal. Reaction conditions: [Phenol] = 25 ppm, catalyst = 0.2 g/L and T = 25 ^{o}C.

A general pseudo first order kinetics for phenol degradation was employed to estimate the kinetic rates, as shown in equation below.

$$\ln\left(\frac{C}{Co}\right) = -k \bullet t \qquad (8.7)$$

Where k is the apparent first order rate constant of phenol removal, C is the concentration of phenol at various time (t). C_o is the initial phenol concentration. Using this model ln(C/Co) versus time produced straight lines as shown in **Figure**

8.4. The rate constants at varying PMS concentrations are shown in **Table 8.2**. As seen, rate constant will decrease as the concentration of PMS decreases.

Table 8.2. Rate constant at different feed concentration of PMS

Initial PMS concentration	Rate constant min^{-1}	R^2
6.5 mmol	0.3943	0.967
5.2 mmol	0.2661	0.991
2.6 mmol	0.1921	0.952
1.3 mmol	0.1409	0.982

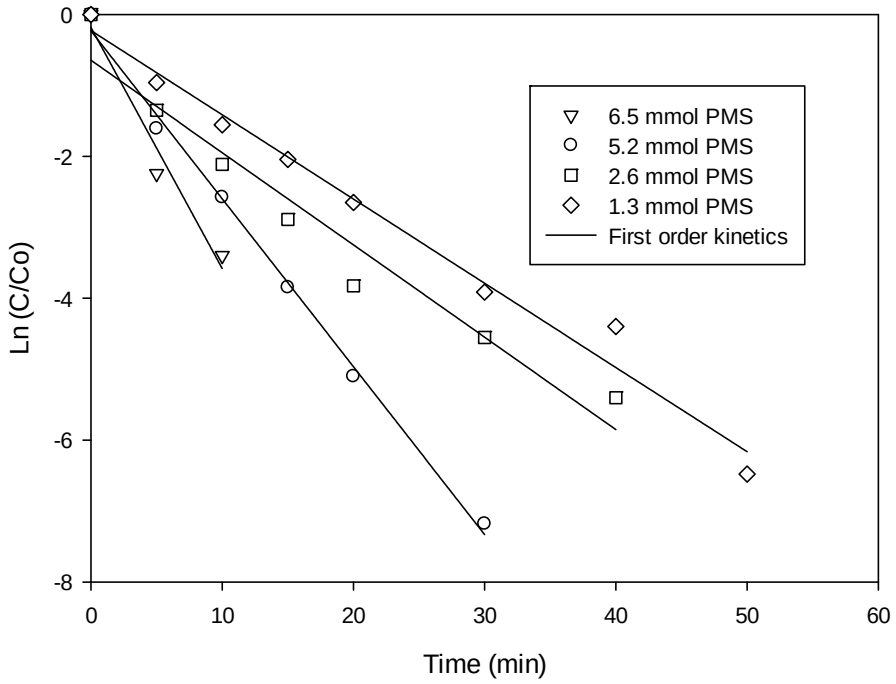

Figure 8.4. Ln (C/Co) versus time in phenol degradation at different oxidant concentration.

It is believed that phenol degradation also depended on initial concentration of phenol in solution. **Figure 8.5** shows phenol degradation at various concentrations between 25 and 100 ppm. At high phenol concentration, removal efficiency tended to decrease. At 25 ppm, phenol removal is very fast and achieves 100% degradation within 15 min, whereas at phenol concentrations of 50, 75 and 100 ppm, the

degradation rate is slower and phenol removal will achieve at only 85, 62, and 42%, respectively in 90 min.

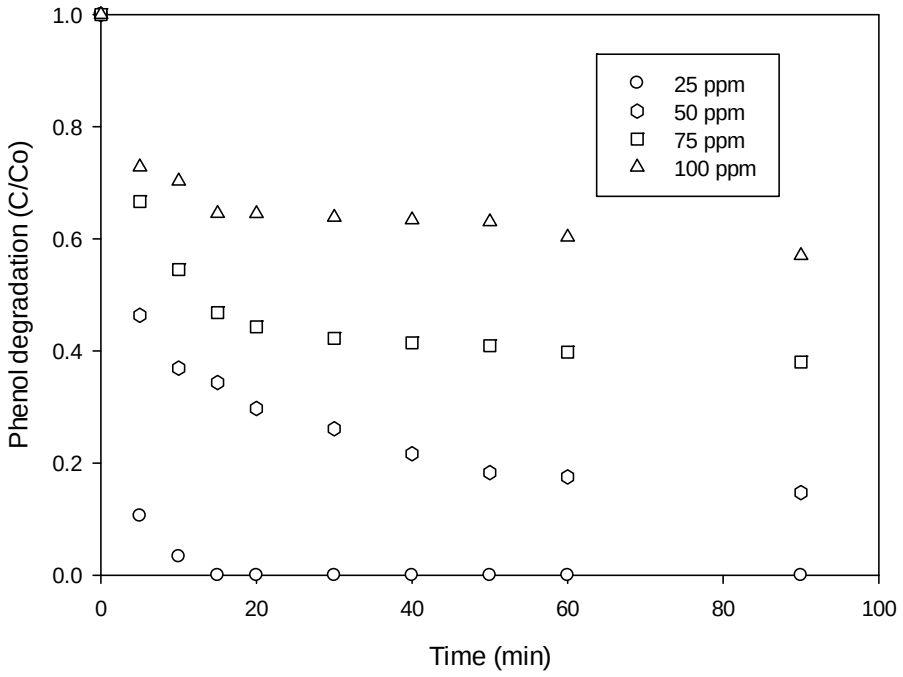

Figure 8.5. Effect of phenol concentration on phenol removal. Reaction conditions: catalyst = 0.2 g/L, PMS = 6.5 mmol/L, and T = 25 ^{o}C.

The effect of PAC loading in solution on phenol degradation is shown in **Figure 8.6**. An increase in PAC amount in the solution increased the phenol degradation efficiency. A complete removal of phenol could be reached within 15 min at 0.2 g/L PAC loading. Whereas 70.5% and 40% removals could be reached at PAC loading of 0.1 and 0.06 g/L, respectively. For phenol degradation, increased catalyst loading would enhance adsorption and provides additional sites for generation of active sulphate radicals, thus enhancing phenol degradation.

Furthermore, temperature is also a variable influencing catalyst activity and phenol degradation. **Figure 8.7** shows the reduction of phenol concentration versus time at various temperatures of 25 - 45 ^{o}C. As seen that the rate of reaction would increase with increased temperature. At temperature of 25 ^{o}C, phenol removal would reach 85% at 50 ppm in 90 min. While in the same duration and phenol concentration at temperatures of 35 and 45 ^{o}C, removal efficiency obtained are 91, and 95%,

respectively. Using the first order kinetic rate constant, the activation energy for this heteregeneous phenol decomposition was found to be 17.6 kJ/mol. It should be noted that phenol degradation in PAC-PMS system would be ascribed to adsorption and oxidation.

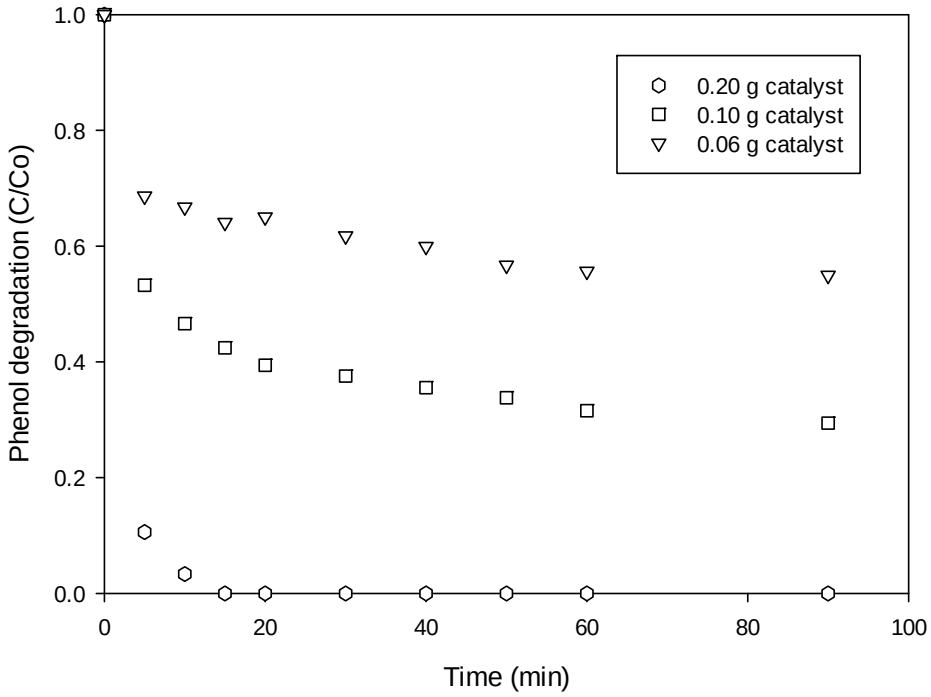

Figure 8.6. Effect of catalyst loading on phenol removal. Reaction conditions: [Phenol] = 25 ppm, PMS = 6.5 mmol/L, and T = 25 ^{o}C.

In this study, it would be difficult to distinguish the contribution of each part (adsorption and oxidation). Thus, the activation energy value obtained would refer to the combined processes. Previously, we have investigated several heterogeneous carbon supported Co and Ru, such as Co/AC, Co/CX (carbon-xerogel) and RuO_2/AC, in activation of PMS for phenol degradation and the activation energies obtained are presented in **Table 8.3**. As can be seen, that PAC presented lower activation energy than AC supported Co and Ru catalysts.

Table 8.3. Activation of heterogeneous catalysts with PMS for phenol degradation.

Catalyst	Activation energy (kJ/mol)	Reference
Co/AC	59.7	[8]
Co/CX-1	48.3	[21]
Co/CX-G	62.9	[21]
RuO_2/AC	61.4	[22]
PAC	17.6	This work

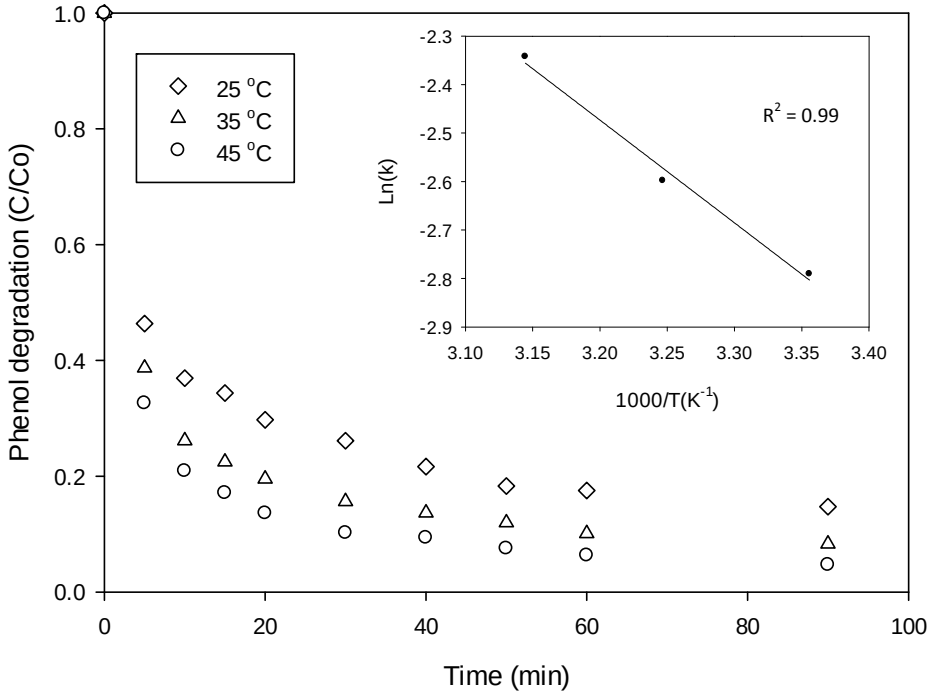

Figure 8.7. Effect of temperature on phenol removal. Reaction conditions: [Phenol] = 50 ppm, catalyst = 0.2 g/L, and PMS = 6.5 mmol/L.

8.3.4 Reactivity of spent PAC catalyst and reusability

Figure 8.8 shows the catalytic activity of recycled PAC for phenol degradation. As can be seen, the catalytic activity significantly reduced in the second use, suggesting deactivation of the catalyst. In the second use, phenol degradation was 34% at 15 min compared with 100% in the first use. Furthermore, for PAC second use after thermal treatment at 500 ^{o}C for 1 hour, it appears that the catalyst activity increases again although unlike the first use and 62% phenol degradation can be achieved at 15 min.

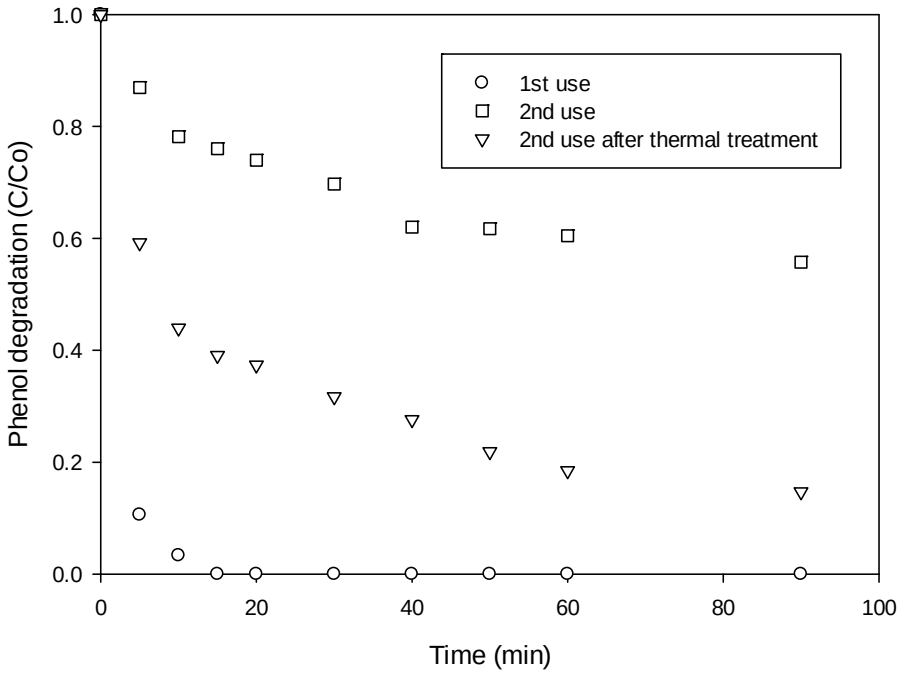

Figure 8.8. Phenol removal in tests of recycled PAC catalyst. Reaction conditions: [Phenol] = 25 ppm, catalyst = 0.2 g/L, and PMS = 6.5 mmol/L.

8.3.5 Role of powder activated carbon catalyst in phenol degradation

During catalytic oxidation of toxic organics, powder activated carbon primarily acted as an adsorbent for phenol, as shown in **Figure 8.1**. This may increase the probability of a reaction between peroxymonosulphate and phenol. Powder activated carbon also catalyses the decomposition of peroxymonosulphate into free radicals, such as sulphate radicals. These sulphate radicals are very active in oxidation reactions in the aqueous phase. Then, sulphate radicals and phenol can react on the catalyst surface to produce simple molecular compounds including CO_2 and H_2O (Eqs. 8.3 – 8.6). Although the peroxymonosulphate decomposition mechanism is not completely understood, the electron transfer from the surface of powder activated carbon has been suggested to take place during the reaction. According to the mechanism, the reaction might be initiated by a reducing site transferring an electron to

peroxymonosulphate to produce sulphate radicals. Moreno-Castilla et al. [23] investigated activated carbon cloth with H_2O_2 for the removal of amitrole from aqueous solution. The studies have suggested that a basic site on carbon surface promotes H_2O_2 decomposition into hydroxyl and perydroxyl radicals, thereby enhanching the oxidation of organic compounds in liquid. They also found that the surface sites may be delocalized π electrons from the graphene layers (C-π), which transfering electrons according to the mechanism as follows:

$$C - \pi + H_2O_2 \longrightarrow C - \pi^+ + OH^- + OH^\bullet \quad (8.8)$$

$$C - \pi^+ + H_2O_2 \longrightarrow C - \pi + H^+ + HO_2^\bullet \quad (8.9)$$

Thus, the current study using peroxymonosulphate as an oxidant will be in similar consequences. The reaction initiated by the activation of peroxymonosulphate by a reducing site in a Fenton like reaction to produce a $SO_4^{-\bullet}$ radical. This sulphate radical can then react with phenol as shown in **Figure 8.9**.

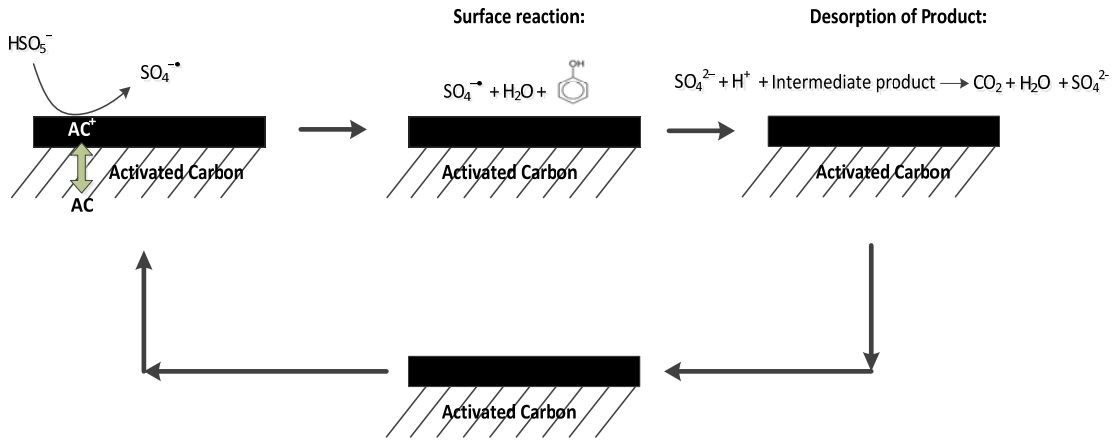

Figure 8.9. Mechanism for phenol removal during powder activated carbon (PAC) enhanced peroxymonosulphate.

8.4 Conclusions

PAC can be a cheap, green and effective catalyst in activation of H_2O_2, PDS and PMS to produce hydroxyl and sulphate radicals for phenol degradation. PAC exhibited higher activity than GAC and higher activity in PMS activation. Phenol degradation can be achieved in a short time with PAC/PMS. High PAC and PMS concentrations in solution will make high phenol degradation efficiency. Phenol degradation followed the first-order kinetics and activation energy of the catalyst was obtained as 17.6 kJ/mol.

References

1. Huang, C.-P. and Y.-H. Huang, *Application of an active immobilized iron oxide with catalytic H_2O_2 for the mineralization of phenol in a batch photo-fluidized bed reactor.* Applied Catalysis A: General, 2009. **357**(2): p. 135-141.

2. Calleja, G., J.A. Melero, F. Martínez, and R. Molina, *Activity and resistance of iron-containing amorphous, zeolitic and mesostructured materials for wet peroxide oxidation of phenol.* Water Research, 2005. **39**(9): p. 1741-1750.

3. Fajerwerg, K. and H. Debellefontaine, *Wet oxidation of phenol by hydrogen peroxide using heterogeneous catalysis Fe-ZSM-5: a promising catalyst.* Applied Catalysis B: Environmental, 1996. **10**(4): p. L229-L235.

4. Imamura, S., A. Doi, and S. Ishida, *Wet oxidation of ammonia catalyzed by cerium-based composite oxides.* Industrial & Engineering Chemistry Product Research and Development, 1985. **24**(1): p. 75-80.

5. Alvarez, P.M., D. McLurgh, and P. Plucinski, *Copper oxide mounted on active carbon as catalyst for wet air oxidation of aqueous phenol. 2. Catalyst stability.* Industrial & Engineering Chemistry Product Research and Development, 2002. **2002**(41): p. 2153-2158.

6. Baldrian, P., V. Merhautová, J. Gabriel, F. Nerud, P. Stopka, M. Hrubý, and M.J. Benes, *Decolorization of synthetic dyes by hydrogen peroxide with heterogeneous catalysis by mixed iron oxides.* Applied Catalysis B: Environmental, 2006. **66**(3-4): p. 258-264.

7. Stüber, F., J. Font, A. Fortuny, C. Bengoa, A. Eftaxias, and A. Fabregat, *Carbon materials and catalytic wet air oxidation of organic pollutants in wastewater.* Topics in Catalysis, 2005. **33**(1): p. 3-50.

8. Shukla, P.R., S. Wang, H. Sun, H.M. Ang, and M. Tadé, *Activated carbon supported cobalt catalysts for advanced oxidation of organic contaminants in aqueous solution.* Applied Catalysis B: Environmental, 2010. **100**(3-4): p. 529-534.

9. Faria, P.C.C., J.J.M. Órfão, and M.F.R. Pereira, *Activated carbon catalytic ozonation of oxamic and oxalic acids.* Applied Catalysis B: Environmental, 2008. **79**(3): p. 237-243.

10. Auer, E., A. Freund, J. Pietsch, and T. Tacke, *Carbons as supports for industrial precious metal catalysts.* Applied Catalysis A: General, 1998. **173**(2): p. 259-271.

11. Aguilar, C., R. García, G. Soto-Garrido, and R. Arraigada, *Catalytic oxidation of aqueous methyl and dimethylamines by activated carbon.* Topics in Catalysis, 2005. **33**(1): p. 201-206.

12. Huang, H.-H., M.-C. Lu, J.-N. Chen, and C.-T. Lee, *Catalytic decomposition of hydrogen peroxide and 4-chlorophenol in the presence of modified activated carbons.* Chemosphere, 2003. **51**(9): p. 935-943.

13. Georgi, A. and F.-D. Kopinke, *Interaction of adsorption and catalytic reactions in water decontamination processes: Part I. Oxidation of organic contaminants with hydrogen peroxide catalyzed by activated carbon.* Applied Catalysis B: Environmental, 2005. **58**(1–2): p. 9-18.

14. Masura Kimura, I.M., *Discovery of the Activated-Carbon Radical AC^+ and the Novel Oxidation-Reactions Comprising the AC/AC^+ Cycle as a Catalyst in an Aqueous Solution.* Bulletin of the Chemical Society of Japan, 1994. **67**(9).

15. Saputra E., M.S., *Red mud and fly ash supported Co catalysts for phenol oxidation.* Catalysis Today, 2011.

16. Huang, K.-C., R.A. Couttenye, and G.E. Hoag, *Kinetics of heat-assisted persulfate oxidation of methyl tert-butyl ether (MTBE).* Chemosphere, 2002. **49**(4): p. 413-420.

17. Shukla, P.R., S. Wang, H.M. Ang, and M.O. Tadé, *Photocatalytic oxidation of phenolic compounds using zinc oxide and sulphate radicals under artificial solar light.* Separation and Purification Technology, 2010. **70**(3): p. 338-344.

18. Santos, V.P., M.F.R. Pereira, P.C.C. Faria, and J.J.M. Órfão, *Decolourisation of dye solutions by oxidation with H_2O_2 in the presence of modified activated carbons.* Journal of Hazardous Materials, 2009. **162**(2–3): p. 736-742.

19. Yao, Y., Z. Yang, D. Zhang, W. Peng, H. Sun, and S. Wang, *Magnetic $CoFe_2O_4$–Graphene Hybrids: Facile Synthesis, Characterization, and Catalytic Properties.* Industrial & Engineering Chemistry Research, 2012. **51**(17): p. 6044-6051.

20. Anipsitakis, G.P. and D.D. Dionysiou, *Radical Generation by the Interaction of Transition Metals with Common Oxidants.* Environmental Science & Technology, 2004. **38**(13): p. 3705-3712.

21. Sun, H., H. Tian, Y. Hardjono, C.E. Buckley, and S. Wang, *Preparation of cobalt/carbon-xerogel for heterogeneous oxidation of phenol.* Catalysis Today, 2012. **186**(1): p. 63-68.

22. Muhammad, S., P.R. Shukla, M.O. Tadé, and S. Wang, *Heterogeneous activation of peroxymonosulphate by supported ruthenium catalysts for phenol degradation in water.* Journal of Hazardous Materials, 2012. **215–216**(0): p. 183-190.

23. Moreno-Castilla, C., M.A. Fontecha-Cámara, M.A. Álvarez-Merino, M.V. López-Ramón, and F. Carrasco-Marín, *Activated carbon cloth as adsorbent and oxidation catalyst for the removal of amitrole from aqueous solution.* Adsorption, 2011. **17**(3): p. 413-419.

Chapter 9

Conclusions and Future Work

Abstract

The work presented in this thesis focused on catalytic oxidation of toxic organics using peroxymonosulfate as an oxidant in the presence of manganese oxides or activated carbon catalysts. Both catalysts were selected due to low toxicity to the environment. Manganese oxides with several different phases and shapes have been synthesized and tested for degradation of phenol as a model compound for wastewater treatment and both catalysts are very promising materials for replacing toxic Co^{2+} for activation of peroxymonosulfate to produce sulfate radicals for organic oxidation. All kinetic studies presented in this thesis suggest that the degradation of phenol in manganese oxide followed first-order kinetic model.

9.1. Conclusions

In general, the main objectives of the research described in the previous chapters have been achieved satisfactorily. Some manganese oxide catalysts with different phases, shapes and morphologies have been successfully synthesized, such as MnO, MnO_2, Mn_2O_3, and Mn_3O_4, using hydrothermal, solvothermal and sol-gel methods. In addition, other manganese oxide catalysts supported on Activated Carbon (AC), and Graphene Oxide (GO) also have been successfully synthesized using an impregnation method. Furthermore, the synthesized catalysts of α-, β-, γ-MnO_2, MnO, α-Mn_2O_3, γ-Mn_3O_4, α-Mn_2O_3@α-MnO_2 core/shell, Mn/AC, and Mn/GO have been characterized and tested for adsorption and heterogeneous oxidation reaction for phenol degradation in aqueous solution. Further, it was observed that adsorption may increase the probability of reaction between peroxymonosulfate and phenol, and phenol degradation on all heterogeneous catalysts followed the first-order kinetics. Moreover, it was also found that several parameters such as the concentration of phenol, catalyst loading, loading peroxymonosulfate, and temperature are key factors affecting the phenol oxidation process.

9.1.1 Catalytic oxidation of phenolics using MnO_2 and peroxymonosulfate

1. Three different types of α-MnO_2 with crystalline and amorphous structure (α-MnO_2-300, α-MnO_2-500 and α-MnO_2-140) have been synthesized using hydrothermal and sol-gel method. Based on XRD pattern and TEM images, α-MnO_2-300 is an amorphous phase with a spherical shape, while α-MnO_2-500 and α-MnO_2-140 are a crystalline with nanorods and nanowires, respectively. In phenol oxidation reaction, crystalline MnO_2 demonstrated high activity. Nanowired MnO_2-140 produced the highest phenol degradation with 100% phenol degradation and 99% TOC reduction in 90 min and it also exhibited high stability. MnO_2-300 with mesoporous structure gave the lowest activity and less stability. The activity shows an order of α-MnO_2-300 < α-MnO_2-500 < α-MnO_2-140. The reaction rate was observed to follow the first-order kinetics with the rate of reaction increasing with temperature.

2. Three one-dimensional MnO_2 nanoparticles with different crystallographic phase, α-, β-, γ-MnO_2 have been successfully synthesized using hydrothermal method. Characterization results by SEM confirm that α-, β -, γ-MnO_2 are in morphologies of nanowires, nanorods and nanotubes, respectively. The α-, β-, γ-MnO_2 are effective catalysts for the activation of peroxymonosulfate to generate sulfate radicals for phenol degradation depending on surface area and crystalline structure. Among them, α-MnO_2 nanowires has the highest activity in removing phenol which completes removal of phenol in 60 min at phenol concentrations ranging in 25-100 ppm. The activity shows an order of α-MnO_2 > γ-MnO_2 > β-MnO_2. Kinetic studies show that phenol degradation on the α-MnO_2 follows the first-order kinetics with the activation energy of 21.9 kJ/mol.

9.1.2 Manganese oxide catalysts at different oxidation states

1. Four different types of manganese oxide at different oxidation states (MnO, MnO_2, Mn_2O_3, and Mn_3O_4) have been synthesized using thermal and hydrothermal methods. Based on XRD pattern and SEM images, MnO is a rock salt structured, while MnO_2, Mn_2O_3, and Mn_3O_4 are a rutile, "C" bixbyite and spinel, respectively.
2. In phenol oxidation reaction, catalytic activities of Mn oxides were found to be closely related to the chemical states of Mn. Mn_2O_3 is highly effective in heterogeneous activation of PMS to produce sulfate radicals for phenol degradation compared with other catalysts (MnO, MnO_2, and Mn_3O_4). The activity shows an order of Mn_2O_3 > MnO > Mn_3O_4 > MnO_2. The reaction rate was observed to follow first order kinetics and activation energy was obtained as 11.4 kJ/mol.
3. One of the Mn_2O_3 disadvantage in relation with its activity on phenol oxidation is reduced catalytic activity of catalyst in the use of a second if the catalyst was recovered by simple water washing. Deactivation of Mn_2O_3 could be attributed to intermediate deposition on surface and chemical phase change.

9.1.3 Metal oxide catalysts with spinel structure.

1. Spinel structure samples, Mn_3O_4, Co_3O_4, and Fe_3O_4, have been successfully synthesized using hydrothermal and solvothermal methods. The redox reactions were observed to follow redox potential of catalysts.
2. Among the catalysts, Mn_3O_4 and Co_3O_4 are highly effective in heterogeneous activation of peroxymonosulfate to generate sulfate radicals with the activity order of $Co_3O_4 \sim Mn_3O_4 > Fe_3O_4$.
3. Kinetic studies show that phenol degradation on the Mn_3O_4 and Co_3O_4 follows the first-order kinetics with the activation energies of 38.5 and 66.2 kJ/mol, respectively.

9.1.4 α-Mn_2O_3@α-MnO_2 core/shell nanocomposite catalysts.

1. α-Mn_2O_3@α-MnO_2 core/shell nanocomposite catalyst has been successfully synthesized using a hydrothermal method. Characterization results by SEM confirm that α-Mn_2O_3@α-MnO_2 core/shell is in morphology of uniform ellipsoid structure. The ellipsoid is actually composed of an inside core (α-Mn_2O_3) and an outside shell (α-MnO_2).
2. The core/shell material is highly effective in heterogeneous activation of peroxymonosulfate to produce sulfate radicals for phenol degradation. Catalyst loading, peroxymonosulfate concentration, phenol concentration, and temperature are key factors affecting the phenol oxidation process.
3. Kinetic studies show that phenol degradation on the α-Mn_2O_3@α-MnO_2 core/shell follows the first-order kinetics with the activation energy of 39.9 kJ/mol.

9.1.5 Carbon supported manganese catalysts.

1. Two types of manganese oxide supported on commercial activated carbons (AC-P and AC-N) and graphene oxide (GO) have been successfully synthesized using an impregnated method. Characterization results by

XRD and SEM-EDS confirm that the active metal manganese on the activated carbons is in form of MnO_2 and Mn_3O_4, while manganese species in graphene oxide were not identified.

2. The three oxide catalysts supported on AC-P, AC-N, and GO are effective for generating sulphate radicals in the presence of peroxymonosulfate. Among them, AC-P has the highest activity in removing phenol which completes removal of phenol in 60 min at phenol concentrations ranging in 75-100 ppm.
3. Kinetic studies show that phenol degradation on the Mn/AC-P follows the first-order kinetics with the activation energy of 15.0 kJ/mol.

9.1.6 Activated carbon catalysts.

1. The same type of commercial activated carbon with different particle size which are powder (PAC) and granular (GAC-1 and GAC-2), is effective catalyst for degradation of a toxic organic compound, phenol in the presence of peroxymonosulfate. Among these three catalysts, Powder Activated Carbon (PAC) with the highest surface area, has the highest activity in removing phenol which completes removal of phenol in less than 20 min at phenol concentrations of 25 ppm. The catalysts with a high surface area can provide more active sites to produce more sulfate radical, resulting in high phenol degradation.
2. Comparisons were conducted for three different oxidants such as H_2O_2, peroxydisulfate (PDS), and peroxymonosulfate (PMS) in the presence of PAC catalyst for degradation of a toxic organic compound, phenol. The activity shows an order of PAC/H_2O_2 < PAC/PDS < PAC/PMS in phenol degradation. This experimental results indicating that the catalytic activity is apparently dependent on the oxidation potential of oxidant.
3. Kinetic studies show that phenol degradation on AC-P follows the first-order kinetics with the activation energies of 17.6 kJ/mol.

9.2. Scope of Future Work

1. This research focused on manganese oxides and activated carbon catalysts for catalytic phenol degradation in aqueous solutions. These catalysts presented very good performance in phenol degradation in the presence of peroxymonosulfate. However, these catalysts need to be tested for other pollutants, such as polycyclic aromatic hydrocarbon, dyes, chloride hydrocarbons, etc. It is also recommended to conduct the tests of catalysts with other oxidants, such as hydrogen peroxide, peroxydisulfate, and potassium permanganate.

2. In the current thesis the focus was to explore the activity and stability of catalysts for phenol oxidation reaction. However, further study on the mechanism reaction need to be done to investigate intermediate products which are resulted from the phenol oxidation reaction.

3. In this study, catalytic oxidation of phenol conducted in a batch process has been successfully carried out. However, further study on a continuous process needs to be done to investigate several parameters such as flow rate of feed, residence time, kinetic constants etc. in order to scale up this technology to pilot scale and finally to industrial scale.